# HYPERSONIC AND PLANETARY ENTRY FLIGHT MECHANICS

*Nguyen X. Vinh*

*Adolf Busemann*

*Robert D. Culp*

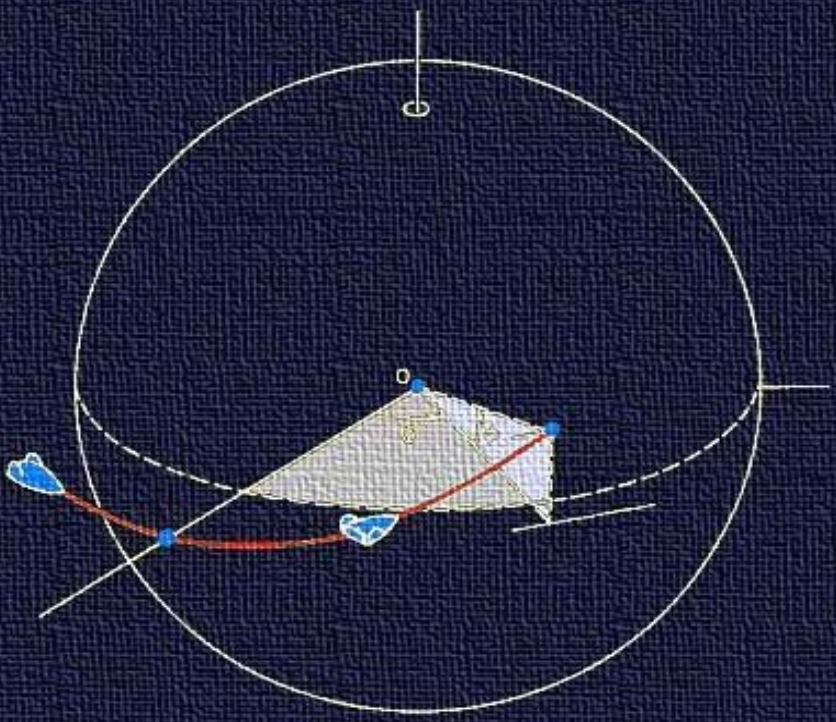

THE UNIVERSITY OF MICHIGAN PRESS

# HYPERSONIC AND PLANETARY ENTRY FLIGHT MECHANICS

# HYPERSONIC AND PLANETARY ENTRY FLIGHT MECHANICS

*Nguyen X. Vinh*

*Adolf Busemann*

*Robert D. Culp*

ANN ARBOR
THE UNIVERSITY OF MICHIGAN PRESS

ISBN 0-472-09304-5
Library of Congress Catalog Card No. 79-57117
Published in the United States of America by
The University of Michigan Press and simultaneously
in Rexdale, Canada, by John Wiley & Sons Canada, Limited
Manufactured in the United States of America

# Preface

The advent of the space shuttle and the prospect of several decades of regular low-altitude earth orbital activity have focused attention on high-speed atmospheric trajectories exemplified by the space shuttle entry. The hypersonic flight mechanics of these trajectories represents a unique field, in that a combination of orbital mechanics and atmospheric flight mechanics is required.

For more than a decade we have worked together in this field, pursuing research under the sponsorship of the National Aeronautics and Space Administration and the United States Air Force, and in teaching various aspects of the subject to advanced undergraduate and graduate students at the University of Michigan and the University of Colorado. During this time, interest in this topic has grown steadily until the demand for such material led to this book.

We have endeavored to make this text valuable as a research tool and reference for current experts in the field, and also as a learning source for engineers and scientists in related fields who want to become involved in entry dynamics. Taken as a whole, this book is a comprehensive and self-contained treatment of hypersonic flight trajectories and atmospheric entry flight mechanics, leading the reader through the classical theories and ending with our modern, unified theory. Every topic is written so as to stand alone; the reader can enter the text at any point to obtain the analysis of particular interest. Every chapter is followed by a list of references which enables a researcher to trace the roots of the subject.

As a textbook, this book is designed to be used in several ways. The first nine chapters serve as a text at the introductory level for senior students interested in orbital and entry flight mechanics. For students with a firm background in aerospace engineering, including aerodynamics, propulsion, and orbital mechanics, this book can be used as the text for a specialized course in atmospheric entry. For these advanced undergraduate and graduate students, chapter 2 and chapters 6 through 13 comprise a suitable text for such a one-semester course. Chapter 18 can be included as time permits. The entire text covers a two-semester sequence at the senior or first-year graduate level which brings the student to a sophisticated understanding of the subject. Finally, used as a textbook for a short

course on entry flight mechanics for engineers working in the space program, the following reading sequence is sufficient: chapter 2 and chapters 10 through 18.

At both the University of Michigan and the University of Colorado, parts of this book have been used as the text for several courses at both the advanced undergraduate and graduate levels. This favorable experience has enabled us to bring out the text in this final form suitable as a useful tool for both research and education. Several of our doctoral students have contributed to the development of a unified theory for planetary entry covered in the second half of the book. It is a pleasure to acknowledge here their collective research efforts. Each individual contribution is fully accounted for in the text. During the whole period of the preparation of this book, from its inception in 1972 until its completion in 1980, Professor Adolf Busemann has provided his eminent leadership, assisted by his gracious wife, Magda. To them this book is dedicated.

It is with gratitude that we acknowledge the support of the NASA Langley Research Center, sponsor of much of the research work which went into this book. Dr. John E. Duberg, at a very early stage, shared our opinion that further basic research on entry trajectories needed to be done. As technical monitors from Langley, Mr. Robert W. Rainey and Mr. Robert S. Dunning have provided enlightening comments on several technical papers and NASA contractor reports generated under NASA research grants. Professor Robert M. Howe, Chairman of the Department of Aerospace Engineering at the University of Michigan, and also the Chairman of the Department of Aerospace Engineering Sciences at the University of Colorado have provided us with much encouragement for this work. It is a pleasure to acknowledge their hospitality during our frequent visits to each other's campus to carry out our teamwork.

The excellent typing of the preliminary manuscript was done by Ms. Shirley Iverson while the final camera-ready copy was professionally prepared by Ms. Ann Gee. Their perseverance and dedication to this work are much appreciated.

We would like to express our deep appreciation to Magda Busemann, Joan Vinh, and Betty Culp for their continual love and encouragement during these years.

# Contents

**Chapter 4. Powered Phase**



**Chapter 5. Return to the Atmosphere**



**Chapter 6. Basic Equations for Planar Entry Trajectories**



**Chapter 7. Analysis of First-Order Planetary Entry Solutions**



**Chapter 8. Loh's Second-Order Theory for Entry Trajectories**

**Chapter 15. Orbit Contraction Due to Atmospheric Drag**



**Chapter 16. Flight with Lift Modulation**



**Chapter 17. Lift Modulation with Constraints on Speed and Flight Path Angle**

**Chapter 18. Lateral Maneuvers**

# Chapter 1

# Planetary Atmospheres and Aerodynamic Forces

## 1-1. INTRODUCTION

To study the effects of aerodynamic forces on trajectories at orbital speeds, it is necessary to model the planetary atmospheres in which the flights take place. Because of the nature of the aerodynamic forces on orbiting and entry vehicles, only a very thin layer of atmosphere near the planet's surface need be considered. This is convenient, for in these lower reaches of the atmosphere the modeling is much simpler.

Many of the more complicated aspects of planetary atmospheres are of no consequence in aerodynamic calculations. For instance, though the atmosphere is composed of a mixture of a number of gases, it may be treated as a uniform gas of unvarying composition throughout the aerodynamically important altitudes.

In fact, the overriding feature of the atmosphere, as far as its effect on the spacecraft is concerned, is the density. The particular composition of the atmosphere can have an important influence on the aerodynamic heating of the vehicle because of the details of the dissociation of the gas after passing through the vehicle's bow shock wave, but the manner in which this is treated in this text accounts for this very simply. Once a particular reference value of aeroheating is determined, the other values are proportional.

The effect of composition on aerodynamic force is negligible. Hence, the concern in modeling the atmosphere will be to conveniently and accurately represent the density.

## 1-2. FUNDAMENTAL ASSUMPTIONS

There are several important assumptions which may be made with respect to any planetary atmosphere. These assumptions will be considered with the goal of providing an analytical representation which lends itself to ease of manipulation while maintaining reasonable accuracy. For high accuracy, tables of density such as in Ref. 1 and detailed models as discussed in Ref. 2 and 3 may be used for particular numerical cases.

### 1-2.1. Assumption of Spherical Symmetry

By far the greatest simplification in analytical atmospheric modeling is achieved by assuming that the atmospheric density is a function only of radial distance, r, from the center of the planet—the assumption of spherical symmetry. Actually, a much better assumption is that the density is a function only of altitude. If the planet's surface were a sphere, then these assumptions would be identical. But the basic figure of all the planets is an oblate spheroid, which has an elliptical cross-section along any meridian. For example, the Earth's ellipticity, the eccentricity of this cross-sectional ellipse, is 0.00335, Table 1-1.

This oblateness of the atmosphere is the greatest deviation from spherical symmetry. However, the tremendous analytical advantages of this assumption justifies this penalty in accuracy. This shortcoming can be easily corrected when necessary. The spherically symmetric model atmosphere is presented as a function of the altitude above the planet's mean sphere. This same density variation is then used as a function of the altitude above the planet's basic oblate spheroid.

This is almost equivalent to assuming the density is constant on surfaces of spheroids with the same ellipticity as that of the planet, and similarly aligned. For example, for Earth if the density at 300 kilometers altitude is referred in this manner to the surface spheroid, it will deviate from a similar spheroid by less than a kilometer (being high at the poles, and conversely low at the equator).

For planets with small ellipticity, the reference spheroid can be conveniently approximated with error $\epsilon^2$, by

$$r = r_E (1 - \epsilon \sin^2 \phi) \tag{1-1}$$

where $r_E$ is the equatorial radius, $\epsilon$ is the ellipticity, and $\phi$ is the latitude.

For particular cases, the oblateness of the atmosphere can be included in this way. However, the complications introduced are severe, and general results are obscured. This approach can be seen in Ref. 4.

Another source of deviation from spherical symmetry is the reaction of the atmosphere to solar activity. At extremely high altitudes the density increases drastically in response to solar radiation. This shows up in several ways— as a diurnal hump of dense atmosphere which follows the Sun as the Earth rotates, as a seasonal density increase which follows summer north and south, as a 27 day cycle responding to a particular solar flare on the rotating surface of the Sun, and as a long period variation corresponding to the eleven year sunspot cycle.

Only rarely do any of these effects descent below 250 kilometers altitude. Since aerodynamic forces are of short-term importance only below about 150 kilometers, these effects are negligible except when considering the slow decay of a high altitude satellite.

### 1-2.2. Assumption of Nonrotating Atmosphere

The atmosphere which the space vehicle encounters is not stationary, but rotates with the planet. For Earth and Mars the aerodynamic forces have immediate effects only at low altitudes, very near the surface. At these altitudes the atmosphere rotates with approximately the angular velocity of the planet. Venus has a denser atmosphere with a much greater effective thickness, but its angular velocity is almost nil, and the rotation of the atmosphere is minuscule. Only on Jupiter and Saturn, of the readily reachable planets, with their fantastic rotational speed, turbulent atmosphere, and lack of a well-defined surface, would the rotating atmosphere deserve special treatment. For the other planets, the speed of the atmosphere past the vehicle contributed by the rotation of the atmosphere is a small percentage of the total speed, Table 1-1.

For example, for Earth, the maximum rotational speed of the atmosphere, encountered at the equator, is about six percent of the circular orbital velocity at low altitude. Thus, the aerodynamic force due to atmospheric rotation has a maximum value of about twelve percent of the aerodynamic force due to the vehicle's speed. In most circumstances it would be far less than this.

It is possible to treat this effect analytically. However, just as for the oblateness of the atmosphere, the rotational effect would depend on the latitude of the vehicle at all times. In addition, it would depend heavily on the inclination of the trajectory to the equator. Inclusion of such detail in an analytical study would do more to obscure than reveal general trends and effects.

An example of such treatment is well-presented in Ref. 4. The effects are so slight, however, that they may easily be accounted for by slight changes in the coefficients of lift and drag for a vehicle. Indeed, the errors in such coefficients probably would already exceed the error caused by neglecting the rotation of the atmosphere.

For all of these reasons, it is usual to assume a nonrotating atmosphere. The assumption is certainly justifiable.

Table 1-1. Relative effects of oblateness and rotation of the atmosphere on aerodynamic force.

| | Ellipticity of basic spheroid, $\epsilon$ | $\frac{\text{surface rotational speed}}{\text{circular orbital speed at surface}}$ |
|---|---|---|
| Venus | 0. | 0% |
| Earth | 0.0034 | 6% |
| Mars | 0.0052 | 7% |
| Jupiter | 0.062 | 30% |
| Saturn | 0.096 | 40% |

### 1-2.3. Assumption of Exponential Atmosphere

A powerful assumption, greatly simplifying atmospheric analyses, which is frequently made, is that the atmospheric density decreases exponentially with altitude. There are several nuances to this assumption which are worth investigating.

There are two basic equations governing the density as a function of altitude. The first is the familiar equation of state for the atmosphere relating its pressure p, density $\rho$ and temperature T

$$p = \rho \frac{R^*}{M} T \tag{1-2}$$

where $R^*$ is the universal gas constant, $8.31439 \times 10^3$ joules/kg - $^oK$, and M is the mean molecular weight of the atmosphere. The second basic equation expresses that the rate of change of pressure must equal the increased weight of the atmosphere supported, as the altitude changes.

$$dp = - \rho g \, dr \tag{1-3}$$

where g is the acceleration of the gravity.

From the equation of state comes

$$\frac{d\rho}{\rho} = \frac{dp}{p} - \frac{dT}{T} \tag{1-4}$$

which, combined with Eq. (1-3), gives

$$\frac{d\rho}{\rho} = - \left[ \frac{gM}{R^* T} + \frac{1}{T} \frac{dT}{dr} \right] dr \tag{1-5}$$

This equation can be rewritten as

$$\frac{d\rho}{\rho} = - \beta \, dr \tag{1-6}$$

where $\beta$, defined as the bracketed term in Eq. (1-5), is the reciprocal of the scale height.

At this point several specific types of density atmospheres, corresponding to different assumptions on $\beta$, are to be considered.

a) The locally exponential atmosphere.

If the coefficient $\beta$ can be considered constant over some small altitude interval, the integrated density function is

$$\frac{\rho}{\rho_o} = e^{-\beta (r - r_o)} \tag{1-7}$$

from which the character of $1/\beta$ as a scale height is apparent. The coefficient $\beta$ is evaluated at the initial, or reference, point indicated by subscript zero.

b) The strictly exponential atmosphere.

If $\beta$ can be considered constant throughout the atmosphere,

Eq. (1-7) holds for all r. In this case the reference level is commonly taken to be the surface of the planet.

c) The isothermal atmosphere.

If the temperature can be considered constant through an altitude interval of the atmosphere, $dT/dr = 0$, and $\beta$ is given by

$$\beta = \frac{gM}{R^* T} \tag{1-8}$$

Since for an inverse-square gravitational force field

$$g = g_o \left(\frac{r_o}{r}\right)^2 , \tag{1-9}$$

the quantity $\beta r^2$ is constant in an isothermal atmosphere. Again, the density is given by the exponential function, Eq. (1-7).

d) The $\beta$ r-constant atmosphere.

In several studies of atmospheric entry (Ref. 5, 6), it has been convenient to consider the dimensionless quantity $\beta r$ as constant. For all the planets this is a large quantity, usually of the order 1000, Table 1-2. In this case, the difference introduced into Eq. (1-6) is additive, of the order of $1/\beta r$. Thus, the exponential atmosphere may be retained while considering $\beta r$ to be constant.

For Earth, the scale height at altitudes below 120 km, stays between about 5 km and 14 km, with a weighted mean value of about 7.1 km. The quantity $\beta r$ varies from 750 to 1300, with a weighted average of 900.

Table 1-2. Scale heights of the planets.

| | Average scale height, $1/\beta$ | Average $\beta r$ |
|---|---|---|
| Venus | 6 - 15 km | 500 - 900 |
| Earth | 7.1 km | 900 |
| Mars | 10.6 km | 350 |
| Jupiter | 25 km ? | 3000 ? |

## 1-3. THE EARTH'S ATMOSPHERE

Of course, the primary interest must be focused on the Earth's atmosphere. In order to make an analytic study of orbital trajectories encountering the Earth's atmosphere, it is necessary to have a simple, but accurate, expression for the density as a function of r. For numerical calculations for particular cases, using a high speed computer, detailed tables, such as those in Ref. 1, or polynomial representations, are used. For detailed computations for a specific vehicle, such an

approach is valuable. However, the intimate knowledge of the Earth's atmosphere which such references make available can be used to generate more easily used functions. In particular, it is convenient to produce piecewise exponential functions, Ref. 7.

An accurate density function can be obtained by considering the effects on density of the variation in scale height, $H \equiv 1/\beta$, and molecular scale temperature, $T_M$.

The molecular scale temperature accounts for both temperature and molecular weight changes with altitude.

$$T_M \equiv \frac{T}{M} M_o \tag{1-10}$$

The standard atmosphere of Ref. 1 shows that both H and $T_M$ may be represented as piecewise linear functions between the altitudes of 54 kilometers and 300 kilometers, Fig. 1-1, which is the region of interest for aerodynamically affected orbital trajectories.

In each of the seven piecewise linear sections the scale height can be written as

$$H \equiv \frac{1}{\beta} = H_i + a(r - r_i) \tag{1-11}$$

and the molecular scale temperature as

$$T_M = T_{M_i} + b(r - r_i) \tag{1-12}$$

where the subscript i indicates the value at some reference point for the section under consideration. The reference points are chosen in such a way that the density expression will give the least deviation from the 1959 ARDC Model Atmosphere, Ref. 1.

The seven sections and the constants for each are given in Tables 1-3 and 1-4. The constants a are dimensionless; the constants b have dimensions $^{\circ}K/km$. If the altitude above mean sea level is h, then the radial distances r and $r_i$ in Eqs. (1-11) and (1-12) can be replaced by h and $h_i$, where $h_i$ is the reference altitude for a given section.

From the equation of state, (1-2), and the equation defining the scale height, (1-6), it is seen that

$$\frac{1}{H} \equiv \beta = -\frac{d}{dr}(\ln p) \tag{1-13}$$

Differentiating the logarithm of p from the equation of state, using the definitions of H and $T_M$, and assuming linear behavior for H, Eq. (1-11), gives

$$d \ln (\rho T_M) = -\frac{dr}{H_i + a(r - r_i)} \tag{1-14}$$

which, when integrated, gives

$$\ln\left(\frac{\rho\, T_M}{\rho_i\, T_{M_i}}\right) = \ln\left[\frac{H_i}{H_i + a(r - r_i)}\right]^{1/a} \tag{1-15}$$

or, what is the same,

$$\frac{\rho}{\rho_i} = \left[\frac{T_{M_i}}{T_{M_i} + b(r - r_i)}\right]\left[\frac{H_i}{H_i + a(r - r_i)}\right]^{1/a} \tag{1-16}$$

where the linear behavior of $T_M$, Eq. (1-12), is assumed.

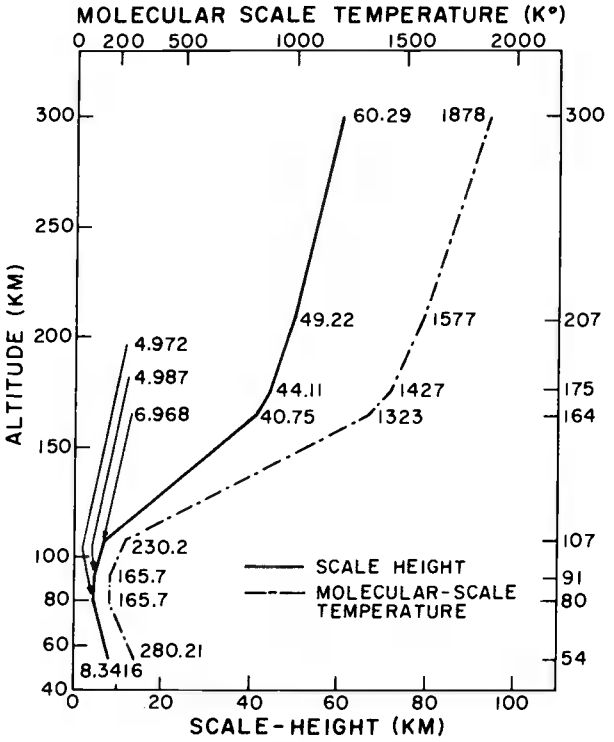


Fig. 1-1. The scale height and molecular scale temperature versus altitude. The values at the endpoints of the sections are noted.

Table 1-3. Reference values of $h_i$, $\rho_i$, $H_i$ and $T_{M_i}$ for the different sections of the Earth's atmosphere.

| Section | Altitude Range (Km) | Reference Values $h_i$ (Km) | $\rho_i$ ($Kg/m^3$) | $H_i$ (Km) | $T_{M_i}$ ($^oK$) |
|---|---|---|---|---|---|
| 1 | 54 ~ 80 | 67 | 1.4975-4 | 6.6597 | 222.8 |
| 2 | 80 ~ 91 | 85 | 7.726-6 | 4.979 | 165.7 |
| 3 | 91 ~ 107 | 99 | 4.504-7 | 5.905 | 195.6 |
| 4 | 107 ~ 164 | 110 | 5.930-8 | 8.731 | 288.2 |
| 5 | 164 ~ 175 | 170 | 7.932-10 | 42.62 | 1381. |
| 6 | 175 ~ 207 | 190 | 4.680-10 | 46.51 | 1498. |
| 7 | 207 ~ 300 | 254 | 1.149-10 | 54.78 | 1730. |

Table 1-4. Values of the constants a and b for the different sections of the Earth's atmosphere.

| Section | Altitude Range (Km) | Constants a | b, $^oK/km$ |
|---|---|---|---|
| 1 | 54 ~ 80 | -0.1296385 | -4.044231 |
| 2 | 80 ~ 91 | 0.1545455 | 0.0 |
| 3 | 91 ~ 107 | 0.1189286 | 3.878571 |
| 4 | 107 ~ 164 | 0.5925240 | 19.17964 |
| 5 | 164 ~ 175 | 0.3054545 | 9.454545 |
| 6 | 175 ~ 207 | 0.1596875 | 4.687500 |
| 7 | 207 ~ 300 | 0.1190323 | 3.236559 |

By introducing two dimensionless parameters, $\delta_H$ and $\delta_{T_M}$, with the Earth's mean radius, $r_e$,

$$\delta_H \equiv \frac{a}{H_i} r_e \qquad \delta_{T_M} \equiv \frac{b}{T_{M_i}} r_e \tag{1-17}$$

one arrives at the basic density equation which takes into account the variation of scale height and molecular scale temperature:

$$\frac{\rho}{\rho_i} = \left[\frac{1}{1+\delta_{T_M}\left(\frac{r-r_i}{r_e}\right)}\right]\left[\frac{1}{1+\delta_H\left(\frac{r-r_i}{r_e}\right)}\right]^{1/a} \tag{1-18}$$

Values for $\delta_H$ and $\delta_{T_M}$ in the seven sections are given in Table 1-5.

Table 1-5. The dimensionless parameters $\delta_H$ and $\delta_{T_M}$ for the Earth's atmosphere (Ref. 7).

| Section | $\delta_H$ | $\delta_{T_M}$ |
|---|---|---|
| 1 | 124.1549 | 126.0780 |
| 2 | 1.9797 | 0.0000 |
| 3 | 128.4549 | 126.4670 |
| 4 | 432.8391 | 424.4544 |
| 5 | 45.7107 | 43.6648 |
| 6 | 21.8982 | 19.9577 |
| 7 | 13.8588 | 11.9322 |

A major simplification can be made by noting that $\delta_H$ and $\delta_{T_M}$ are approximately equal in the seven sections. Setting $\delta_{T_M}$ equal to $\delta_H$ in Eq. (1-18) gives

$$\frac{\rho}{\rho_i} = \left[\frac{1}{1+\delta_H\left(\frac{r-r_i}{r_e}\right)}\right]^{\frac{1+a}{a}} \tag{1-19}$$

which can be rewritten using Eq. (1-11) as

$$\frac{\rho}{\rho_i} = \left[\frac{H_i}{H}\right]^{\frac{1+a}{a}} \tag{1-20}$$

This is the power function density relationship of Billik, Ref. 8, and shows that it is a special case of the more general density expression, Eq. (1-18).

Equations (1-18) and (1-19) with the constants from Table 1-5 yield the maximum percentage deviations from the 1959 ARDC Model Atmosphere given in Table 1-6.

Table 1-6. Maximum percentage deviation from standard atmosphere.

| Section | Eq. (1-18), general density expression | Eq. (1-19), special density expression |
|---|---|---|
| 1 | 0.07% | 0.40% |
| 2 | 0.02% | 0.20% |
| 3 | 0.02% | 0.25% |
| 4 | 0.57% | 1.16% |
| 5 | 0.11% | 0.25% |
| 6 | 0.04% | 0.52% |
| 7 | 0.11% | 1.52% |

## 1-4. HYPERSONIC FLOW

In supersonic flow it is obvious that the velocity of sound is too small to carry a portion of the flow pattern ahead of the moving body. But with increasing Mach number even the lateral extent of the flow pattern shrinks to smaller and smaller Mach angles, until the accumulating gas masses along the surface of the body have to create local velocities of sound high enough to keep the gas density finite and the thickness of the layer from shrinking to zero. The flow around bodies under these conditions, at which the undisturbed Mach number loses importance and the thermodynamical characteristics of the gas at high temperatures gain weight, is called hypersonic flow. Its investigation constitutes an important discipline of gasdynamics to which one author of this text has contributed significantly in its early development. The practical interest in high performance aircraft, guided missiles, and aerodynamically maneuverable spacecraft has brought a new extension to the study of hypersonic flow in engineering because of all the specific questions to make their flights feasible and safe. Here we shall summarize only the basic characteristics of hypersonic flow to help in evaluating the aerodynamic forces on a vehicle configuration in order to analyze its motion in the very high speed range.

Most authors consider as a rough definition of the hypersonic flow regime a supersonic flow in which the Mach number exceeds approximately five. Main characteristics are the following:

1/ The shock waves originating at the leading edge of the body lie close to the body surface. This results in a strong interaction with the boundary layer caused by the surface friction.

2/ The presence of extreme temperatures in the region between the shock waves and the body invalidates the ideal gas concept. At low Mach numbers a diatomic molecule, such as $N_2$ or $0_2$ in air, has five active degrees of freedom: three in translation and two in rotation. As the temperatures behind a shock wave increase with increasing Mach number, the heretofore inert degrees of freedom (vibration, dissociation, and ionization) are activated, causing serious alterations in the thermodynamic properties of the air.

Such complex phenomena create challenging problems. Early reports of their investigations can be found in many specialized texts, such as Refs. 9 and 10. Here we shall be mainly concerned with the practical importance with respect to determining the forces acting on bodies at hypersonic speeds using the most simplifying assumptions.

## 1-5. NEWTONIAN FLOW

At very high Mach numbers, approaching infinity, the shock waves get very close to the body surface, at least for the front part. They would even get closer to the surface when the thermodynamical degrees of freedom are increased toward infinity, for which the ratio of the specific heats $\gamma$ is approaching the value one. It is amazing that for such extremely modern conditions the impact forces of the gas get close to the analytical description of the wind forces on buildings 300 years ago by Sir Isaac Newton, who neglected the thermodynamic movements of the air particles and assumed the free path length to be infinite. Considering an element of the surface $\Delta S$ inclined under an angle $\alpha$ to the direction of the incident flow, (Fig. 1-2), the mass of particles which collide with the surface element in unit time is equal to

$$\Delta m = \rho \Delta S V \sin \alpha \tag{1-21}$$

where $\rho$ is the density of the medium and V the speed of the particles. The force acting on the element $\Delta S$ as a result of the collisions depends on the nature of the interaction between the particles and the body surface.

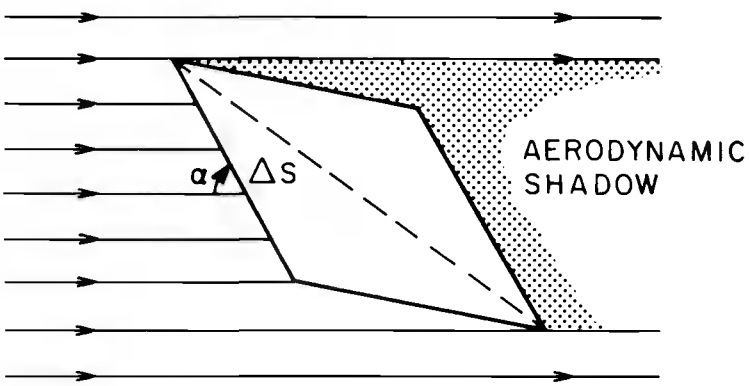


Fig. 1-2. Newtonian flow past double-wedge profile.

For gases Newton assumed an elastic reflection of the particles on a smooth wall, reversing the normal velocity component $V \sin \alpha$ while retaining the tangential component $V \cos \alpha$. However, for what he calls a "continuous medium" (water, oil, and mercury), Newton estimated the normal force to be diminished by one-half, because "the body does not immediately strike against all particles, but presses only the particles that lie next to it, which press the particles beyond, which press other particles and so on." This value is exactly the result for $M \to \infty$ and $\gamma \to 1$, when the free path is small and no thermodynamical particle movements existed before the collision with the body ($M = \infty$) nor would be created at the collision by the energy loss according to the disappearing velocity component $V \sin \alpha$ because of the infinite number of degrees of freedom sharing its heat equivalent ($\gamma = 1$). Dropping simply the normal velocity component $V \sin \alpha$ during the collision creates a normal force on the surface element $\Delta S$

$$\Delta F = \Delta m \; V \sin \alpha = \rho V^2 \, \Delta S \sin^2 \alpha \tag{1-22}$$

Hence we have the Newtonian formula for the pressure coefficient:

$$C_p = 2 \sin^2 \alpha \tag{1-23}$$

It was first observed by Lees (Ref. 11), that a substantial improvement in the agreement of the Newtonian calculations with experimental data for symmetric two-dimensional and axisymmetric flow can be obtained by modifying the formula as

$$C_p = C_p^* \frac{\sin^2 \alpha}{\sin^2 \alpha_o} \tag{1-24}$$

where $C_p^*$ is the value of the pressure coefficient at the leading edge or nose of the body, found from the theory of supersonic flow of an ideal gas, and $\alpha_o$ is the angle between the tangent to the body contour and the free-stream direction. For bodies with blunt noses, we have obviously $\sin \alpha_o = 1$, while $C_p^*$ as a function of the Mach number M and the ratio of the constant specific heats $\gamma$ can be obtained with the aid of the normal shock relations and the Bernoulli integral as

$$C_p^* = \frac{2}{\gamma M^2} \left[ \left( \frac{\gamma + 1}{2} M^2 \right)^{\gamma/(\gamma-1)} \left( \frac{\gamma + 1}{2\gamma M^2 - \gamma + 1} \right)^{1/(\gamma-1)} - 1 \right] \tag{1-25}$$

For $M \to \infty$, we have

$$C_p^* = \frac{2}{\gamma} \left( \frac{\gamma + 1}{2} \right)^{\gamma/(\gamma-1)} \left( \frac{\gamma + 1}{2\gamma} \right)^{1/(\gamma-1)} \tag{1-26}$$

If the simple Newtonian impact theory is used, where any static pressure and skin friction are neglected, the force on the element $\Delta S$ is the impact pressure force. Newton's theory implies

that only those frontal surfaces exposed to the flow can contribute to the aerodynamic force, and pressure forces on rear surfaces in the aerodynamic shadow are negligible, (Fig. 1-2). Now if we divide the forces acting normal on every exposed surface element $\Delta S$ into positive drag components in the direction of the free-stream velocity and lifting components orthogonal to it, then using the simple pressure from Eq. (1-23) at the surface element inclined at an angle $\alpha$ with respect to the incident velocity, we have

$$(C_p)_D = C_p \sin \alpha = 2 \sin^3 \alpha \tag{1-27}$$

and

$$(C_p)_L = C_p \cos \alpha = 2 \sin^2 \alpha \cos \alpha \tag{1-28}$$

For this simple body or, integrated over the surface of a complicated body, Eqs. (1-27) and (1-28) give the drag and lift coefficients, $C_D$ and $C_L$, respectively.

## 1-6. THE DRAG POLAR

On the basis of the simple formulas derived from Newton impact theory, we can determine the hypersonic aerodynamic characteristics of wedges or cone-like bodies when a high degree of accuracy is not required.

As an illustrative example, we shall consider a plane-convex airfoil whose cross-section has the form of an isoceles triangle (Fig. 1-3). Let $\theta$ be the nose angle of the airfoil and $\alpha$ the angle of attack, defined as the angle between the base of the triangle and the direction of the free-stream velocity. We restrict ourselves to the case of small angles $\theta$ and $\alpha$.

Consider the case in which both the lower surface and the forward half of the upper surface are exposed to the flow, $(0 < \alpha < \theta)$. The angle of attack of the lower surface is $\alpha$ while the local angle of attack for the upper surface is clearly $(\theta - \alpha)$

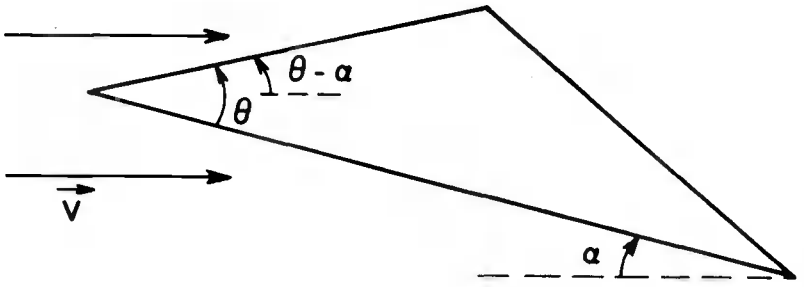


Fig. 1-3. Triangular airfoil at angle of attack.

The lower surface is a flat plate at an incidence $\alpha$ . The lift and drag coefficients are respectively

$$C_{L_1} = 2\alpha^2$$
$$C_{D_1} = 2\alpha^3 \tag{1-29}$$

The total lift and drag coefficients for the airfoil are evaluated using the area of the lower surface as a reference area. Since the front area of the upper surface is practically equal to half of the area of the lower surface for small $\theta$ , the contributions of the lift and drag coefficients from the upper surface, considered as a flat plate at an incidence $(\theta - \alpha)$, are

$$C_{L_2} = -(\theta - \alpha)^2$$
$$C_{D_2} = (\theta - \alpha)^3 \tag{1-30}$$

The total lift and drag coefficients for the complete airfoil are found by simply adding the separate contributions of the individual surface, as long as $0 \leq \alpha \leq \theta$ .

$$C_L = 2\alpha^2 - (\theta - \alpha)^2$$
$$C_D = 2\alpha^3 + (\theta - \alpha)^3 \tag{1-31}$$

In hypersonic flow, a useful small parameter $\tau$ , called the thickness ratio of the body, is defined as the maximum value of the angle between the surface of the forward portion of the body and the free-stream direction. Here, we define $\tau \equiv \theta/2$ , and write the Eqs. (1-31)

$$\frac{C_L}{\tau^2} = 2\left(\frac{\alpha}{\tau}\right)^2 - \left(2 - \frac{\alpha}{\tau}\right)^2$$
$$\frac{C_D}{\tau^3} = 2\left(\frac{\alpha}{\tau}\right)^3 + \left(2 - \frac{\alpha}{\tau}\right)^3 \tag{1-32}$$

The second terms in these expressions are valid only for $\alpha/\tau < 2$ . For large angles of attack, the pressure on the upper surfaces of the airfoil is zero and the airfoil behaves like a flat plate. Both expressions for $C_L/\tau^2$ and $C_D/\tau^3$ are functions only of the ratio $\alpha/\tau$ . The plot of $C_L/\tau^2$ versus $C_D/\tau^3$ is called the drag polar (Fig. 1-4).

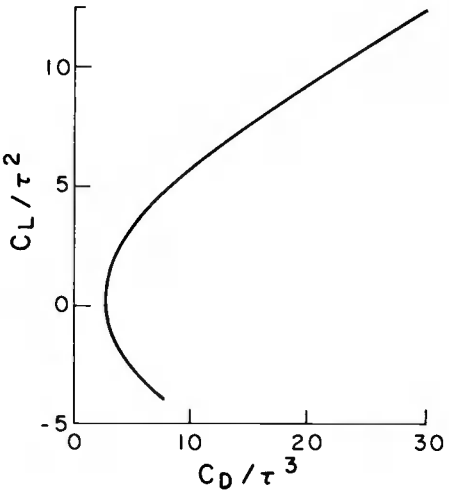


Fig. 1-4. Drag polar for triangular airfoil in hypersonic flow.

## 1-7. THE BUSEMANN FORMULA

For the case of a flow over a wedge or axisymmetric cone, the gas particles move along straight lines in an infinitely thin layer adjacent to the surface in which the density of the gas is infinitely large. The pressure on the surface of the wedge and cone coincides with the pressure behind the shock wave and is determined by the Newtonian formula

$$p = \rho_1 V^2 \sin^2 \alpha \tag{1-33}$$

with subscript 1 denoting the free-stream condition. On a curved body, a particle is constrained within the continuum flow in the shock layer to follow a curved path and the forces required to curve the trajectories of the particles must be taken into consideration. The result is a pressure difference across the shock layer equal to the momentum flow in the layer times the curvature of the layer. The inclusion of this centrifugal force was first proposed by Busemann who gave formulas for the correction (Ref. 12, pp. 276-277).

Based on the assumptions of inelastic collisions, $\gamma = 1$, and the absence of frictional forces, we may assume that the speed of each particle remains unchanged after its collision with the surface and that the particles move along the geodesic lines of the surface. Under this assumption, we refer to Fig. 1-5 for the evaluation of the pressure difference in the layer for two-dimensional and axisymmetric flows.

Let us follow the motion of the particles along the surface of the body after collision. These particles move within an infinitely thin layer depicted in the figure by the body contour and the dashed

line. At the point x , measured along the body contour, the pressure difference dp in the infinitesimal layer composed of particles which have collided with the surface near the point x' and which have the velocity u(x') , is equal to

$$dp = \frac{\rho(x,x')\, u^2(x')}{R(x)}\, dn \tag{1-34}$$

where R(x) is the radius of curvature of the body at the point x , and dn the thickness of the infinitesimal layer of the deviated gas particles, evaluated along the outward normal to the surface.

Let F be the cross-sectional area of the body in a plane normal to the direction of the free-stream flow. By consideration of the conservation of mass in the layer, we have

$$\rho_1 V dF(x') = \rho(x,x')\, u(x')\, \ell(x)\, dn \tag{1-35}$$

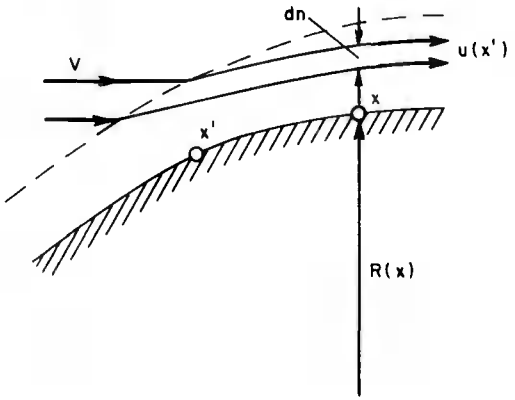


Fig. 1-5. Curved trajectories of gas particles after collisions.

For two-dimensional flow, $\ell(x) = 1$ , and for axisymmetric flow $\ell(x) = 2\pi r(x)$ where r is the radial coordinate for the body of revolution.

The radius of curvature R(x) of the body at the point x is

$$R = -\frac{dx}{d\alpha} = -\frac{1}{\sin\alpha}\,\frac{dr}{d\alpha} \tag{1-36}$$

Using Eqs. (1-35) and (1-36) in Eq. (1-34), we obtain

$$dp = -\rho_1 V \sin\alpha \frac{d\alpha}{dF}\, u(x')\, dF(x') \tag{1-37}$$

Since the velocity component of a particle tangential to the body surface is unaltered by the collision, $u(x') = V \cos[\alpha(x')]$ . Hence,

$$dp = -\rho_1 V^2 \sin\alpha \frac{d\alpha}{dF} \cos\alpha(x')\, dF(x') \tag{1-38}$$

Integrating the equation for dp and taking into account the fact that at the outer boundary of the layer, $p = \rho_1 V^2 \sin^2 \alpha$, we find the pressure on the body surface to be

$$p = \rho_1 V^2 \left(\sin^2 \alpha + \sin \alpha \frac{d\alpha}{dF} \int_{F_o}^{F} \cos \alpha \, dF\right) \qquad (1\text{-}39)$$

This formula was first given by Busemann in Ref. 12. In recent years, it has been used by several authors in their investigations of minimum drag bodies at hypersonic speeds (Ref. 13).

Convex surfaces have a negative value $d\alpha / dF$, and avoid separation only when the pressure is nowhere negative. This implies a finite positive $\alpha$ at the end of the nose.

## References


1. Minzner, R. A., Champion, K. S. W., and Pond, H. L., The ARDC Model Atmosphere, 1959, AFCRC-TR-59-267, 1959.

2. Goody, R. M., and Walker, J. C. G., Atmospheres, Prentice-Hall, Englewood Cliffs, N. Y., 1972.

3. Hunten, D. M., "Lower Atmospheres of the Planets," Chap. 6, Physics of the Solar System, ed. by S. I. Rasool, NASA SP-300, 1972.

4. King-Hele, Desmond, Theory of Satellite Orbits in An Atmosphere, Butterworths, London, 1964.

5. Chapman, D. R., "An Approximate Analytical Method for Studying Entry Into Planetary Atmospheres," NASA TR R-11, 1959.

6. Vinh, N. X., Busemann, A., and Culp, R. D., "Optimum Three-Dimensional Atmospheric Entry," Acta Astronautica, Vol. 2, pp. 593-611, 1975.

7. Busemann, A., Culp, R. D., and Yang, C. Y., "A Study of Very High Altitude Maneuvers Using Aerodynamic Forces," Vol. III, "On the Use of Aerodynamic Forces to Effect Maneuvers of Orbiting Vehicles," ARL TR 74-0104, Vol. III, 1974.

8. Billik, B. H., "Survey of Current Literature on Satellite Lifetime," ARS Journal, November, pp. 1641-1650, 1962.

9. Hayes, W. D., and Probstein, R. F., Hypersonic Flow Theory, Academic Press, New York, 1959.

10. Chernyi, G. G., Introduction to Hypersonic Flow, translated and edited by R. F. Probstein, Academic Press, New York, 1961.

11. Lees, L., Hypersonic Flow, Proc. 5th International Aerodynamics Conference, Los Angeles. Institute of Aerospace Sciences, New York, 1955.

12. Busemann, A., Flüssigkeits-und-Gasbewegung, Handwörterbuch der Naturwissenschaften, Vol. IV, 2nd Edition, pp. 244-279, Gustav Fischer, Jena, 1933.

13. Miele, A., Editor, Theory of Optimum Aerodynamic Shapes, Academic Press, New York, 1965.

# Chapter 2

# Equations for Flight Over a Spherical Planet

## 2-1. INTRODUCTION

In this chapter we shall derive the equations of motion of a vehicle considered as a point mass of mass m flying inside a planetary atmosphere. The motion of the vehicle is defined by

$$\begin{aligned} \vec{r}(t) &= \text{position vector} \\ \vec{V}(t) &= \text{velocity vector} \\ m(t) &= \text{mass} \end{aligned} \tag{2-1}$$

At each instant, it is subject to a total force $\vec{F}$ composed of the gravitational force $m\vec{g}$, the aerodynamic force $\vec{A}$ and a thrusting force $\vec{T}$ provided by the propulsion system.

$$\vec{F} = \vec{T} + \vec{A} + m\vec{g} \tag{2-2}$$

With respect to an inertial system, we have the vector equation

$$m \frac{d\vec{V}}{dt} = \vec{F} \tag{2-3}$$

## 2-2. RELATIVE ANGULAR MOTION

Consider a fixed system $0_1 X_1 Y_1 Z_1$, and another system 0xyz which is rotating with respect to the fixed system.

Let $\vec{i}$, $\vec{j}$, and $\vec{k}$ be the unit vectors along the axes of the rotating system. Let $\vec{A}$ be any arbitrary vector with components $A_x$, $A_y$ and $A_z$ along the rotating axes. Then

$$\vec{A} = A_x \vec{i} + A_y \vec{j} + A_z \vec{k} \tag{2-4}$$

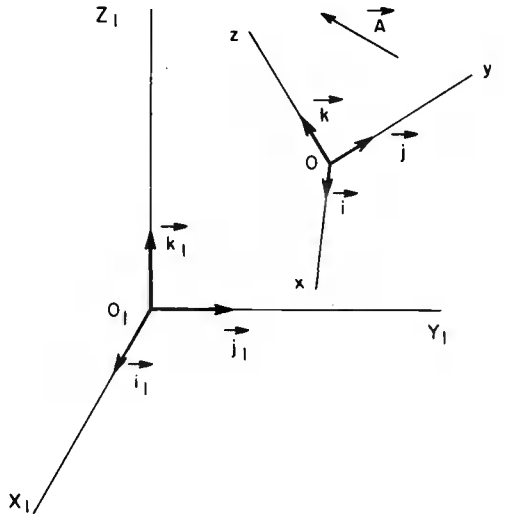


Fig. 2-1. Relative angular motion.

Since 0xyz is rotating, its associated unit vectors $\vec{i}$, $\vec{j}$, and $\vec{k}$ are functions of time. Hence, the time derivative of A, taken with respect to the fixed system, is

$$\frac{d\vec{A}}{dt} = \left( \frac{dA_x}{dt}\vec{i} + \frac{dA_y}{dt}\vec{j} + \frac{dA_z}{dt}\vec{k} \right) + \left( A_x \frac{d\vec{i}}{dt} + A_y \frac{d\vec{j}}{dt} + A_z \frac{d\vec{k}}{dt} \right) \tag{2-5}$$

Now, a point P with position vector $\vec{r}$, fixed in a system rotating with angular velocity $\vec{\omega}$, will have as linear velocity (Fig. 2-2)

$$\vec{V} = \frac{d\vec{r}}{dt} = \vec{\omega} \times \vec{r} \tag{2-6}$$

If $\vec{r}$ is taken as the vector $\vec{i}$, $\vec{j}$, and $\vec{k}$ respectively, we have the Poisson formulas

$$\frac{d\vec{i}}{dt} = \vec{\omega} \times \vec{i}\,, \quad \frac{d\vec{j}}{dt} = \vec{\omega} \times \vec{j}\,, \quad \frac{d\vec{k}}{dt} = \vec{\omega} \times \vec{k} \tag{2-7}$$

Using these relations, together with the definition (2-4), it is seen that the second term on the right-hand side of Eq. (2-5) is

$$A_x \frac{d\vec{i}}{dt} + A_y \frac{d\vec{j}}{dt} + A_z \frac{d\vec{k}}{dt} = \vec{\omega} \times \vec{A} \tag{2-8}$$

The first term can be interpreted as the time derivative of the vector $\vec{A}$ if the vectors $\vec{i}$, $\vec{j}$, and $\vec{k}$ are constant unit vectors. Hence, it is

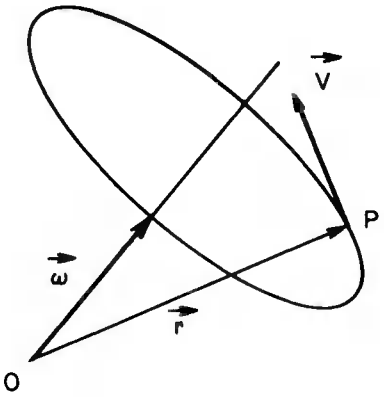


Fig. 2-2. Kinematics of rotation .

the time derivative of $\vec{A}$ with respect to the rotating system 0xyz . We denote it by

$$\frac{\delta \vec{A}}{\delta t} = \frac{dA_x}{dt}\vec{i} + \frac{dA_y}{dt}\vec{j} + \frac{dA_z}{dt}\vec{k} \qquad (2\text{-}9)$$

and write Eq. (2-5) as

$$\frac{d\vec{A}}{dt} = \frac{\delta \vec{A}}{\delta t} + \vec{\omega} \times \vec{A} \qquad (2\text{-}10)$$

This is the formula for transforming the time derivative of a vector from one system to another rotating system.

## 2-3. BASIC EQUATIONS OF MOTION

The inertial reference frame $0X_1Y_1Z_1$ is taken such that 0 is at the center of the gravitational field of a spherical planet and the $0X_1Y_1$ plane is the equatorial plane. The 0XYZ reference frame is fixed with respect to the planet, hence it is rotating with an angular velocity $\vec{\omega}$ assumed constant and directed along the Z-axis (Fig. 2-3).

The vector equation (2-3) is written with respect to the inertial frame. In deriving the equations of motion we shall use the planet-fixed axes as the reference frame. Hence, putting $\vec{A} = \vec{r}$ in Eq. (2-10) and then taking its time derivative, we have the expression for the absolute acceleration $d\vec{V}/dt$ .

$$\frac{d\vec{r}}{dt} = \frac{\delta \vec{r}}{\delta t} + \vec{\omega} \times \vec{r}$$

$$\frac{d\vec{V}}{dt} = \frac{\delta}{\delta t}\left[\frac{\delta \vec{r}}{\delta t} + \vec{\omega} \times \vec{r}\right] + \vec{\omega} \times \left[\frac{\delta \vec{r}}{\delta t} + \vec{\omega} \times \vec{r}\right]$$

or since $\delta\vec{\omega}/\delta t = 0$ ,

$$\frac{d\vec{V}}{dt} = \frac{\delta^2\vec{r}}{\delta t^2} + 2\vec{\omega} \times \frac{\delta\vec{r}}{\delta t} + \vec{\omega} \times (\vec{\omega} \times \vec{r}) \qquad (2\text{-}11)$$

The vector equation (2-3) now becomes, with the planet-fixed system used as the reference frame,

$$m\frac{\delta^2\vec{r}}{\delta t^2} = \vec{F} - 2m\vec{\omega} \times \frac{\delta\vec{r}}{\delta t} - m\vec{\omega} \times (\vec{\omega} \times \vec{r}) \qquad (2\text{-}12)$$

For convenience, we change the notation for the time derivative and write it as

$$m\frac{d\vec{V}}{dt} = \vec{F} - 2m\vec{\omega} \times \vec{V} - m\vec{\omega} \times (\vec{\omega} \times \vec{r}) \qquad (2\text{-}13)$$

with $\vec{V}$ being the velocity with respect to the planet, and the time derivative taken with respect to planet-fixed axes.

In this planetocentric system, the position vector $\vec{r}$ is defined by its magnitude r, its longitude $\theta$ (measured from the X-axis, in the equatorial plane, positively eastward), and its latitude $\phi$ (measured from the equatorial plane, along a meridian, and positively northward).

It is convenient to evaluate different vectors in Eq. (2-13) by their components in a rotating coordinate system 0xyz such that the x-axis is along the position vector, the y-axis in the equatorial plane positive toward the direction of motion and orthogonal to the x-axis, and the z-axis completing a right-handed system (Fig. 2-3).

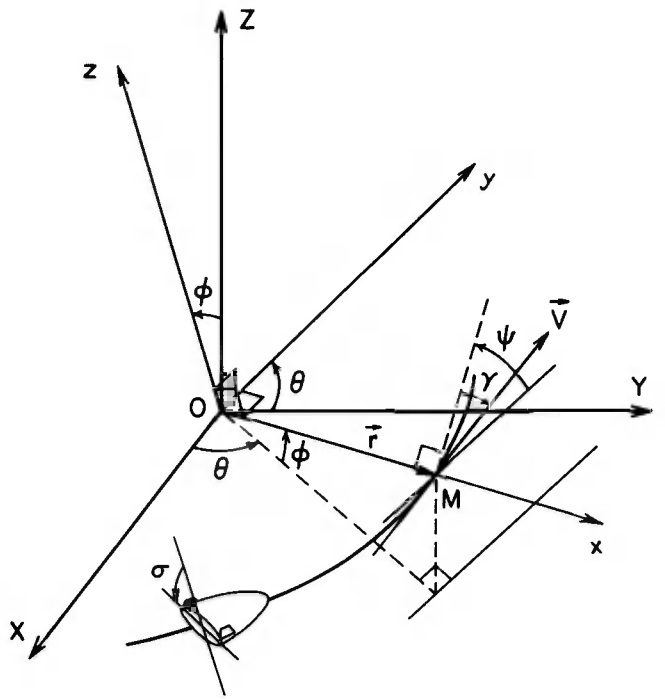


Fig. 2-3. Coordinate systems.

Let $\gamma$ be the angle between the local horizontal plane (that is, the plane passing through the vehicle and orthogonal to the vector $\vec{r}$), and the velocity $\vec{V}$. The angle $\gamma$ is termed the flight path angle and is positive when $\vec{V}$ is above the horizontal plane. Let $\psi$ be the angle between the local parallel of latitude and the projection of $\vec{V}$ on the horizontal plane. The angle $\psi$ is termed the heading and is measured positively in the right-handed direction about the x-axis. Let $\vec{i}, \vec{j}$, and $\vec{k}$ be the unit vectors along the axes of the rotating system $0xyz$. We have

$$\vec{r} = r\vec{i} \tag{2-14}$$

and

$$\vec{V} = (V\sin\gamma)\vec{i} + (V\cos\gamma\cos\psi)\vec{j} + (V\cos\gamma\sin\psi)\vec{k} \tag{2-15}$$

On the other hand, the angular velocity $\vec{\omega}$ can be represented by

$$\vec{\omega} = (\omega\sin\phi)\vec{i} + (\omega\cos\phi)\vec{k} \tag{2-16}$$

Hence

$$\vec{\omega}\times\vec{V} = -(\omega V\cos\gamma\cos\phi\cos\psi)\vec{i} + \omega V(\sin\gamma\cos\phi - \cos\gamma\sin\phi\sin\psi)\vec{j} + \omega V\cos\gamma\sin\phi\cos\psi\vec{k} \tag{2-17}$$

and

$$\vec{\omega}\times(\vec{\omega}\times\vec{r}) = -\omega^2 r\cos^2\phi\,\vec{i} + \omega^2 r\sin\phi\cos\phi\,\vec{k} \tag{2-18}$$

In the force $\vec{F}$, the gravity force is simply

$$m\vec{g} = -mg(r)\vec{i} \tag{2-19}$$

The aerodynamic force $\vec{A}$ can be decomposed into a drag force $\vec{D}$ opposite to the velocity vector $\vec{V}$ and a lift force $\vec{L}$ orthogonal to it. In symmetric flight the thrust vector $\vec{T}$ is always in the lift-drag plane. Let $\epsilon$ be the angle between the velocity vector $\vec{V}$ and the thrust $\vec{T}$. Then, we can decompose the thrust into a component $T\cos\epsilon$ along the velocity and a component $T\sin\epsilon$ along the lift force. It is convenient for the derivation of the equations to group the components of aerodynamic and propulsive force and define

$$\begin{aligned} F_T &= T\cos\epsilon - D \\ F_N &= T\sin\epsilon + L \end{aligned} \tag{2-20}$$

where $F_T$ is the component of the aerodynamic and propulsive forces along the velocity vector and $F_N$ is their component orthogonal to it in the lift-drag plane. In vector form, since $\vec{F}_T$ is along $\vec{V}$, we can refer to Eq. (2-15) to write

$$\vec{F}_T = (F_T\sin\gamma)\vec{i} + (F_T\cos\gamma\cos\psi)\vec{j} + (F_T\cos\gamma\sin\psi)\vec{k} \tag{2-21}$$

In planar flight, the vector $\vec{F}_N$ is in the $(\vec{r}, \vec{V})$ plane, that is the vertical plane, and there is no lateral force. By control action, if we rotate the vector $\vec{L}$, and hence also the vector $\vec{F}_N$, about the velocity vector $\vec{V}$, we create a lateral component of the force $\vec{F}_N$ that has the effect of changing the orbital plane. To resolve the force $\vec{F}_N$ or its collinear force $\vec{L}$ into components along the rotating axes, we refer to Fig. 2-4. The vertical plane considered is the $(\vec{r}, \vec{V})$ plane. Assume the vector $\vec{L}$ is rotated out of this plane through an angle $\sigma$. The angle $\sigma$ which is the angle between the vector $\vec{L}$ and the $(\vec{r}, \vec{V})$ plane will be referred to as the roll, or the bank, angle. The force $\vec{F}_N$ is decomposed into a component $\overrightarrow{F_N \cos\sigma}$ in the vertical plane and orthogonal to $\vec{V}$ and a component $\overrightarrow{F_N \sin\sigma}$ orthogonal to the vertical plane. Let x', y', and z' be the axes from the position M of the vehicle, parallel to the rotating axes x, y, and z. Let $x_1$, $y_1$ and $z_1$ be the axes from the point M, along the direction of $\overrightarrow{F_N \cos\sigma}$, $\vec{V}$ and $\overrightarrow{F_N \sin\sigma}$ respectively. The system $Mx_1y_1z_1$ is deduced from the system Mx'y'z' by a rotation $\psi$ in the horizontal plane, followed by a rotation $\gamma$ in the vertical plane. Hence, we have the transformation matrix equation

$$\begin{bmatrix} x' \\ y' \\ z' \end{bmatrix} = \begin{bmatrix} 1 & 0 & 0 \\ 0 & \cos\psi & -\sin\psi \\ 0 & \sin\psi & \cos\psi \end{bmatrix} \begin{bmatrix} \cos\gamma & \sin\gamma & 0 \\ -\sin\gamma & \cos\gamma & 0 \\ 0 & 0 & 1 \end{bmatrix} \begin{bmatrix} x_1 \\ y_1 \\ z_1 \end{bmatrix} \tag{2-22}$$

or

$$\begin{bmatrix} x' \\ y' \\ z' \end{bmatrix} = \begin{bmatrix} \cos\gamma & \sin\gamma & 0 \\ -\sin\gamma\cos\psi & \cos\gamma\cos\psi & -\sin\psi \\ -\sin\gamma\sin\psi & \cos\gamma\sin\psi & \cos\psi \end{bmatrix} \begin{bmatrix} x_1 \\ y_1 \\ z_1 \end{bmatrix} \tag{2-23}$$

Since the components of $\vec{F}_N$ in the $Mx_1y_1z_1$ system are $x_1 = F_N \cos\sigma$, $y_1 = 0$, $z_1 = F_N \sin\sigma$, we deduce the components of $\vec{F}_N$ along the system Mx'y'z', or what is the same, along the rotating system 0xyz

$$\vec{F}_N = (F_N \cos\sigma \cos\gamma)\,\vec{i} - (F_N \cos\sigma \sin\gamma\cos\psi + F_N \sin\sigma \sin\psi)\,\vec{j} - (F_N \cos\sigma \sin\gamma\sin\psi - F_N \sin\sigma \cos\psi)\,\vec{k} \tag{2-24}$$

In summary, we have resolved all the vector terms in Eq. (2-13) into components along the rotating axes 0xyz.

In order to take the time derivative of the vectors $\vec{r}$ and $\vec{V}$ with respect to the planet-fixed system 0XYZ, we need to evaluate the angular velocity vector $\vec{\Omega}$ of the rotating axes. The system 0xyz is obtained from the system 0XYZ by a rotation $\theta$ about the positive Z-axis, followed by a rotation $\phi$ about the negative y-axis. Hence the angular velocity $\vec{\Omega}$ of the rotating system 0xyz is

$$\vec{\Omega} = (\sin\phi \frac{d\theta}{dt})\,\vec{i} - (\frac{d\phi}{dt})\,\vec{j} + (\cos\phi \frac{d\theta}{dt})\,\vec{k} \tag{2-25}$$

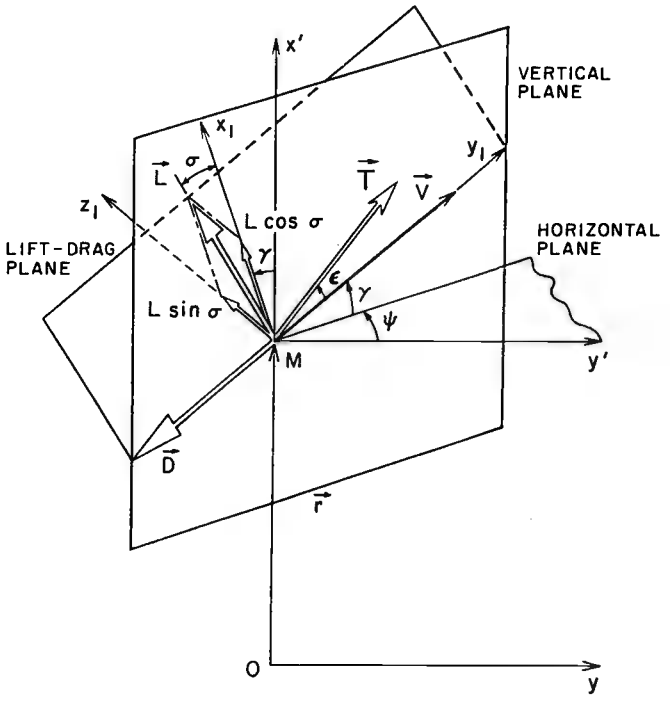


Fig. 2-4. Aerodynamic forces and thrust components.

We use Eqs. (2-7) with $\vec{\Omega}$ instead of $\vec{\omega}$ to deduce the time derivative of $\vec{i}$, $\vec{j}$, and $\vec{k}$.

$$\frac{d\vec{i}}{dt} = \vec{\Omega} \times \vec{i} = (\cos\phi \frac{d\theta}{dt}) \vec{j} + (\frac{d\phi}{dt}) \vec{k}$$

$$\frac{d\vec{j}}{dt} = \vec{\Omega} \times \vec{j} = -(\cos\phi \frac{d\theta}{dt}) \vec{i} + (\sin\phi \frac{d\theta}{dt}) \vec{k} \qquad (2\text{-}26)$$

$$\frac{d\vec{k}}{dt} = \vec{\Omega} \times \vec{k} = -(\frac{d\phi}{dt}) \vec{i} - (\sin\phi \frac{d\theta}{dt}) \vec{j}$$

If we take the time derivative of $\vec{r}$, as given by Eq. (2-14), using the first of the Eqs. (2-26) for the derivative of $\vec{i}$, we have

$$\frac{d\vec{r}}{dt} = (\frac{dr}{dt}) \vec{i} + (r\cos\phi \frac{d\theta}{dt}) \vec{j} + (r\frac{d\phi}{dt}) \vec{k} \qquad (2\text{-}27)$$

Identifying this equation with Eq. (2-15) yields three scalar equations

$$\frac{dr}{dt} = V \sin\gamma$$

$$\frac{d\theta}{dt} = \frac{V \cos\gamma \cos\psi}{r \cos\phi} \qquad (2\text{-}28)$$

$$\frac{d\phi}{dt} = \frac{V \cos\gamma \sin\psi}{r}$$

These equations are the kinematic equations.

On the other hand, if we take the derivative of the velocity vector $\vec{V}$, as given by Eq. (2-15), using Eqs. (2-26) for the derivatives of the unit vectors $\vec{i}$, $\vec{j}$, and $\vec{k}$, and subsequently Eqs. (2-28) for $d\theta/dt$ and $d\phi/dt$, we have

$$\frac{d\vec{V}}{dt} = \left[\sin\gamma \frac{dV}{dt} + V\cos\gamma \frac{d\gamma}{dt} - \frac{V^2}{r}\cos^2\gamma\right]\vec{i}$$

$$+ \left[\cos\gamma\cos\psi \frac{dV}{dt} - V\sin\gamma\cos\psi \frac{d\gamma}{dt} - V\cos\gamma\sin\psi \frac{d\psi}{dt} + \frac{V^2}{r}\cos\gamma\cos\psi(\sin\gamma - \cos\gamma\sin\psi\tan\phi)\right]\vec{j}$$

$$+ \left[\cos\gamma\sin\psi \frac{dV}{dt} - V\sin\gamma\sin\psi \frac{d\gamma}{dt} + V\cos\gamma\cos\psi \frac{d\psi}{dt} + \frac{V^2}{r}\cos\gamma(\sin\gamma\sin\psi + \cos\gamma\cos^2\psi\tan\phi)\right]\vec{k} \qquad (2\text{-}29)$$

By substituting into the basic vector equation (2-13), using Eqs. (2-17), (2-18), (2-19), (2-21) and (2-24), we obtain three scalar equations

$$\sin\gamma \frac{dV}{dt} + V\cos\gamma \frac{d\gamma}{dt} - \frac{V^2}{r}\cos^2\gamma = \frac{1}{m}F_T\sin\gamma + \frac{1}{m}F_N\cos\sigma\cos\gamma - g + 2\omega V\cos\gamma\cos\phi\cos\psi + \omega^2 r\cos^2\phi$$

$$\cos\gamma \frac{dV}{dt} - V\sin\gamma \frac{d\gamma}{dt} - V\cos\gamma\tan\psi \frac{d\psi}{dt} + \frac{V^2}{r}\cos\gamma(\sin\gamma - \cos\gamma\sin\psi\tan\phi) = \frac{1}{m}F_T\cos\gamma - \frac{1}{m}(F_N\cos\sigma\sin\gamma + F_N\sin\sigma\tan\psi) - \frac{2\omega V}{\cos\psi}(\sin\gamma\cos\phi - \cos\gamma\sin\phi\sin\psi)$$

$$\cos\gamma \frac{dV}{dt} - V\sin\gamma \frac{d\gamma}{dt} + \frac{V\cos\gamma}{\tan\psi} \frac{d\psi}{dt} + \frac{V^2}{r}\cos\gamma\left(\sin\gamma + \frac{\cos\gamma\cos\psi\tan\phi}{\tan\psi}\right) = \frac{1}{m}F_T\cos\gamma - \frac{1}{m}\left(F_N\cos\sigma\sin\gamma - \frac{F_N\sin\sigma}{\tan\psi}\right) - 2\omega V\frac{\cos\gamma\sin\phi}{\tan\psi} - \omega^2 r\frac{\sin\phi\cos\phi}{\sin\psi} \qquad (2\text{-}30)$$

Solving for the derivatives $dV/dt$, $d\gamma/dt$, and $d\psi/dt$, we get the three scalar equations:

$$\frac{dV}{dt} = \frac{1}{m} F_T - g \sin\gamma + \omega^2 r \cos\phi \,(\sin\gamma \cos\phi - \cos\gamma \sin\phi \sin\psi)$$

$$V\frac{d\gamma}{dt} = \frac{1}{m} F_N \cos\sigma - g\cos\gamma + \frac{V^2}{r}\cos\gamma + 2\omega V \cos\phi \cos\psi + \omega^2 r \cos\phi \,(\cos\gamma \cos\phi + \sin\gamma \sin\phi \sin\psi)$$

$$V\frac{d\psi}{dt} = \frac{1}{m}\frac{F_N \sin\sigma}{\cos\gamma} - \frac{V^2}{r}\cos\gamma\cos\psi\tan\phi + 2\omega V(\tan\gamma\cos\phi\sin\psi - \sin\phi) - \frac{\omega^2 r}{\cos\gamma}\sin\phi\cos\phi\cos\psi \qquad (2\text{-}31)$$

These three equations are the force equations. The presence of the $\omega$ term is due to the rotation of the planet. If we assume that the atmosphere is at rest with respect to the planet, then it has the same rotation as the planet. In general, $\omega$ is small and the term $\omega^2 r$ can be neglected. On the other hand, the term $2\omega V$, called the Coriolis acceleration, has an important effect in a high-speed, long-range flight. For an accurate analysis, especially in the problem of computing the trajectory of a ballistic missile, the term should be retained. In this book, we shall mainly be concerned with the variations of the speed and altitude of the vehicle in the main portion of the trajectory where high deceleration develops. For this purpose, we can also ignore the effect of the Coriolis, that is, we shall assume that the planet, and hence the atmosphere, is nonrotating, $\omega = 0$.

Then, the equations become

$$\frac{dV}{dt} = \frac{1}{m} F_T - g \sin\gamma$$

$$V\frac{d\gamma}{dt} = \frac{1}{m} F_N \cos\sigma - g\cos\gamma + \frac{V^2}{r}\cos\gamma \qquad (2\text{-}32)$$

$$V\frac{d\psi}{dt} = \frac{1}{m}\frac{F_N \sin\sigma}{\cos\gamma} - \frac{V^2}{r}\cos\gamma\cos\psi\tan\phi$$

where the force components $F_T$ and $F_N$ are defined in Eqs. (2-20) for the case of powered flight. In this case, the mass of the vehicle is varying and we add the equation for the mass flow rate

$$\frac{dm}{dt} = -\frac{T}{c} \qquad (2\text{-}33)$$

where T is the thrust and c a parameter characterizing the propellant used in the propulsion system on board the vehicle. In the case of nonthrusting flight, which is usually the case for high speed entry into planetary atmosphere, we have $T = 0$, $F_T = -D$ and $F_N = L$. Hence, the three force equations for entry trajectories are

$$\frac{dV}{dt} = -\frac{D}{m} - g \sin\gamma$$

$$V\frac{d\gamma}{dt} = \frac{L\cos\sigma}{m} - g\cos\gamma + \frac{V^2}{r}\cos\gamma \qquad (2\text{-}34)$$

$$V\frac{d\psi}{dt} = \frac{L\sin\sigma}{m\cos\gamma} - \frac{V^2}{r}\cos\gamma\cos\psi\tan\phi$$

## References

1. Lass, H., Vector and Tensor Analysis, McGraw-Hill Book Co., Inc., New York, 1950.

2. Busemann, A., Vinh, N. X., and Culp, R. D., "Solution of the Exact Equations for Three-Dimensional Atmospheric Entry Using Directly Matched Asymptotic Expansions," NASA CR-2643, 1976.

3. Greenwood, D. T., Principles of Dynamics, Prentice-Hall, Inc., Englewood Cliffs, New Jersey, 1965.

# Chapter 3

# Performance in Extra-Atmospheric Flight

## 3-1. INTRODUCTION

Beginning here, we shall analyze the performance of long-range hypervelocity vehicles. The flight is assumed to take place in the plane containing the great circle arc, between the take-off point and the landing point. The flight is thought of in two phases as illustrated in Fig. 3-1.

a/ The powered phase, in which sufficient kinetic energy provided by the propulsion system is imparted to the vehicle to bring it, under a proper guidance, to a prescribed position and velocity in space. The trajectory followed is the arc AB in Fig. 3-1. The point B is referred to as the burnout position.

b/ The unpowered phase, in which the vehicle travels to its destination under the influence of the gravity and aerodynamic forces. The trajectory followed is the arc BC.

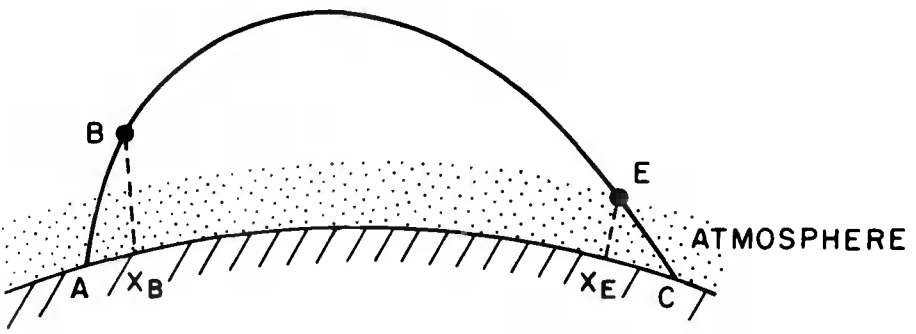


Fig. 3-1. Trajectory of long range hypervelocity vehicle.

The powered phase is generally short, and the corresponding longitudinal range during launch, $x_B$ , is small compared to the radius of the Earth. Hence, the trajectory can be analyzed using the flat Earth assumption. This is done in Chapter 4. For a short range flight, the unpowered phase is performed entirely in the dense layer of the atmosphere. For long range flight, if the total energy imparted to the vehicle at the burnout position B is sufficiently high, with a proper orientation of the burnout velocity, the trajectory followed will have a portion entirely outside the dense layer of the atmosphere. This portion of the trajectory is represented by the arc BE in Fig. 3-1. The corresponding contribution to the range, $(x_E - x_B)$ , may be large. This is one of the most interesting features in hypersonic flight. For long-range operation, hypervelocity vehicles may reduce the cost in fuel consumption since the range $(x_E - x_B)$ can be made infinite with finite energy input. In this respect, Sänger and Bredt were among the first to recognize the favorable connection between speed and range (Ref. 1). The idea leads to the concept of present-day shuttle vehicles where, after the powered phase, the subsequent trajectory is entirely flown outside the atmosphere for several days and the required mission is accomplished without additional energy input. When it comes time to return to the Earth a rocket may be fired to deflect the trajectory such that it intersects the atmosphere of the Earth at a certain point E called the entry position. The subsequent trajectory is called the reentry trajectory. This portion of the trajectory is illustrated by the arc EC in Fig. 3-1.

In this chapter, we shall be concerned with the extra-atmospheric portion of the flight trajectory, namely the arc BE . We shall assume that space is completely free of atmosphere. Hence, from classical orbital mechanics, the trajectory is a Keplerian conic. The reentry phase will be analyzed in subsequent chapters.

## 3-2. THE TRAJECTORY EQUATION

In the plane of motion, the position of the vehicle, considered as a point mass represented by the point M , is defined in polar coordinates by its radial distance r from the center of the Earth O , and the angle $\theta$ between the vectors $\overrightarrow{OB}$ and $\overrightarrow{OM}$ (Fig. 3-2). With the aerodynamic force neglected, the vehicle is subject only to the gravitational attraction which, for a spherical earth, is directed toward the center O with a force per unit mass

$$\frac{F_r}{m} = -\frac{\mu}{r^2} \tag{3-1}$$

where m is the mass of the vehicle, and $\mu$ a positive constant

$$\mu = Gm_e \tag{3-2}$$

$m_e$ is the mass of the Earth and G a universal constant. This yields a value of $\mu$ for Earth:

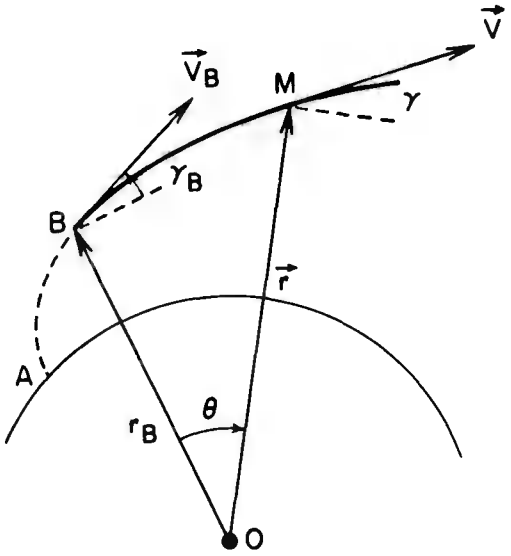


Fig. 3-2. Geometry of the trajectory.

$$\mu = 398603.2 \frac{km^3}{sec^2}$$

Since the force is central, its component $F_\theta$ along the direction perpendicular to the position vector $\vec{r}$ is zero. Hence, we can write the equations of the motion in polar coordinates

$$\ddot{r} - r\dot{\theta}^2 = -\frac{\mu}{r^2} \tag{3-3}$$

$$r\ddot{\theta} + 2\dot{r}\dot{\theta} = 0 \tag{3-4}$$

The dot represents derivatives taken with respect to time. By integrating Eq. (3-4) directly, we obtain

$$r^2\dot{\theta} = h \tag{3-5}$$

where $h$ is a constant. Since $r\dot{\theta}$ is the velocity component orthogonal to the position vector, Eq. (3-5) shows that the constant $h$ is the angular momentum per unit mass.

The equation for $r$, Eq. (3-3), can be integrated by the change of variable

$$r = \frac{1}{s} \tag{3-6}$$

Using $\theta$ as the new independent variable to replace the time gives

$$\dot{r} = \frac{dr}{d\theta}\frac{d\theta}{dt} = \dot{\theta}\frac{d}{d\theta}\left(\frac{1}{s}\right) = -\frac{\dot{\theta}}{s^2}\frac{ds}{d\theta} \tag{3-7}$$

Since, from Eqs. (3-5) and (3-6)

$$\dot{\theta} = hs^2 \tag{3-8}$$

we can write Eq. (3-7) as

$$\dot{r} = -h\frac{ds}{d\theta} \tag{3-9}$$

Therefore,

$$\ddot{r} = -h\frac{d^2s}{d\theta^2}\frac{d\theta}{dt} = -h^2s^2\frac{d^2s}{d\theta^2} \tag{3-10}$$

Making these substitutions into Eq. (3-3) we obtain the linear equation in s

$$\frac{d^2s}{d\theta^2} + s = \frac{\mu}{h^2} \tag{3-11}$$

The general solution of this equation is

$$s = \frac{\mu}{h^2} + C\cos(\theta - \theta_o) \tag{3-12}$$

where C and $\theta_o$ are two constants of integration. Returning to the variable r, we write

$$r = \frac{p}{1 + e\cos(\theta - \theta_o)} \tag{3-13}$$

where by definition

$$p \equiv h^2/\mu \tag{3-14}$$

and

$$e \equiv Ch^2/\mu \tag{3-15}$$

Equation (3-13) represents a family of conic sections. The center of attraction O is a common focus for the family. The dimensionless parameter e is called the eccentricity of the conic, and the parameter p, which has the dimension of length, is the semilatus rectum, or the conic parameter. The polar equation involves three constants, p, e and $\theta_o$. These constants are specified by the values of the radial distance $r_B$, the speed $V_B$ and the flight path angle $\gamma_B$ at the burn-

out position B . The flight path angle $\gamma$ along the trajectory is measured positive upward from the local horizontal to the velocity vector $\vec{V}$ .

## 3-3. CHARACTERISTIC VALUES OF A TRAJECTORY

Once the initial values $r_B$ , $V_B$ and $\gamma_B$ are specified, the trajectory followed by the vehicle is well-determined. With each trajectory, there are associated a number of characteristic values which are constants of the motion. In this section, we shall define these values and interpret their physical meanings.

First, using Eq. (3-5), we rewrite Eq. (3-3) as

$$\ddot{r} - \frac{h^2}{r^3} = -\frac{\mu}{r^2} \tag{3-16}$$

Multiplying the equation by $\dot{r}$ , we have

$$\dot{r}\ddot{r} - \frac{h^2\dot{r}}{r^3} = -\frac{\mu\dot{r}}{r^2}$$

or equivalently

$$\frac{1}{2}\frac{d}{dt}\left(\dot{r}^2 + \frac{h^2}{r^2}\right) = \frac{d}{dt}\left(\frac{\mu}{r}\right)$$

By integrating and replacing $h^2$ by $(r^2\dot{\theta})^2$ , we obtain

$$\frac{1}{2}\left[\dot{r}^2 + (r\dot{\theta})^2\right] - \frac{\mu}{r} = \mathcal{E} \tag{3-17}$$

where $\mathcal{E}$ is a constant of integration. If $V_r$ is the radial component and $V_\theta$ the transverse component of the velocity, $V_r = \dot{r}$ and $V_\theta = r\dot{\theta}$ , and

$$V^2 = V_r^2 + V_\theta^2 = \dot{r}^2 + (r\dot{\theta})^2 \tag{3-18}$$

Hence Eq. (3-17) can be written as

$$\frac{1}{2}V^2 - \frac{\mu}{r} = \mathcal{E} \tag{3-19}$$

At each point along its trajectory, the vehicle has, per unit mass, a kinetic energy equal to $(1/2)V^2$ and a potential energy from which is derived the gravitational force. Since the gravitational force per unit mass has the magnitude $\mu/r^2$ , the potential energy at a distance $r$ is $-\mu/r$ , if we select the level of the potential energy such that it

has the value zero at infinity. Hence, relation (3-19) states that the total energy per unit mass, along the trajectory, is constant. The equation is called the energy integral or the vis-viva integral.

Next, by a rotation of the direction of reference, we can make $\theta_o = 0$ and $e \geq 0$ in the polar equation (3-13) for the trajectory. Hence we consider

$$r = \frac{p}{1 + e \cos \theta} \tag{3-20}$$

In this form, the angle $\theta$ is no longer measured from the position vector $\vec{r}_B$, but from a new reference direction which we shall determine later. Equation (3-20) is the general equation of a conic section. The radial distance $r$ remains finite if $0 \leq e < 1$. This condition defines a family of closed curves, ellipses. If the trajectory does not intersect the boundary of the Earth's atmosphere, the vehicle returns to its initial condition for each variation of $2\pi$ of the angle $\theta$. Hence, we shall refer to the trajectory as an orbit. The distance $r$ remains the same when we change $\theta$ into $-\theta$. The elliptic orbit is symmetric with respect to the polar axis (Fig. 3-3). The minimum value of $r$ is called the pericenter distance $r_p$. It is obtained by setting $\theta = 0$ in Eq. (3-20). We have

$$r_p = \frac{p}{1 + e} \tag{3-21}$$

We see now that the reference direction is the direction toward the point P of closest distance called the pericenter. The maximum value of $r$, $r_a$, is called the apocenter distance. It is obtained by setting $\theta = \pi$ in Eq. (3-20). We have

$$r_a = \frac{p}{1 - e} \tag{3-22}$$

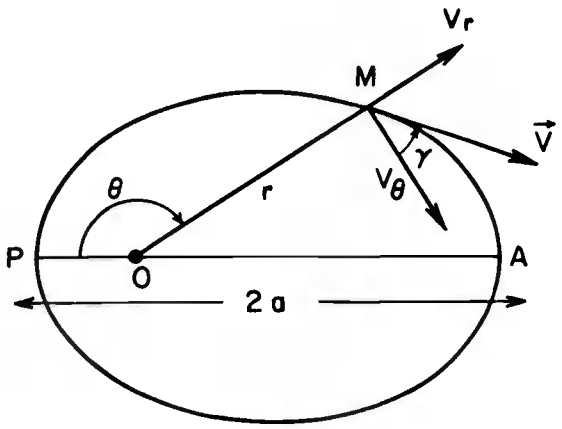


Fig. 3-3. Elliptic orbit.

The point of farthest distance, the point A , is called the apocenter. For the Earth, the point P and the point A are also called the perigee and the apogee, respectively. They are the apses of the elliptic orbit, and the line joining P and A is called the line of apses. The distance 2a between the apses is defined as the major axis of the ellipse. Hence

$$2a = r_p + r_a = \frac{p}{1+e} + \frac{p}{1-e} = \frac{2p}{(1-e^2)} \tag{3-23}$$

This gives the relation for the semi-latus rectum

$$p = a(1-e^2) \tag{3-24}$$

Therefore, in terms of a and e , the expression for $r_p$ and $r_a$ can be written as

$$r_p = a(1-e) \quad , \quad r_a = a(1+e) \tag{3-25}$$

Now, by taking the derivative of Eq. (3-20), we have

$$\dot{r} = \frac{pe \sin\theta}{(1+e\cos\theta)^2} \frac{d\theta}{dt}$$

Using Eqs. (3-5) and (3-20) and noticing that $V_r = \dot{r}$ , we have

$$V_r = \frac{h}{p} e \sin\theta \tag{3-26}$$

On the other hand, in evaluating $V_\theta = r\dot{\theta}$ , we have

$$V_\theta = \frac{h}{p} (1+e\cos\theta) \tag{3-27}$$

The Eqs. (3-26) and (3-27) give the expressions for the radial and transverse components of the velocity along the orbit as functions of the polar angle. The magnitude of $\vec{V}$ is given by Eq. (3-18) written as

$$V = \frac{h}{p} \sqrt{1 + e^2 + 2e\cos\theta} \tag{3-28}$$

Since $h^2 = \mu p$ by Eq. (3-14), using the relation (3-24) we can rewrite this expression as

$$V = \sqrt{\frac{\mu}{a(1-e^2)}} \sqrt{1 + e^2 + 2e\cos\theta} \tag{3-29}$$

This equation gives the magnitude of the velocity along the orbit as a function of $\theta$ . It passes through a maximum at the pericenter,

$\theta = 0$ , and a minimum at the apocenter, $\theta = \pi$ . We have

$$V_p = \sqrt{\frac{\mu(1+e)}{a(1-e)}} \quad , \quad V_a = \sqrt{\frac{\mu(1-e)}{a(1+e)}} \tag{3-30}$$

The flight path angle at each point along the orbit is given by

$$\sin\gamma = \frac{V_r}{V} \quad , \quad \cos\gamma = \frac{V_\theta}{V} \quad , \quad \tan\gamma = \frac{V_r}{V_\theta} \tag{3-31}$$

Hence, using the Eqs. (3-26) - (3-28), we have

$$\sin\gamma = \frac{e\sin\theta}{\sqrt{1+e^2+2e\cos\theta}} \quad , \quad \cos\gamma = \frac{1+e\cos\theta}{\sqrt{1+e^2+2e\cos\theta}}$$

$$\tan\gamma = \frac{e\sin\theta}{1+e\cos\theta} \tag{3-32}$$

If we use $r = r_p$ , and $V = V_p$ to evaluate the constant energy $\mathcal{E}$ in the vis-viva integral, (3-19), we have

$$\mathcal{E} = -\frac{\mu}{2a} \tag{3-33}$$

This shows that the total energy of the orbit is a function solely of the major axis. With this value for $\mathcal{E}$ , we rewrite the energy integral

$$V^2 = \mu\left(\frac{2}{r} - \frac{1}{a}\right) \tag{3-34}$$

This very important relation expresses the speed along the elliptical orbit in terms of the radial distance $r$ .

We have defined the elliptic orbit as an orbit with an eccentricity such that $0 \leq e < 1$ . The two limiting cases are the cases where $e = 0$ , and $e \to 1$ .

When $e = 0$ , the Eq. (3-20) shows that the radial distance is constant. The orbit is circular. From the Eqs. (3-26) and (3-27) with $e = 0$ , we see that the radial component of the velocity is zero, while the normal component of the velocity is constant. This component, which is tangential to the circular orbit, is called the circular speed. The circular speed can also be obtained from Eq. (3-34) by putting $a = r$ . Thus,

$$V_{cir} = \sqrt{\frac{\mu}{r}} \tag{3-35}$$

The other limiting case is obtained by making $e \to 1$ . From Eq. (3-23), we see that, holding the semilatus rectum $p$ constant,

when $e \to 1$, the major axis of the ellipse tends to infinity. We say that in the limiting case $e = 1$, the orbit is a parabola. The equation of the conic, Eq. (3-20), with $e = 1$, becomes

$$r = \frac{p}{1 + \cos\theta} = \frac{p}{2\cos^2\frac{\theta}{2}} \tag{3-36}$$

The closest distance is obtained for $\theta = 0$

$$r_p = \frac{p}{2} \tag{3-37}$$

The farthest distance, when $\theta = \pi$, is infinite. Since the trajectory has an infinite branch, the vehicle along a parabolic flight path escapes to infinity, though it takes infinite time. For this reason, the speed along a parabolic trajectory is called the escape speed. From Eq. (3-34) we see in the limiting case, when $a \to \infty$, the escape speed is

$$V_{escape} = \sqrt{\frac{2\mu}{r}} \tag{3-38}$$

It is obvious that, at any distance $r$, the condition for a circular orbit is that Eq. (3-35) holds, together with the condition that the direction of the velocity is perpendicular to the position vector. In contrast, for a parabolic orbit, condition (3-38) is necessary and sufficient.

Now Eq. (3-5) can be written

$$\dot{A} = \frac{1}{2} r^2 \dot{\theta} = \frac{h}{2} \tag{3-39}$$

The quantity $\dot{A}$ is called the areal velocity. It represents the rate at which the position vector sweeps out area. We see that this rate is constant for a given orbit. For an elliptic orbit, if we integrate the equation over a full period $T$ we obtain

$$\frac{h}{2} T = \pi a^2 \sqrt{1 - e^2} = \text{Area of ellipse} \tag{3-40}$$

But from the Eqs. (3-14) and (3-24)

$$h = \sqrt{\mu p} = \sqrt{\mu a(1 - e^2)} \tag{3-41}$$

Therefore the period is

$$T = 2\pi \sqrt{\frac{a^3}{\mu}} \tag{3-42}$$

Just as is the energy $\mathcal{E}$, the period, $T$, in elliptical motion is a function solely of the major axis.

## 3-4. TIME OF FLIGHT ALONG THE ORBIT

Consider the Eq. (3-39) written as

$$dt = \frac{1}{h} r^2 \, d\theta \tag{3-43}$$

Using the polar equation (3-20) for $r$, we have the time of flight from the pericenter to a position $M$ defined by the polar angle $\theta$

$$t = \frac{p^2}{h} \int_0^{\theta} \frac{d\theta}{(1 + e\cos\theta)^2} = \frac{p^2}{h(1 - e^2)^{3/2}} S(\theta)$$

or

$$t = \sqrt{\frac{a^3}{\mu}} \, S(\theta) \tag{3-44}$$

where the function $S(\theta)$ is given by

$$S(\theta) = - \frac{e\sqrt{1 - e^2}\sin\theta}{1 + e\cos\theta} + 2 \arctan \left( \sqrt{\frac{1 - e}{1 + e}} \tan \frac{\theta}{2} \right) \tag{3-45}$$

Let $M_1$ and $M_2$ be two points along the orbit with polar angle $\theta_1$ and $\theta_2$. The time of flight for the vehicle to travel the arc $M_1M_2$ is

$$t_2 - t_1 = \sqrt{\frac{a^3}{\mu}} \, [ S(\theta_2) - S(\theta_1)] \tag{3-46}$$

Using Eq. (3-42) we can write

$$\frac{t_2 - t_1}{T} = \frac{1}{2\pi} [ S(\theta_2) - S(\theta_1)] \tag{3-47}$$

The time of flight along an elliptic orbit can also be obtained by simple geometric considerations. First we shall give some properties related to an ellipse.

An ellipse can be obtained from a circle of center $\omega$ and radius $a$, called the principal circle, by an affine reduction with ratio $b/a$ (Fig. 3-4). From each point $M'$ on the circle, the corresponding point $M$ on the ellipse is obtained by reducing the ordinate of $M'$ by the factor $b/a$. Hence when $M'$ is at the point $B'$, the corresponding point on the ellipse is $B$ such that $\omega B = b$. The minor axis of the ellipse is $2b$. In celestial mechanics, the polar angle $\theta$ defining the point $M$, measured from the pericenter, is called the true anomaly. On the other hand, the angle $E$ measured at the center $\omega$ of the principal circle from the pericenter, defining the point $M'$ on the principal circle, is called the eccentric anomaly. Using Cartesian coordinates as shown in Fig. 3-4, with the eccentric anomaly as the parameter, we can write the coordinates of the point $M'$ moving along the principal circle

$$x' = a \cos E$$
$$y' = a \sin E \qquad (3\text{-}48)$$

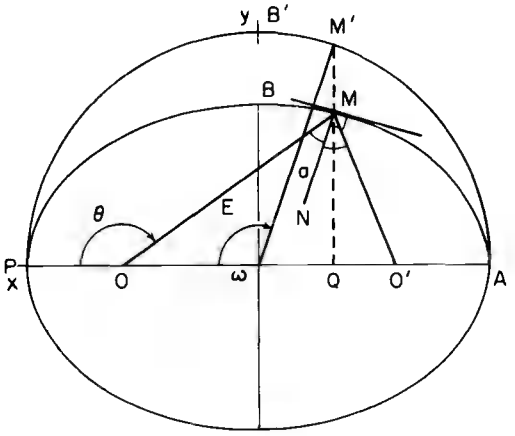


Fig. 3-4. True anomaly and eccentric anomaly.

Using the affinity described above, the Cartesian coordinates of the point on the ellipse are

$$x = a \cos E$$
$$y = b \sin E \qquad (3\text{-}49)$$

From this, we can verify the familiar Cartesian equation of the ellipse

$$\frac{x^2}{a^2} + \frac{y^2}{b^2} = 1 \qquad (3\text{-}50)$$

The point $O'$, symmetric to the point $O$ with respect to the center $\omega$, is called the second focus, or the vacant focus of the ellipse. A main property of the ellipse is that the sum of the distances from any point $M$ on the ellipse to the foci $O$ and $O'$ remains constant and equal to the major axis, that is

$$MO + MO' = 2a \qquad (3\text{-}51)$$

Another property is that the bisector $MN$ of the angle $OMO'$ is the normal at the point $M$ to the ellipse. Hence, this bisector is orthogonal to the tangent at $M$.

The distance $OO' = 2c$ is called the focal distance. From Fig. 3-4 we have

$$c = \omega O = \omega P - OP = a - a(1 - e)$$

Therefore

$$c = ae \tag{3-52}$$

On the other hand, since $OB = a$ , from the triangle $OB\omega$

$$b^2 = a^2 - c^2$$

or

$$b = a\sqrt{1 - e^2} \tag{3-53}$$

The ellipse can be considered as the projection of the principal circle, the angle $\alpha$ between the planes containing the circle and the ellipse, respectively, being such that $\cos \alpha = b/a$ . We have shown that the time of flight from the pericenter $P$ to the point $M$ is proportional to the area $POM$ swept by the radius vector $OM$ . By using the notation Area $POM = (POM)$ , we write

$$t = K \cdot (POM)$$

where $K$ is a coefficient of proportionality. But

$$\begin{aligned}(POM) &= \frac{b}{a}(POM') \\ &= \frac{b}{a}[(P\omega M') - (O\omega M')] \\ &= \frac{b}{2a}[a^2E - a^2 e \sin E]\end{aligned}$$

Hence

$$t = \frac{Kab}{2}[E - e \sin E] \tag{3-54}$$

The coefficient $K$ is obtained by taking $E = 2\pi$ , which corresponds to the time $t$ equal to a full period of revoluation $T$ . Hence

$$T = Kab\pi \tag{3-55}$$

Compared with Eq. (3-42)

$$\frac{Kab}{2} = \sqrt{\frac{a^3}{\mu}} \tag{3-56}$$

Hence, the time of flight from the pericenter in terms of the eccentric anomaly $E$ is given by

$$M = E - e \sin E \tag{3-57}$$

where $M$ is a non-dimensional time

$$M = \sqrt{\frac{\mu}{a^3}}\, t \tag{3-58}$$

Equation (3-57) is the well-known Kepler's equation. The variable $M$, expressed in radians, is called the mean anomaly.

Finally, it is easy to derive relations between the true anomaly $\theta$ and the eccentric anomaly $E$. From Fig. 3-4, we have

$$\overline{OQ} = \overline{O\omega} + \overline{\omega Q}$$

or

$$r \cos\theta = -ae + a \cos E \tag{3-59}$$

Using Eq. (3-20) for $r$, with $p = a(1 - e^2)$, we have

$$\frac{(1 - e^2)\cos\theta}{1 + e\cos\theta} = \cos E - e$$

Hence,

$$\cos\theta = \frac{\cos E - e}{1 - e\cos E}, \quad \cos E = \frac{e + \cos\theta}{1 + e\cos\theta} \tag{3-60}$$

From this,

$$\sin\theta = \frac{\sqrt{1 - e^2}\sin E}{1 - e\cos E}, \quad \sin E = \frac{\sqrt{1 - e^2}\sin\theta}{1 + e\cos\theta} \tag{3-61}$$

Also,

$$\tan^2\frac{\theta}{2} = \frac{1 - \cos\theta}{1 + \cos\theta} = \frac{(1 + e)(1 - \cos E)}{(1 - e)(1 + \cos E)} = \frac{(1 + e)}{(1 - e)}\tan^2\frac{E}{2}$$

That is,

$$\tan\frac{\theta}{2} = \sqrt{\frac{1 + e}{1 - e}}\tan\frac{E}{2} \tag{3-62}$$

Quite often, we use the expression for the radial distance $r$ in terms of the eccentric anomaly $E$. Using Eq. (3-60) in Eq. (3-59), we have

$$r = a(1 - e\cos E) \tag{3-63}$$

## 3-5. THE ELEMENTS OF THE ORBIT IN TERMS OF THE INITIAL CONDITION

Let us now follow the trajectory, starting from the burnout position B . The quantities $r_B$ , $V_B$ , and $\gamma_B$ are known, together with the direction from the center of the Earth O to the position B . We propose in this section to calculate the quantities related to the orbit followed by the vehicle in terms of the information obtained at burnout (Fig. 3-5).

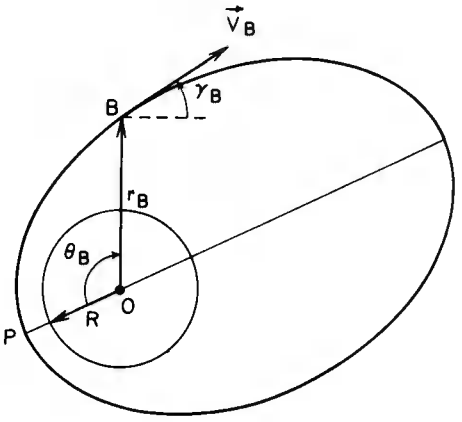


Fig. 3-5. The orbit from burnout conditions.

It is convenient to define the non-dimensional burnout speed $u_B$ as the ratio of the speed $V_B$ , to the circular speed at distance $r_B$

$$u_B = \frac{V_B}{\sqrt{\mu / r_B}} \tag{3-64}$$

We shall assume that the orbit is elliptic, that is $u_B < \sqrt{2}$ . First, by applying the energy integral, Eq. (3-34), at the point B , we have

$$V_B^2 = \mu\left(\frac{2}{r_B} - \frac{1}{a}\right)$$

From this equation, the major-axis is

$$\frac{a}{r_B} = \frac{1}{2 - u_B^2} \tag{3-65}$$

Since the angular momentum is constant along an orbit, it can be evaluated at the burnout position

$$h = r_B V_B \cos \gamma_B \tag{3-66}$$

Using Eq. (3-41), with the major-axis obtained from Eq. (3-65), we have for the eccentricity

$$e = \sqrt{1 - u_B^2 (2 - u_B^2) \cos^2 \gamma_B} \tag{3-67}$$

or

$$e = \sqrt{\sin^2 \gamma_B + (1 - u_B^2)^2 \cos^2 \gamma_B} \tag{3-68}$$

From Eqs. (3-65) and (3-68) for $a$ and $e$, we have for the apocenter distance and the pericenter distance from Eq. (3-25)

$$\frac{r_a}{r_B} = \frac{1}{2 - u_B^2} \left[ 1 + \sqrt{\sin^2 \gamma_B + (1 - u_B^2)^2 \cos^2 \gamma_B} \right] \tag{3-69}$$

and

$$\frac{r_p}{r_B} = \frac{1}{2 - u_B^2} \left[ 1 - \sqrt{\sin^2 \gamma_B + (1 - u_B^2)^2 \cos^2 \gamma_B} \right] \tag{3-70}$$

The condition for the orbit to intersect the Earth's atmosphere, assumed to be spherical, with a finite radius $R$, is that $r_p \leq R$. Hence, in terms of the initial conditions, we have the condition for intersection

$$\frac{R}{r_B} \geq \frac{1}{2 - u_B^2} \left[ 1 - \sqrt{\sin^2 \gamma_B + (1 - u_B^2)^2 \cos^2 \gamma_B} \right] \tag{3-71}$$

The orientation of the orbit is given by the angle $\theta_B$ between the direction to the pericenter and the direction to the burnout position $B$. This angle is obtained by replacing in Eq. (3-20) $r$ and $\theta$ by $r_B$ and $\theta_B$. We have

$$\cos \theta_B = \frac{1}{e} \left[ \frac{a}{r_B} (1 - e^2) - 1 \right]$$

or, using Eqs. (3-65) and (3-67)

$$\cos \theta_B = \frac{u_B^2 \cos^2 \gamma_B - 1}{\sqrt{1 - u_B^2 (2 - u_B^2) \cos^2 \gamma_B}} \tag{3-72}$$

Therefore,

$$\sin \theta_B = \frac{u_B^2 \sin\gamma_B \cos\gamma_B}{\sqrt{1 - u_B^2(2-u_B^2)\cos^2\gamma_B}} \tag{3-73}$$

and

$$\tan \theta_B = \frac{u_B^2 \sin\gamma_B \cos\gamma_B}{u_B^2 \cos^2\gamma_B - 1} \tag{3-74}$$

## 3-6. MINIMUM-ENERGY ORBIT

Let us consider the case where the vehicle, after ascending to the highest altitude, at the apocenter A , returns and intersects the Earth's atmosphere at the entry point E at a distance R from the center of attraction O (Fig. 3-6). This is the case where the inequality (3-71) for intersection is satisfied. The angle $\phi$ between the positions B and E , measured at the center of attraction O , is called the range angle. From Fig. 3-6, it is seen that

$$\phi = \theta_E - \theta_B \tag{3-75}$$

where $\theta_E$ is the polar angle defining the entry position E . The angle $\theta_B$ is given by Eq. (3-72). The angle $\theta_E$ is obtained by replacing in the Eq. (20) r and $\theta$ by R and $\theta_E$. We have

$$\cos \theta_E = \frac{1}{e}\left[\frac{a}{R}(1 - e^2) - 1\right] \tag{3-76}$$

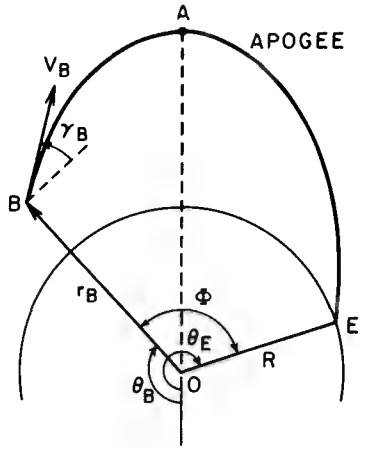


Fig. 3-6. The range angle .

Using Eq. (3-65) for the semi-major axis we have

$$\frac{a}{R} = \frac{r_B}{R}\,\frac{a}{r_B} = \frac{\lambda}{2 - u_B^2} \tag{3-77}$$

where

$$\lambda = \frac{r_B}{R} \tag{3-78}$$

is the ratio of the radial distances to the point B and E, respectively. Hence,

$$\cos\theta_E = \frac{\lambda u_B^2 \cos^2\gamma_B - 1}{\sqrt{1 - u_B^2(2 - u_B^2)\cos^2\gamma_B}} \tag{3-79}$$

The range angle is then

$$\phi = \arccos\frac{1}{e}(\lambda u_B^2 \cos^2\gamma_B - 1) - \arccos\frac{1}{e}(u_B^2\cos^2\gamma_B - 1) \tag{3-80}$$

where e is given by Eq. (3-67). We notice that when the point B is at the top of the atmosphere, $r_B = R$, and $\lambda = 1$. Since the point E is beyond the apocenter, $\theta_E = 2\pi - \theta_B$, and Eq. (3-80) becomes

$$\phi = 2[\pi - \arccos\frac{1}{e}(u_B^2\cos^2\gamma_B - 1)] \tag{3-81}$$

The range can be evaluated when the trajectory intersects the Earth's atmosphere. In the limiting case, where we have an equality in condition (3-71), the trajectory is tangent at its pericenter to the circle with center O and radius R representing the atmosphere in the plane of the motion. The flight path angle at the point of tangency, which is also the limiting position of the entry point E, is zero. The trajectory is called the grazing trajectory. By simple geometric considerations, it is seen that the range angle for the grazing trajectory is given by $\phi_G = 2\pi - \theta_B$. Hence, from Eq. (3-74),

$$\tan\phi_G = \frac{u_B^2 \sin\gamma_B \cos\gamma_B}{1 - u_B^2\cos^2\gamma_B} \tag{3-82}$$

This equation can be written as

$$\sin\phi_G - u_B^2 \sin(\phi_G + \gamma_B)\cos\gamma_B = 0 \tag{3-83}$$

Equation (3-80) for the range gives $\phi$ as a function of two

parameters $u_B$ and $\gamma_B$. For a given initial velocity $u_B$, there exists a value of the initial flight path angle $\gamma_B$ such that the range angle is a maximum. Conversely, for a prescribed range angle $\phi$, Eq. (3-80) gives the initial velocity $u_B$ as function of the initial flight path angle $\gamma_B$. There exists an angle $\gamma_B$ giving the minimum velocity $u_B$ to achieve the prescribed range angle. Since by Eq. (3-65) the minimum of $u_B$ corresponds to the minimum of the semimajor axis $a$, which in turn, by Eq. (3-33), corresponds to the minimum of the total energy $\mathcal{E}$, such an orbit is called the minimum-energy orbit.

To calculate the minimum-energy orbit, it is convenient to rewrite Eq. (3-80) in the implicit form

$$f(\phi, \lambda, u_B, \gamma_B) = 0 \tag{3-84}$$

For this purpose, we write Eq. (3-75)

$$\cos \theta_E = \cos (\phi + \theta_B)$$

or

$$\cos \theta_E = \cos \phi \cos \theta_B - \sin \phi \sin \theta_B$$

From the Eqs. (3-72), (3-73) and (3-79)

$$1 - \lambda u_B^2 \cos^2 \gamma_B = \cos\phi (1 - u_B^2 \cos^2 \gamma_B) + \sin\phi \, u_B^2 \sin\gamma_B \cos\gamma_B$$

or

$$f(\phi, \lambda, u_B, \gamma_B) = \frac{1 - \cos\phi}{u_B^2 \cos^2 \gamma_B} + \frac{\cos(\phi + \gamma_B)}{\cos \gamma_B} - \lambda = 0 \tag{3-85}$$

Now, consider the case where the points B and E are prescribed. The Eq. (3-85) gives the relation between the initial speed $u_B$ and the initial flight path angle $\gamma_B$ to achieve the prescribed range $\phi$. We write the equation

$$\frac{(1 - \cos\phi)}{u_B^2} \tan^2 \gamma_B - \sin\phi \tan\gamma_B + \frac{1 - \cos\phi}{u_B^2} + \cos\phi - \lambda = 0 \tag{3-86}$$

For each initial speed $u_B$, this equation, considered as a quadratic equation in $\tan \gamma_B$, gives two values $\gamma_B$. Hence, there exist two trajectories connecting the points B and E. One is called the high trajectory, and the other the low trajectory. The two trajectories coincide when the equation has a double root. In this case we have

$$\sin^2\phi - \frac{4(1 - \cos\phi)}{u_B^2} \left[ \frac{(1 - \cos\phi)}{u_B^2} + \cos\phi - \lambda \right] = 0 \tag{3-87}$$

We notice that if we consider Eq. (3-85) as an implicit equation giving $u_B$ as function of $\gamma_B$, for a prescribed range angle $\phi$, then by taking its derivative with respect to $\gamma_B$

$$\frac{\partial f}{\partial u_B}\frac{du_B}{d\gamma_B} + \frac{\partial f}{\partial \gamma_B} = 0$$

The minimum of $u_B$ with respect to $\gamma_B$ corresponds to $du_B/d\gamma_B = 0$, that is, $\partial f/\partial \gamma_B = 0$, which is the same condition as for Eq. (3-86) to have a double root. Hence Eq. (3-87), when solved, provides the minimum speed $u_B$ for a prescribed range angle $\phi$, with an initial distance ratio $\lambda$. Solving for $u_B$, we have by taking the positive root

$$u_B^2 = \frac{1}{\cos^2\frac{\phi}{2}}\left[\cos\phi - \lambda + \sqrt{\lambda^2 - 2\lambda\cos\phi + 1}\right] \tag{3-88}$$

The corresponding flight path angle $\gamma_B$ is given by the double root of Eq. (3-86). We have

$$\tan\gamma_B = \frac{u_B^2}{2\tan\frac{\phi}{2}} \tag{3-89}$$

In the simple case where the point B is at the top of the atmosphere, we have $\lambda = 1$. The Eqs. (3-88) and (3-89) are reduced to

$$u_B^2 = \frac{2\sin\frac{\phi}{2}}{1+\sin\frac{\phi}{2}} \tag{3-90}$$

and

$$\tan\gamma_B = \frac{\cos\frac{\phi}{2}}{1+\sin\frac{\phi}{2}} = \tan\left(\frac{\pi}{4} - \frac{\phi}{4}\right) \tag{3-91}$$

That is,

$$\gamma_B = \frac{\pi}{4} - \frac{\phi}{4} \tag{3-92}$$

We see that, for the case of the minimum-energy orbit, when the burnout and the entry positions are at the same distance from the center of attraction, the initial speed and the initial flight path angle are given by simple expressions in terms of the range angle $\phi$. In this case, the other elements of the flight path can also be expressed in terms of the range angle.

For the semi-major axis, using Eq. (3-65) with $r_B = R$, and Eq. (3-90) we have

$$\frac{a}{R} = \frac{1}{2}(1 + \sin\frac{\phi}{2}) \tag{3-93}$$

For the eccentricity, we write Eq. (3-67)

$$e = \sqrt{1 - \frac{u_B^2(2 - u_B^2)}{1 + \tan^2\gamma_B}} \tag{3-94}$$

Using Eqs. (3-90) and (3-91), we have, after simplification

$$e = \frac{\cos\frac{\phi}{2}}{1 + \sin\frac{\phi}{2}}, \quad 1 - e^2 = \frac{2\sin\frac{\phi}{2}}{1 + \sin\frac{\phi}{2}} \tag{3-95}$$

We notice from Eq. (3-91) that

$$e = \tan\gamma_B \tag{3-96}$$

The apocenter distance of the trajectory can be seen to be

$$\frac{r_a}{R} = \frac{1}{2}(1 + \sin\frac{\phi}{2} + \cos\frac{\phi}{2}) \tag{3-97}$$

For the time of flight between the two points B and E , we use Kepler's equation, Eq. (3-57). Let $E_1$ and $E_2$ be the eccentric anomalies corresponding to the point B and E , respectively. Then the time of flight is given by

$$\sqrt{\frac{\mu}{a^3}}(t_2 - t_1) = E_2 - E_1 - e(\sin E_2 - \sin E_1)$$

Obviously, when $\lambda = 1$ , the points B and E are symmetric with respect to the line of apses. Hence

$$E_2 = 2\pi - E_1$$

Therefore,

$$\sqrt{\frac{\mu}{a^3}}(t_2 - t_1) = 2(\pi - E_1 + e\sin E_1) \tag{3-98}$$

On the other hand, if $\theta_1$ is the true anomaly of the point B

$$\theta_1 = \pi - \frac{\phi}{2}, \quad \sin\theta_1 = \sin\frac{\phi}{2}, \quad \cos\theta_1 = -\cos\frac{\phi}{2} \tag{3-99}$$

Using Eq. (3-61) for $\theta$ and Eq. (3-95) for $e$ we have

$$\sin(\pi - E_1) = \sin E_1 = \frac{\sqrt{1-e^2}\sin\theta_1}{1+e\cos\theta_1} = \sqrt{\frac{2\sin\frac{\phi}{2}}{1+\sin\frac{\phi}{2}}}$$

and

$$e\sin E_1 = \frac{\cos\frac{\phi}{2}}{1+\sin\frac{\phi}{2}}\sqrt{\frac{2\sin\frac{\phi}{2}}{1+\sin\frac{\phi}{2}}}$$

Upon substituting into Eq. (3-98) and using Eq. (3-93) for $a$, we have

$$\sqrt{\frac{2\mu}{R^3}}(t_2 - t_1) = \left(1+\sin\frac{\phi}{2}\right)^{3/2} \arcsin\sqrt{\frac{2\sin\frac{\phi}{2}}{1+\sin\frac{\phi}{2}}} + \cos\frac{\phi}{2}\sqrt{2\sin\frac{\phi}{2}} \qquad (3\text{-}100)$$

## 3-7. EFFECTS OF VARIATIONS OF THE INITIAL CONDITION IN THE ELEMENTS AT ENTRY

The trajectory followed by the vehicle during reentry depends strongly on the condition at the reentry position $E$. Hence, it is interesting to study the resulting errors at the entry position $E$ due to an error incurred at the burnout position $B$.

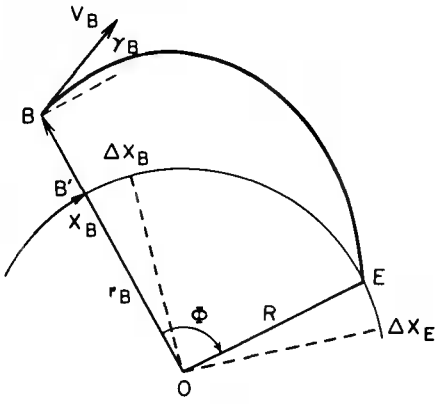


Fig. 3-7. Error in the range angle.

First, we consider the variation in the curvilinear range (Fig. 3-7)

$$x = R\phi \qquad (3\text{-}101)$$

The parameters specifying the burnout condition are $r_B$, $V_B$ and $\gamma_B$, and the curvilinear distance $x_B$ from the origin to the projection

of the burnout position B on the top of the atmosphere. It is apparent that, from the rotational symmetry of the force field, any error in linear range $\Delta x_B$, incurred at the burnout position will be translated into an equal error $\Delta x_E$ of the range

$$\Delta x_E = \Delta x_B \tag{3-102}$$

We shall now evaluate the error $\Delta x$, or equivalently the error $\Delta\phi$ in the range as function of an error $\Delta r_B$, $\Delta V_B$ or $\Delta\gamma_B$ incurred at the burnout position. For this purpose we rewrite Eq. (3-85) with the velocity $V_B$ appearing explicitly

$$f(\phi, \lambda, V_B, \gamma_B) = \frac{1 - \cos\phi}{\frac{R}{\mu}\lambda V_B^2 \cos^2\gamma_B} + \frac{\cos(\phi + \gamma_B)}{\cos\gamma_B} - \gamma = 0 \tag{3-103}$$

Then, the differential of f is

$$\Delta f = \frac{\partial f}{\partial \phi}\Delta\phi + \frac{\partial f}{\partial \lambda}\Delta\lambda + \frac{\partial f}{\partial V_B}\Delta V_B + \frac{\partial f}{\partial \gamma_B}\Delta\gamma_B = 0$$

Holding $V_B$ and $\gamma_B$ constant, the change in the range $\Delta\phi$, due to a change in the ratio of the radial distance $\Delta\lambda$ is

$$\frac{\Delta\phi}{\Delta\lambda} = -\frac{\partial f/\partial\lambda}{\partial f/\partial\phi} \tag{3-104}$$

Similarly,

$$\frac{\Delta\phi}{\partial V_B} = -\frac{\partial f/\partial V_B}{\partial f/\partial\phi} \tag{3-105}$$

and

$$\frac{\Delta\phi}{\Delta\gamma_B} = -\frac{\partial f/\partial\gamma_B}{\partial f/\partial\phi} \tag{3-106}$$

By evaluating the partial derivatives, we have the following formulae for computing the error in the range angle

$$\frac{\Delta\phi}{\Delta\lambda} = \frac{1 - \cos\phi + \lambda u_B^2 \cos^2\gamma_B}{\lambda\left[\sin\phi - u_B^2 \sin(\phi + \gamma_B)\cos\gamma_B\right]}$$

$$\frac{\Delta\phi}{\Delta V_B} = \frac{2(1 - \cos\phi)}{V_B\left[\sin\phi - u_B^2 \sin(\phi + \gamma_B)\cos\gamma_B\right]} \tag{3-107}$$

$$\frac{\Delta\phi}{\Delta\gamma_B} = \frac{-2(1-\cos\phi)\sin\gamma_B + u_B^2 \sin\phi\cos\gamma_B}{\cos\gamma_B[\sin\phi - u_B^2 \sin(\phi+\gamma_B)\cos\gamma_B]} \tag{3-107}$$

Now, consider the quantity in the square brackets in the denominators of the Eqs. (3-107)

$$\Delta = \sin\phi - u_B^2 \sin(\phi+\gamma_B)\cos\gamma_B \tag{3-108}$$

$\Delta = 0$ when

$$\sin\phi - u_B^2 \sin(\phi+\gamma_B)\cos\gamma_B = 0 \tag{3-109}$$

This is the same as Eq. (3-83) for grazing trajectory. Hence, in general, $\Delta$ is not vanishing and keeps the same sign which we can easily verify as the positive sign. Since $1-\cos\phi \geq 0$, from the first two equations (3-107), we see that the ratio $\Delta\phi / \Delta\lambda$ and $\Delta\phi / \Delta V_B$ are positive. Any increase in the initial altitude, or in the initial speed, provides an increase in the range. On the other hand, from the third equation (3-107), the ratio $\Delta\phi / \Delta\gamma_B$ changes its sign when

$$2(1-\cos\phi)\sin\gamma_B = u_B^2 \sin\phi\cos\gamma_B$$

or

$$\tan\gamma_B = \frac{u_B^2}{2\tan\frac{\phi}{2}} \tag{3-110}$$

This equation is the same as Eq. (3-89) for the minimum-energy trajectory. Along a minimum-energy trajectory, the variation of $\Delta\phi$ is always negative, and is of the second order in $\Delta\gamma_B$. We have

$$\Delta\phi = \cancel{\frac{\partial\phi}{\partial\gamma_B}}\,\Delta\gamma_B + \frac{1}{2}\frac{\partial^2\phi}{\partial\gamma_B^2}(\Delta\gamma_B)^2 + \ldots \tag{3-111}$$

By taking the derivative of the third of equations (3-107) with respect to $\gamma_B$, and using the relations for the minimum-energy trajectory, we have

$$\frac{\partial^2\phi}{\partial\gamma_B^2} = -\frac{4\sin^2\frac{\phi}{2}}{\Delta\cos^2\gamma_B} \tag{3-112}$$

Now, using Eq. (3-89) for a minimum-energy trajectory we have

$$\Delta = \sin\phi - u_B^2 \sin(\phi + \gamma_B)\cos\gamma_B$$

$$= 2\sin\frac{\phi}{2}\left[\cos\frac{\phi}{2} - \frac{\sin\gamma_B \sin(\phi+\gamma_B)}{\cos\frac{\phi}{2}}\right]$$

$$= 2\tan\frac{\phi}{2}\left[\cos^2\frac{\phi}{2}\cos^2\gamma_B + \sin^2\frac{\phi}{2}\sin^2\gamma_B - 2\sin\frac{\phi}{2}\cos\frac{\phi}{2}\sin\gamma_B\cos\gamma_B\right]$$

or

$$\Delta = 2\tan\frac{\phi}{2}\cos^2(\gamma_B + \frac{\phi}{2})$$

Therefore, a perturbation $\Delta\gamma_B$ in the initial flight path angle, along a minimum-energy trajectory, corresponds to an error in the range angle given by

$$\Delta\phi = -\frac{\sin\phi}{2\cos^2\gamma_B\cos^2(\gamma_B + \frac{\phi}{2})}(\Delta\gamma_B)^2 \qquad (3\text{-}113)$$

In this case, using Eq. (3-89) in the first two of equations (3-107), we have for the error in the range angle with respect to an error in the initial altitude and in the initial speed, along a minimum-energy trajectory

$$\frac{\Delta\phi}{\Delta\lambda} = \frac{\sin\phi + \lambda\sin 2\gamma_B}{2\lambda\cos^2(\gamma_B+\frac{\phi}{2})} \qquad (3\text{-}114)$$

and

$$\frac{\Delta\phi}{\Delta V_B} = \frac{\sin\phi}{V_B\cos^2(\gamma_B+\frac{\phi}{2})} \qquad (3\text{-}115)$$

In the special case where the point B is at the top of the atmosphere, $r_B = R$, and

$$2\cos^2(\gamma_B+\frac{\phi}{2}) = 1 + \cos(2\gamma_B + \phi)$$

But from Eq. (3-92), $2\gamma_B + \phi = \frac{\pi}{2} + \frac{\phi}{2}$. Hence,

$$2\cos^2(\gamma_B + \frac{\phi}{2}) = 1 - \sin\frac{\phi}{2} \qquad (3\text{-}116)$$

The Equations (3-113) - (3-115) become

$$\Delta\phi = -4 \tan \frac{\phi}{2} (\Delta\gamma_B)^2 \tag{3-117}$$

$$\frac{\Delta\phi}{\Delta\lambda} = \frac{1}{\cos \frac{\phi}{2}} (1 + \sin \frac{\phi}{2})(1 + 2 \sin \frac{\phi}{2}) \tag{3-118}$$

$$\frac{\Delta\phi}{\Delta V_B} = \frac{4}{V_B} \tan \frac{\phi}{2} (1 + \sin \frac{\phi}{2}) \tag{3-119}$$

Now, let us consider the variations in the entry speed $V_E$ and the entry flight path angle $\gamma_E$ . From the energy integral, Eq. (3-19), we have the relation connecting the elements at the burnout position B and the entry position E

$$\frac{1}{2} V_B^2 - \frac{\mu}{r_B} = \frac{1}{2} V_E^2 - \frac{\mu}{R} \tag{3-120}$$

On the other hand, by evaluating the angular momentum at these points, we have

$$r_B V_B \cos \gamma_B = R V_E \cos \gamma_E \tag{3-121}$$

The differentials of Eqs. (3-120) and (3-121) give

$$V_B \Delta V_B + \frac{\mu}{r_B^2} \Delta r_B = V_E \Delta V_E \tag{3-122}$$

and

$$(V_B \cos\gamma_B) \Delta r_B + (r_B \cos\gamma_B) \Delta V_B - (r_B V_B \sin\gamma_B) \Delta\gamma_B$$

$$= (R \cos\gamma_E) \Delta V_E - (R V_E \sin\gamma_E) \Delta\gamma_E \tag{3-123}$$

For an error $\Delta V_B$ in the burnout speed alone, the corresponding error in the entry speed is given by Eq. (3-122) with $\Delta r_B = 0$

$$\frac{\Delta V_E}{\Delta V_B} = \frac{V_B}{V_E} \tag{3-124}$$

From Eq. (3-123) the error in the entry angle is obtained by putting $\Delta r_B = 0$ and $\Delta\gamma_B = 0$

$$(\tan\gamma_E)\,\Delta\gamma_E = \frac{\Delta V_B}{V_B}\left(\frac{V_B^2}{V_E^2} - 1\right) \tag{3-125}$$

For an error in the initial altitude, the error in the entry speed is

$$\frac{\Delta V_E}{V_E} = \left(\frac{\Delta r_B}{r_B}\right)\left(\frac{\mu}{r_B}\right)\frac{1}{V_E^2}$$

In terms of $\lambda$ and $u_B$, this is

$$\frac{\Delta V_E}{V_E} = \frac{1}{[\,u_B^2 + 2(\lambda - 1)\,]}\left(\frac{\Delta\lambda}{\lambda}\right) \tag{3-126}$$

The corresponding error in the entry angle is

$$(\tan\gamma_E)\,\Delta\gamma_E = -\frac{u_B^2 + 2\lambda - 3}{u_B^2 + 2\lambda - 2}\left(\frac{\Delta\lambda}{\lambda}\right) \tag{3-127}$$

Finally, for an error in the initial flight path angle $\gamma_B$ alone, there is no error in the entry speed. The error in the entry angle is given by

$$(\tan\gamma_E)\,\Delta\gamma_E = (\tan\gamma_B)\,\Delta\gamma_B \tag{3-128}$$

We notice from Eqs. (3-125), (3-127) and (3-128) that the entry angle is particularly sensitive for a grazing trajectory, $\gamma_E = 0$.

## References

1. Sänger, E., and Bredt, J., "A Rocket Drive for Long Range Bombers," Translation No. CGD-32, Bureau of Aeronautics, Navy Department, 1944.

2. Anthony, M. L., "Free Flight Missile Trajectories," Vistas in Astronautics, Vol. II, Pergamon Press, New York, 1959.

3. Dunning, R. S., "The Orbital Mechanics of Flight Mechanics," NASA SP-325, 1973.

4. Arora, K. L., and Vinh, N. X., "Maximum Range of Ballistic Missiles," SIAM Review, Vol. 7, No. 4, 1965.

# Chapter 4

# Powered Phase

## 4-1. INTRODUCTION

In this chapter, we shall analyze the trajectory of the vehicle from the launching pad, point A, to the burnout position, point B. During the thrusting phase, the energy provided by the propellant is transformed into potential energy through the increase in the altitude of the vehicle, and kinetic energy through its increase in speed. Also, a part of the energy provided by the propulsion system is dissipated in the form of heat by action of the aerodynamic drag. The powered phase is the phase during which it is possible to have a guidance system to control the trajectory such that at the end of the thrusting program, the vehicle reaches a prescribed position B, specified by the position vector $\overrightarrow{r_B}$, and a prescribed velocity $\overrightarrow{V_B}$. We have seen in the preceding chapter that the trajectory required by the mission may be completely specified by these conditions at burnout.

The guidance is achieved by the following modes of control.

a/ Control of the thrusting force $\vec{T}$. This control is performed by the direction of the vector thrust. Its magnitude can also be controlled by the variation of the mass flow rate.

b/ Besides the main engine, the vehicle can be equipped with several small rockets providing lateral thrusting forces for its guidance. We shall assume that the resultant thrusting force of all the engines is represented by the vector thrust $\vec{T}$.

c/ Control of the aerodynamic force $\vec{A}$. This control is performed by varying the angle of attack of the vehicle and possibly by varying its aerodynamic configuration. In three-dimensional flight, the aerodynamic force is also a function of the bank angle.

## 4-2. THE EQUATIONS OF MOTION

To write the equations of motion, we shall assume that the trajectory lies in the plane of the great circle containing the launch point A and the burnout position B. Hence, it is necessary that all the forces involved be contained in that plane. This leads to the assumption that the vehicle has a plane of symmetry and that the velocity vector $\vec{V}$, the aerodynamic force $\vec{A}$ and the thrusting force $\vec{T}$ are

all contained in that plane. The duration of the powered phase is generally short and it is convenient for a first-order approximation to assume that the Earth is an adequate inertial reference and in this reference system the atmosphere is at rest.

The center of mass M of the vehicle is defined by its coordinates x and z in a ground coordinate system Axz , where the axis Ax is the horizontal at the launching point A taken as the origin of the coordinates, with positive x in the direction of motion, and the axis Az is the vertical at the point A, taken positively up (Fig. 4-1).

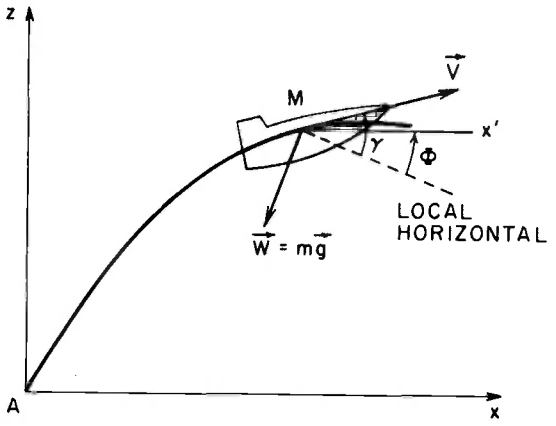


Fig. 4-1. Ground inertial system.

At any point along its trajectory, the flight path angle of the vehicle is defined as the angle between the local horizontal (the plane perpendicular to the gravitational force $m\vec{g}$), and the velocity vector $\vec{V}$. The angle $\phi$ between the local horizontal and the line Mx' drawn parallel to the horizontal Ax of the launch point is precisely the range angle as defined in the preceding chapter.

At each instant t , the vehicle is subject to three forces (Fig. 4-2).

a/ The gravitational force $\vec{W} = m\vec{g}$ applied at the center of mass M .

b/ The aerodynamic force $\vec{A}$ applied at the aerodynamic center P . The aerodynamic force can be decomposed into a drag force $\vec{D}$ in the opposite direction to the velocity $\vec{V}$ , and a lift force $\vec{L}$ orthogonal to it.

c/ A propulsive force represented by the thrust vector $\vec{T}$ , applied at a point Q . To simplify the force diagram we shall assume that the three points M , P and Q are aligned and constitute a body axis, fixed with respect to the vehicle. Then the angle of attack $\alpha$ can be conveniently measured from this body axis to the velocity vector $\vec{V}$ . The thrust angle $\epsilon$ is defined as the angle between the body axis and the direction of the thrust.

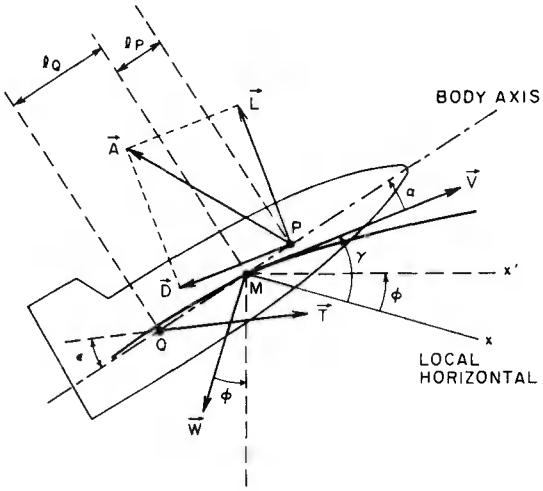


Fig. 4-2. Forces acting on the vehicle.

Using Newton's second law, we can write the equation of motion in vector form

$$m \frac{d\vec{V}}{dt} = \vec{T} + \vec{A} + \vec{W} \tag{4-1}$$

where $m$ is the mass of the vehicle. By projecting this equation into the tangent and the normal to the trajectory of the vehicle we have

$$m \frac{dV}{dt} = T \cos(\epsilon - \alpha) - D - W \sin\gamma \tag{4-2}$$

and

$$-mV \frac{d(\gamma - \phi)}{dt} = T \sin(\epsilon - \alpha) - L + W \cos\gamma \tag{4-3}$$

These equations are the dynamical equations. They can be obtained directly from the general equations for flight over a spherical Earth derived in Chapter 2.

The lift and the drag forces are assumed to have the form

$$L = \frac{1}{2} \rho S C_L V^2$$

$$D = \frac{1}{2} \rho S C_D V^2 \tag{4-4}$$

where $\rho$ is the atmospheric mass density, and $S$ a reference area.

The coefficients $C_L$ and $C_D$ are lift and drag coefficients. They are functions of the angle of attack $\alpha$, the Mach number $M$ and the Reynolds number $R_e$

$$C_L = C_L(\alpha, M, R_e)$$

$$C_D = C_D(\alpha, M, R_e) \tag{4-5}$$

The longitudinal range $x$, and the altitude $z$ are obtained from the kinematic relations

$$x = \int_0^t V \cos(\gamma - \phi)\, dt \tag{4-6}$$

$$z = \int_0^t V \sin(\gamma - \phi)\, dt \tag{4-7}$$

Finally we have the pitching moment equation, describing the motion of the vehicle about the center of mass

$$B \frac{d^2}{dt^2}(\gamma + \alpha - \phi) = L \ell_P \cos\alpha + D \ell_P \sin\alpha - T \ell_Q \sin\epsilon - M_q - K \frac{d(\gamma + \alpha - \phi)}{dt} \tag{4-8}$$

where $B$ is the moment of inertial of the vehicle about an axis passing through the center of mass and perpendicular to the plane of symmetry, $\ell_P$ the distance between $P$ and $M$ and $\ell_Q$ the distance between $Q$ and $M$. The term $M_q$ is the aerodynamic pitching moment, and the term $Kd(\gamma + \alpha - \phi)/dt$ represents the moment due to the mass flow of the gas ejected from the propulsion system.

The thrust can be written as

$$\vec{T} = -\beta \vec{V}_{re} + (p_e - p_o) A_e \vec{n}_e \tag{4-9}$$

where $\beta \equiv -dm/dt$ is the overall mass flow, $V_{re}$ the average relative velocity, $p_e$ the average pressure and $A_e$ the area over the exit of the engine. It is assumed that the tangential stress over the exit area is negligible. The unit vector $\vec{n}_e$ normal to the area $A_e$ is positively directed inward. Finally, $p_o$ is the average free stream pressure. For simplicity, we may assume that the vectors in Eq. (4-9) are all collinear and write the one dimensional equation as

$$T = \beta V_{re} + (p_o - p_e) A_e \tag{4-10}$$

We define the effective exhaust velocity $c$ as

$$c = V_{re} + (p_o - p_e) \frac{A_e}{\beta} \tag{4-11}$$

Hence, the expression for the thrust magnitude is simply

$$T = \beta c = - c \frac{dm}{dt} \tag{4-12}$$

This equation gives the thrust in terms of the mass flow rate and the parameter $c$ which can be characterized as a function of the propellant used in the propulsion system on board the vehicle. In engineering practice, we may use the specific impulse $I_{sp}$ as an alternate parameter which specifies the thrust performance. It is defined as the thrust impulse per unit mass of propellant or

$$I_{sp} = - \frac{Tdt}{dm} = \frac{T}{\beta} \tag{4-13}$$

From the last two equations, it is seen that the specific impulse $I_{sp}$ may be alternatively defined as the thrust obtained per unit mass flow which is precisely the same as the effective exhaust velocity. But it is a common practice to use different units for $I_{sp}$ and $c$ through the relationship

$$c = g I_{sp} \tag{4-14}$$

where $g$ is the acceleration of gravity. Therefore, while $c$ is given in meters per second, $I_{sp}$ is given in seconds.

Using Eqs. (4-11) and (4-14) we have

$$I_{sp} = \frac{V_{re}}{g} + \frac{(p_o - p_e)}{g\beta} A_e \tag{4-15}$$

The mass flow rate can be computed from

$$\beta = C_\beta p_c A_c \tag{4-16}$$

where

$C_\beta$ = mass flow coefficient, function of the propellant

$p_c$ = average pressure in the combustion chamber. This pressure is also called the operating pressure.

$A_c$ = area of the throat of the nozzle

Hence

$$I_{sp} = \frac{V_{re}}{g} + \frac{(p_o - p_e)}{g\, C_\beta\, p_c} \frac{A_e}{A_c} \tag{4-17}$$

The ratio of the areas $A_e / A_c$ can be expressed in terms of the expansion factor $p_c / p_e$ as

$$\frac{A_c}{A_e} = \left(\frac{k+1}{2}\right)^{\frac{1}{k-1}} \left(\frac{p_e}{p_c}\right)^{\frac{1}{k}} \sqrt{\left(\frac{k+1}{k-1}\right)\left(1 - \frac{p_e}{p_c}\right)^{\frac{k-1}{k}}} \tag{4-18}$$

where $k$ is the ratio of the specific heats.

From these relations, we see that the specific impulse is a function of the following four factors

1. The nature of the propellant ($C_\beta$, $V_{re}$, $k$).
2. The operating pressure $p_c$.
3. The expansion factor $p_c / p_e$.
4. The altitude of flight (g and $p_o$ are functions of the altitude).

For a given type of propellant, we can evaluate its specific impulse under some reference conditions. These conditions are:

For a solid propellant, $p_c$ = 70 atm., $p_c / p_e$ = 70/1 at sea level.

For a liquid propellant, $p_c$ = 25 atm., $p_c / p_e$ = 25/1 at sea level.

Let the specific impulse of the given propellant evaluated at these reference conditions be denoted $(I_{sp})_o$. Then we define the coefficient

$$i_{sp} \equiv \frac{I_{sp}}{(I_{sp})_o} \tag{4-19}$$

This dimensionless coefficient characterizing the propellant under the actual operating condition is now a function of four parameters--the ratio of the specific heats $k$, the altitude $z$, the pressure in the combustion chamber $p_c$ and the expansion ratio $p_c / p_e$. If we assume that the ratio of the specific heats is the same for all propellants, then the function $i_{sp} = f(z, p_c, p_c / p_e)$ can be tabulated for practical reference.

For an anlytical integration of the equations of motion, we shall assume that, under normal operational conditions, the specific impulse $I_{sp}$, or equivalently the effective exhaust velocity $c$, is constant.

Finally, if $R$ is the radius of the Earth, then the range angle $\phi$ is seen to be given by

$$\tan \phi = \frac{x}{R + z} \tag{4-20}$$

Now we see that, for each stage of the rocket vehicle, the dynamical equations, Eqs. (4-2) and (4-3), the kinematic equations, Eqs. (4-6) and (4-7), the moment equation, Eq. (4-8), and the mass flow program equation, Eq. (4-12), constitute a system of six equations for the following eight unknowns:

$\begin{Bmatrix} x \\ z \end{Bmatrix}$ = coordinates of the center of mass

$\begin{Bmatrix} V \\ \gamma \end{Bmatrix}$ = components of the velocity vector

$m$ = mass of the vehicle

$\alpha$ = angle of attack

$\epsilon$ = angle of the thrust

$T$ = magnitude of the thrust

Therefore, to specify the flight trajectory, we have at our disposal two control variables. They may be taken to be the thrust magnitude $T$, and the thrust direction $\epsilon$. On the other hand, for a fully controlled flight, the angle of attack $\alpha$ has to be adjusted constantly to render the moment equation, Eq. (4-8), identically satisfied. Consequently, with a flight program fully controlled, the remaining equations constitute a system of five equations--the Eqs. (4-2) and (4-3), (4-6) and (4-7), and the Eq. (4-12)--which provide the solution for the variables $x$, $z$, $V$, $\gamma$ and $m$ as functions of the time $t$.

If the time history of the thrust magnitude $T(t)$ is prescribed in advance, then by integrating the mass flow equation, Eq. (4-12), we have the variation of the mass as a function of the time. If we assume a constant mass flow rate, then $m$ is a decreasing linear function of the time. In general, the mass of the vehicle is a decreasing function with respect to time as shown in Fig. 4-3.

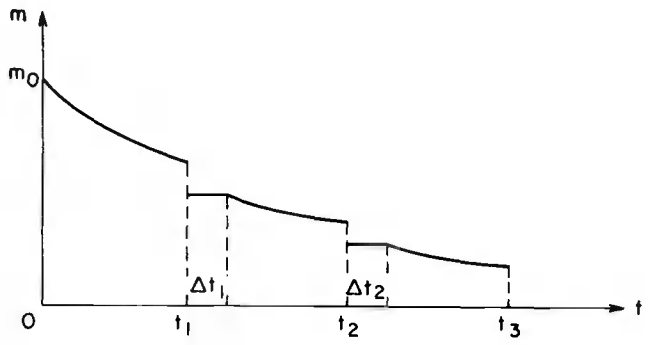


Fig. 4-3. The variation of the mass of a multi-stage rocket vehicle.

The figure represents the variation of the mass of a multi-stage rocket. The first stage of the rocket is operating between the initial time and the time $t_1$ . At $t_1$ the first stage is released providing a discontinuity in the mass of the vehicle. If a lapse of time $\Delta t_1$ exists before the engine in the second stage is ignited, during that time the vehicle is in coast flight with constant mass. Next m continues to decrease between the time $(t_1 + \Delta t_1)$ and $t_2$ and so on. In the subsequent analysis, we shall assume that all the $\Delta t_i$ are zero.

The remaining control variable can be selected either as the angle of attack $\alpha$ , or the thrust angle $\epsilon$ or a combination of both by specifying a relation between these variables and possible other variables also. With this selection the ascending program is completely specified.

In general, in considering an ascending program, we are trying to obtain the optimum of some performance criterion. For example, for a preprogrammed motor, we would like to select a time history for the thrust orientation such that the range achieved is a maximum. Problems like these involve the calculus of variations or the equivalent modern control theory and will not be discussed here. From an engineering standpoint, the selection of a best flight control program is severely restricted by other technical constraints. For example, for a thrusting flight giving the maximum range, it can be shown, upon using not unrealistic assumptions, that the flight must be at maximum lift-to-drag ratio, with the thrust directed orthogonally to the aerodynamic force, and hence making a constant angle with the velocity vector. But the thrust angle $\epsilon$ , due to the technical construction of the propulsion system, cannot deviate at a large angle from the axis of the vehicle. In general $\epsilon$ is constrained by a maximum angle $\epsilon_{max}$ of a few degrees from the main thrusting line.

Another factor to be considered is the normal acceleration. In general, due to structural constraints, this acceleration is severely limited. Hence, for practical purposes, we are led to adopt some simple ascending program which is satisfactory for the analysis during the preliminary stage of the design project. The simplifying hypotheses will provide an analytical solution to the problem considered. The analytical solution has the advantage that it displays explicitly the many relationships among the different variables allowing a global analysis. For example, the solution will give the approximate size of the engine, and the weight of the propellant required to launch a certain given payload (final weight of the vehicle) into a prescribed final orbit. From these approximate data, with the aid of high speed computers, we may update the numerical results to obtain the exact solution to the problem.

## 4-3. ASCENDING TRAJECTORY AT CONSTANT FLIGHT PATH ANGLE

The equations of motion derived in section 4-2 cannot be integrated analytically. For a prescribed initial condition, and a specified thrusting program, numerical integration using high speed computers has to be performed in order to obtain the variables describing the dynamical system as functions of the time.

For advanced planning purposes, it is useful to adopt some simplifying assumptions in order to obtain an analytical solution of the ascen-

ding powered flight. Such a solution will give explicit relationships among the different variables and permit a preliminary selection of the size of the vehicle, its aerodynamic characteristics, the propulsion system required to perform a given mission. With these data we can then use numerical integration to readjust the different characteristic values.

There exists a simple ascending law which can be used to approximate the real powered flight trajectory. Using this program, as a first approximation, we can assume that, after lift-off, the vehicle essentially follows a straight line trajectory having a constant angle of inclination with respect to the local horizontal. In reality, if the flight path angle is constant, the trajectory will be a logarithmic spiral in the plane of the motion, but since we shall assume a flat Earth model for the gravitational field, the trajectory with constant flight path is essentially a straight line.

More specifically, we shall use the following assumptions to simplify the equations in section 4-2:

a/ The powered flight trajectory involves short longitudinal range and a relatively small altitude compared to the radius of the Earth. Hence, from Eq. (4-20)

$$\tan \phi \approx \frac{X}{R} \approx 0$$

Therefore, we can use $\phi = 0$ in the equations in section 4-2. This assumption is usually called the flat Earth assumption.

b/ For the same reason, the acceleration of gravity $g$ can be considered constant for the altitude range considered.

c/ We shall neglect the aerodynamic force.

With these assumptions, the dynamical equations, Eqs. (4-2) and (4-3) become, as can be seen from the simplifying force diagram in Fig. 4-4

$$m \frac{dV}{dt} = T \cos (\epsilon - \alpha) - W \sin \gamma \qquad (4\text{-}21)$$

$$-mV \frac{d\gamma}{dt} = T \sin (\epsilon - \alpha) + W \cos \gamma \qquad (4\text{-}22)$$

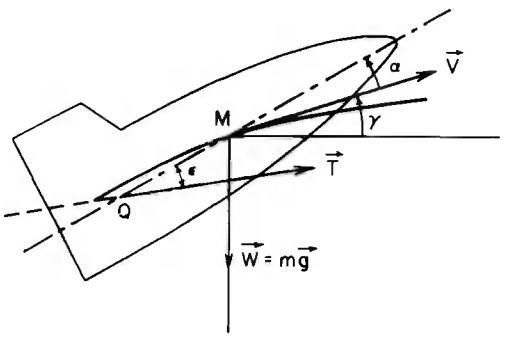


Fig. 4-4. Simple force diagram neglecting aerodynamic force and the curvature of the Earth.

Since we assume that $\gamma$ = constant, then $d\gamma/dt = 0$. Hence, from Eq. (4-22) we have the relation between the thrust and the weight

$$T \sin(\alpha - \epsilon) = W \cos\gamma \tag{4-23}$$

In general, for rocket flight the thrust is large as compared to the weight. Hence from this equation we see that the angle $(\alpha - \epsilon)$ is necessarily small and we can take $\cos(\epsilon - \alpha) \approx 1$ in Eq. (4-21). Then we have the simplified equation

$$m\frac{dV}{dt} = T - W \sin\gamma \tag{4-24}$$

Using Eq. (4-12) for the thrust we rewrite this equation, using the relation $W = mg$

$$dV = -c\frac{dm}{m} - g \sin\gamma\, dt \tag{4-25}$$

To integrate this equation for a multi-stage rocket vehicle, we refer to the Fig. 4-3 and assume that all the time intervals $\Delta t_i$ between the separation of the ith stage and the engine ignition of the $(i+1)$th stage are zero. Then by integrating Eq. (4-25) starting from the time $t_{i-1}$ of the separation of the $(i-1)$th stage, we have during the operation of the ith stage

$$V(t) = V_{i-1} - c_i \log\frac{m_i(t)}{m_{i_0}} - g \sin\gamma t' \tag{4-26}$$

where

$V(t)$ = instantaneous speed at the time $t$
$V_{i-1}$ = speed at the initial time of burning of the ith stage
$c_i$ = effective exhaust velocity of the ith stage
$m_i(t)$ = instantaneous mass at the time $t$
$m_{i_0}$ = mass at the initial time of burning of the ith stage
$t'$ = $t - t_{i-1}$, time interval from the initial time of burning of the ith stage

Now, consider the operation of one single stage. For example, let us assume that the vehicle is a single-stage rocket. At the burnout time $t_1$ of this stage, the change in the speed is

$$\Delta V = V_1 - V_0 = c \log\frac{m_0}{m_1} - g t_1 \sin\gamma \tag{4-27}$$

where $c$ is the effective exhaust velocity of the stage considered, $m_0 = m_{1_0}$ is the initial mass and $m_1 = m_1(t_1)$ is the final mass of the vehicle. If we neglect the gravitational force, we have for the change in the speed

$$\Delta V = c \log \frac{m_0}{m_1} \tag{4-28}$$

We see that, in this case, $\Delta V$ can be used as a measure of the fuel consumption. This quantity is called the characteristic velocity of the maneuver. From this simple formula, we can see that $\Delta V$ must have a certain upper limit. The exhaust velocity has an upper limit which depends on the propulsion system used. For example, ordinary chemical propulsion systems currently provide exhaust velocities up to 3000 m/ sec, with a theoretical maximum in the neighborhood of 4000 m/ sec. On the other hand, the ratio of the masses $m_0 / m_1$ also cannot be made arbitrarily large. Let $\Delta m = m_0 - m_1$ be the mass of the fuel spent. Then we define the fuel ratio

$$f \equiv \frac{\Delta m}{m_0} = 1 - \frac{m_1}{m_0} \tag{4-29}$$

so that we can write Eq. (4-28)

$$\Delta V = c \log \frac{1}{1 - f} \tag{4-30}$$

It is obvious that $f$ can never approach unity, since any amount of fuel always requires a certain provision of structure for its operation. Therefore, the characteristic velocity for a single stage is limited due to technological constraints. Some optimistic predictions advance a figure in the neighborhood of 9000 m/ sec for its ultimate value.

Equation (4-30) gives the performance of a single stage rocket in the hypothetical situation of gravity-free, vacuum space. If we include the gravitational force, the increase in the speed during a thrusting phase of a stage is given by Eq. (4-27). The term $gt_1 \sin\gamma$ characterizes the losses due to the gravitational force. Because of this component, the performance of a single stage rocket is further limited. Therefore, to obtain high final speed, one must use a multi-stage rocket.

Let $\tau$ be the total burning time for a rocket vehicle having $n$ stages. By repeated application of Eq. (4-26), we have the final speed at burnout, assuming a zero initial speed.

$$V_B = \sum_{i=1}^{n} \Delta V_i = -\left[ \sum_{i=1}^{n} c_i \log \mu_i \right] - g\tau \sin\gamma \tag{4-31}$$

where $\mu_i$ is the ratio of the masses of the ith stage, defined as

$$\mu_i \equiv \frac{m_{i1}}{m_{i0}} = \frac{\text{mass of the vehicle at burnout of ith stage}}{\text{mass of the vehicle at initial time of ith stage}} \tag{4-32}$$

For the range and the altitude at the end of the powered phase, we use the Eqs. (4-6) and (4-7) with $\phi = 0$ , and $\gamma$ = constant. We have

$$\frac{x_B}{\cos\gamma} = \int_0^\tau V(t)\,dt$$

$$\frac{z_B}{\sin\gamma} = \int_0^\tau V(t)\,dt \qquad (4\text{-}33)$$

Using $V(t)$ as given by Eq. (4-26) to evaluate the integral, we have, for the case of constant mass flow $\beta$ , ($\beta \equiv -dm/dt$) ,

$$x_B = \cos\gamma \left\{ \sum_{i=1}^{n} \left[ V_{i-1}\tau_i + c_i\tau_i\left(1 + \frac{\mu_i}{1-\mu_i}\log\mu_i\right)\right] - \frac{1}{2}g\tau^2\sin\gamma \right\} \qquad (4\text{-}34)$$

where $\tau_i$ is the burning time of the ith stage. The final altitude is simply

$$z_B = x_B \tan\gamma \qquad (4\text{-}35)$$

## 4-4. OPTIMUM STAGING

The final speed of a rocket vehicle, having a prescribed number of stages is given by Eq. (4-31). This expression for $V_B$ is a function of the characteristic parameters $c_i$ and $\mu_i$ of the different stages, of the constant flight path angle $\gamma$ and the total burning time $\tau$ of the powered phase. By these considerations one may ask the following question:

"Is there an optimum distribution of the masses of different stages such that, for a prescribed burnout speed $V_B$ , the ratio $m_L/m_F$ of the initial mass at launching to the final mass at the end of the powered phase is a minimum? "

If such a solution exists, it therefore gives the lightest rocket for a prescribed payload (final mass $m_F$) for a prescribed final speed $V_B$ .

In solving this problem, we write the ratio of the masses

$$\frac{m_L}{m_F} = \frac{m_1}{m_2}\cdot\frac{m_2}{m_3}\cdot\ldots\cdot\frac{m_n}{m_{n+1}} = \prod_{i=1}^{n}\frac{1}{s_i} \qquad (4\text{-}36)$$

where to ease the notation, in this section, we have used the subscripts as follows

$m_i$ - total mass of the vehicle at the initial burning time of the ith stage. This mass is also referred to as the gross mass of the ith stage.

From Eq. (4-36) we see that we have defined the ratio $s_i$, called the staging ratio, as

$$s_i = \frac{m_{i+1}}{m_i} \tag{4-37}$$

We notice that $s_i$ is the ratio of the gross mass of the $(i+1)$th stage to the gross mass of the ith stage, the masses are all evaluated at the initial burning time of the corresponding stage. Also it is seen that $m_1 = m_L$ is the initial gross mass of the rocket vehicle, while $m_{n+1} = m_F$ is the resulting payload of the operation.

There is a basic difference between the ratio $\mu_i$ as defined by Eq. (4-32) and the staging ratio $s_i$ as defined by Eq. (4-37). This is illustrated by Fig. 4-5 showing the mass distribution in the ith stage of a rocket vehicle

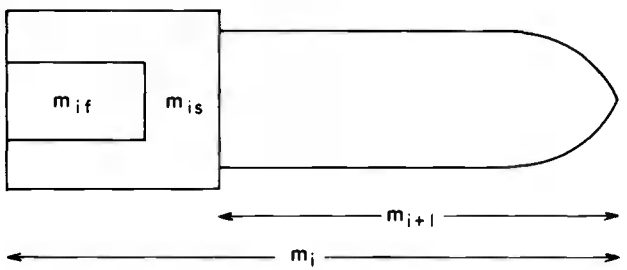


Fig. 4-5. Distribution of the masses in the ith stage of a rocket vehicle.

The total mass shown is the gross mass $m_i$ of the ith stage. The mass $m_{if}$ denotes the mass of the fuel used during the operation of the ith stage, while the mass $m_{is}$ denotes the mass of the structural components of the propulsion system used in the operation of the ith stage. This mass is to be discarded leaving the mass $m_{i+1}$ as the initial mass for the operation of the $(i+1)$th stage. Hence, the mass of the vehicle at burnout of the ith stage is

$$m_{il} = m_i - m_{if} = m_{is} + m_{i+1} \tag{4-38}$$

Since we have used $m_i = m_{i0}$ to denote the mass of the rocket vehicle at the initial time of the ith stage, the ratio $\mu_i$, as defined by Eq. (4-32) now becomes

$$\mu_i = \frac{m_i - m_{if}}{m_i} = 1 - \frac{m_{if}}{m_i} \tag{4-39}$$

On the other hand, the staging ratio $s_i$, as defined by Eq. (4-37) is

$$s_i = \frac{m_{i+1}}{m_i} = 1 - \frac{(m_{if} + m_{is})}{m_i} \tag{4-40}$$

We define the structural ratio $\omega_i$ for the propulsion system used in the operation of the ith stage as

$$\omega_i = \frac{m_{is}}{m_{if} + m_{is}} \tag{4-41}$$

Using this relation in Eq. (4-40) we have

$$s_i = 1 - \frac{1}{(1 - \omega_i)} \frac{m_{if}}{m_i} \tag{4-42}$$

By eliminating $(m_{if}/ m_i)$ between the Eqs. (4-39) and (4-42), we have the relation

$$s_i = \frac{\mu_i - \omega_i}{1 - \omega_i} \tag{4-43}$$

We can now formulate the optimization problem as follows.

The final speed $V_B$, the climb angle $\gamma$ and the total burning time $\tau$ are given. That is, we have from Eq. (4-31)

$$-\sum_{i=1}^{n} c_i \log \mu_i = V_B + g\tau \sin \gamma = V_0$$

where $V_0$ is therefore prescribed. We write this equation as a constraining relation

$$f(\mu_i) \equiv \sum_{i=1}^{n} c_i \log \mu_i + V_0 = 0 \tag{4-44}$$

The number of stages $n$, the different propellant characteristics $c_i$, and the different structural ratios $\omega_i$ are also given. Find a mass distribution $\mu_1, \mu_2, \ldots\ldots, \mu_n$ such that the following function

$$g(\mu_i) = \prod_{i=1}^{n} s_i = \prod_{i=1}^{n} \frac{(\mu_i - \omega_i)}{(1 - \omega_i)} \tag{4-45}$$

is a maximum. This is equivalent to minimizing the product of $1/ s_i$.

In solving this problem, we introduce a Lagrange multiplier $\lambda$ to form the augmented function

$$F(\mu_i) \equiv g(\mu_i) + \lambda f(\mu_i) \tag{4-46}$$

The solution to the problem is obtained by solving the system of $(n+1)$ equations

$$\frac{\partial F}{\partial \mu_i} = 0 \ , \ f(\mu_i) = 0 \tag{4-47}$$

for the $(n+1)$ unknowns $\mu_1$ , $\mu_2$ , . . . , $\mu_n$ and $\lambda$ . Explicitly, we write the first $n$ equations

$$\frac{\partial F}{\partial \mu_i} = \frac{1}{(1-\omega_i)} \prod_{\substack{j=1 \\ j\neq i}}^{n} \frac{(\mu_j - \omega_j)}{(1-\omega_j)} + \lambda \frac{c_i}{\mu_i} = 0 \tag{4-48}$$

For each of the $n$ equations (4-48), we have

$$\frac{\mu_i}{c_i(\mu_i - \omega_i)} = - \frac{\lambda}{\prod_{i=1}^{n} [\ (\mu_i - \omega_i)/(1-\omega_i)\ ]}$$

Since the right-hand side is the same for all equations, it is a constant and we introduce a new constant $K$ to replace the Lagrange multiplier $\lambda$

$$\frac{\mu_i}{c_i(\mu_i - \omega_i)} \equiv \frac{1}{K} \tag{4-49}$$

These $n$ equations can also be put into the form

$$\mu_i = \frac{c_i \omega_i}{c_i - K} \tag{4-50}$$

The problem is then to evaluate the constant $K$ . Using this expression in the constraining relation (4-44), we have

$$\sum_{i=1}^{n} c_i \log \frac{c_i \omega_i}{c_i - K} = - V_0 \tag{4-51}$$

The sum of the logarithms can be written as the logarithm of a product

$$\log \prod_{i=1}^{n} \left( \frac{c_i \omega_i}{c_i - K} \right)^{c_i} = - V_0 \tag{4-52}$$

That is,

$$\prod_{i=1}^{n} \left( \frac{c_i \omega_i}{c_i - K} \right)^{c_i} = e^{-V_0}$$

Or finally, by separating the unknown K

$$\prod_{i=1}^{n} (c_i - K)^{c_i} = e^{V_0} \prod_{i=1}^{n} (c_i \omega_i)^{c_i} \tag{4-53}$$

This equation can be solved for K , and subsequently the mass distribution $\mu_1$ , $\mu_2$, ..., $\mu_n$ is obtained from Eq. (4-50). Obviously the equation (4-53) can only be solved numerically. To obtain an explicit solution, simplifying assumptions have to be made. We have the following special cases.

### 4-4.1. All the Propulsion Systems are Similar

If we assume that all the stages use the same propellant, and regardless of the difference in size, it is possible to achieve the same structural ratio for all the stages, we have

$$\begin{aligned} c_1 &= c_2 = \ldots = c_n = c \\ \omega_1 &= \omega_2 = \ldots = \omega_n = \omega \end{aligned} \tag{4-54}$$

Then, by Eq. (4-50), the mass distribution is the same for each stage. We have

$$\mu_1 = \mu_2 = \ldots = \mu_n = \mu = \frac{c\omega}{c - K} \tag{4-55}$$

The equation (4-53) for K becomes

$$(c - K)^{nc} = e^{V_0} (c\omega)^{nc}$$

Solving for K

$$K = c\left[ 1 - \omega e^{V_0/nc} \right] \tag{4-56}$$

Using this solution in Eq. (4-55), we have for the common mass ratio

$$\mu = e^{-V_0/nc} \tag{4-57}$$

We notice, by Eq. (4-43), that the staging ratios are also the same

$$s_1 = s_2 = \ldots = s_n = s = \frac{\mu - \omega}{1 - \omega}$$

or, explicitly in terms of the given characteristics

$$s = \frac{\omega}{1-\omega}\left[\frac{e^{-V_0/nc}}{\omega} - 1\right] \tag{4-58}$$

The final payload is then obtained in terms of the gross mass of the vehicle at launching

$$m_F = m_L \left(\frac{\omega}{1-\omega}\right)^n \left[\frac{e^{-V_0/nc}}{\omega} - 1\right]^n \tag{4-59}$$

Finally, from Eq. (4-31), we have the final speed

$$V_B = -nc \log \mu - g\tau \sin \gamma \tag{4-60}$$

The special case we have analyzed is highly hypothetical. Nevertheless, the solution is obtained in closed form and it provides a first estimation of the distribution of the masses for different stages.

4-4.2. The Propellant Used is the Same for All Stages

If we assume that the propellant used is the same for all stages, but because of technological construction, the structural ratios are all different, then we have the simplification

$$c_1 = c_2 = \ldots = c_n = c \tag{4-61}$$

Equation (4-53) for $K$ becomes

$$(c-K)^{nc} = e^{V_0} c^{nc} (\omega_1 \omega_2 \ldots \omega_n)^c \tag{4-62}$$

Solving for $K$,

$$K = c\left[1 - (\omega_1 \omega_2 \ldots \omega_n)^{1/n} e^{V_0/nc}\right] \tag{4-63}$$

The mass distribution is given by Eq. (4-50).

$$\mu_i = \frac{\omega_i}{(\omega_1 \omega_2 \ldots \omega_n)^{1/n}} e^{-V_0/nc} \tag{4-64}$$

We notice that the ratio $\mu_i/\omega_i$ is the same for all stages. On the other hand, by Eq. (4-43), the staging ratio is

$$s_i = \frac{\omega_i}{(1-\omega_i)}\left[\frac{e^{-V_0/nc}}{(\omega_1 \omega_2 \ldots \omega_n)^{1/n}} - 1\right] \tag{4-65}$$

The final payload is

$$m_F = m_L \left[ \frac{e^{-V_0/nc}}{(\omega_1 \omega_2 \cdots \omega_n)^{1/n}} - 1 \right]^n \prod_{i=1}^{n} \left( \frac{\omega_i}{1 - \omega_i} \right) \quad (4\text{-}66)$$

Finally, we have for the final speed

$$V_B = -c \sum_{i=1}^{n} \log \mu_i - g\tau \sin \gamma \quad (4\text{-}67)$$

It is easy to verify that the equations in this section are reduced to the equations derived in the preceding section if we put $\omega_1 = \omega_2 = \cdots = \omega_n = \omega$ .

### 4-4.3. The Structural Ratios are the Same for All Stages

The special case considered in the previous section is very close to the practical realization of a multi-stage rocket vehicle. There exists another special case, namely when technological realization allows a common structural ratio for all the stages although different propellants are used. Then we have the simplification

$$\omega_1 = \omega_2 = \cdots = \omega_n = \omega \quad (4\text{-}68)$$

In this case the equation (4-53) cannot be solved explicitly for $K$ . The mass ratio is here

$$\mu_i = \frac{\omega c_i}{c_i - K} \quad (4\text{-}69)$$

It is seen that $\mu_i$ is a decreasing function of $c_i$ . Therefore, if the propellants used are such that $c_1 < c_2$ , we have $\mu_1 > \mu_2$ . The staging ratio is given by Eq. (4-43) written as

$$s_i = \frac{1}{(1 - \omega)} (\mu_i - \omega) \quad (4\text{-}70)$$

We see that it varies in the same direction as $\mu_i$ .

### References

1. Dorleac, B., and Poggi, J., "Performances et Structures du Missile Balistique," Lecture notes, Ecole Nationale Supérieure de l'Aéronautique et de l'Espace, 1960.

2. Schurmann, E. E. H., "Optimum Staging Technique for Multistaged Rocket Vehicles," ARS Journal, Vol. 27, No. 8, 1957.

# Chapter 5

# Return to the Atmosphere

## 5-1. INTRODUCTION

In Chapter 3, the trajectory for flight outside the atmosphere, assumed to be spherical with a finite radius $R$, was considered. We have seen that, if the burnout position $B$, (Fig. 3-1), is outside the atmosphere, the resulting trajectory is a Keplerian conic until the atmosphere is reencountered. In the case of an elliptic trajectory, if the periapsis distance $r_p$ is less than the radius $R$ of the atmosphere, a condition expressed by the inequality (3-71), the trajectory will intersect the atmosphere at a point $E$, the entry position. In the case where inequality (3-71) is not satisfied, the vehicle will be in an elliptic orbit around the Earth if the initial speed is less than the escape speed, that is if

$$V_B \leq \sqrt{\frac{2\mu}{r_B}} \tag{5-1}$$

After the mission has been accomplished, to bring back the vehicle, one must perform a series of maneuvers to change the initial orbit, designated by $\mathcal{E}_1$, to a final orbit, $\mathcal{E}_2$, intersecting the atmosphere at the entry position $E$ (Fig. 5-1). From this point on, the vehicle is in the atmosphere and follows a flight path subject to the gravitational and atmospheric forces. The flight path from the entry position $E$ to the landing point $C$ is called the reentry flight path and its analysis is the subject of several later chapters. In this chapter, we shall be concerned with the maneuver performed to change the nonintersecting orbit $\mathcal{E}_1$ into the intersecting orbit $\mathcal{E}_2$. In general, the means of accomplishing a change of orbit, or transfer, will be by firing the rocket on board the vehicle to change its velocity, thus propelling the vehicle into a new orbit. If the rocket engine provides a high thrust, the burning time is generally short, compared to the orbital period. Hence, it can be assumed that, during a thrusting phase, the position of the vehicle remains essentially unchanged while the velocity undergoes a change impulsively. Furthermore, we shall be concerned with the last orbital change before reentry. Hence the orbit $\mathcal{E}_1$ is the final nonintersecting orbit resulting from a series of maneuvers. At a point $D$ in this orbit, referred to as the deorbit position, a velocity

impulse $\overrightarrow{\Delta V}$ will be applied to the vehicle to change the initial velocity $\overrightarrow{V_1}$ into a new velocity $\overrightarrow{V_2}$, thus injecting the vehicle into the descending orbit $\mathcal{E}_2$. This orbit, initiated from the point D, intersects the atmosphere at the entry position E at a distance R from the center of the Earth. The speed $V_e$, and the flight path angle $\gamma_e$ at the point E will be referred to as the entry speed and the entry flight path angle.

In the subsequent analysis, we shall assume that the initial orbit $\mathcal{E}_1$ and the deorbit position D are prescribed. Hence, we have the polar equation of the initial orbit (Fig. 5-1)

$$r = \frac{a_1(1 - e_1^2)}{1 + e_1 \cos\theta} \tag{5-2}$$

where $a_1$ is the semimajor axis, and $e_1$ the eccentricity of the orbit $\mathcal{E}_1$. The deorbit position D is defined by the polar angle $\theta_D$ measured from the direction to the periapsis of the initial orbit taken as direction of reference. The distance from the center of the Earth to the point D is denoted by $r_D$. It is given by Eq. (5-2) with $\theta = \theta_D$. In general the point D is on the second half of the orbit, that is, $\theta_D \geq \pi$. The firing of the rocket is performed at a point of the orbit where the vehicle is on its way toward the periapsis. From the previous analyses, it is seen that, if $\theta_D$ is specified, $V_1$ and $\gamma_1$ at the point D are also known. The angle $\phi$ between the directions to the deorbit position D and the entry position E, measured at the center of attraction O, is the range angle. It is function of the descending orbit $\mathcal{E}_2$.

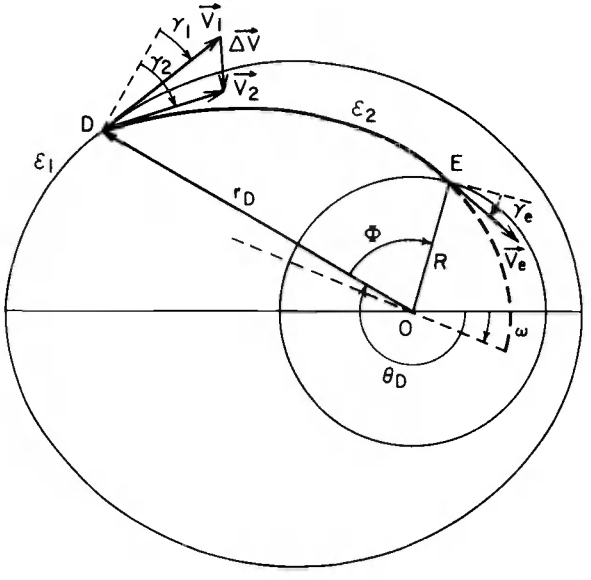


Fig. 5-1. The descending trajectory.

A successful recovery of the vehicle depends on the condition at entry, namely on the location of the point $E$, the entry speed $V_e$, and the entry flight path angle $\gamma_e$. Therefore, in this chapter we shall consider several types of descending trajectory $\mathcal{E}_2$. Each family of trajectories, initiated from the deorbit position $D$, is such that a certain condition at the entry position $E$ is prescribed. More specifically, we shall successively consider families of trajectories such that:

a/ the entry speed $V_e$ is prescribed.
b/ the entry angle $\gamma_e$ is prescribed.
c/ the entry position, or equivalently (for the planar case under consideration) the range angle $\phi$ is prescribed.

The first two problems are associated with the safe recovery of the vehicle since the heating and the deceleration during atmospheric entry depends on the entry speed and the entry angle. The last problem is associated with the selection of the landing point.

In each problem we shall first evaluate the impulse velocity required to achieve the entry condition specified. It will be shown that, for each problem, there exists a family of descending trajectories satisfying the prescribed entry condition. Next we shall compute the trajectory requiring the minimum $\Delta V$. The minimum of this characteristic velocity also corresponds to the minimum fuel consumption of the maneuver.

## 5-2. DESCENT TRAJECTORY FOR GIVEN ENTRY SPEED

In this section, we shall consider the family of descent trajectories initiated from the deorbit position $D$ such that the resulting speed $V_e$ at the entry position $E$ is equal to a prescribed value.

At the point $D$, velocity impulse $\overrightarrow{\Delta V}$ is applied to the vehicle to change the initial velocity $\overrightarrow{V_1}$ into a new velocity $\overrightarrow{V_2}$ called the deorbit velocity. The resulting flight path $\mathcal{E}_2$ is the descent flight path. It intersects the atmosphere at the entry position $E$. Along the trajectory $\mathcal{E}_2$, the total energy is constant as shown by Eq. (3-19). By evaluating this constant energy at the points $D$ and $E$, respectively, we have

$$V_2^2 - \frac{2\mu}{r_D} = V_e^2 - \frac{2\mu}{R} \tag{5-3}$$

where from Eq. (5-2), the radial distance $r_D$ to the deorbit position $D$ is prescribed and is given by

$$r_D = \frac{a_1(1 - e_1^2)}{1 + e_1 \cos \theta_D} \tag{5-4}$$

with $\theta_D$ the true anomaly specifying the point $D$.

We define the nondimensional speeds

$$u_1 \equiv \frac{V_1}{\sqrt{\mu/r_D}} \quad , \quad u_2 \equiv \frac{V_2}{\sqrt{\mu/r_D}} \quad , \quad u_e \equiv \frac{V_e}{\sqrt{\mu/r_D}} \quad , \quad \Delta u \equiv \frac{\Delta V}{\sqrt{\mu/r_D}} \tag{5-5}$$

Note that $\sqrt{\mu/r_D}$ is the circular speed evaluated at distance $r_D$. We shall use $\vec{u}_i$ to denote the scaled velocity $\vec{V}_i / \sqrt{\mu/r_D}$. Distances are measured in units of $R$, with the nondimensional distances defined as

$$\lambda \equiv \frac{r_D}{R} \quad , \quad \alpha_1 \equiv \frac{a_1}{R} \quad , \quad \alpha_2 \equiv \frac{a_2}{R} \tag{5-6}$$

In terms of the nondimensional quantities, Eq. (5-3) becomes

$$u_2^2 - 2 = u_e^2 - 2\lambda \tag{5-7}$$

Then the required dimensionless deorbit speed $u_2$ to achieve the prescribed dimensionless entry speed $u_e$ is

$$u_2 = \sqrt{u_e^2 + 2(1 - \lambda)} \tag{5-8}$$

It is convenient for the analysis to define a velocity axis system $Dxy$, the hodograph space, such that its origin is at the deorbit position $D$, the y-axis along the position vector $\vec{r}_D$, positive outward, and the x-axis along the perpendicular to the position vector, positive toward the direction of the motion. Note that the axis $Dx$ represents the horizontal at the point $D$. In this axis system, the initial velocity $\vec{u}_1$ is defined in polar coordinates by the dimensionless speed $u_1$ and the flight path angle $\gamma_1$ (Fig. 5-2)

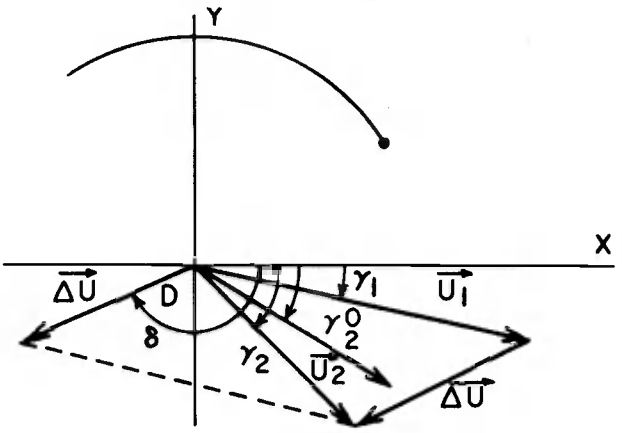


Fig. 5-2. Dimensionless velocity space.

Since the initial orbit is given and the deorbit position prescribed, $u_1$ and $\gamma_1$ are known quantities. From

$$V_1^2 = \mu\left(\frac{2}{r_D} - \frac{1}{a_1}\right)$$

comes

$$u_1 = \sqrt{\frac{2\alpha_1 - \lambda}{\alpha_1}} \tag{5-9}$$

The flight path angle is given by Eq. (3-32).

$$\cos\gamma_1 = \frac{1 + e_1 \cos\theta_D}{\sqrt{1 + e_1^2 + 2e_1\cos\theta_D}}$$

Using Eqs. (5-4) and (5-6), we can write

$$\cos\gamma_1 = \alpha_1\sqrt{\frac{(1 - e_1^2)}{\lambda(2\alpha_1 - \lambda)}}$$

$$\sin\gamma_1 = \pm\sqrt{\frac{\lambda(2\alpha_1 - \lambda) - \alpha_1^2(1 - e_1^2)}{\lambda(2\alpha_1 - \lambda)}} \tag{5-10}$$

Now consider Eq. (5-8) for the deorbit speed $u_2$. Since $u_e$ and $\lambda$ are prescribed, it is seen that $u_2$ is constant for all possible descent trajectories. Hence, the locus of the terminus of the velocity $\overrightarrow{u_2}$ in the hodograph space is a circle centered at D and having a given radius $u_2$ as given by Eq. (5-8). For each direction of this velocity, defined by the flight path angle $\gamma_2$, we have a vector $\overrightarrow{u_2}$. The required velocity impulse $\overrightarrow{\Delta u}$ is such that

$$\overrightarrow{u_1} + \overrightarrow{\Delta u} = \overrightarrow{u_2}$$

Its magnitude is obtained by applying the law of cosines to the velocity triangle in Fig. 5-2. Thus,

$$\Delta u = \sqrt{u_1^2 + u_2^2 - 2u_1u_2\cos(\gamma_2 - \gamma_1)} \tag{5-11}$$

The direction of $\overrightarrow{\Delta u}$ is defined by the angle $\delta$ from the horizontal Dx. Applying the law of sines to the velocity triangle in Fig. 5-2, we have

$$\sin(\delta - \gamma_2) = \frac{u_1}{\Delta u}\sin(\gamma_2 - \gamma_1) \tag{5-12}$$

From Eq. (5-11) and (5-12) it is apparent that the deorbit flight path angle $\gamma_2$ for the descending trajectory can be used as a parameter. To each angle $\gamma_2$ corresponds an impulse velocity $\overrightarrow{\Delta u}$, and hence, a trajectory $\mathcal{E}_2$. The elements of this trajectory can be obtained by using the equations derived in Section 3-5, with the subscript B replaced by subscript 2, and $r_B$ by $r_D$.

We have for the semimajor axis of $\mathcal{E}_2$

$$\frac{a_2}{r_D} = \frac{1}{2 - u_2^2}$$

or

$$\alpha_2 = \frac{\lambda}{2\lambda - u_e^2} \tag{5-13}$$

For the eccentricity of the descending trajectory, by using Eq. (3-67) we have

$$e_2 = \sqrt{1 - (2\lambda - u_e^2)[u_e^2 + 2(1 - \lambda)] \cos^2 \gamma_2} \tag{5-14}$$

The periapsis distance is given by

$$\frac{r_{p_2}}{r_D} = \frac{1 - \sqrt{1 - (2\lambda - u_e^2)[u_e^2 + 2(1 - \lambda)] \cos^2 \gamma_2}}{2\lambda - u_e^2} \tag{5-15}$$

Hence we have the condition for the trajectory $\mathcal{E}_2$ to intersect the atmosphere

$$\frac{1}{\lambda} \geq \frac{1 - \sqrt{1 - (2\lambda - u_e^2)[u_e^2 + 2(1 - \lambda)] \cos^2 \gamma_2}}{2\lambda - u_e^2}$$

Solving for $\gamma_2$, we have the condition

$$\cos \gamma_2 \leq \frac{u_e}{\lambda \sqrt{u_e^2 + 2(1 - \lambda)}} \tag{5-16}$$

This condition restricts the locus of the terminus of the vector $\overrightarrow{u_2}$ in the velocity space to an arc of a circle (Fig. 5-2).

The entry angle at the entry position is obtained by writing that the angular momentum is constant along the descent orbit. We have, by evaluating this constant at the point D and at the point E, respectively

$$r_D V_2 \cos \gamma_2 = R V_e \cos \gamma_e$$

Hence, in terms of the dimensionless variables

$$\cos \gamma_e = \frac{\lambda u_2 \cos \gamma_2}{u_e}$$

or

$$\cos \gamma_e = \frac{\lambda \sqrt{u_e^2 + 2(1 - \lambda)}}{u_e} \cos \gamma_2 \qquad (5\text{-}17)$$

The orientation of the descent trajectory $\mathcal{E}_2$ is defined by the angle $\omega$ between the reference direction, which has been taken as the direction to the periapsis of the initial orbit, and the direction to the periapsis of the descent trajectory (Fig. 5-3). The angle $\omega$ is called the longitude of periapsis of the descent trajectory.

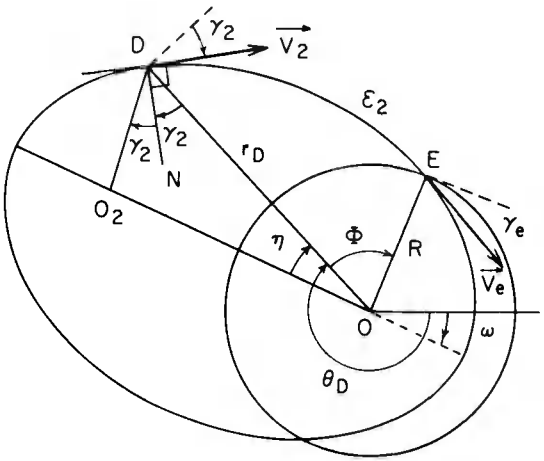


Fig. 5-3. Geometry of the descent trajectory.

To evaluate the angle $\omega$, let us recall two important properties of the ellipse already mentioned in section 3-4. Let $O_2$ be the second focus of the elliptic trajectory $\mathcal{E}_2$, the first focus being the center O. The line $OO_2$ is the line of apses.

First, if D is a point on the ellipse $\mathcal{E}_2$, then

$$DO + DO_2 = 2a_2 \qquad (5\text{-}18)$$

where $a_2$ is the semimajor axis of $\mathcal{E}_2$.

Next, if DN is the normal to the ellipse at the point D, then, DN is the bisector of the angle $ODO_2$. Since the flight path angle

$\gamma_2$ at the point D is defined as the angle between the horizontal at D, which is perpendicular to the position vector $\overrightarrow{OD}$, and the velocity $\overrightarrow{V_2}$, which is tangent to the ellipse at the point D, this property is expressed by the relation

$$\measuredangle ODO_2 = 2\gamma_2 \tag{5-19}$$

Now let $\eta$ be the angle between the vectors $\overrightarrow{OD}$ and $\overrightarrow{OO_2}$ (Fig. 5-3). Using the law of sines in the triangle $ODO_2$ and the property expressed by Eq. (5-19) we have

$$\frac{DO_2}{\sin \eta} = \frac{OO_2}{\sin 2\gamma_2} = \frac{OD}{\sin(2\gamma_2 + \eta)}$$

But $OO_2 = 2a_2e_2$, and by the property expressed by Eq. (5-18) $DO_2 = 2a_2 - r_D$. Hence,

$$\frac{2a_2 - r_D}{\sin \eta} = \frac{2a_2e_2}{\sin 2\gamma_2} = \frac{r_D}{\sin(2\gamma_2 + \eta)} \tag{5-20}$$

Therefore, the first equation (5-20) gives

$$\sin \eta = \frac{(2\alpha_2 - \lambda)}{2\alpha_2 e_2} \sin 2\gamma_2$$

or

$$\sin \eta = \frac{[u_e^2 + 2(1 - \lambda)] \sin 2\gamma_2}{2\sqrt{1 - (2\lambda - u_e^2)[u_e^2 + 2(1 - \lambda)] \cos^2 \gamma_2}} \tag{5-21}$$

Another expression for $\eta$ is obtained by using the second equation (5-20). We have

$$\tan \eta = \frac{(2a_2 - r_D) \sin 2\gamma_2}{r_D - (2a_2 - r_D) \cos 2\gamma_2} = \frac{(2\alpha_2 - \lambda) \sin 2\gamma_2}{\lambda - (2\alpha_2 - \lambda) \cos 2\gamma_2}$$

or

$$\tan \eta = \frac{[u_e^2 + 2(1 - \lambda)] \sin 2\gamma_2}{(2\lambda - u_e^2) - [u_e^2 + 2(1 - \lambda)] \cos 2\gamma_2}$$

$$= \frac{[u_e^2 + 2(1 - \lambda)] \tan \gamma_2}{[(2\lambda - 1) - u_e^2] + \tan^2 \gamma_2} \tag{5-22}$$

The longitude of periapsis of the descending trajectory $\mathcal{E}_2$ is then given by

$$\omega = \theta_D - (\pi + \eta) \tag{5-23}$$

Finally, the range angle $\phi$ from the deorbit position to the entry position is given by Eq. (3-80), written as

$$\phi = \arccos \frac{1}{e_2} (\lambda u_2^2 \cos^2 \gamma_2 - 1) - \arccos \frac{1}{e_2} (u_2^2 \cos^2 \gamma_2 - 1) \tag{5-24}$$

## 5-3. MINIMUM IMPULSE FOR ENTRY AT GIVEN SPEED

We have seen in the preceding section that, if the entry speed alone is specified, then there exists a family of descent trajectories which is a function of the deorbit angle $\gamma_2$. To each angle $\gamma_2$ corresponds a descent trajectory, and hence an impulsive change, $\overrightarrow{\Delta u}$, in the velocity. The magnitude of this impulse, the characteristic velocity, is a measure of the fuel consumption for the maneuver. In this section we shall compute this particular descent trajectory such that $\Delta u$ is a minimum.

Let $\gamma_2^o$ be the limiting value of the angle $\gamma_2$ selected as the parameter for optimization. This value $\gamma_2^o$ is given by the equality sign in condition (5-16). Then from Fig. 5-2, if $\gamma_2^o \leq \gamma_1$, to minimize $\Delta u$, we must select $\gamma_2 = \gamma_1$. The velocity impulse $\overrightarrow{\Delta u}$ is tangential to the initial orbit, at the deorbit point D, to reduce the speed from $u_1$ to $u_2$. Hence, we have the condition for optimum tangential deorbit for a given entry speed

$$\frac{u_e}{\lambda \sqrt{u_e^2 + 2(1 - \lambda)}} \geq \cos \gamma_1 \tag{5-25}$$

Using Eq. (5-10) for $\cos \gamma_1$, we can write this condition

$$u_e^2 \leq \frac{2\lambda (\lambda - 1)(1 - e_1^2) \alpha_1^2}{\lambda (1 - e_1^2) \alpha_1^2 - 2\alpha_1 + \lambda} \tag{5-26}$$

This condition expresses that, for a given initial orbit with a prescribed deorbit position, the prescribed entry speed $u_e$ must be less than a certain value for an optimum tangential deorbit to be possible.

For tangential optimum deorbit, we have the following results obtained by putting $\gamma_2 = \gamma_1$ in the general expressions for the descent trajectory derived in the previous section.

First,

$$\cos \gamma_2 = \cos \gamma_1 = \alpha_1 \sqrt{\frac{(1 - e_1^2)}{\lambda (2\alpha_1 - \lambda)}} \tag{5-27}$$

The minimum characteristic velocity is simply

$$\Delta u = u_1 - u_2 \tag{5-28}$$

where $u_2$ and $u_1$ are given by Eq. (5-8) and Eq. (5-9), respectively. The direction of the optimum velocity impulse is given by

$$\delta = \pi + \gamma_1 \tag{5-29}$$

The major axis is the same as given by Eq. (5-13) but the expression for the eccentricity becomes

$$e_2 = \sqrt{1 - (2\lambda - u_e^2)\,[\,u_e^2 + 2(1 - \lambda)]\,\cos^2 \gamma_1} \tag{5-30}$$

Using Eq. (5-27) we can rewrite this expression

$$e_2 = \sqrt{1 - \frac{\alpha_1^2 (1 - e_1^2)(2\lambda - u_e^2)\,[\,u_e^2 + 2(1 - \lambda)]}{\lambda (2\alpha_1 - \lambda)}} \tag{5-31}$$

The entry angle is given by Eq. (5-17) written as

$$\cos \gamma_e = \frac{\alpha_1}{u_e} \sqrt{\frac{\lambda (1 - e_1^2)[\,u_e^2 + 2(1 - \lambda)]}{(2\alpha_1 - \lambda)}} \tag{5-32}$$

The longitude of periapsis of the descent trajectory is given by Eq. (5-23), where now the expression for the angle $\eta$ is

$$\tan \eta = \frac{\alpha_1 [u_e^2 + 2(1 - \lambda)]\ \sqrt{(1 - e_1^2)[\,\lambda (2\alpha_1 - \lambda) - \alpha_1^2 (1 - e_1^2)]}}{\lambda (2\alpha_1 - \lambda) - \alpha_1^2 (1 - e_1^2)\,[\,u_e^2 + 2(1 - \lambda)]} \tag{5-33}$$

The range angle is given by Eq. (5-24). The polar equation of the entry orbit is

$$r = \frac{p_2}{1 + e_2 \cos (\theta - \omega)} \tag{5-34}$$

where $e_2$ is given by Eq. (5-31) and

$$\frac{p_2}{R} = \alpha_2 (1 - e_2^2) = \frac{\alpha_1^2 (1 - e_1^2)[\,u_e^2 + 2(1 - \lambda)]}{(2\alpha_1 - \lambda)} \tag{5-35}$$

The entry position E is defined by the polar angle $\theta_E$

$$\theta_E = \theta_D + \phi \tag{5-36}$$

where $\phi$ is the range angle. $\theta_E$ can also be computed from Eq. (5-34) with $r = R$ and $\theta = \theta_E$.

A tangential deorbit is optimum when the entry velocity is small as constrained by the inequality (5-26). When this inequality is not satisfied, the minimum deorbit angle $\gamma_2^o$ for the descent trajectory to intersect the atmosphere is larger than the initial flight path angle $\gamma_1$ (Fig. 5-4).

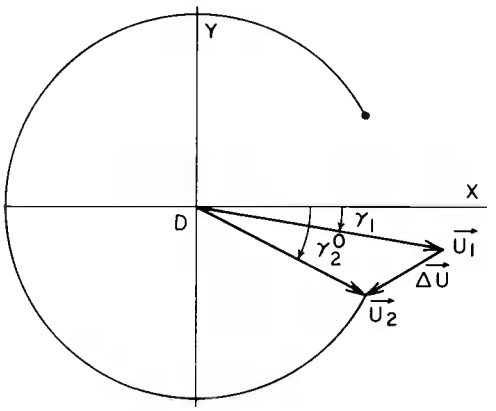


Fig. 5-4. Minimum velocity impulse when $\gamma_2^o \geq \gamma_1$.

In this case, as can be seen in Fig. 5-4, the minimum $\Delta u$ corresponds to $\gamma_2 = \gamma_2^o$. Since the limiting value of $\gamma_2$ is given by the equality sign in (5-16), we have

$$\cos \gamma_2 = \frac{u_e}{\lambda \sqrt{u_e^2 + 2(1 - \lambda)}} \tag{5-37}$$

The minimum characteristic velocity is given by Eq. (5-11), and its direction by Eq. (5-12) with the value of $\gamma_2$ obtained from Eq. (5-37). Using Eq. (5-37) in Eq. (5-17) we see that $\cos \gamma_e = 1$. Hence, the entry is grazing

$$\gamma_e = 0 \tag{5-38}$$

The eccentricity of the descending orbit is given by Eq. (5-14), which by virtue of Eq. (5-37), becomes

$$e_2 = \frac{u_e^2 - \lambda}{\lambda} \tag{5-39}$$

The longitude of periapsis of the descent orbit is given by Eq. (5-23). To evaluate the angle $\eta$, we notice from Eqs. (5-14), (5-21) and (5-22) that

$$\cos \eta = \frac{(2\lambda - u_e^2) - [u_e^2 + 2(1-\lambda)] \cos 2\gamma_2}{2e_2} \tag{5-40}$$

From Eq. (5-37)

$$\cos 2\gamma_2 = 2\cos^2\gamma_2 - 1 = \frac{u_e^2(2-\lambda^2) - 2\lambda^2(1-\lambda)}{\lambda^2[u_e^2 + 2(1-\lambda)]}$$

Hence, upon substituting into Eq. (5-40), with the aid of Eq. (5-39) we have

$$\cos \eta = \frac{\lambda^2 - u_e^2}{\lambda(u_e^2 - \lambda)} \tag{5-41}$$

The polar equation of the entry orbit is

$$r = \frac{p_2}{1 + e_2 \cos(\theta - \omega)} \tag{5-42}$$

where now, by using Eqs. (5-13) and (5-39)

$$\frac{p_2}{R} = \alpha_2(1 - e_2^2) = \frac{u_e^2}{\lambda} \tag{5-43}$$

The position of entry is given by the polar angle $\theta_E$. It is obtained by putting $r = R$, and $\theta = \theta_E$ in Eq. (5-42).

## 5-4. DESCENT TRAJECTORY FOR GIVEN ENTRY ANGLE

In this section we shall consider the family of descending trajectories initiated from the deorbit position $D$, such that the resulting flight path angle $\gamma_e$ at the entry position $E$ is equal to a prescribed value.

The notation used is the same as in the previous sections. We now write the equations for the conservation of energy and conservation of angular momentum, Eqs. (5-7) and (5-17), using the dimensionless variables defined by Eqs. (5-5) and (5-6).

$$u_2^2 - 2 = u_e^2 - 2\lambda \tag{5-44}$$

and

$$u_e \cos\gamma_e = \lambda u_2 \cos\gamma_2 \tag{5-45}$$

In the hodograph space Dxy as defined in section 5-2, let x and y be the components of the deorbit velocity $\overrightarrow{u_2}$. Then

$$\begin{aligned} x &= u_2 \cos\gamma_2 \\ y &= u_2 \sin\gamma_2 \end{aligned} \tag{5-46}$$

Therefore

$$u_2^2 = x^2 + y^2 \tag{5-47}$$

Using these equations, we rewrite Eqs. (5-44) and (5-45)

$$(x^2 + y^2) - 2 = u_e^2 - 2\lambda$$

$$u_e \cos\gamma_e = \lambda x \tag{5-48}$$

By eliminating $u_e$ between these two equations, we have

$$\frac{x^2}{\dfrac{2(\lambda - 1)\cos^2\gamma_e}{(\lambda^2 - \cos^2\gamma_e)}} - \frac{y^2}{2(\lambda - 1)} = 1 \tag{5-49}$$

This is the equation of a hyperbola symmetric with respect to the axes in the velocity coordinates system Dxy (Fig. 5-5).

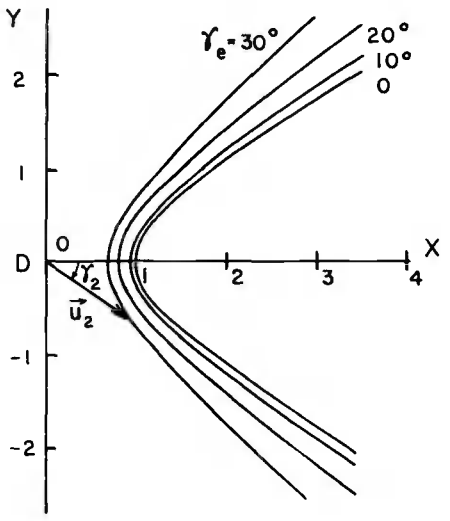


Fig. 5-5. Locus of the terminus of the deorbit velocity for entry at given angle.

The equation expresses that, for a deorbit from a prescribed position $D$, at a given distance $\lambda$, in such a way that the entry angle $\gamma_e$ is equal to a prescribed value, the terminus of the deorbit velocity $\overrightarrow{u_2}$ must be on a branch of a hyperbola defined by Eq. (5-49). Each hyperbola corresponds to a specified entry angle $\gamma_e$. In particular, when the entry is grazing, $\cos \gamma_e = 1$, and we have the limiting hyperbola

$$\frac{x^2}{\frac{2}{(\lambda + 1)}} - \frac{y^2}{2(\lambda - 1)} = 1 \qquad (5\text{-}50)$$

Figure 5-5 gives the plots of several hyperbolas, loci of the terminus of the deorbit velocity $\overrightarrow{u_2}$, for several values of $\gamma_e$, and for an initial distance ratio $\lambda = 1.18$.

To each prescribed value $\gamma_e$, we have a branch of an hyperbola. When the terminus of the vector $\overrightarrow{u_2}$ moves along this hyperbola, it generates a family of descent trajectories, all intersecting the atmosphere at a point $E$ at a distance $R$, with the prescribed entry angle $\gamma_e$. The deorbit angle $\gamma_2$ can be used as a parameter for the family.

If the entry speed is also prescribed, then the magnitude of $u_2$ is prescribed as given by Eq. (5-8). The descending orbit is obtained by finding the intersection of the circle of radius $u_2$ and the hyperbola given by Eq. (5-49). We have, by using the Eqs. (5-8) and (5-46)

$$\begin{aligned} x^2 &= [u_e^2 + 2(1 - \lambda)] \cos^2 \gamma_2 \\ y^2 &= [u_e^2 + 2(1 - \lambda)] \sin^2 \gamma_2 \end{aligned} \qquad (5\text{-}51)$$

To simplify the notation, we rewrite Eq. (5-49) as

$$Ax^2 - By^2 = 1 \qquad (5\text{-}52)$$

where

$$\begin{aligned} A &\equiv \frac{\lambda^2 - \cos^2 \gamma_e}{2(\lambda - 1) \cos^2 \gamma_e} \\ B &\equiv \frac{1}{2(\lambda - 1)} \end{aligned} \qquad (5\text{-}53)$$

By substituting the Eqs. (5-51) into Eq. (5-52) and solving for $\gamma_2$, we have

$$\cos \gamma_2 = \frac{u_e \cos \gamma_e}{\lambda \sqrt{u_e^2 + 2(1 - \lambda)}} \qquad (5\text{-}54)$$

The branch of the hyperbola corresponding to the velocity $\vec{u}_2$ pointing in the same direction as the motion along the initial orbit corresponds to a solution providing two points of intersection, hence two values for $\gamma_2$. One solution $\gamma_2 > 0$, gives a high descent orbit, while the other, $\gamma_2 < 0$, gives a low descent orbit. The solutions are real when

$$\frac{u_e \cos \gamma_e}{\lambda \sqrt{u_e^2 + 2(1 - \lambda)}} \leq 1 \tag{5-55}$$

or, that is, when

$$u_e \geq \lambda \sqrt{\frac{2(\lambda - 1)}{\lambda^2 - \cos^2 \gamma_e}} \tag{5-56}$$

For a given entry angle $\gamma_e$, there exists a lower bound for a predetermined entry speed for an entry trajectory to be physically possible. On the other hand, we can write Eq. (5-55) in terms of a condition on $\gamma_e$

$$\cos \gamma_e \leq \frac{\lambda \sqrt{u_e^2 + 2(1 - \lambda)}}{u_e} \tag{5-57}$$

Hence, if the entry speed is prescribed, there exists a lower bound for the entry angle $\gamma_e$, for an entry trajectory to be physically possible.

By prescribing both $\gamma_e$ and $u_e$, for a given initial orbit, that is, for a given $\alpha_1$ and $e_1$, we can also vary the deorbit position, by varying $\lambda$, to satisfy the physical constraints on the entry. To study the influence of $\lambda$ on the condition for entry, we rewrite the condition (5-56)

$$\frac{V_e}{\sqrt{\frac{\mu}{R}}} \geq \sqrt{\frac{2\lambda(\lambda - 1)}{\lambda^2 - \cos^2 \gamma_e}} \tag{5-58}$$

With $\gamma_e$ fixed, the right hand side of the inequality (5-58) is an increasing function of $\lambda$. Hence its minimum corresponds to the position of deorbit at the periapsis of the initial orbit.

$$\lambda = \alpha_1 (1 - e_1) \tag{5-59}$$

We conclude that, when $V_e$ and $\gamma_e$ are both prescribed, for a given initial orbit, single-impulse deorbit is always possible if the following condition is satisfied

$$\frac{V_e}{\sqrt{\frac{\mu}{R}}} \geq \sqrt{\frac{2\alpha_1(1-e_1)\,[\alpha_1(1-e_1)-1]}{\alpha_1^2(1-e_1)^2-\cos^2\gamma_e}} \tag{5-60}$$

We now return to the case where only the entry angle $\gamma_e$ is prescribed. Then, there exists a family of deorbit trajectories initiating from a prescribed deorbit position D . Using the deorbit flight path angle $\gamma_2$ as a parameter for this family, we can calculate the elements of the descent trajectory selected. This can be obtained by expressing the entry speed $u_e$ in terms of the variables $\lambda$, $\gamma_e$, and $\gamma_2$ and then substituting into the equations obtained in section 5-2. For $u_e$ we have from Eq. (5-54)

$$u_e = \lambda \sqrt{\frac{2(\lambda-1)}{\lambda^2\cos^2\gamma_2-\cos^2\gamma_e}}\cos\gamma_2 \tag{5-61}$$

The deorbit speed $u_2$ is given by Eq. (5-45).

$$u_2 = \sqrt{\frac{2(\lambda-1)}{\lambda^2\cos^2\gamma_2-\cos^2\gamma_e}}\cos\gamma_e \tag{5-62}$$

The magnitude of the velocity impulse $\overrightarrow{\Delta u}$ , and its direction $\delta$ , are given by the Eqs. (5-11) and (5-12) respectively, with the initial speed given by Eq. (5-9) and the initial flight path angle by Eq. (5-10). The dimensionless semimajor axis of the descending trajectory is given by Eq. (5-13), written with the value of $u_e$ given by Eq. (5-61) as

$$\alpha_2 = \frac{\lambda^2\cos^2\gamma_2-\cos^2\gamma_e}{2(\lambda\cos^2\gamma_2-\cos^2\gamma_e)} \tag{5-63}$$

The eccentricity of the descending trajectory is given by Eq. (5-14). In terms of $\lambda$ , $\gamma_e$ and $\gamma_2$ , this is

$$e_2 = \sqrt{1-\frac{4\lambda(\lambda-1)(\lambda\cos^2\gamma_2-\cos^2\gamma_e)\cos^2\gamma_e\cos^2\gamma_2}{(\lambda^2\cos^2\gamma_2-\cos^2\gamma_e)^2}} \tag{5-64}$$

The longitude of periapsis of the descent trajectory is given by Eq. (5-23), where now the angle $\eta$ is given in terms of the selected variables as

$$\tan \eta = \frac{2(\lambda - 1)\cos^2 \gamma_e \tan \gamma_2}{[\lambda^2 - (2\lambda - 1)\cos^2 \gamma_e] - \cos^2 \gamma_e \tan^2 \gamma_2} \tag{5-65}$$

The polar equation of the entry trajectory is

$$r = \frac{p_2}{1 + e_2 \cos(\theta - \omega)} \tag{5-66}$$

where $e_2$ is given by Eq. (5-64) and

$$\frac{p_2}{R} = \frac{2\lambda(\lambda - 1)\cos^2 \gamma_e \cos^2 \gamma_2}{\lambda^2 \cos^2 \gamma_2 - \cos^2 \gamma_e} \tag{5-67}$$

The position of entry E is defined by its polar angle $\theta_E$ which is obtained by putting $r = R$, and $\theta = \theta_E$ in the polar Eq. (5-66).

## 5-5. MINIMUM IMPULSE FOR ENTRY AT GIVEN ANGLE

We have seen in the preceding section that, for an entry at a prescribed angle initiating from a prescribed deorbit position, there exists a family of descent trajectories which is a function of the deorbit angle $\gamma_2$. These trajectories are such that the terminus of the deorbit velocity $\overrightarrow{u_2}$ is on a hyperbola defined by Eq. (5-52). In this section we shall select from among the descent trajectories in this family the one that results in a minimum characteristic velocity $\Delta u$. That particular trajectory is called the optimum deorbit trajectory for a prescribed entry angle.

In the hodograph space (Fig. 5-6), consider a hyperbola, the locus of the terminus of $\overrightarrow{u_2}$ for a given entry angle $\gamma_e$. In this hodograph space, the initial velocity $\overrightarrow{u_1}$ is prescribed. Let $x_1$ and $y_1$ be the projections of $\overrightarrow{u_1}$ on the axes of the coordinates system $Dxy$. We have from Eqs. (5-9) and (5-10)

$$x_1 = u_1 \cos \gamma_1 = \sqrt{\frac{\alpha_1(1 - e_1^2)}{\lambda}}$$

$$y_1 = u_1 \sin \gamma_1 = \pm \sqrt{\frac{\lambda(2\alpha_1 - \lambda) - \alpha_1^2(1 - e_1^2)}{\lambda \alpha_1}} \tag{5-68}$$

The minus sign for $y_1$ is taken if the point D is on the second half of the initial orbit.

The minimum $\Delta u$ is obtained by finding the shortest distance from the point with coordinates $(x_1, y_1)$ to the hyperbola. Let superscript $(*)$ denote the optimum elements. The point with coordinates

$(x^*, y^*)$ giving the terminus of the optimum deorbit velocity $\overrightarrow{u_2}^*$ on the hyperbola defined by Eq. (5-52) is the point where the normal to the hyperbola passes through the point $(x_1, y_1)$.

Let the equation of this hyperbola be

$$f(x, y) = Ax^2 - By^2 - 1 = 0 \tag{5-69}$$

where A and B are defined by Eq. (5-53). The components of the normal to the hyperbola are given by

$$\frac{\partial f}{\partial x} = 2Ax$$

$$\frac{\partial f}{\partial y} = -2By \tag{5-70}$$

Requiring that this normal be collinear to the vector $\overrightarrow{\Delta u}$ gives

$$\frac{x - x_1}{Ax} = -\frac{y - y_1}{By} \tag{5-71}$$

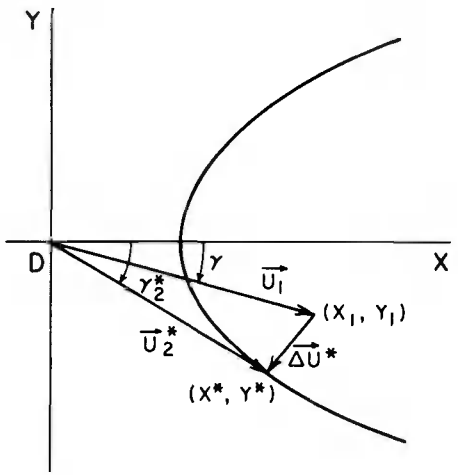


Fig. 5-6. Optimum velocity triangle for entry at given angle.

The set of Eqs. (5-69) and (5-71), gives the coordinates $(x^*, y^*)$, components of the optimum deorbit velocity $\overrightarrow{u_2}^*$.

It is convenient to use the deorbit angle $\gamma_2$ as the variable. Let

$$z \equiv \tan \gamma_2^* = \frac{y^*}{x^*} \tag{5-72}$$

be the tangent of the optimum deorbit angle. Then from Eqs. (5-71) and (5-72) we have

$$x^* = \frac{Ay_1 + Bx_1 z}{(A + B)z}$$

$$y^* = \frac{Ay_1 + Bx_1 z}{(A + B)} \tag{5-73}$$

Upon substituting into Eq. (5-69) we have a quartic equation in $z$

$$A_0 z^4 + A_1 z^3 + A_2 z^2 + A_3 z + A_4 = 0 \tag{5-74}$$

where the coefficients $A_i$ are given by

$$\begin{aligned} A_0 &\equiv B^3 x_1^2 \\ A_1 &\equiv 2AB^2 x_1 y_1 \\ A_2 &\equiv A^2 B y_1^2 - AB^2 x_1^2 + (A + B)^2 \\ A_3 &\equiv -2A^2 B x_1 y_1 \\ A_4 &\equiv -A^3 y_1^2 \end{aligned} \tag{5-75}$$

Hence, the optimum deorbit flight path angle is obtained by solving a quartic equation. In general, this equation gives four roots corresponding to four normals drawn from the point $(x_1, y_1)$ to the hyperbola defined by Eq. (5-69). One of these roots corresponds to the minimum of $\Delta u$.

The elements of the optimum deorbit trajectory can be easily obtained in terms of $z$ by using the general equations derived in the preceding section.

First the components of the deorbit velocity $\vec{u}_2^*$ are given by Eq. (5-73). Next, the minimum characteristic velocity is simply

$$\Delta u^* = \sqrt{(x^* - x_1)^2 + (y^* - y_1)^2} \tag{5-76}$$

The direction of $\vec{\Delta u}^*$ is the direction of the normal to the hyperbola which has components $(Ax^*, -By^*)$. Hence, if $\delta^*$ is the optimum angle of $\vec{\Delta u}^*$, measured from the x-axis, we have

$$\tan \delta^* = -\frac{B}{A} z = -\frac{z \cos^2 \gamma_e}{\lambda^2 - \cos^2 \gamma_e} \tag{5-77}$$

The entry speed is given by Eq. (5-61). Since

$$\cos^2 \gamma_2^* = \frac{1}{1 + \tan^2 \gamma_2^*} = \frac{1}{1 + z^2}$$

then

$$u_e^* = \lambda \sqrt{\frac{2(\lambda - 1)}{\lambda^2 - (1 + z^2)\cos^2 \gamma_e}} \tag{5-78}$$

The optimum deorbit speed is given by Eq. (5-62) written as

$$u_2^* = \sqrt{\frac{2(\lambda - 1)(1 + z^2)}{\lambda^2 - (1 + z^2)\cos^2 \gamma_e}} \cos \gamma_e \tag{5-79}$$

The dimensionless semimajor axis of the optimum deorbit trajectory is given by Eq. (5-63). We have

$$\alpha_2^* = \frac{\lambda^2 - (1 + z^2)\cos^2 \gamma_e}{2[\lambda - (1 + z^2)\cos^2 \gamma_e]} \tag{5-80}$$

The eccentricity of this orbit is

$$e_2^* = \sqrt{1 - \frac{4\lambda(\lambda - 1)[\lambda - (1 + z^2)\cos^2 \gamma_e]\cos^2 \gamma_e}{[\lambda^2 - (1 + z^2)\cos^2 \gamma_e]^2}} \tag{5-81}$$

The longitude of periapsis of the optimum deorbit trajectory is given by Eq. (5-23) with the angle $\eta$ expressed in terms of $\lambda$, $\gamma_e$ and $z$ as

$$\tan \eta = \frac{2(\lambda - 1) z \cos^2 \gamma_e}{[\lambda^2 - (2\lambda - 1)\cos^2 \gamma_e] - z^2 \cos^2 \gamma_e} \tag{5-82}$$

The polar equation of the entry orbit is given by Eq. (5-66) where $e_2$ is given by Eq. (5-81) and

$$\frac{p_2^*}{R} = \frac{2\lambda(\lambda - 1)\cos^2 \gamma_e}{\lambda^2 - (1 + z^2)\cos^2 \gamma_e} \tag{5-83}$$

The position of entry E is defined by its polar angle $\theta_E$ which is obtained by putting $r = R$ and $\theta = \theta_E$ in the polar Eq. (5-66).

The formulae (5-78) - (5-83) are expressed in terms of the variable $z = \tan \gamma_2^*$, solution of the quartic equation (5-74). By using, instead of $z$, the components $x^*$ and $y^*$ of the optimum deorbit velocity $\vec{u}_2^*$ as given by the Eqs. (5-73), we have the following alternate formulae.

The optimum deorbit speed is

$$u_2^* = \sqrt{x^{*2} + y^{*2}} \tag{5-84}$$

Hence, we have from Eq. (5-44) for the entry speed

$$u_e^* = \sqrt{x^{*2} + y^{*2} + 2(\lambda - 1)} \tag{5-85}$$

Also, from Eq. (5-13)

$$\alpha_2 = \frac{\lambda}{2 - (x^{*2} + y^{*2})} \tag{5-86}$$

The eccentricity is obtained from Eq. (5-14). With the aid of Eqs. (5-51) and (5-85), it is seen that

$$e_2^* = \sqrt{(x^{*2} - 1)^2 + x^{*2} y^{*2}} \tag{5-87}$$

For the angle $\eta$ in the evaluation of the longitude of periapsis of the optimum deorbit trajectory through Eq. (5-23), we rewrite Eq. (5-22)

$$\tan \eta = \frac{u_2^2 \tan \gamma_2}{(1 - u_2^2) + \tan^2 \gamma_2}$$

Then, using the Eqs. (5-72) and (5-84) to simplify the expression

$$\tan \eta = \frac{x^* y^*}{1 - x^{*2}} \tag{5-88}$$

Finally,

$$\frac{p_2^*}{R} = \alpha_2^* (1 - e_2^{*2})$$

or using Eqs. (5-86) and (5-87),

$$\frac{p_2^*}{R} = \lambda x^{*2} \tag{5-89}$$

## 5-6. DESCENT TRAJECTORY FOR A GIVEN ENTRY POSITION

In this section we shall consider the family of descent trajectories initiated from the deorbit position D and intersecting the atmosphere at a prescribed position E . This entry position can be defined by the range angle $\phi$ measured from the initial position vector $\overrightarrow{OD}$ (Fig. 5-7).

Let $u_2$ be the deorbit speed and $\gamma_2$ the deorbit flight path angle at the point D . They are the initial speed and flight path angle for the descending trajectory $\mathcal{E}_2$ . The equation relating the initial speed, flight path angle, radial distance and range angle has been derived in Chapter 3 , Eq. (3-86). We rewrite this equation, using subscript 2 to replace subscript B

$$\frac{(1-\cos\phi)}{u_2^2}\tan^2\gamma_2 - \sin\phi\tan\gamma_2 + \frac{(1-\cos\phi)}{u_2^2} + \cos\phi - \lambda = 0 \tag{5-90}$$

In the hodograph space Dxy as defined in section 5-2, let x and y be the projection of the deorbit velocity $\overrightarrow{u_2}$ on the axes

$$\begin{aligned} x &= u_2\cos\gamma_2 \\ y &= u_2\sin\gamma_2 \end{aligned} \tag{5-91}$$

Hence,

$$\begin{aligned} u_2^2 &= x^2 + y^2 \\ \tan\gamma_2 &= \frac{y}{x} \end{aligned} \tag{5-92}$$

By substituting Eq. (5-92) into Eq. (5-90) and rearranging, we have

$$(\lambda - \cos\phi)\,x^2 + (\sin\phi)xy - (1-\cos\phi) = 0 \tag{5-93}$$

In the velocity coordinates system Dxy , this equation is the equation of a hyperbola having the asymptotes

$$\begin{aligned} x &= 0 \\ y &= -\frac{(\lambda-\cos\phi)}{\sin\phi}\,x \end{aligned} \tag{5-94}$$

Hence, the first asymptote is the y-axis. For a geometric interpretation of the second asymptote, we consider the triangle ODE , and evaluate the tangent of the angle ODE . Let E' be the projection of the point E on the axis OD . Then

$$\tan \measuredangle ODE = \frac{EE'}{DE'} = \frac{R \sin\phi}{r_D - R\cos\phi}$$

Hence,

$$\tan \measuredangle ODE = \frac{\sin\phi}{\lambda - \cos\phi} \tag{5-95}$$

Thus, the second asymptote of the hyperbola given by Eq. (5-93) is the line DE .

Equation (5-93) shows that, for the descent trajectory initiated from the point D , to intersect the atmosphere at a prescribed position E defined by the range angle $\phi$ , the terminus of the deorbit velocity $\overrightarrow{u_2}$ must be on that hyperbola. When the terminus of the vector $\overrightarrow{u_2}$ moves on that hyperbola, it generates a family of descent trajectories. Using the deorbit flight path angle $\gamma_2$ as the parameter for this family, we can calculate the elements of the descent orbit in terms of $\lambda$ , $\phi$ and $\gamma_2$ . Let

$$z \equiv \tan\gamma_2 \tag{5-96}$$

Then, if x and y are the components of the deorbit velocity $\overrightarrow{u_2}$ in the Dxy axis system,

$$y = xz \tag{5-97}$$

By substituting into Eq. (5-93) and solving for x , we have

$$x = \sqrt{\frac{(1-\cos\phi)}{(\lambda - \cos\phi) + z\sin\phi}} \tag{5-98}$$

and therefore

$$y = z\sqrt{\frac{(1-\cos\phi)}{(\lambda - \cos\phi) + z\sin\phi}} \tag{5-99}$$

The deorbit speed can be obtained by directly solving Eq. (5-90).

$$u_2 = \sqrt{\frac{(1-\cos\phi)(1+z^2)}{(\lambda - \cos\phi) + z\sin\phi}} \tag{5-100}$$

For the other elements of the descent trajectory, we only need to evaluate the entry speed $u_e$ in terms of $\lambda$ , $\phi$ and $z = \tan\gamma_2$ , and then substitute into the equations derived in section 5-2. From Eq. (5-7) we obtain

$$u_e = \sqrt{2(\lambda - 1) + \frac{(1-\cos\phi)(1+z^2)}{(\lambda - \cos\phi) + z\sin\phi}} \tag{5-101}$$

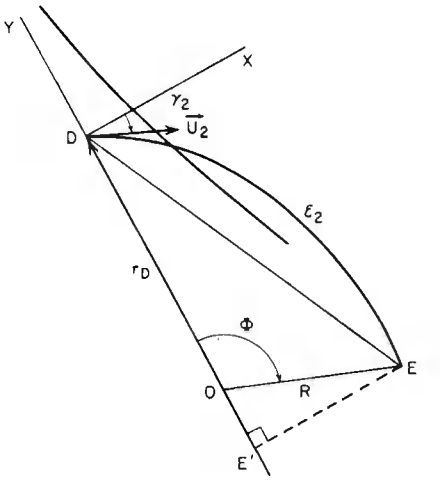


Fig. 5-7. The hyperbola which is the locus of the terminus of the deorbit velocity for entry at given position.

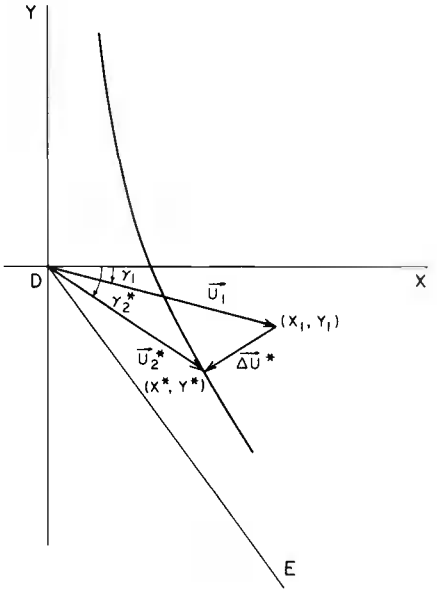


Fig. 5-8. Optimum velocity triangle for entry at given position.

The impulsive change in the velocity $\overrightarrow{\Delta u}$ , and its direction $\delta$ , are given by Eqs. (5-11) and (5-12), respectively, with the initial speed given by Eq. (5-9) and the initial flight path angle by Eq. (5-10).

The entry flight path angle is given by Eq. (5-17). We have

$$\cos\gamma_e = \frac{\lambda}{u_e}\sqrt{\frac{u_e^2 + 2(1-\lambda)}{(1+z^2)}} \tag{5-102}$$

where $u_e$ is given by Eq. (5-101). The dimensionless semimajor axis of the descent orbit is given by Eq. (5-13), written with the value of $u_e$ given by Eq. (5-101) as

$$\alpha_2 = \frac{\lambda\left[(\lambda - \cos\phi) + z\sin\phi\right]}{(2\lambda - 1) - \cos\phi + 2z\sin\phi - (1-\cos\phi)z^2} \tag{5-103}$$

The eccentricity of the descent orbit is given by Eq. (5-14).

$$e_2 = \frac{\sqrt{2(1-\cos\phi)z^2 + 2(\lambda-1)z\sin\phi + (\lambda-1)^2}}{\left[(\lambda - \cos\phi) + z\sin\phi\right]} \tag{5-104}$$

The longitude of periapsis of the descent orbit is given by Eq. (5-23) where now the angle $\eta$ is given in terms of the selected variables as

$$\tan\eta = \frac{(1-\cos\phi)z}{(\lambda - 1) + z\sin\phi} \tag{5-105}$$

The polar equation of the entry orbit is

$$r = \frac{p_2}{1 + e_2\cos(\theta - \omega)} \tag{5-106}$$

where $e_2$ is given by Eq. (5-104) and

$$\frac{p_2}{R} = \frac{\lambda(1-\cos\phi)}{(\lambda - \cos\phi) + z\sin\phi} \tag{5-107}$$

The position of entry E is, of course, specified by the prescribed range angle $\phi$ .

## 5-7. MINIMUM IMPULSE FOR ENTRY AT GIVEN POSITION

We have seen in the preceding section that, for an entry at a prescribed position, initiating from a given point D on the initial orbit, there exists a family of descent trajectories which is a function of the deorbit flight path angle $\gamma_2$ . These trajectories are such that the terminus of the deorbit velocity $\vec{u}_2$ is on a branch of hyperbola defined by Eq. (5-93). In this section we shall select from among the descent trajectories in this family the one that results in a minimum characteristic velocity $\Delta u$ . That particular trajectory is called the optimum deorbit trajectory for a prescribed entry position.

In the hodograph space (Fig. 5-8), consider the hyperbola which is the locus of the terminus of $\vec{u}_2$ for a given entry position defined by the range angle $\phi$ . In this hodograph space, the initial velocity $\vec{u}_1$ is prescribed. Its projections $x_1$ and $y_1$ on the axis system Dxy are given by Eq. (5-68).

As for the problem of minimum impulse for entry at a given angle solved in section 5-5, we obtain the minimum of $\Delta u$ by finding the shortest distance from the point with coordinates $(x_1 , y_1)$ to the hyperbola defined by Eq. (5-93).

Again, let superscript (*) denote the optimum elements. The point with coordinates $(x^* , y^*)$ on the hyperbola giving the terminus of the optimum deorbit velocity $\vec{u}_2^*$ is the point where the normal to the hyperbola passes through the point $(x_1 , y_1)$ . We write the equation of this hyperbola

$$f(x, y) = (\lambda - \cos\phi)\, x^2 + (\sin\phi)\, xy - (1 - \cos\phi) = 0 \qquad (5\text{-}108)$$

The components of the normal to the hyperbola are given by

$$\frac{\partial f}{\partial x} = 2(\lambda - \cos\phi)\, x + y \sin\phi$$

$$\frac{\partial f}{\partial y} = x \sin\phi \qquad (5\text{-}109)$$

Requiring that this normal be collinear to the vector $\vec{\Delta u}$ gives

$$\frac{x - x_1}{2(\lambda - \cos\phi)\, x + y \sin\phi} = \frac{y - y_1}{x \sin\phi} \qquad (5\text{-}110)$$

The set of equations (5-108) and (5-110) gives the coordinates $(x^* , y^*)$ , components of the optimum deorbit velocity $\vec{u}_2^*$ . It is convenient to use the variable z as defined by Eq. (5-96). Then the components of the vector $\vec{u}_2$ are given in terms of z by Eqs. (5-98) and (5-99). Upon substituting these equations into Eq. (5-110) and rearranging we have a quartic equation in z

$$B_0 z^4 + B_1 z^3 + B_2 z^2 + B_3 z + B_4 = 0 \qquad (5\text{-}111)$$

where the coefficients $B_i$ are

$$
\begin{aligned}
B_0 &\equiv (1 - \cos\phi)\sin^2\phi \\
B_1 &\equiv 4(1 - \cos\phi)(\lambda - \cos\phi)\sin\phi - y_1^2 \sin^3\phi \\
B_2 &\equiv 2(1 - \cos\phi)(2\lambda^2 - 4\lambda\cos\phi + 3\cos^2\phi - 1) \\
&\quad + 2x_1 y_1 \sin^3\phi - 5y_1^2(\lambda - \cos\phi)\sin^2\phi \\
B_3 &\equiv -4(1 - \cos\phi)(\lambda - \cos\phi)\sin\phi - x_1^2 \sin^3\phi \\
&\quad + 6x_1 y_1 (\lambda - \cos\phi)\sin^2\phi - 8y_1^2(\lambda - \cos\phi)^2 \sin\phi \\
B_4 &\equiv (1 - \cos\phi)\sin^2\phi - x_1^2(\lambda - \cos\phi)\sin^2\phi \\
&\quad + 4x_1 y_1(\lambda - \cos\phi)^2 \sin\phi - 4y_1^2(\lambda - \cos\phi)^3
\end{aligned}
\tag{5-112}
$$

Hence, the optimum deorbit flight path angle is obtained by solving a quartic equation. In general, this equation gives four roots corresponding to four normals drawn from the point $(x_1, y_1)$ to the hyperbola given by Eq. (5-93). One of these roots corresponds to the minimum of $\Delta u$.

The elements of the optimum deorbit trajectory are obtained by using the value of $z$ computed from the quartic equation (5-111) in the general equations for descending trajectory derived in the previous section.

By using, instead of $z$, the components $x^*$ and $y^*$ of the optimum deorbit velocity $\vec{u}_2^*$ as computed from Eqs. (5-98) and (5-99), we also can calculate the elements of the descending trajectory using the alternate formulas, Eqs. (5-84) - (5-89).

## References


1. Fosdick, G. E., and Anthony, M. L., "Three-Dimensional Pulse Optimization for Vehicles Disorbiting from Circular Orbits," Research Report No. R-61-13, The Martin Company, Denver, 1961.

2. Vinh, N. X., "A Geometrical Study of Re-Entry Transfer Orbits," ARL Report, USAF, No. 63-241, December 1963.

3. Busemann, A., Vinh, N. X., and Culp, R. D., "Geometric Constraints of the Disorbit Problem," AAS preprint No. 66-122, First Space Flight Mechanics Specialist Conference, Denver, July 1966. Conference Proceedings, Vol. 11 in the AAS Series in Sciences and Technology.

4. Busemann, A., and Vinh, N. X., "Geometric Theory of Optimum Disorbit Problems," NASA CR-750, April 1967.

# Chapter 6

# Basic Equations for Planar Entry Trajectories

## 6-1. INTRODUCTION

In Chapter 5 we considered the trajectory of the vehicle from the deorbit position D to the entry position E . This point E is assumed to be at the top of the sensible atmosphere. Thus, until now, the trajectory has been analyzed for flight in a vacuum. From here on , this text will treat the portion of the flight path beyond the point E , referred to as the entry trajectory.

Along the entry trajectory, the aerodynamic force is no longer negligible. In fact, it plays an important role as a braking force to reduce the speed of the vehicle to the point such that the terminal phase of the flight before landing can be conducted as a vertical free fall using a system of parachutes for soft landing for vehicles with no lift capability, or as a gliding flight at low speed as an ordinary airplane for vehicles which can generate aerodynamic lift.

## 6-2. ENERGY DISCUSSION OF THE TRAJECTORY IN PHASE SPACE

The equations of motion of a vehicle flying in a Newtonian gravitational force field and subject to thrust and aerodynamic force were derived in Chapter 2, Eqs. (2-28) and (2-32). We shall assume that along the fundamental part of the entry trajectory where the deceleration undergoes rapid change, the engine is shut off at all times. Hence, with $T = 0$ , and using Eqs. (4-4) for the lift and drag forces, we have the planar equations of motion in the plane of a great circle (Fig. 6-1).

$$\frac{dV}{dt} = -\frac{\rho S C_D V^2}{2m} - g(r)\sin\gamma$$

$$V\frac{d\gamma}{dt} = \frac{\rho S C_L V^2}{2m} - \left[g(r) - \frac{V^2}{r}\right]\cos\gamma$$

$$\frac{dr}{dt} = V\sin\gamma \qquad (6\text{-}1)$$

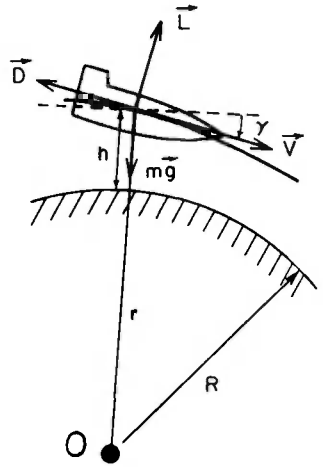


Fig. 6-1. Geometry of the entry trajectory.

where $V$ is the speed of the vehicle, $\gamma$ the flight path angle measured from the local horizontal, positively up, and $r$ the radial distance from the center of the planet. The atmospheric density $\rho$ and the acceleration of gravity $g$ are, in general, functions of the distance $r$.

$$\rho = \rho(r) \quad , \quad g = g(r) \tag{6-2}$$

The reference area $S$ has some conventional value, used to evaluate the lift coefficient $C_L$ and the drag coefficient $C_D$. In general, these coefficients are functions of the angle of attack $\alpha$, the Mach number $M$, and the Reynolds number $R_e$

$$C_L = C_L(\alpha, M, R_e)$$

$$C_D = C_D(\alpha, M, R_e) \tag{6-3}$$

In hypersonic flight however, it is generally assumed that $C_L$ and $C_D$ are functions of the angle of attack only.

For a given vehicle, if the initial conditions are prescribed, $r = r_o$, $V = V_o$, and $\gamma = \gamma_o$ at $t = 0$, and if a flight program is prescribed by specifying the angle of attack function $\alpha = \alpha(t)$, then with Eqs. (6-2) and (6-3), the system of equations (6-1) can be integrated, at least numerically, giving the time histories of the variables $r(t)$, $V(t)$, and $\gamma(t)$. In the following we shall mainly interest ourselves in the flight program of constant $\alpha$. In this case the coefficients $C_L$ and $C_D$ in Eqs. (6-1) are constants.

It is convenient to write the Eqs. (6-1) in nondimensional form. For this purpose, let $r_o$ be a reference radial distance. Frequently $r_o$ is taken as the radius of the planet, assumed homogeneous and spherical, but for reasons which shall be clearly justified later, we shall take $r_o$ as the initial radial distance. We define the dimensionless variables

$$u \equiv \frac{1}{2}\left(\frac{V^2}{g_o r_o}\right) \quad , \quad z \equiv \frac{r_o}{r} \tag{6-4}$$

where $u$ is the dimensionless kinetic energy, and, for a Newtonian force field, $z$ is the negative of the potential energy. The acceleration of gravity is then

$$g = g_o \left(\frac{r_o}{r}\right)^2 \tag{6-5}$$

where $g_o$ is the acceleration of the gravity at the reference distance. With $r_o$ as the initial distance, the initial value of $z$ is $z_o = 1$.

Using $z$ as the new independent variable, we eliminate the time and rewrite Eqs. (6-1) as

$$\frac{du}{dz} = \frac{r_o \rho S C_D u}{m z^2 \sin\gamma} + 1$$

$$\frac{d\phi}{dz} = \frac{r_o \rho S C_L}{2m z^2} + \left(\frac{1}{z} - \frac{1}{2u}\right)\phi \tag{6-6}$$

where

$$\phi \equiv \cos\gamma \tag{6-7}$$

The system of Eqs. (6-6) constitutes the exact equations for flight in a Newtonian force field, subject to aerodynamic forces. Its integration requires specifying the law of variation for the atmospheric density, $\rho$, as a function of the independent variable $z$.

The system of Eqs. (6-6) is exact. Hence, for flight in a vacuum, that is when $\rho \to 0$, we expect to obtain the trajectory in the form of a Keplerian orbit. Putting $\rho = 0$ in the Eqs. (6-6), we have the system

$$\frac{du}{dz} = 1$$

$$\frac{d\phi}{dz} = \left(\frac{1}{z} - \frac{1}{2u}\right)\phi \tag{6-8}$$

Integrating the first equation yields the vis viva integral

$$u = z + C \tag{6-9}$$

where $C$ is a constant representing the total energy. Substituting this relation into the second equation (6-8) and integrating gives

$$\sigma \equiv \frac{\phi\sqrt{u}}{z} = K \tag{6-10}$$

where $K$ is a new constant of integration.

The definitions (6-4) and (6-7) of $u$, $z$, and $\phi$ show that

$$\sigma = \frac{rV\cos\gamma}{\sqrt{2g_o r_o^3}} \tag{6-11}$$

Hence, Eq. (6-10) is a statement of the conservation of angular momentum for flight in a vacuum.

The Keplerian trajectory can be conveniently visualized in the cylindrical coordinate space ($z$, $\sigma$, $u$) (Fig. 6-2).

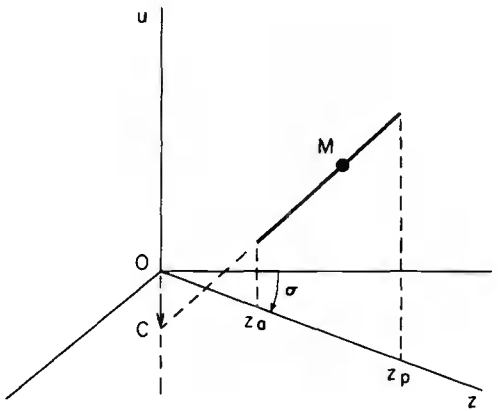


Fig. 6-2. Drag-free trajectory in phase space.

The trajectory is in the plane $\sigma$ = constant. In this plane, it is a segment of a straight line representing the equation (6-9). This line makes an angle of 45° with the $u$ axis (Fig. 6-3). By the definitions (6-4) of $u$ and $z$, the trajectory lies in the positive ($u$, $z$) space. When $C < 0$, it is an ellipse, and the radial distance is bounded. The variable $z$ oscillates between a minimum $z_a$ corresponding to the apogee distance, and a maximum $z_p$ corresponding to the perigee distance. On the other hand, the kinetic energy is a minimum where the radial distance is maximum, and it is a maximum for a minimum of $r$. When $C = 0$, the trajectory is a parabola, and since $z_a = 0$, the maximum distance is infinity. At the point at infinity, the kinetic energy of the system is zero. When $C > 0$, the trajectory is a hyperbola. But, at the point at infinity where the potential energy is zero, there is a residual kinetic energy equal to $C$.

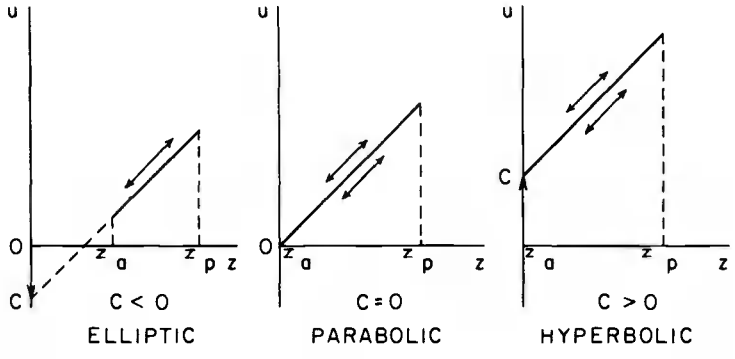


Fig. 6-3. Three types of Keplerian orbits.

When $\rho \neq 0$ , the total energy and the angular momentum are no longer constant. Still, it is possible to discuss the variations of these quantities and have some insight into the behavior of the trajectory by considering the phase space $(z\ ,\ \sigma\ ,\ u)$ .

Let $\xi$ be the vehicle total energy when aerodynamic force is encountered. We have

$$\xi = u - z \tag{6-12}$$

From the first equation (6-6)

$$\frac{d\xi}{dz} = \frac{r_o \rho S C_D u}{m z^2 \sin\gamma} \tag{6-13}$$

From the last equation (6-1), it follows that

If $\sin\gamma > 0$ , r increases and z decreases.

If $\sin\gamma < 0$ , r decreases and z increases.

In both cases the total energy, $\xi$ , of the system is decreasing, as seen in Eq. (6-13). Hence, $\xi$ is a convenient dimensionless independent variable.

On the other hand, the definition (6-10) of the angular momentum, $\sigma$ , show that

$$\frac{d\sigma}{dz} = \frac{\sqrt{u}}{z}\frac{d\phi}{dz} + \frac{\phi}{2z\sqrt{u}}\frac{du}{dz} - \frac{\phi\sqrt{u}}{z^2}$$

With the aid of the equations (6-6) we have

$$\frac{d\sigma}{dz} = \frac{r_o \rho S \sqrt{u}}{2mz^3}\left(C_L + \frac{C_D}{\tan\gamma}\right) \tag{6-14}$$

If $\tan\gamma < 0$ , $z$ increases. Thus, for the angular momentum to decrease, the condition

$$C_L + \frac{C_D}{\tan\gamma} < 0 \tag{6-15}$$

must be satisfied. If high lift is developed, for example in the case of a pull-up maneuver, the condition may be violated, and the angular momentum can increase. On the other hand, if $\tan\gamma > 0$ , $z$ decreases. Then, decreasing angular momentum requires that

$$C_L + \frac{C_D}{\tan\gamma} > 0 \tag{6-16}$$

The condition is always satisfied for positive lift. But for large negative lift, the angular momentum can increase.

Thus, we have obtained some very general conclusions for the variations of the total energy and of the angular momentum of the dynamical system representing the motion of the vehicle without regard to a specific law of variation for the atmospheric density. These criteria are very useful for the qualitative discussion of the asymptotic behavior of the dynamical system represented by the point $M$ in the phase space (Fig. 6-2). For example, if we consider the trajectory of a satellite starting out at very high altitude, with an initially elliptic orbit, and subject to aerodynamic force besides the gravitational force, then first we see that, in the phase space $(z, \sigma, u)$ , the point $M$ is constantly on a ruled surface generated by the equations

$$\begin{aligned} \sigma &= \sigma(t) \\ u &= z + \xi(t) \end{aligned} \tag{6-17}$$

with $\xi(t)$ being a decreasing function of the time $t$ . Let $R$ be the radius of the planet. By the physical constraint $r > R$ , in the phase space of Fig. (6-2) , both $z_a$ and $z_p$ tend to $r_o/R$ with

$$z_a \leq \frac{r_o}{R} \leq z_p$$

Also, since $u > 0$ , the limit of $\xi$ is

$$\xi(t_o) \geq \xi(t) \geq -\max z_p$$

Furthermore, for a vehicle with no lift capability, putting $C_L = 0$ and dividing Eq. (6-13) by Eq. (6-14), gives

$$\frac{d\xi}{d\sigma} = \frac{2z\sqrt{u}}{\phi}$$

which is, using definition (6-10)

$$\frac{d\xi}{d\sigma} = \frac{2u}{\sigma} \tag{6-18}$$

This shows that the angular momentum $\sigma(t)$ is also decreasing.

## 6-3. THE FUNDAMENTAL EQUATIONS

The system of nonlinear differential equations (6-6) can be integrated for any specified vehicle from a prescribed initial condition, once the law of variation of the atmospheric density is known. We shall assume an exponential atmosphere of the form

$$\rho = \rho_s e^{-\beta h} \tag{6-19}$$

where $h$ is the altitude above the surface of the planet

$$h = r - R \tag{6-20}$$

with $R$ being the radius of the planet. $\beta$ is the reciprocal of the scale height and $\rho_s$ is the atmospheric density at the surface. Using an average value for $\beta$ in the altitude range of interest, we can treat it as essentially a constant.

For an analytic integration of the equations of motion, we introduce an altitude variable $\eta$ proportional to the atmospheric density

$$\eta = \frac{\rho S C_D}{2m\beta} \tag{6-21}$$

Then using the exponential law, Eq. (6-19)

$$\frac{d\eta}{\eta} = -\beta\, dr = \frac{\beta r_o}{z^2}\, dz \tag{6-22}$$

With this change of variable Eqs. (6-6) are transformed into

$$\begin{aligned} \frac{du}{d\eta} &= \frac{2u}{\sin\gamma} + \frac{z^2}{\beta r_o \eta} \\ \frac{d\phi}{d\eta} &= \frac{C_L}{C_D} - \frac{z^2}{\beta r_o \eta}\left(\frac{1}{2u} - \frac{1}{z}\right)\phi \end{aligned} \tag{6-23}$$

This system is the fundamental system of equations for planar entry trajectories. The system is exact in the sense that the equations are valid for flight in a Newtonian force field. The atmosphere is specified by prescribing the value of $\beta r_o$ as shown in Table 1-2 (e.g., $\beta r_o = 900$ for the Earth's atmosphere). The flight parameter is specified by the constant lift-to-drag ratio, $C_L / C_D$. For the

integration of the entry equations, the values $u_o$, $\eta_o$ and $\gamma_o$ at the initial time are given. Rigorously speaking, the variable $z = r/r_o$ in the equations can be expressed in terms of the atmospheric density $\eta$ through Eq. (6-21). This will require the specification of the drag parameter, that is the value of $SC_D/m\beta$. A simplification can be made by noticing that in the fundamental equations, Eq. (6-23), the variable $\eta$ which is proportional to the atmospheric density undergoes strong variation while within the relatively thin layer of the atmosphere, as compared to the radius of the planet, we have for all practical purpose $z = r/r_o \approx 1$. Mathematically, this can be clearly seen in Eq. (6-22) by noticing that the value of $\beta r_o$ is large, of the order of $10^3$. With this simplification, we are led to the basic equations for atmospheric entry

$$\frac{du}{d\eta} = \frac{2u}{\sin\gamma} + \frac{1}{\beta r_o \eta}$$

$$\frac{d\phi}{d\eta} = \frac{C_L}{C_D} - \frac{1}{\beta r_o \eta}\left(\frac{1}{2u} - 1\right)\phi \qquad (6\text{-}24)$$

One characteristic feature with these equations is that for entry from very high altitude, we have $\eta_o \approx 0$. Hence, besides the values for the atmospheric parameter, $\beta r_o$, and lift-to-drag ratio, $C_L/C_D$, we only need to specify the initial values $u_o$ and $\gamma_o$ for the integration without regard to other physical characteristics of the vehicle. In other words, for a given planetary atmsophere, using the same lift-to-drag ratio $C_L/C_D$, with the same initial condition in $u_o$ and $\gamma_o$, the relationships between $u$, $\gamma$ and $\eta$ are the same regardless of the mass, size and shape of the vehicle. The only difference is that the actual altitude during entry, for any specified vehicle, is ultimately computed by Eq. (6-21) for the corresponding drag parameter.

The basic equations we have derived are adequate for a preliminary analysis of the phenomena encountered during atmospheric entry of a hypervelocity vehicle. This will be done in Chapters 7, 8 and 9. In Chapter 7, first order solutions for planetrary entry will be obtained. A second order theory for entry trajectories as developed by Loh will be the subject of Chapter 8. Chapter 9 concerns the aerodynamic heating during entry. The rest of the text will be devoted to more sophisticated theories for planetary entry.

## References

1. Vinh, N. X., and Brace, F., "An Energy Approach to Atmospheric Entry," Lecture notes, University of Michigan, 1972.

2. Vinh, N. X., Busemann, A., and Culp, R. D., "Optimum Three-Dimensional Atmospheric Entry," Acta Astronautica, Vol. 2, pp. 593-611, 1975.

3. Loh, W. H. T., Dynamics and Thermodynamics of Planetary Entry, Prentice Hall, Inc., Englewood Cliffs, New Jersey, 1963.

# Chapter 7

# Analysis of First-Order Planetary Entry Solutions

## 7-1. INTRODUCTION

To help in the understanding of the basic physical phenomena encountered by a vehicle during its descent through a planetary atmosphere, in this chapter we shall derive several first-order solutions for planetary entry by making, separately for each case, the necessary physical assumptions. Each type of trajectory will be analyzed in detail. In particular, we shall be concerned with the variations during the entry of the altitude, the speed, and the acceleration of the vehicle. Other physical quantities associated with the dynamic pressure over the vehicle, and the heating phenomena will be analyzed in Chapter 9. The study of the physical quantities associated with an entry trajectory is important since not only the knowledge of the variations of these quantities is of great assistance in the preliminary planning of the design of a specific type of entry vehicle, but also it provides the basic information with which one can construct new and accurate theories for analyzing entry trajectories.

For convenience, we recall the basic equations for entry trajectories in the plane of a great circle

$$\frac{du}{d\eta} = \frac{2u}{\sin\gamma} + \frac{1}{\beta r_o \eta}$$

$$\frac{d\phi}{d\eta} = \frac{C_L}{C_D} - \frac{1}{\beta r_o \eta}\left(\frac{1}{2u} - 1\right)\phi \qquad (7\text{-}1)$$

where $\beta r_o$ is a constant and by definition

$$u \equiv \frac{1}{2}\left(\frac{V^2}{g_o r_o}\right), \quad \phi \equiv \cos\gamma \qquad (7\text{-}2)$$

while $r_o$ is the initial distance from the center of the planet and $g_o$ is the acceleration of gravity at this reference level. The equations were obtained by assuming that, at each instant, $r = R + h \approx r_o$, where R is the radius of the planet and h is the flight atltitude. The altitude is obtained through the variation of the density of the atmosphere

which is related to the dimensionless variable $\eta$ by the relation

$$\eta \equiv \frac{SC_D\rho_s}{2m\beta} e^{-\beta h} \tag{7-3}$$

It is generally assumed, in first-order theory, that the component of the gravity along the tangent to the flight path can be neglected compared to the drag. This is equivalent to neglecting the second term on the right-hand side of the first equation (7-1). Hence, we write it as

$$\frac{du}{d\eta} = \frac{2u}{\sin\gamma} \tag{7-4}$$

The second equation (7-1) is maintained in its general form. We rewrite it with the physical meaning of each term

$$\frac{d\phi}{d\eta} = \underbrace{\frac{C_L}{C_D}}_{\text{lift force}} - \frac{1}{\beta r_o \eta}\Big(\underbrace{\frac{1}{2u}}_{\text{gravity force}} - \underbrace{1}_{\text{centrifugal force}}\Big)\phi \tag{7-5}$$

Two quantities of interest along an entry trajectory are the distance traveled, and the deceleration. First, we have

$$\frac{ds}{dt} = V \tag{7-6}$$

where $s$ is the arc length travelled since the initial time. On the other hand, the equation for the speed $V$ with the tangential component of the gravity $g\sin\gamma$, neglected is

$$\frac{dV}{dt} = -\frac{\rho SC_D V^2}{2m} \tag{7-7}$$

Hence,

$$\frac{dV}{ds} = -\frac{\rho SC_D V}{2m} \tag{7-8}$$

Using the definitions (7-2) and (7-3) for $u$ and $\eta$, we have

$$\frac{d}{du}\left(\frac{s}{r_o}\right) = -\frac{1}{2\beta r_o \eta u} \tag{7-9}$$

This equation, upon integration, gives the distance travelled along the flight path. The tangential deceleration is simply

$$a = -\frac{dV}{dt} \tag{7-10}$$

Using Eq. (7-7), in dimensionless form, we have

$$\frac{a}{g_o} = 2\beta r_o \eta u \tag{7-11}$$

Another quantity of interest is the time of flight. It is obtained by integrating Eq. (7-7). In dimensionless form, it is

$$\frac{d}{du}\left(\sqrt{\frac{2g_o}{r_o}}\, t\right) = -\frac{1}{2\beta r_o \eta u^{3/2}} \tag{7-12}$$

The following sections discuss the integration of the equations of motion given above under various approximations relative to the nature of the entry trajectories.

## 7-2. GLIDING ENTRY AT SMALL FLIGHT PATH ANGLES

The main assumption for this type of entry trajectory is that the flight path angle is small, that is

$$\sin\gamma \approx \gamma \,, \quad \cos\gamma \approx 1 \tag{7-13}$$

If in Eq. (7-5) we consider the variation of $\phi = \cos\gamma$ as negligibly small, this leads to the assumption of equilibrium glide at small flight path angles as first formulated by Sänger and Bredt (Ref. 1). We have

$$\frac{C_L}{C_D} - \frac{1}{\beta r_o \eta}\left(\frac{1}{2u} - 1\right) = 0 \tag{7-14}$$

Solved for $u$, this is

$$u = \frac{1}{2[\,1 + \beta r_o (C_L/C_D)\,\eta\,]} \tag{7-15}$$

On the other hand, if $u$ is used as the independent variable, the variation in the altitude is given by

$$\beta r_o \eta = \frac{(1-2u)}{2(C_L/C_D)\,u} = \frac{1 - (V^2/g_o r_o)}{(C_L/C_D)(V^2/g_o r_o)} \tag{7-16}$$

Figure 7-1 gives the plot of $1/\beta r_o \eta$ versus $V/\sqrt{g_o r_o}$ for different values of the lift-to-drag ratio, $C_L/C_D$. The ordinate of the figure varies as the altitude. It is seen that the speed decreases as the altitude decreases during the glide.

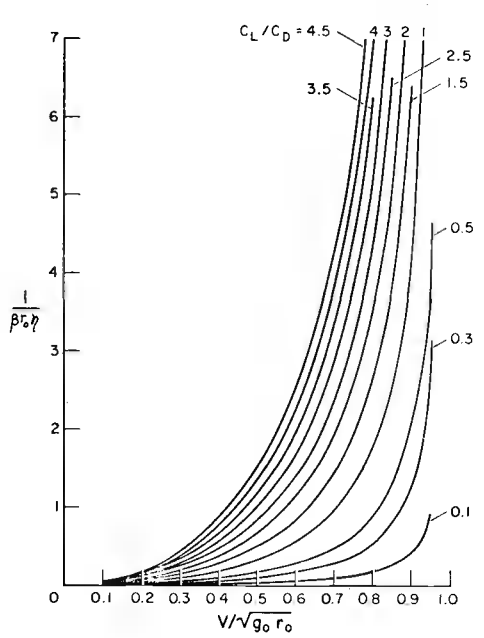


Fig. 7-1. Gliding entry at small flight path angle.
Velocity - altitude diagram for different values of lift-to-drag ratio.

The flight path angle is obtained from Eq. (7-4). We have, by taking the derivative of Eq.(7-15) with respect to $u$

$$\beta r_o \sin\gamma = -\frac{1}{(C_L/C_D)\,u} \tag{7-17}$$

From Eq. (7-9), we have for the distance travelled, using Eq. (7-16) for $\eta$

$$\frac{d}{du}\left(\frac{s}{r_o}\right) = \frac{(C_L/C_D)}{(2u-1)} \tag{7-18}$$

Integrating from the initial value $u_o$ gives

$$\frac{s}{r_o} = \frac{1}{2}\left(\frac{C_L}{C_D}\right)\log\frac{1-2u}{1-2u_o} \tag{7-19}$$

We see that, for any prescribed final speed $u_f$, the distance travelled $s_f$ is maximized by using the maximum lift-to-drag ratio. Using the final speed $V_f \approx 0$, the total range is given by

$$\frac{s_f}{r_o} = \frac{1}{2}\left(\frac{C_L}{C_D}\right)\log\frac{1}{1-(V_o^2/g_o r_o)} \tag{7-20}$$

The total range $(s_f / r_o)$ is plotted in Fig. 7-2 in terms of the initial speed $V_o / \sqrt{g_o r_o}$ for different values of lift-to-drag ratio.

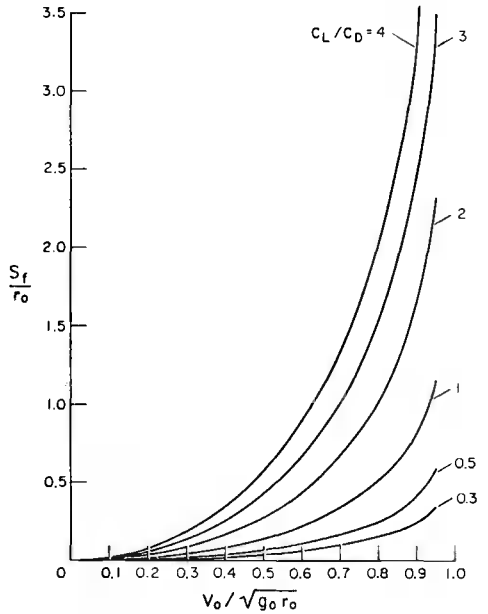


Fig. 7-2. Gliding entry at small flight path angle. Total range in terms of initial speed .

The time of flight is obtained by integrating Eq. (7-12). We have, first by substituting Eq. (7-16) into Eq. (7-12)

$$\frac{d}{du}\left(\sqrt{\frac{2g_o}{r_o}}\,t\right) = \left(\frac{C_L}{C_D}\right)\frac{1}{(2u-1)\,u^{1/2}} \tag{7-21}$$

Integrating from the initial value $u_o$ gives

$$\sqrt{\frac{g_o}{r_o}}\,t = \frac{1}{2}\left(\frac{C_L}{C_D}\right)\log\left[\frac{1+\sqrt{2u_o}}{1-\sqrt{2u_o}}\right]\left[\frac{1-\sqrt{2u}}{1+\sqrt{2u}}\right] \tag{7-22}$$

For any prescribed final speed $u_f$, the total time of flight $t_f$ is maximized by using the maximum lift-to-drag ratio. Using $u_f \approx 0$, we have the total flying time.

$$\sqrt{\frac{g_o}{r_o}}\,t_f = \frac{1}{2}\left(\frac{C_L}{C_D}\right)\log\left[\frac{1+V_o/\sqrt{g_o r_o}}{1-V_o/\sqrt{g_o r_o}}\right] \tag{7-23}$$

Finally, from Eq. (7-11) we have the deceleration along the gliding entry trajectory

$$\frac{a}{g_o} = \frac{1 - 2u}{(C_L/C_D)} = \frac{1 - (V^2/g_o r_o)}{(C_L/C_D)} \tag{7-24}$$

As the speed decreases, the deceleration increases continuously along the descending trajectory and it is minimized by using the maximum lift-to-drag ratio.

The first-order solution of this section is known as the first-order solution of Eggers, Allen and Neice (Ref. 2).

## 7-3. GLIDING ENTRY AT MEDIUM AND LARGE FLIGHT PATH ANGLES

When the flight path angle is not small, the condition of equilibrium glide is no longer maintained. On the right-hand side of Eq. (7-5) the lift force is predominant while the difference between the centrifugal force and the gravity force remains small. Hence, we have the simplified equation

$$\frac{d\phi}{d\eta} = \frac{C_L}{C_D} \tag{7-25}$$

and upon integrating from the initial time

$$\cos\gamma - \cos\gamma_o = \frac{C_L}{C_D}(\eta - \eta_o) \tag{7-26}$$

Combining the Eqs. (7-4) and (7-25) to eliminate $\eta$ we have

$$u\frac{d\gamma}{du} = -\frac{1}{2}\left(\frac{C_L}{C_D}\right) \tag{7-27}$$

which integrates to

$$\frac{u}{u_o} = \exp\left[\frac{2(\gamma_o - \gamma)}{(C_L/C_D)}\right] \tag{7-28}$$

Equations (7-26) and (7-28) constitute the first-order solution of Lees for gliding entry at medium positive lift-to-drag ratio and medium flight path angle (Ref. 3).

Using Eq. (7-11), with the solution (7-26) for $\eta$ and (7-28) for $u$, we have for the deceleration, by taking $\eta_o \approx 0$

$$\frac{a}{g_o} = \frac{2\beta r_o u_o}{(C_L/C_D)}(\cos\gamma - \cos\gamma_o)\exp\left[\frac{2(\gamma_o - \gamma)}{(C_L/C_D)}\right] \tag{7-29}$$

Since, by this expression, "a" is a function of $\gamma$ alone, the maximum deceleration occurs at a value of $\gamma$ obtained by solving the equation $da/d\gamma = 0$ . We have

$$\frac{1}{2}\left(\frac{C_L}{C_D}\right)\sin\gamma = \cos\gamma_o - \cos\gamma \tag{7-30}$$

This equation can be written as a quadratic equation in $\tan(\gamma/2)$

$$(1+\cos\gamma_o)\tan^2\frac{\gamma}{2} - \left(\frac{C_L}{C_D}\right)\tan\frac{\gamma}{2} - (1-\cos\gamma_o) = 0 \tag{7-31}$$

The equation has two roots, one positive and one negative. For a descending trajectory, we take the negative root

$$\tan\frac{\gamma}{2} = \frac{1}{2(1+\cos\gamma_o)}\left[\frac{C_L}{C_D} - \sqrt{\left(\frac{C_L}{C_D}\right)^2 + 4\sin^2\gamma_o}\right] \tag{7-32}$$

Using this critical value for $\gamma$ in Eqs. (7-28) and (7-29), we have the corresponding speed and the maximum deceleration. The altitude at which the maximum deceleration occurs is given by Eq. (7-26) with $\gamma$ as given by Eq. (7-32). Let subscript (*) denote the condition at the point of maximum deceleration. We have

$$\left(\frac{C_L}{C_D}\right)(\eta_* - \eta_o) = \cos\gamma_* - \cos\gamma_o = -\frac{1}{2}\left(\frac{C_L}{C_D}\right)\sin\gamma_*$$

Therefore

$$\eta_* - \eta_o = -\frac{\tan\frac{\gamma_*}{2}}{1+\tan^2\frac{\gamma_*}{2}} \tag{7-33}$$

Another form of this equation is obtained by combining it with Eq.(7-31)

$$\eta_* - \eta_o = -\frac{(1+\cos\gamma_o)\tan\frac{\gamma_*}{2}}{2+(C_L/C_D)\tan\frac{\gamma_*}{2}}$$

Using the solution (7-32), we have explicitly for the critical altitude where the maximum deceleration occurs, in terms of the lift-to-drag ratio $(C_L/C_D)$ , and the initial flight path angle $\gamma_o$

$$\eta_* - \eta_o = \frac{\sqrt{(C_L/C_D)^2 + 4\sin^2\gamma_o} - (C_L/C_D)}{4+[(C_L/C_D)/(1+\cos\gamma_o)]\left[(C_L/C_D) - \sqrt{(C_L/C_D)^2+4\sin^2\gamma_o}\right]} \tag{7-34}$$

When the initial flight path angle is small

$$\frac{4 \sin^2 \gamma_o}{(C_L/C_D)^2} \ll 1$$

and the square root can be approximated by

$$\sqrt{(C_L/C_D)^2 + 4 \sin^2 \gamma_o} \approx \left(\frac{C_L}{C_D}\right)\left[1 + \frac{2 \sin^2 \gamma_o}{(C_L/C_D)^2}\right]$$

The expression for $\eta_*$ becomes

$$\eta_* - \eta_o = \frac{2 \sin^2 \frac{\gamma_o}{2}}{(C_L/C_D)} \tag{7-35}$$

In this case, the critical flight path angle, as given by Eq. (7-32), becomes

$$\tan \frac{\gamma_*}{2} = - \frac{2 \sin^2 \frac{\gamma_o}{2}}{(C_L/C_D)} \tag{7-36}$$

If the flight path angle is not too large, we have the approximate relation

$$\gamma_* = - \frac{\gamma_o^2}{(C_L/C_D)} \tag{7-37}$$

In this case, we obtain from Eq. (7-28) the critical speed where maximum deceleration occurs

$$\frac{V_*}{V_o} = \exp\left(\frac{\gamma_o}{C_L/C_D}\right) \tag{7-38}$$

The maximum deceleration is simply

$$\frac{a_*}{g_o} = \frac{\beta r_o u_o \gamma_o^2}{(C_L/C_D)} \exp\left(\frac{2\gamma_o}{C_L/C_D}\right) \tag{7-39}$$

The solution obtained by Lees applies to circular speed entry. For supercircular speed entry, it has been generalized by Ting (Ref. 4). In this case, the second term on the right-hand side of Eq. (7-5) is not negligible since for large values of $u$, the difference $[(1/2u) - 1]$ is not small. To obtain the expression for the flight path angle Ting used the approximation

$$\left(\frac{1}{2u} - 1\right)\phi \approx \frac{1}{2u_o} - 1$$

Then, we have the equation

$$\frac{d\phi}{d\eta} = \frac{C_L}{C_D} - \frac{1}{\beta r_o \eta}\left(\frac{1}{2u_o} - 1\right) \tag{7-40}$$

Upon integrating and using the initial conditions, we have

$$\cos\gamma - \cos\gamma_o = \left(\frac{C_L}{C_D}\right)(\eta - \eta_o) - \frac{1}{\beta r_o}\left(\frac{1}{2u_o} - 1\right)\log\frac{\eta}{\eta_o} \tag{7-41}$$

For small flight path angles, we have Ting's first-order solution for entry at supercircular speed

$$\gamma = -\left[\gamma_o^2 - 2\left(\frac{C_L}{C_D}\right)(\eta - \eta_o) + \frac{2}{\beta r_o}\left(\frac{1}{2u_o} - 1\right)\log\frac{\eta}{\eta_o}\right]^{1/2} \tag{7-42}$$

Next, we write Eq. (7-5)

$$-\sin\frac{d\gamma}{d\eta} = \frac{C_L}{C_D} - \frac{1}{\beta r_o \eta}\left(\frac{1}{2u} - 1\right) \tag{7-43}$$

Combining this equation with Eq. (7-4) to eliminate $\eta$, we have

$$\frac{du}{u} = -\frac{d\gamma}{\frac{1}{2}\left[\frac{C_L}{C_D} - \frac{1}{\beta r_o \eta}\left(\frac{1}{2u} - 1\right)\right]} \tag{7-44}$$

Considering the denominator on the right-hand side of this equation as constant, we have, upon integrating

$$\text{Log}\,\frac{u}{u_o} = \frac{\gamma_o - \gamma}{\frac{1}{2}\left[\frac{C_L}{C_D} - \frac{1}{\beta r_o \eta}\left(\frac{1}{2u} - 1\right)\right]} \tag{7-45}$$

Equations (7-42) and (7-45) constitute Ting's solution for entry from supercircular speed (Ref. 4).

## 7-4. BALLISTIC ENTRY AT LARGE FLIGHT PATH ANGLES

When the aerodynamic force is in the form of pure drag, we have ballistic entry. For ballistic entry, $C_L = 0$ . The general assumption is that ballistic entry involves short range so that the assumption of flat Earth applies. In Eq. (7-5), if we neglect the centrifugal force, we have

$$\frac{d\phi}{d\eta} = - \frac{1}{2\beta r_o \eta u} \tag{7-46}$$

From this equation, because of the small factor $1/2 \beta r_o$ , it is seen that for relatively steep trajectories, the dimensionless atmospheric density $\eta$ will quickly become finite and the right-hand side can be put equal to zero. Since the term is the gravity term, this is equivalent to neglecting the gravity force compared with the drag force which is large during the fundamental portion of a steep ballistic entry trajectory. We shall first conduct the investigation under this assumption and later modify the solution to include the effect of the gravitational force.

### 7-4.1. Analysis Neglecting Gravity

If gravity is neglected, the integration of Eq. (7-46), with the right-hand side put equal to zero, yields

$$\cos \gamma = \cos \gamma_o \tag{7-47}$$

We conclude that, for ballistic entry, the flight path angle remains nearly constant and the trajectory is essentially a small portion of a spiral. Using this solution, Eq. (7-4) can be integrated to give

$$\frac{u}{u_o} = \exp \left[ \frac{2(\eta - \eta_o)}{\sin \gamma_o} \right] \tag{7-48}$$

Equations (7-47) and (7-48) constitute the first-order solution for ballistic entry at large flight path angles as given by Gazley (Ref. 5), Allen and Eggers (Ref. 6) and Chapman (Ref. 7).

Equation (7-48), with $\eta_o \approx 0$ , can be written as

$$\frac{V}{V_o} = \exp \left( \frac{\eta}{\sin \gamma_o} \right) \tag{7-49}$$

It is seen that V decreases as the radius of a logarithmic spiral (Fig. 7-3).

In the figure, the angle $\eta$ is measured in radians. Let $\sigma$ be the constant angle between $\vec{V}$ and the tangent to the spiral. We have

$$\tan \sigma = \sin \gamma_o < 0 \tag{7-50}$$

V decreases more rapidly with the altitude for larger initial flight path angles. On the other hand, by the definition (7-3) of $\eta$, for each value of the altitude, $\eta$ is larger for larger values of the drag coefficient and smaller values of the wing loading $(mg_o/S)$. Hence, the speed decreases more rapidly with a larger drag coefficient and a smaller wing loading. The deceleration is given by Eq. (7-11). We have, using the solution (7-48) for $u$,

$$\frac{a}{g_o} = 2\beta r_o u_o \eta \exp\left[\frac{2(\eta - \eta_o)}{\sin \gamma_o}\right] \tag{7-51}$$

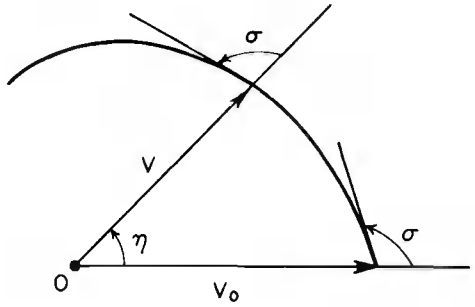


Fig. 7-3. Variation of the speed during ballistic entry.

The maximum deceleration occurs at the altitude $\eta_*$ obtained by solving the equation $da/d\eta = 0$. We have

$$\eta_* = -\frac{1}{2} \sin \gamma_o \tag{7-52}$$

From the definition (7-3) of $\eta$, this critical altitude is positive if

$$-\sin \gamma_o \leq \frac{SC_D \rho_s}{m\beta} \tag{7-53}$$

If this inequality is not satisfied, the deceleration continues to increase and reaches a maximum at the altitude zero. In this case, the maximum deceleration is

$$\frac{a_*}{g_o} = 2\beta r_o u_o \eta_s \exp\left[\frac{2(\eta_s - \eta_o)}{\sin \gamma_o}\right] \tag{7-54}$$

where $\eta_s$ is the value of $\eta$ at sea level

$$\eta_s = \frac{SC_D \rho_s}{2m\beta}, \tag{7-55}$$

The corresponding value of $u$ is

$$u_* = u_o \exp\left[\frac{2(\eta_s - \eta_o)}{\sin\gamma_o}\right] \tag{7-56}$$

In the case where the strict inequality in (7-53) is satisfied the maximum deceleration occurs at an altitude $h_*$ above the surface of the planet. The corresponding value of $\eta$ is given by Eq. (7-52). Using this value in Eq. (7-48) with $\eta_o \approx 0$, we have

$$\frac{u_*}{u_o} = \frac{1}{e}$$

Therefore

$$V_* = \frac{V_o}{\sqrt{e}} = 0.607\, V_o \tag{7-57}$$

Thus, the point on the ballistic entry trajectory where the speed has decreased to about 60.7% of its initial value is the point of maximum deceleration. The maximum value of the deceleration is obtained from Eq. (7-51) with $\eta_*$ as given by Eq. (7-52). We have

$$\frac{a_*}{g_o} = -\frac{\beta r_o u_o}{e} \sin\gamma_o \tag{7-58}$$

We see that the maximum deceleration is proportional to the quantity $-u_o \sin\gamma_o$ and is independent of the physical characteristics of the vehicle.

Figure 7-4 presents the speed-altitude relationship, Eq. (7-49), for different values of the initial flight path angle. The use of the dimensionless quantity $\eta$ is convenient since the diagram applies to any type of vehicle regardless of its physical characteristics. For each specified vehicle, one can compute its sea level value $\eta_s$ by Eq. (7-55) and deduce the speed ratio at this level. This also applies to any level by using the corresponding value $\rho$.

Figure 7-5 presents the deceleration-altitude relationship, Eq. (7-51) for different values of the initial flight path angle. It is convenient for the plot to write this equation as

$$\frac{a}{2\beta r_o g_o u_o} = \eta \exp\left(\frac{2\eta}{\sin\gamma_o}\right) \tag{7-59}$$

In this way, the diagram can be used for any type of entry vehicle at any initial speed. The line of maximum deceleration is the hyperbola

$$\left(\frac{1}{\eta}\right)\left(\frac{a}{2\beta r_o g_o u_o}\right) = \frac{1}{e} = 0.36788 \tag{7-60}$$

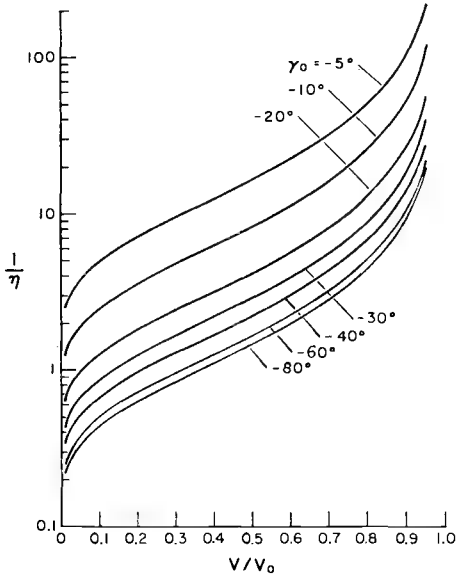


Fig. 7-4. Ballistic entry at large flight path angle. Speed - altitude diagram for several values of the initial angle.

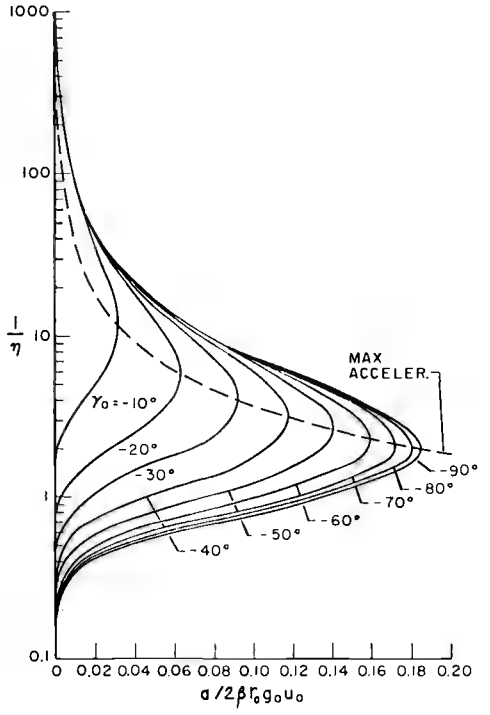


Fig. 7-5. Ballistic entry at large flight path angle. Acceleration - altitude diagram for several values of the initial angle.

7-4.2. Analysis Including Gravity

The results in the previous section are obtained by neglecting the gravitational force. If the effect of gravitational force is retained, then for ballistic entry, under the flat Earth assumption, the Eqs. (7-1) are reduced to

$$\frac{du}{d\eta} = \frac{2u}{\sin\gamma} + \frac{1}{\beta r_o \eta}$$

$$\frac{d\phi}{d\eta} = -\frac{\phi}{2\beta r_o \eta u} \tag{7-61}$$

The first of these equations is now integrated under the assumption that the flight path angle is nearly constant and can be put equal to its initial value. Hence we have the linear equation

$$\frac{du}{d\eta} - \frac{2u}{\sin\gamma_o} = \frac{1}{\beta r_o \eta} \tag{7-62}$$

Using a new dimensionless atmospheric density $\alpha$ such that

$$\alpha = -\frac{2\eta}{\sin\gamma_o} \tag{7-63}$$

we can write the solution of Eq. (7-62) as (Ref. 8)

$$u = \frac{1}{\beta r_o} \exp(-\alpha)[\,\mathrm{Ei}(\alpha) + C] \tag{7-64}$$

where $C$ is a constant of integration and the exponential-integral function $\mathrm{Ei}(\alpha)$ is defined as

$$\mathrm{Ei}(\alpha) = \int_{-\infty}^{\alpha} \frac{e^t}{t}\, dt \tag{7-65}$$

This integral function is tabulated in Ref. 9. The constant of integration $C$ in Eq. (7-64) is evaluated using the initial condition. It is seen from this equation that the kinetic energy of the vehicle, or equivalently its speed, passes through a maximum for a falue of $\alpha$ satisfying the equation

$$\mathrm{Ei}(\alpha) + C = \frac{\exp(\alpha)}{\alpha} \tag{7-66}$$

If the constant of integration $C$ has been obtained from the initial condition, this equation can be solved for $\alpha$. Upon substituting back into Eq. (7-64) we have the value for the maximum kinetic energy

$$u = \frac{1}{\beta r_o \alpha} \tag{7-67}$$

Now, using Eq. (7-11), we have for the deceleration

$$-\frac{a}{g_o \sin\gamma_o} = \alpha \exp(-\alpha)[\,\mathrm{Ei}(\alpha) + C] \tag{7-68}$$

The deceleration has a maximum at the altitude where

$$\mathrm{Ei}(\alpha) + C = \frac{\exp(\alpha)}{\alpha - 1} \tag{7-69}$$

Again, if the constant $C$ has been evaluated, using the initial condition, this equation can be solved for $\alpha$ and, by the definition (7-63), for $\eta$, yielding the altitude where maximum deceleration occurs. Combining the last two equations, we have the maximum deceleration

$$-\frac{a_*}{g_o \sin\gamma_o} = \frac{\alpha}{\alpha - 1} \tag{7-70}$$

where $\alpha$ is obtained by solving Eq. (7-69). Maximum deceleration occurs at a positive altitude if

$$\mathrm{Ei}(\alpha_s) + C - \frac{\exp(\alpha_s)}{\alpha_s - 1} > 0 \tag{7-71}$$

where $\alpha_s$ is the value of $\alpha$ at sea level, that is

$$\alpha_s = -\frac{2\eta_s}{\sin\gamma_o} = -\frac{SC_D\rho_s}{m\beta \sin\gamma_o} \tag{7-72}$$

If the vehicle's physical characteristics are such that inequality (7-71) is not satisfied, then the deceleration monotonically increases during the balistic entry and reaches its highest level at sea level. This maximum deceleration is given by

$$-\frac{a_*}{g_o \sin\gamma_o} = \alpha_s \exp(-\alpha_s)\,[\,\mathrm{Ei}(\alpha_s) + C] \tag{7-73}$$

From Eq. (7-64) the constant of integration $C$ is given by

$$C = \beta r_o u_o \exp(\alpha_o) - \mathrm{Ei}(\alpha_o) \quad . \tag{7-74}$$

where

$$\alpha_o = -\frac{2\eta_o}{\sin \gamma_o} \tag{7-75}$$

On the other hand, a series expansion of the exponential function is

$$Ei(\alpha) = \gamma_E + \log \alpha + \sum_{n=1}^{\infty} \frac{\alpha^n}{n\, n!} \tag{7-76}$$

where $\gamma_E = 0.577215...$ is the Euler constant. Hence, for entry from high altitude, $\alpha_o \approx 0$ and an approximate expression for C is

$$C = \beta r_o u_o (1+\alpha_o) - \alpha_o - \gamma_E - \log \alpha_o \tag{7-77}$$

## 7-5. SKIP ENTRY

A trajectory of interest for a lifting hypervelocity vehicle is the skip trajectory. In the skipping phase, the vehicle enters the atmosphere, negotiates a turn, and is ejected from the atmosphere. This type of maneuver can be used to achieve a change in the orbital plane. Only the maneuver at constant lift-to-drag ratio in a vertical plane will be analyzed in this section. The skip trajectory involves a short longitudinal range. Hence the flat Earth assumption will be used; that is, we shall neglect the centrifugal force. Furthermore, since the gravitational force is, on the average, much smaller than the aerodynamic force, we can neglect completely the gravitational force in the equations of motion.

With these assumptions, we deduce from the general equations (7-1), the equations of motion governing a skip trajectory.

$$\frac{du}{d\eta} = \frac{2u}{\sin \gamma}$$

$$\frac{d\phi}{d\eta} = \frac{C_L}{C_D} \tag{7-78}$$

The second equation can be integrated to give

$$\cos \gamma - \cos \gamma_o = \frac{C_L}{C_D}(\eta - \eta_o) \tag{7-79}$$

The vehicle exits at a final altitude level $\eta_f$ equal to the initial altitude $\eta_o$. Hence,

$$\gamma_f = -\gamma_o \tag{7-80}$$

This shows that, for a skip maneuver at constant angle of attack, the ejection angle is equal to the absolute value of the entry angle.

At the lowest point of a skip trajectory, $\gamma = 0$ . The minimum altitude is then

$$\eta = \eta_o + \frac{1 - \cos \gamma_o}{(C_L/C_D)} \tag{7-81}$$

For this altitude to be positive, it is necessary that

$$\frac{1 - \cos \gamma_o}{(C_L/C_D)} < \frac{SC_D\rho_s}{2m\beta}$$

where the condition $\eta_o \approx 0$ has been assumed. We can write the condition as

$$\sin^2 \frac{\gamma_o}{2} < \frac{g_o\rho_s C_L}{4\beta\,(mg_o/S)} \tag{7-82}$$

This provides the safety limit on the entry angle for a vehicle with specified lift capability and wing loading condition.

To obtain the velocity distribution along a skip trajectory, we combine the two equations (7-78) to obtain

$$\frac{d\gamma}{du} = -\frac{1}{2u}\left(\frac{C_L}{C_D}\right) \tag{7-83}$$

Integration gives

$$\frac{u}{u_o} = \exp\left[\frac{2(\gamma_o - \gamma)}{(C_L/C_D)}\right] \tag{7-84}$$

or in terms of V

$$\frac{V}{V_o} = \exp\left[\frac{(\gamma_o - \gamma)}{(C_L/C_D)}\right] \tag{7-85}$$

Hence, since $\gamma_f = -\gamma_o$ the final velocity is

$$\frac{V_f}{V_o} = \exp\left(\frac{2\gamma_o}{C_L/C_D}\right) \tag{7-86}$$

Equations (7-79) and (7-85) constitute the first-order solution for a skip trajectory as originally derived by Eggers, Allen and Neice (Ref. 2).

The distance travelled is given by Eq. (7-9) which, combined with Eq. (7-83), provides

$$\frac{d}{d\gamma}\left(\frac{s}{r_o}\right) = \frac{1}{\beta r_o (C_L/C_D)\,\eta} \tag{7-87}$$

Using the solution (7-79) for $(C_L/C_D)\,\eta$, we can write this equation

$$\frac{d}{d\gamma}(\beta s) = \frac{1}{(\cos\gamma - \cos\gamma_i)} \tag{7-88}$$

where the modified initial angle $\gamma_i$ is defined by

$$\cos\gamma_i = \cos\gamma_o - \left(\frac{C_L}{C_D}\right)\eta_o \tag{7-89}$$

The integration of Eq. (7-88) is simple. We have

$$\beta s = \frac{1}{\sin\gamma_i} \log\left[\frac{\tan\frac{\gamma}{2} + \tan\frac{\gamma_i}{2}}{\tan\frac{\gamma}{2} - \tan\frac{\gamma_i}{2}}\right]\left[\frac{\tan\frac{\gamma_o}{2} - \tan\frac{\gamma_i}{2}}{\tan\frac{\gamma_o}{2} + \tan\frac{\gamma_i}{2}}\right] \tag{7-90}$$

using $\gamma_i$ with its positive argument.

If we consider the range $x$, then by the differential relation

$$dx = \cos\gamma\, ds \tag{7-91}$$

the equation to be integrated is

$$\frac{d}{d\gamma}(\beta x) = \frac{\cos\gamma}{(\cos\gamma - \cos\gamma_i)} \tag{7-92}$$

Integration from the initial distance $x_o = 0$ gives the solution

$$\beta x = \gamma - \gamma_o + \cot\gamma_i \log\left[\frac{\tan\frac{\gamma}{2} + \tan\frac{\gamma_i}{2}}{\tan\frac{\gamma}{2} - \tan\frac{\gamma_i}{2}}\right]\left[\frac{\tan\frac{\gamma_o}{2} - \tan\frac{\gamma_i}{2}}{\tan\frac{\gamma_o}{2} + \tan\frac{\gamma_i}{2}}\right] \tag{7-93}$$

The tangential deceleration is given by Eq. (7-11), written with subscript $t$, as

$$\frac{a_t}{g_o} = 2\beta r_o\, \eta u \tag{7-94}$$

It is informative to follow Miele, (Ref. 8), in considering also the normal deceleration

$$\frac{a_n}{g_o} = \frac{V}{g_o}\frac{d\gamma}{dt} = 2\beta r_o \left(\frac{C_L}{C_D}\right) \eta u \tag{7-95}$$

Hence, the total deceleration is

$$\frac{a}{g_o} = \sqrt{1 + \left(\frac{C_L}{C_D}\right)^2}\ 2\beta r_o\, \eta u \tag{7-96}$$

The total deceleration and its two components are proportional to $\eta u$. All pass through their respective maxima at the same time. We need only consider

$$\frac{a_t}{2\beta r_o g_o} = \eta u = \frac{u_o}{(C_L/C_D)}(\cos\gamma - \cos\gamma_o) \exp\left[\frac{2(\gamma_o - \gamma)}{(C_L/C_D)}\right] \tag{7-97}$$

The analytical solution for $\eta$ and $u$, as well as the expression for the deceleration have the same mathematical form as the expressions obtained by Lees for gliding entry at medium and large flight path angles as derived in Section 7-3. Hence, the discussion for the maximum deceleration is identical to that in Section 7-3. The pertinent remark to be added here is that, from Eq. (7-36), one can see that the peak deceleration occurs during the descending phase.

Furthermore, it should be noted that although for the two cases the resulting differential equations are identical, hence, providing identical solutions, the physical assumptions are different. For the skip trajectory, if we return to Eq. (7-5) with the different forces labelled, each of the gravity force and the centrifugal force is small compared to the lift force, since it will require a relatively high lift-to-drag ratio to negotiate a skip trajectory. On the other hand, for gliding flight at medium and large flight path angles, one uses a moderate lift-to-drag ratio. The gravity force and the centrifugal force, considered separately, may have the same order of magnitude as the lift force. The assumption used is that their combined effect is negligible compared to the effect due to the lift, hence the combined term may be put equal to zero. To retain this effect, instead of putting it equal to zero, we may hold it constant for the integration. In doing so, we used the so-called Loh's assumption. Loh's theory for the entry trajectory, which is a second-order theory, will be presented in Chapter 8.

## References

1. Sänger, E., and Bredt, J., "A Rocket Drive for Long Range Bombers," Translation No. CGD-32, Technical Information Branch, Navy Dept., 1944.

2. Eggers, A.J., Allen, H.J., and Neice, S.E., "A Comparative Analysis of the Performance of Long-Range Hypervelocity Vehicles," NACA TN 4046, 1957.

3. Lees, L., Hastwig, F.W., and Cohen, C.B., "Use of Aerodynamic Lift During Entry into the Earth's Atmosphere," ARS Journal, pp. 633-641, September, 1959.

4. Ting, L., and Wang, K., "An Approximate Analytic Solution of Re-Entry Trajectory with Aerodynamic Forces," ARS Journal, pp. 565-566, June, 1960.

5. Gazley, C., "Deceleration and Heating of a Body Entering a Planetary Atmosphere from Space," The RAND Corporation Report P-955, February 1957.

6. Allen, H.J., and Eggers, A.J., "A Study of the Motion and Aerodynamic Heating of Missiles Entering the Earth's Atmosphere at High Supersonic Speeds," NACA TR 1381, 1958.

7. Chapman, D.R., "An Approximate Analytical Method for Studying Entry into Planetary Atmospheres," NASA Technical Report R-11, 1959.

8. Miele, A., Flight Mechanics, Vol. 1, Addison-Wesley Publishing Company Inc., Reading, Massachusetts, 1962.

9. National Bureau of Standards, Tables of Sine, Cosine and Exponential Integrals, Vols. 1 and 2, 1940.

# Chapter 8

# Loh's Second-Order Theory for Entry Trajectories

## 8-1. INTRODUCTION

In Chapter 6, we derived the dimensionless exact equations for entry at constant lift-to-drag ratio in the plane of a great circle. The set of fundamental equations of entry are not solvable analytically, even with the usual assumption considering the acceleration of gravity constant. However, upon restricting the solution to a limited region of application, one can obtain several first-order approximate analytical solutions as presented in Chapter 7. Each of these solutions is then valid for one type of entry. On the other hand, Loh has derived a more general solution which covers the entire range of lift-to-drag ratios and initial flight path angles (Ref. 1). We shall refer to his solution as Loh's second-order solution.

Loh's theory is empirical, and is based on data from extensive numerical integration of entry trajectories. Nevertheless, it proves to be very accurate, even for trajectories with varying lift-to-drag ratio (Ref. 2).

In formulating Loh's assumption, we consider the fundamental equations, Eqs. (6-23)

$$\frac{du}{d\eta} = \frac{2u}{\sin\gamma} + \frac{z^2}{\beta r_o \eta}$$

$$\frac{d\phi}{d\eta} = \frac{C_L}{C_D} - \frac{z^2}{\beta r_o \eta}\left(\frac{1}{2u} - \frac{1}{z}\right)\phi \qquad (8\text{-}1)$$

where, as before,

$$u \equiv \frac{1}{2}\left(\frac{V^2}{g_o r_o}\right), \quad z \equiv \frac{r_o}{r}, \quad \phi \equiv \cos\gamma \qquad (8\text{-}2)$$

with $r_o$ the initial radial distance. The variable $\eta$ is proportional to the atmospheric density, and is defined as

$$\eta = \frac{SC_D}{2m\beta}\rho \tag{8-3}$$

Loh's first assumption is to take $z = 1$ in the fundamental equations, Eqs. (8-1). Thus, we have the basic equations for planetary entry

$$\begin{aligned}\frac{du}{d\eta} &= \frac{2u}{\sin\gamma} + \frac{1}{\beta r_o \eta} \\ \frac{d\phi}{d\eta} &= \frac{C_L}{C_D} - \frac{1}{\beta r_o \eta}\left(\frac{1}{2u} - 1\right)\phi\end{aligned} \tag{8-4}$$

Loh considered this system as the system of exact equations for entry, but, as seen here, it is obtained by neglecting the altitude as compared to the reference radial distance.

Let

$$G \equiv \frac{1}{\beta r_o \eta}\left(\frac{1}{2u} - 1\right)\phi \tag{8-5}$$

Although the right-hand side of this equation is a function of the variables $\eta$, $u$ and $\phi$, all varying with the time, Loh observed through extensive numerical integration for different types of entry trajectories, that the term remains nearly constant for each trajectory. Therefore, he used the assumption that $G$ is constant for the purpose of integration with respect to either $\eta$ or $\gamma$. A possible interpretation of this phenomenon can be seen by observing that the expression for $G$ is the difference between the gravity force and the centrifugal force along the normal to the flight path. For curvilinear flight over a spherical Earth, this difference remains nearly constant. In keeping this term, these effects are retained in the solution, with any resulting error from the assumption coming entirely from the fluctuation between the two forces. Such fluctuation is small.

## 8-2. UNIFIED SOLUTION FOR ENTRY

With $G$ considered as constant, the second Eq. (8-4) is written

$$\frac{d\phi}{d\eta} = \frac{C_L}{C_D} - G \tag{8-6}$$

where, for constant lift-to-drag ratio, the right-hand side of this equation is constant. The integration is immediate,

$$\cos\gamma - \cos\gamma_o = \left[\frac{C_L}{C_D} - G\right](\eta - \eta_o) \tag{8-7}$$

This equation can be rearranged to give the expression for the flight path angle in terms of $\eta$ and $u$.

$$\cos\gamma = \frac{\cos\gamma_o + (C_L/C_D)\,\eta(1 - \eta_o/\eta)}{1 + (1/\beta r_o)(1 - \eta_o/\eta)[(1/2u) - 1]} \tag{8-8}$$

To integrate the first equation (8-4), Eq. (8-6) is rewritten as

$$-\sin\gamma \frac{d\gamma}{d\eta} = \frac{C_L}{C_D} - G \tag{8-9}$$

Then, with $\gamma$ as the independent variable of integration, Eq. (8-4) is

$$\frac{du}{d\gamma} + \frac{2u}{[(C_L/C_D) - G]} = -\frac{\sin\gamma}{\beta r_o \eta[(C_L/C_D) - G]}$$

Using the solution (8-7) to rearrange the right-hand side of this equation gives

$$\frac{du}{d\gamma} + \frac{2u}{[(C_L/C_D) - G]} = -\frac{\sin\gamma}{\beta r_o\{\cos\gamma - \cos\gamma_o + \eta_o[(C_L/C_D) - G]\}}$$

Since $\eta_o \approx 0$, the final equation for $u$ is

$$\frac{du}{d\gamma} + \frac{2u}{[(C_L/C_D) - G]} = \frac{\sin\gamma}{\beta r_o(\cos\gamma_o - \cos\gamma)} \tag{8-10}$$

Let

$$K \equiv \frac{2}{[(C_L/C_D) - G]} \tag{8-11}$$

and

$$f(\gamma) \equiv \frac{\sin\gamma}{\beta r_o(\cos\gamma_o - \cos\gamma)} \tag{8-12}$$

The equation for $u$ is a non-homogeneous, linear equation:

$$\frac{du}{d\gamma} + Ku = f(\gamma) \tag{8-13}$$

If we treat $G$ as essentially constant, $K$ is a constant for constant lift-to-drag ratio entry. Then Eq. (8-13) can be integrated:

$$u = C e^{-K\gamma} + F(\gamma) \tag{8-14}$$

where $C$ is the constant of integration, and $F(\gamma)$ represents the integral

$$F(\gamma) \equiv e^{-K\gamma} \int e^{K\gamma} f(\gamma)\, d\gamma \tag{8-15}$$

The constant of integration $C$ can be evaluated by using the initial conditions

$$\gamma = \gamma_o \ , \quad u = u_o \ , \quad \eta = \eta_o \tag{8-16}$$

It should be noted that, although $K$ is treated essentially as a constant for the purpose of integration, when the solution is obtained explicitly in the form (8-14), both terms on the right-hand side of this solution are now functions of $u$, $\gamma$ and $\eta$ through the definitions (8-5) and (8-11) of $G$ and $K$. Hence, in evaluating the constant of integration $C$, one may choose either to consider $K$ as a function of $u$, $\gamma$ and $\eta$ or as a constant evaluated at some specific point along the trajectory. If $C$ is evaluated by considering $K$ as varying, then

$$u = u_o e^{(K_o\gamma_o - K\gamma)} + [\, F(\gamma) - e^{(K_o\gamma_o - K\gamma)} F(\gamma_o)] \tag{8-17}$$

where

$$K_o \equiv \frac{2}{(C_L/C_D) - (1/\beta r_o \eta_o)\,[\,(1/2u_o) - 1]\cos\gamma_o} \tag{8-18}$$

The two equations (8-8) and (8-17) constitute Loh's unified solution for entry. In general, the function $F(\gamma)$ as given by the integral (8-15) cannot be expressed in terms of elementary functions, but series solutions are available (Ref. 1). The equations can be solved for any two of the three variables $u$, $\gamma$ and $\eta$ in terms of the remaining one. From the value of $\eta$, one can recover the real altitude through the definition (8-3) written as

$$\eta \equiv \frac{SC_D\rho_s}{2m\beta} e^{-\beta h} \tag{8-19}$$

The drag parameter of the vehicle is involved only at this step. Hence, as far as the relationship between the dimensionless kinetic energy $u$ and the flight path angle $\gamma$ is concerned, it is dependent on the value of the drag parameter only through the initial value $\eta_o$. Practically, for entry from very high altitude $\eta_o$ is zero. Thus, the relationship between $u$ and $\gamma$ is completely independent of the drag parameter. In this case the value $K_o$ as defined by (8-18) should be evaluated at some intermediate point of the trajectory other than the initial point to avoid the singularity caused by taking $\eta_o = 0$.

## 8-3. SECOND-ORDER SOLUTION FOR ENTRY

In general, the unified solution as presented by Loh is too tedious to use since the two governing equations, Eqs. (8-8) and (8-17) are transcendental in the variables $u$, $\gamma$ and $\eta$. But the second term in the expression (8-17) for $u$ contains the factor $1/\beta r_o$ by the definition (8-12) of the function $f(\gamma)$, which is generally small. For the Earth, $\beta r_o = 900$, and according to Table 1-2, the values of $\beta r_o$ for the planets Venus, Mars and Jupiter are 500, 350 and 3000 respectively. Therefore, except for the cases where extreme accuracy at the terminal phase of flight is desired or for the cases involving planetary atmospheres in which the values of $\beta r_o$ are unforeseeably small, one can omit the term with the factor $1/\beta r_o$ in the expression (8-17) for $u$. In this case, the solution becomes

$$\cos\gamma = \frac{\cos\gamma_o + (C_L/C_D)\,\eta(1 - \eta_o/\eta)}{1 + (1/\beta r_o)(1 - \eta_o/\eta)[(1/2u) - 1]} \tag{8-20}$$

and

$$\log\left(\frac{u}{u_o}\right) = \frac{2(\gamma_o - \gamma)}{(C_L/C_D) - (1/\beta r_o\,\eta)[(1/2u) - 1]\cos\gamma} \tag{8-21}$$

Equations (8-20) and (8-21) form the basic second-order solution as derived by Loh. From these two equations, any two of the three variables $u$, $\gamma$ and $\eta$ can be determined in terms of the remaining one. The equations are still transcendental in the variables. To ease the numerical computation, whenever $\eta_o/\eta \ll 1$, Eq. (8-20) can be approximated by

$$\cos\gamma = \frac{\cos\gamma_o + (C_L/C_D)\,\eta}{1 + (1/\beta r_o)[(1/2u) - 1]} \tag{8-22}$$

On the other hand, Eq. (8-21), when solved for $\eta$, gives

$$\eta = \frac{(1/\beta r_o)[(1/2u) - 1]\cos\gamma \log(u/u_o)}{(C_L/C_D)\log(u/u_o) - 2(\gamma_o - \gamma)} \tag{8-23}$$

Eliminating $\eta$ between the last two equations yields

$$\gamma = \gamma_o - \frac{1}{2}\left(\frac{C_L}{C_D}\right)\log\left(\frac{u}{u_o}\right)\left[1 + \frac{1}{\beta r_o}\,\frac{[(1/2u) - 1]}{[1 - (\cos\gamma_o/\cos\gamma)]}\right]^{-1} \tag{8-24}$$

This transcendental equation can be solved for $\gamma$ in terms of $u$. Subsequently, the corresponding value of $\eta$ can be obtained from Eq. (8-23), or more accurately from Eq. (8-20), rewritten as

$$\frac{C_L}{C_D}(\eta - \eta_o) = (\cos\gamma - \cos\gamma_o) + \frac{1}{\beta r_o}\left(1 - \frac{\eta_o}{\eta}\right)\left(\frac{1}{2u} - 1\right)\cos\gamma$$

For $\eta_o/\eta \ll 1$, the right-hand side can be simplified. This gives approximately the dimensionless atmospheric density $\eta$ representing the variation of the altitude

$$\eta = \eta_o + \left(\frac{C_L}{C_D}\right)^{-1}\left[(\cos\gamma - \cos\gamma_o) + \frac{1}{\beta r_o}\left(\frac{1}{2u} - 1\right)\cos\gamma\right] \tag{8-25}$$

Loh has shown that the second-order solution, as derived, is very accurate compared with the exact numerical solution (Ref. 1). However, it should be noted that the exact equations as considered by Loh are the equations (8-4) obtained by taking $z = 1$. The theory is based on computational experience showing that, during the process of integration, the term $G$ is nearly constant. This explains the accuracy of the theory. A physical explanation of this phenomenon will be given in the next section when we show how the second-order solution is reduced to different first-order solutions.

## 8-4. REDUCTION OF THE SECOND-ORDER SOLUTION TO FIRST-ORDER SOLUTIONS

As presented in Chapter 7, several authors have obtained first-order solutions for different cases of entry trajectories. The procedures followed in deriving these solutions are the same. First, the type of entry trajectory is examined, and then approximations are made based on physical reasoning, and the basic equations for entry are simplified allowing simple integrations to obtain the solution in closed form. Each of the solutions is then only valid for a specified type of entry trajectory. The second-order solution obtained by Loh is a unified solution in the sense that it is valid for all types of entry trajectories. Hence, upon appropriate simplifications, it should be reducible to the different types of entry solutions if the empirical observation made by Loh is consistent with the physical entry phenomena.

The second-order solution derived by Loh as presented in the previous section is reproduced here for convenience of discussion.

$$\cos\gamma = \frac{\cos\gamma_o + (C_L/C_D)\,\eta(1 - \eta_o/\eta)}{1 + (1/\beta r_o)(1 - \eta_o/\eta)[(1/2u) - 1]} \tag{8-26}$$

$$\log\left(\frac{u}{u_o}\right) = \frac{2(\gamma_o - \gamma)}{(C_L/C_D) - (1/\beta r_o\,\eta)[(1/2u) - 1]\cos\gamma} \tag{8-27}$$

An alternate expression is

$$\gamma = \gamma_o - \frac{1}{2}\left(\frac{C_L}{C_D}\right)\log\left(\frac{u}{u_o}\right)\left[1+\frac{1}{\beta r_o}\frac{[(1/2u)-1]}{[1-(\cos\gamma_o/\cos\gamma)]}\right]^{-1} \tag{8-28}$$

The solution has been derived based on the assumption that a combined gravity and centrifugal term G is constant. This G term is defined as

$$G \equiv \frac{1}{\beta r_o \eta}\left(\frac{1}{2u}-1\right)\cos\gamma \tag{8-29}$$

As has been observed, this term represents the difference between the gravity force and the centrifugal force along the normal to the flight path. We shall derive the different first-order solutions from Loh's second-order solution and at the same time try to justify his empirical assumption.

### 8-4.1. Gliding Entry at Small Flight Path Angles

When the flight path angle is small, $\cos\gamma \approx \cos\gamma_o \approx 1$. Thus, Eq. (8-26) becomes, with $\eta_o \approx 0$

$$\frac{1}{\beta r_o}\left(\frac{1}{2u}-1\right) = \left(\frac{C_L}{C_D}\right)\eta \tag{8-30}$$

Or, solving for u

$$u = \frac{1}{2[1+\beta r_o (C_L/C_D)\,\eta]} \tag{8-31}$$

which is identical to the first-order solution, Eq. (7-18), for gliding entry derived in Chapter 7. Now, Eq. (8-29) with $\cos\gamma \approx 1$ can be written as

$$\frac{1}{\beta r_o}\left(\frac{1}{2u}-1\right) = G\eta \tag{8-32}$$

By comparing the two Eqs. (8-30) and (8-32), we see that the nearly constant term G is, in this case, nearly equal to the constant lift-to-drag ratio. It also can be seen in Eq. (8-6) that, for gliding entry at small flight path angles, $\phi = \cos\gamma$ is nearly unity and the right-hand side of this equation is nearly zero. The condition

$$\frac{C_L}{C_D} - \frac{1}{\beta r_o \eta}\left(\frac{1}{2u}-1\right)\cos\gamma = 0 \tag{8-33}$$

is called the condition of equilibrium glide. That is, there is nearly exact balancing among the lift force, the gravitational force and the centrifugal force along the flight path for $\gamma \approx 0$ . This assumption was first formulated by Sänger and Bredt in Ref. 3.

Now Eq. (8-28) is written as

$$\frac{\gamma_o - \gamma}{\cos\gamma - \cos\gamma_o} = \frac{(1/2)(C_L/C_D)\log(u/u_o)}{(\cos\gamma - \cos\gamma_o) + (1/\beta r_o)[(1/2u) - 1]\cos\gamma}$$

$$\approx \frac{\beta r_o}{2}\left(\frac{C_L}{C_D}\right)\log\left(\frac{u}{u_o}\right)\left(\frac{1}{2u} - 1\right)^{-1} \qquad (8\text{-}34)$$

The left-hand side of this equation, for $\gamma \approx \gamma_o$ , can be approximated by

$$\frac{\gamma_o - \gamma}{\cos\gamma - \cos\gamma_o} = \frac{\gamma_o - \gamma}{2\sin\frac{1}{2}(\gamma + \gamma_o)\sin\frac{1}{2}(\gamma_o - \gamma)} \approx \frac{1}{\sin\frac{1}{2}(\gamma + \gamma_o)} \approx \frac{1}{\sin\gamma}$$

On the other hand, for entry from near circular speed, $2u_o \approx 1$ , and the logarithm term on the right-hand side of Eq. (8-34) is approximated by

$$\log\left(\frac{u}{u_o}\right) \approx \log 2u = -\log\left(\frac{1}{2u}\right) = -\frac{\left(\frac{1}{2u} - 1\right)}{\frac{1}{2u}} + \ldots \approx -2u\left(\frac{1}{2u} - 1\right)$$

With these approximations, Eq. (8-34) is reduced to the final result for the small flight path angle in the form

$$\beta r_o \sin\gamma = -\frac{1}{(C_L/C_D)\,u} \qquad (8\text{-}35)$$

which is identical to Eq. (7-17) derived in Chapter 7. Equations (8-31) and (8-35) form the first-order solution of Eggers, Allen and Neice (Ref. 4) for gliding entry at small flight path angle. The derivation of Eq. (8-35) directly from the second-order solution is somewhat delicate because it involves the ratio of small quantities. A more direct way is to use the first Eq. (8-4) with the second term on the right-hand side neglected. This is equivalent to assuming that the component of the gravity force on the tangent to the flight path is negligible compared to the drag force. Then,

$$\frac{du}{d\eta} = \frac{2u}{\sin\gamma}$$

Using the first-order solution (8-31) to evaluate the derivative $du/d\eta$ yields directly Eq. (8-35)

### 8-4.2. Gliding Entry at Medium and Large Flight Path Angles

When the flight path angle is not small, we neglect the terms with coefficient $1/\beta r_o$ in Loh's second-order solution. Then the Eqs. (8-26) and (8-27) are reduced to

$$\cos\gamma - \cos\gamma_o = \frac{C_L}{C_D}(\eta - \eta_o) \tag{8-36}$$

and

$$\frac{u}{u_o} = \exp\left[\frac{2(\gamma_o - \gamma)}{(C_L/C_D)}\right] \tag{8-37}$$

Equations (8-36) and (8-37) are the first-order solutions of Eggers, Allen and Neice (Ref. 4) and Lees (Ref. 5) for skip entry and gliding entry at medium and large flight path angles. They have been derived by different approaches in Chapter 7. In the present analysis, this case corresponds to considering the term G as negligibly small. Hence, Loh's assumption, the empirical assumption of considering G as nearly constant, is essentially correct.

### 8-4.3. Ballistic Entry at Large Flight Path Angles

For ballistic entry, $C_L = 0$. This, along with neglecting the term with coefficient $1/\beta r_o$ in Eq. (8-26), gives

$$\cos\gamma = \cos\gamma_o \tag{8-38}$$

Since the flight path angle is nearly constant, the trajectory is essentially a spiral in the plane of the great circle. If we keep the term $1/\beta r_o$ in Eq. (8-26) to retain the small variation in the flight path angle, then

$$\cos\gamma - \cos\gamma_o = -\frac{1}{\beta r_o \eta}(\eta - \eta_o)\left(\frac{1}{2u} - 1\right) \tag{8-39}$$

Now Eq. (8-27), with the constant term $\cos\gamma$ as unity, is

$$2(\gamma_o - \gamma) = -\frac{1}{\beta r_o \eta}\log\left(\frac{u}{u_o}\right)\left(\frac{1}{2u} - 1\right) \tag{8-40}$$

The ratio of the last two equations yields

$$\frac{1}{(\eta - \eta_o)}\log\left(\frac{u}{u_o}\right) = \frac{2(\gamma_o - \gamma)}{\cos\gamma - \cos\gamma_o} \approx \frac{2}{\sin\gamma}$$

The last step in approximating the equation above is accomplished by using $\gamma \approx \gamma_o$ as done previously. Hence, the expression for the velocity is

$$\frac{u}{u_o} = \exp\left[\frac{2(\eta - \eta_o)}{\sin\gamma}\right] \tag{8-41}$$

Equations (8-38) and (8-41) form the first-order solution of Gazley (Ref. 6), Allen and Eggers (Ref. 7) and Chapman (Ref. 8) for ballistic entry at large flight path angles. Since they are here derived from Loh's second-order solution, they involve his assumed nearly constant $G$, the combined gravity and centrifugal force. Let us examine the validity of this conjecture of Loh. Comparing the two equations (8-29) and (8-39) we see that

$$G = \frac{\cos\gamma(\cos\gamma_o - \cos\gamma)}{(\eta - \eta_o)} \tag{8-42}$$

Hence, except along the initial portion of the trajectory, this term can be considered as small if $\gamma \approx \gamma_o$. In fact, as has been presented in Chapter 7, for the direct derivation of the first-order solution for ballistic entry we put $C_L = 0$, $G = 0$ in the second Eq. (8-4) and have upon integration

$$\cos\gamma = \cos\gamma_o$$

Hence the constancy of the term $G$, being small in this case, is explained.

### 8-4.4. Skip Entry at Large Flight Path Angles

Along a skip trajectory, the vehicle enter the atmosphere, negotiates a turn in the vertical plane and returns to the vacuum. Hence, if the flight continues under the action of the gravity, each portion of atmospheric flight is joined to the next by a ballistic arc. In Chapter 7, it has been seen that the original solution was developed by Eggers, Allen and Neice (Ref. 4) with the assumption that, in the turning process, the aerodynamic lift is the predominant force and the gravity force can be neglected. While the original derivation considers a flat Earth model, we can retain the curvature of the Earth in the combined Loh's $G$ term and set it equal to zero compared to the lift term. That is, the second Eq. (8-4) now becomes

$$\frac{d\phi}{d\eta} = \frac{C_L}{C_D} \tag{8-43}$$

Integration gives the solution

$$\cos\gamma - \cos\gamma_o = \frac{C_L}{C_D}(\eta - \eta_o) \tag{8-44}$$

This equation can also be obtained from Loh's second-order solution, Eq. (8-26) by neglecting the term G in it. Using the same assumption in Eq. (8-27) we have for the speed

$$\frac{u}{u_o} = \exp\left[\frac{2(\gamma_o - \gamma)}{(C_L/C_D)}\right] \tag{8-45}$$

## References


1. Loh, W. H. T., Dynamics and Thermodynamics of Planetary Entry, Prentice Hall, Inc., Englewood Cliffs, New Jersey, 1963.

2. Speyer, J., and Womble, M., "Approximate Optimal Atmospheric Entry Trajectories," J. of Spacecraft and Rockets, Vol. 8, pp. 1120-1126, Nov.-Dec., 1971.

3. Sänger, E., and Bredt, J., "A Rocket Drive for Long Range Bombers," Translation CGD - 32, Technical Information Branch, Navy Dept., 1944.

4. Eggers, A. J., Jr., Allen, H. J., and Neice, S. E., "A Comparative Analysis of the Performance of Long-Range Hypervelocity Vehicles," NACA TN 4046, 1957.

5. Lees, L., Hastwig, F. W., and Cohen, C. B., "Use of Aerodynamic Lift During Entry into the Earth's Atmosphere," ARS Journal, pp. 633-641, September 1959.

6. Gazley, C., "Deceleration and Heating of a Body Entering a Planetary Atmosphere from Space," The RAND Corporation Report, P-955, February 1957.

7. Allen, H. J., and Eggers, A. J., "A Study of the Motion and Aerodynamic Heating of Missiles Entering the Earth's Atmosphere at High Supersonic Speeds," NACA TR 1381, 1958.

8. Chapman, D. R., "An Approximate Analytical Method for Studying Entry into Planetary Atmospheres," NASA Technical Report R-11, 1959.

# Chapter 9

# Aerodynamic Heating

## 9-1. INTRODUCTION

The various first-order solutions developed in Chapter 7 are now employed to analyze the thermal problems encountered in hypersonic flight. The study is of fundamental interest to scientists and engineers involved in design of space vehicles and in planning flight operations for a given mission. In space-flight, achieving a maximum payload is always a factor of prime consideration. A relatively important fraction of this payload is used in the protection and cooling process during entry if the spacecraft is to be recovered. During entry the total heat transferred to a spacecraft from the environment must be absorbed by some coolant material or radiated away. But any heat absorbing material has a maximum allowable temperature and therefore can accept only a given amount of heat per unit weight. Hence, the total heat input to the vehicle must be kept as low as possible.

On the other hand, often the coolant material is simply the protective wall of the vehicle exposed to the oncoming airstream, and it follows that the selection of this material is dictated by the required structural strength and rigidity for the vehicle. An important criterion determining the required structural performance of the vehicle is the dynamic pressure encountered, which is a function of the entry trajectory flown. In structural analysis, it is known that the strength of the structure is a function of the stresses induced by the temperature gradients within the material. Since these temperature gradients are proportional to the time rate of heat input, the maximum time rate of heat input is also a parameter of prime interest in the design of the vehicle. Hence, three of the most important parameters of the entry trajectory are the total heat input along the trajectory, the maximum rate of aerodynamic heating and the maximum dynamic pressure.

This mechanism of heat flow into a vehicle during entry was investigated at an early time by Allen and Eggers (Ref. 1). Since then, because of the many possible combinations of speed regimes and aerodynamic shapes, numerous technical papers have been published. But the basic aspects of the aerodynamic heating during entry are still the same. Only numerical factors for different heat transfer formulas and their validity in terms of the regime of the speed vary with the different authors. Hence, in this chapter, we shall follow Allen and Eggers (Ref. 1) in analyzing the three most important aspects of aerodynamic heating

during entry; namely,

1. The total heat input, $Q$.
2. The time rate and maximum time rate of average heat input per unit area, $q_{av} = dH_{av}/dt$ and
$$(q_{av})_{max} = (dH_{av}/dt)_{max} .$$
3. The time rate and maximum time rate of local stagnation region heat input per unit area, $q_s = dH_s/dt$ and $(q_s)_{max} = (dH_s/dt)_{max}$.

For easy reference, the notation introduced in this chapter is summarized below:

$A$ surface area, $m^2$

$C_F$ equivalent skin-friction coefficient

$C_p$ specific heat of atmosphere at constant pressure, k cal/kgm $^oK$

$h$ convective heat transfer coefficient, k cal/$m^2$ sec $^oK$

$H$ convective heat transfer per unit area, k cal/$m^2$

$k$ fraction of the heating rate at any point to the heating rate at stagnation point

$\kappa$ constant in stagnation point heat-transfer equation, k cal/$m^{3/2}$ sec

$q$ time rate of heat input per unit area, k cal/$m^2$ sec

$\bar{q}$ dimensionless $q$

$Q$ convective heat transferred, k cal

$R$ radius of curvature of body surface at stagnation point, m

$T$ temperature, $^oK$

Subscript

$o$ conditions at reference, initial condition

$av$ average values

$f$ final conditions

$\ell$ local conditions

$e$ exit conditions

$r$ recovery conditions

$s$ stagnation conditions, also conditions at sea level

$w$ wall condition

## 9-2. HEAT FLOW INTO THE VEHICLE

A vehicle entering a planetary atmosphere possesses a large amount of total energy. When it encounters the atmosphere at high speed, a shock wave system will form ahead of the part of the vehicle exposed to the oncoming airstream. The resulting deceleration of the flow induces the formation of a high temperature region in the inviscid flow between the shock system and the body. In addition, the velocity of the stream relative to the vehicle vanishes at the surface (zero-slip condition), producing a further increase in the static enthalpy of the fluid. Therefore, if the temperature at a small distance from the body is higher than the surface temperature, thermal energy flows into the body. The heat transfer is made up of two basic processes:

a/ convective heating associated with the transport processes in the boundary layer,

b/ radiant heating associated both with the radiation from the high-temperature gas to the vehicle, and the radiation away from the hot surface of the vehicle.

To simplify the analysis, Allen and Eggers have assumed that:

1. Convective heat transfer predominates and radiation effects could be ignored.

2. Real gas effects may be neglected.

3. Shock-wave boundary-layer interaction may be neglected.

4. Reynolds analogy is applicable.

5. The Prandtl number is unity.

Of the first assumption, the radiation effects that are neglected include the radiation from the surface of the body and the radiation to the body from the high-temperature disturbed air between the shock wave and the surface. The first simplification is based on the fact that the maximum allowable surface temperature will be about the same for a variety of entry vehicles, regardless of shape, and as a consequence the radiation away from the surface will be approximately the same. Hence, neglecting this form of heat transfer should not alter the qualitative effect of the relative heating investigated. The second simplification, namely neglecting the radiative heat transfer from the disturbed air, is purely for qualitative evaluation and is not applicable to very blunt and heavy shapes at entry speeds about $3,000$ m/sec .

In the second assumption, the neglect of real-gas effects in the flow, particularly dissociation, on convective heat transfer is a good assumption for entry speeds up to $3,000$ m/sec . In any case, it is a conservative assumption resulting in heating rates higher than actual rates.

In the third assumption, it has been shown by Lees and Probstein (Ref. 2), and by Li and Nagamatsu (Ref. 3), that shock-wave boundary-layer interaction may significantly increase laminar skin-friction coefficients on a flat plate at zero incidence and at Mach numbers in excess of about $10$ . Hence, this assumption should not be used for high entry speed of the order of $6,000$ m/sec or higher.

The assumptions of Reynolds analogy and constant Prandtl number taken as unity also restricts the entry speed to the range of less than 3,000 m/sec . It is for the purpose of simplifying the analysis that these assumptions were made. Hence, they should be removed for an accurate quantitative evaluation of the aerodynamic heating during entry of a specific vehicle. Nevertheless, the qualitative and explicit results obtained with these assumptions remain generally valid for an estimate of heat transport phenomena as a function of the aerodynamic shape of the vehicle, and the type of entry trajectory.

On the basis of the foregoing assumptions, for large Mach numbers, the difference between the local recovery temperature of the air, $T_r$ , and the wall temperature, $T_w$ , can be expressed as

$$(T_r - T_w)_\ell = \frac{V^2}{2C_p} \tag{9-1}$$

where the subscript $\ell$ denotes local conditions at a point on the body surface.

Now, by Reynolds analogy, the local heat-transfer coefficient $h_\ell$ , for the assumed Prandtl number of unity, is

$$h_\ell = \frac{1}{2} C_{F_\ell} C_{p_\ell} \rho_\ell V_\ell \tag{9-2}$$

where $C_{F_\ell}$ is the local skin-friction coefficient based on conditions just outside the boundary layer.

The time rate of convective heat transfer from the air to any element of surface of the body may be expressed by

$$\frac{dH}{dt} = h_\ell (T_r - T_w)_\ell \tag{9-3}$$

Hence,

$$\frac{dH}{dt} = \frac{V^2}{4C_p} (C_{F_\ell} C_{p_\ell} \rho_\ell V_\ell) \tag{9-4}$$

Equation (9-4) can be integrated over the surface $A$ of a body to yield the time rate of heat input

$$\frac{dQ}{dt} = \int_A \frac{dH}{dt} dA = \frac{1}{4} C_F A \rho V^3 \tag{9-5}$$

where assuming $C_{p_\ell} = C_p$

$$C_F = \frac{1}{A} \int_A C_{F_\ell} \left(\frac{\rho_\ell}{\rho}\right) \left(\frac{V_\ell}{V}\right) dA \tag{9-6}$$

The parameter $C_F$ is termed the " equivalent skin-friction coefficient" and will be assumed constant at a mean value for a particular vehicle (Refs. 4-5).

The time rate of average heat input per unit area may be obtained from Eq. (9-5) as

$$q_{av} = \frac{dH_{av}}{dt} = \frac{1}{A}\frac{dQ}{dt} = \frac{1}{4} C_F \rho V^3 \tag{9-7}$$

Consider next the local convective heat transfer at a stagnation point in the region of the foremost part of the body. According to Lees (Ref. 6), the heating rate at any point on a body is a fraction

$$k = \frac{q}{q_s} \tag{9-8}$$

of the heating rate $q_s$ at a stagnation point of radius of curvature $R$

$$q_s = \frac{\kappa}{\sqrt{R}} \left(\frac{\rho}{\rho_o}\right)^n \left(\frac{V}{V_o}\right)^m \tag{9-9}$$

where $\kappa$ is a constant. The constant exponents $n$ and $m$ depend on the type of boundary-layer flow. For laminar flow, we have $n = 1/2$ and under the assumptions that the viscosity coefficient varies as the square root of the absolute temperature and that flow between the bow shock wave and the stagnation point is incompressible we can use the value $m = 3$ (Ref. 1).

Hence, we shall consider

$$q_s = \frac{\kappa}{\sqrt{R}} \left(\frac{\rho}{\rho_o}\right)^{1/2} \left(\frac{V}{\sqrt{g_o r_o}}\right)^3 \tag{9-10}$$

## 9-3. DIMENSIONLESS VARIABLES

With the expressions obtained for different thermal quantities in terms of the atmospheric density $\rho$ and the speed $V$, we are now in a position to study the heating during entry using the first-order solutions derived in Chapter 7. The dimensionless variables introduced for developing first-order solutions are

$$u \equiv \frac{1}{2}\left(\frac{V^2}{g_o r_o}\right), \qquad \eta \equiv \frac{SC_D}{2m\beta}\rho \tag{9-11}$$

where the subscript zero denotes a reference condition, usually the initial condition.

It is convenient for the analysis to write the thermal quantities

in terms of these dimensionless variables. Using definitions (9-11) in Eq. (9-7), the time rate of average heat input per unit area is

$$q_{av} = \left[\frac{\sqrt{2m\beta}}{SC_D}(g_o r_o)^{3/2} C_F\right] \bar{q}_{av} \tag{9-12}$$

where

$$\bar{q}_{av} = \eta u^{3/2} \tag{9-13}$$

The expression for the time rate of local heat per unit area, Eq. (9-10), is

$$q_s = \left[\frac{4\kappa}{\sqrt{R}}\sqrt{\frac{m\beta}{SC_D\rho_o}}\right] \bar{q}_s \tag{9-14}$$

where

$$\bar{q}_s = \eta^{1/2} u^{3/2} \tag{9-15}$$

Finally, the total heat input is obtained by integrating Eq. (9-5). It is advantageous to integrate this equation with respect to $u$, though the relation (7-12) of Chapter 7, written as

$$\frac{d}{du}\left(\sqrt{\frac{2g_o}{r_o}}\, t\right) = -\frac{1}{2\beta r_o \eta u^{3/2}} \tag{9-16}$$

Hence, we can write the equation for $Q$

$$\frac{dQ}{du} = -\frac{AC_F}{2}\left(\frac{m}{SC_D}\right) g_o r_o \tag{9-17}$$

Integrating from $u_o$ to $u$

$$Q = \frac{AC_F}{2}\left(\frac{m}{SC_D}\right) g_o r_o (u_o - u) \tag{9-18}$$

## 9-4. ENTRY OF A BALLISTIC VEHICLE

For ballistic entry, the solution obtained in Chapter 7 is

$$\frac{u}{u_o} = \exp\left[\frac{2(\eta - \eta_o)}{\sin\gamma_o}\right] \tag{9-19}$$

Hence, with $\eta_o \approx 0$

$$Q = \frac{AC_F}{2} \left(\frac{m}{SC_D}\right) g_o r_o u_o \left[1 - \exp \frac{2\eta}{\sin \gamma_o}\right] \tag{9-20}$$

Since $u_o = (1/2) V_o^2 / g_o r_o$, the fraction of the initial kinetic energy which is transferred to the vehicle in the form of heat can be written as

$$\frac{Q}{\frac{1}{2} m V_o^2} = \frac{1}{2} \left(\frac{AC_F}{SC_D}\right) \left[1 - \exp \frac{2\eta}{\sin \gamma_o}\right] \tag{9-21}$$

For a relatively light vehicle $\eta_f >> 1$ and since $\sin \gamma_o < 0$, the ratio is reduced to

$$\frac{Q_f}{\frac{1}{2} m V_o^2} = \frac{1}{2} \left(\frac{AC_F}{SC_D}\right) \tag{9-22}$$

where subscript f denotes the final condition.

To minimize the heat convected to the vehicle, the ratio of the skin-friction coefficient $C_F$ to the total drag coefficient $C_D$ must be made as small as possible. This is achieved by a blunt body. Since a light vehicle is subject to sharply decreasing speed due to the aerodynamic force, Eq. (9-22) can also be obtained directly from Eq. (9-18) by taking $u_f \approx 0$. For a relatively dense ballistic vehicle, $\eta_f$ is small and

$$1 - \exp \frac{2\eta_f}{\sin \gamma_o} \approx - \frac{2\eta_f}{\sin \gamma_o} = - \frac{SC_D \rho_f}{m\beta \sin \gamma_o}$$

Hence,

$$\frac{Q_f}{\frac{1}{2} m V_o^2} = - \frac{\rho_f AC_F}{2m\beta \sin \gamma_o} \tag{9-23}$$

The skin-friction coefficient must be minimized to have the smallest total heat transferred.

With the solution (9-19) the dimensionless time rate of average heat input per unit area, Eq. (9-13), was found to be

$$\bar{q}_{av} = u_o^{3/2} \eta \exp \left(\frac{3\eta}{\sin \gamma_o}\right) \tag{9-24}$$

The expression has a maximum value when

$$\eta = -\frac{1}{3}\sin\gamma_o \tag{9-25}$$

This gives

$$(\bar{q}_{av})_{max} = -\frac{1}{3e}\,u_o^{3/2}\sin\gamma_o \tag{9-26}$$

This is only possible with a vehicle such that

$$\eta_s > -\frac{1}{3}\sin\gamma_o \tag{9-27}$$

where $\eta_s$ denotes the value of $\eta$ at sea level. The speed at which the maximum average heating rate occurs is obtained by substituting (9-25) into (9-19)

$$u = \frac{u_o}{e^{2/3}}\,, \qquad \frac{V}{V_o} = \frac{1}{e^{1/3}} \tag{9-28}$$

We notice that this critical value of the speed is independent of the vehicle physical characteristics. The altitude $h$ at which the maximum heating rate occurs is obtained by solving Eq. (9-25) for $h$.

$$h = \frac{1}{\beta}\log\left[-\frac{3SC_D\rho_s}{2m\beta\sin\gamma_o}\right] \tag{9-29}$$

This critical altitude is a function of the vehicle drag parameter and entry angle. If condition (9-27) is not satisfied, then the maximum heating rate occurs at sea level,

$$(\bar{q}_{av})_{max} = u_o^{3/2}\eta_s\exp\left(\frac{3\eta_s}{\sin\gamma_o}\right) \tag{9-30}$$

Figure 9-1 plots the average heating rate, $\bar{q}_{av}/u_o^{3/2}$ versus the "altitude" $1/\eta$ for different values of the entry angle $\gamma_o$. As in Chapter 7, the diagrams can be used for any type of ballistic entry vehicles. The line of maximum heating rate is the hyperbola

$$\left(\frac{1}{\eta}\right)\left(\frac{q_{av}}{u_o^{3/2}}\right) = \frac{1}{e} \tag{9-31}$$

If we consider the dimensionless time rate of local heat input per unit area, Eq. (9-15), then using the solution (9-19) for ballistic entry, we have

$$\bar{q}_s = u_o^{3/2} \eta^{1/2} \exp\left(\frac{3\eta}{\sin \gamma_o}\right) \tag{9-32}$$

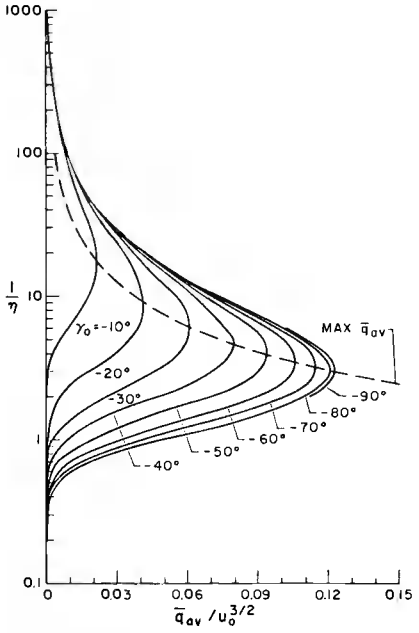


Fig. 9-1. Ballistic entry at large flight path angle. Average heating rate - Altitude diagram for several values of the initial angle.

The expression has a maximum value when

$$\eta = -\frac{1}{6} \sin \gamma_o \tag{9-33}$$

This gives

$$(\bar{q}_s)_{max} = u_o^{3/2} \sqrt{-\frac{1}{6e} \sin \gamma_o} \tag{9-34}$$

The altitude where the maximum heating rate occurs, as a function of the vehicle drag parameter and entry angle is given by

$$h = \frac{1}{\beta} \log\left(-\frac{3SC_D\rho_s}{m\beta \sin \gamma_o}\right) \tag{9-35}$$

where $\rho_s$ is the atmospheric density at sea level. The altitude is positive if

$$\eta_s > -\frac{\sin \gamma_o}{6} \tag{9-36}$$

If the inequality is not satisfied, the maximum heating rate occurs at sea level and has the value

$$(\bar{q}_s)_{max} = u_o^{3/2} \eta_s^{1/2} \exp\left(\frac{3\eta_s}{\sin \gamma_o}\right) \tag{9-37}$$

Figure 9-2 plots the heating rate $\bar{q}_s / u_o^{3/2}$ versus the altitude $1/\eta$ for different values of the entry angle $\gamma_o$. The diagrams can be used for any type of ballistic entry vehicle. The line of maximum heating rate is the curve

$$\left(\frac{1}{\eta}\right) \left(\frac{\bar{q}_s}{u_o^{3/2}}\right)^2 = \frac{1}{e} \tag{9-38}$$

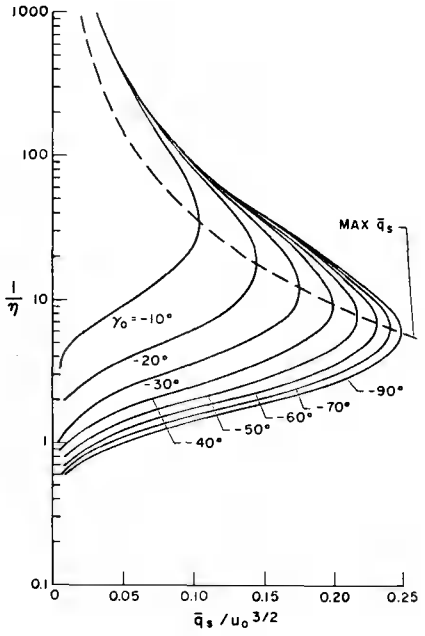


Fig. 9-2. Ballistic entry at large flight path angle. Heating-rate - Altitude diagram for several values of the initial angle.

## 9-5. ENTRY OF A GLIDE VEHICLE

For gliding entry, the solution obtained in Chapter 7 is

$$\eta = \frac{(1 - 2u)}{2\beta r_o (C_L/C_D)\, u} \tag{9-39}$$

The heat transfer to the vehicle is given by Eq. (9-18) which, for $u_f \approx 0$ is reduced to the same expression (9-22) as given for a light ballistic entry vehicle.

The time rate of average heat input per unit area is obtained by substituting solution (9-39) into Eq. (9-13)

$$\bar{q}_{av} = \frac{(1 - 2u)\, u^{1/2}}{2\beta r_o (C_L/C_D)} \tag{9-40}$$

It follows that the maximum average heat input rate occurs at

$$u = \frac{1}{6} \quad , \quad \frac{V}{\sqrt{g_o r_o}} = \frac{\sqrt{3}}{3} \tag{9-41}$$

This value of the speed is independent of the lift-to-drag ratio and vehicle physical characteristics. The corresponding maximum value of the average heat input rate is

$$(\bar{q}_{av})_{max} = \frac{1}{3\sqrt{6}\ \beta r_o (C_L/C_D)} \tag{9-42}$$

If we consider the dimensionless time rate of local heat input per unit area, Eq. (9-15), then using the solution (9-39) for gliding entry, we have

$$\bar{q}_s = \frac{(1 - 2u)^{1/2}\, u}{\sqrt{2\beta r_o (C_L/C_D)}} \tag{9-43}$$

The maximum time rate of local heat input occurs at

$$u = \frac{1}{3} \quad , \quad \frac{V}{\sqrt{g_o r_o}} = \frac{\sqrt{6}}{3} \tag{9-44}$$

Again, this value of the speed is independent of the lift-to-drag ratio and vehicle physical characteristics. The corresponding maximum value of the local heating rate is

$$(\bar{q}_s)_{max} = \frac{1}{3\sqrt{6\beta r_o (C_L/C_D)}} \tag{9-45}$$

## 9-6. ENTRY OF A SKIP VEHICLE

For skip entry, the solution obtain in Chapter 7 is

$$\cos\gamma - \cos\gamma_o = \frac{C_L}{C_D}(\eta - \eta_o) \tag{9-46}$$

for the altitude and

$$\frac{u}{u_o} = \exp\left[\frac{2(\gamma_o - \gamma)}{C_L/C_D}\right] \tag{9-47}$$

for the speed. The flight path angle $\gamma$ is used as the independent variable.

First, for the total heat input, the integral (9-18) is valid. Let $u_e = u_1$ be the value of $u$ at the first exit. The resulting heat flow after the first skipping phase $Q_1$ is

$$Q_1 = \frac{AC_F}{2}\left(\frac{m}{SC_D}\right) g_o r_o (u_o - u_1) \tag{9-48}$$

After a free flight in space, the vehicle reenters for another skipping phase with the same entry speed $u_1$. Then, if $u_n$ is the exit speed at the end of the nth skip, the total heat input is

$$Q = \frac{AC_F}{2}\left(\frac{m}{SC_D}\right) g_o r_o \sum_{k=1}^{n} (u_{k-1} - u_k) \tag{9-49}$$

It is clear that we have finally

$$Q = \frac{AC_F}{2}\left(\frac{m}{SC_D}\right) g_o r_o (u_o - u_f) \tag{9-50}$$

if $u_o$ is the initial value of $u$ and $u_f$ is its final value.

One may be led to believe that the final value $u_f$ is small. In general, a skipping trajectory is possible for high values of $C_L/C_D$ coupled with a small flight path angle $\gamma$. For constant $C_L/C_D$ the skipping phase may end at a relatively high value of $u_f$ and the remaining portion of atmospheric flight is effected as a glide trajectory at high lift-to-drag ratio. In any case, since the integral (9-18) is valid for all types of entry trajectories, and for lifting entry $u_f \approx 0$,

the resulting total heat input for a skip trajectory is

$$\frac{Q_f}{\frac{1}{2} m V_o^2} = \frac{1}{2} \left( \frac{A C_F}{S C_D} \right) \tag{9-51}$$

which is identical to the result obtained for light ballistic vehicle entry, Eq. (9-22), and also for gliding entry.

Now, using the Eqs. (9-46) and (9-47) in the expression (9-13) for the time rate of average heat input per unit area, we have

$$\bar{q}_{av} = u_o^{3/2} \frac{(\cos\gamma - \cos\gamma_o)}{(C_L/C_D)} \exp\left[ \frac{3(\gamma_o - \gamma)}{(C_L/C_D)} \right] \tag{9-52}$$

The maximum heating rate occurs when $d\bar{q}_{av}/d\gamma = 0$ .

$$3(\cos\gamma - \cos\gamma_o) + \left( \frac{C_L}{C_D} \right) \sin\gamma = 0 \tag{9-53}$$

As in Chapter 7, we can write this equation as a quadratic equation in $\tan(\gamma/2)$ . Upon solving we have the critical value of $\gamma$ where the maximum heating rate occurs

$$\tan\frac{\gamma}{2} = \frac{(C_L/C_D) - \sqrt{(C_L/C_D)^2 + 9\sin^2\gamma_o}}{3(1+\cos\gamma_o)} \tag{9-54}$$

In general, a skip trajectory is effected at high lift-to-drag ratios and small entry angles such that

$$\frac{9\sin^2\gamma_o}{(C_L/C_D)^2} \ll 1 \tag{9-55}$$

so that, in this case, the critical $\gamma$ can be evaluated from

$$\tan\frac{\gamma}{2} \approx -\frac{3}{(C_L/C_D)} \sin^2\frac{\gamma_o}{2} \tag{9-56}$$

In terms of the flight path angle, the time rate of local heat input per unit area, Eq. (9-15), is

$$\bar{q}_s = u_o^{3/2} \frac{(\cos\gamma - \cos\gamma_o)^{1/2}}{(C_L/C_D)^{1/2}} \exp\left[ \frac{3(\gamma_o - \gamma)}{(C_L/C_D)} \right] \tag{9-57}$$

At the point of maximum heating rate

$$6(\cos\gamma - \cos\gamma_o) + \left(\frac{C_L}{C_D}\right)\sin\gamma = 0 \tag{9-58}$$

Solving for this equation, we have

$$\tan\frac{\gamma}{2} = \frac{(C_L/C_D) - \sqrt{(C_L/C_D)^2 + 36\sin^2\gamma_o}}{6(1+\cos\gamma_o)} \tag{9-59}$$

In the case where assumption (9-55) is valid, we have approximately

$$\tan\frac{\gamma}{2} \approx -\frac{6}{(C_L/C_D)}\sin^2\frac{\gamma_o}{2} \tag{9-60}$$

The maximum values for $\bar{q}_{av}$ and $\bar{q}_s$ are obtained by using the corresponding critical values of $\gamma$. In the case where the small angle approximation is used, since the critical $\gamma$ is of the order of $\gamma_o^2$, we have explicitly

$$(\bar{q}_{av})_{max} = \frac{u_o^{3/2}\gamma_o^2}{2(C_L/C_D)}\exp\left[\frac{3\gamma_o}{(C_L/C_D)}\right] \tag{9-61}$$

and

$$(\bar{q}_s)_{max} = \frac{u_o^{3/2}\gamma_o}{\sqrt{2(C_L/C_D)}}\exp\left[\frac{3\gamma_o}{(C_L/C_D)}\right] \tag{9-62}$$

## 9-7. COMPARATIVE ANALYSIS OF THE PERFORMANCE OF HYPERVELOCITY VEHICLES

Any detailed analysis of the performance would require variational theory and hence is not within the stated goal of this work. Nevertheless, since some of the performance criteria such as range, time of flight, speed and design parameters, such as convective heat and heat rate, are obtained in explicit form, it is possible to have some qualitative appraisal of the performance of a hypervelocity vehicle using different entry modes. In the past, space vehicles were designed for a specified entry mode. In the beginning, they were all of the ballistic entry type vehicles. A new generation of space vehicles has lifting capability. Through attitude control the lift coefficient can be modulated in the range from $C_L = 0$ to $C_L = C_{L_{max}}$. Correspondingly, for a specified lifting vehicle, with a prescribed drag polar, the lift-to-drag ratio can be modulated from zero to $(C_L/C_D)_{max}$. We shall restrict ourselves to performance at constant lift-to-drag ratio. Lift-

modulation to achieve prescribed constraints will be examined in the final chapters.

Since we consider a versatile lifting vehicle, it is proper to discuss entry modes rather than entry vehicles. The three entry modes that have been discussed are:

1. Ballistic entry.
2. Glide entry.
3. Skip entry.

Any vehicle considered is supposed to have the capability of entering a planetary atmosphere in any of these three modes or using any combination of modes in following an overall, composite trajectory.

First, from the range standpoint, ballistic entry is the least effective mode. For skip entry, the range for each separate skipping phase is short but each atmospheric portion of the flight trajectory is followed by a Keplerian portion in space adding significant distance to the total range. As a matter of fact, with a high initial entry speed, a skip trajectory can achieve infinite range while a glide trajectory totally immersed in the atmosphere is condemned to a finite range. Thus, there exists an initial speed such that there is equal range for skip entry and glide entry, with gliding flight achieving the longer range at lower initial speed.

From considerations of aerodynamic heating, with the possible exception of the relatively dense vehicle in the ballistic mode, in all three modes, the hypervelocity vehicle expends the major part of its kinetic energy in flight and receives in exchange heat by convection according to the simplified formula

$$\frac{Q_f}{\frac{1}{2}mV_o^2} = \frac{1}{2}\left(\frac{AC_F}{SC_D}\right) \tag{9-63}$$

To minimize this fraction, that is to reduce the total heat transfer by convection, it is necessary to determine how the ratio of friction force to total drag force can be reduced. This matter was discussed in detail in Ref. 1 in connection with a purely ballistic vehicle and it was demonstrated that the ratio could be reduced by employing high pressure-drag shapes, that is, blunted shapes. On the other hand, in the skip and glide modes the geometric configuration of the vehicle will be slender and the above ratio may reach the order of 0.1 which is quite high for vehicle materials to absorb. In skip or glide modes one must, therefore, consider the possibility of the vehicle radiating a significant part of this heat back to the surrounding atmosphere. This problem has been discussed in Ref. 4, and it is found that in a high lift-to-drag ratio glide mode, if the surface temperature is allowed to reach a high level, the vehicle can radiate heat at a rate equal to the maximum average convective heat transfer rate. Furthermore, in the gliding mode the vehicle may require less coolant than in the ballistic mode. The reason for this is that although in the gliding mode the same vehicle will receive more heat, the gliding time is much longer, by a factor of perhaps one hundred. Therefore, with a sufficiently

high radiant heat transfer rate the glide vehicle can return to the atmosphere most of the heat it receives by convection.

In general, for a lifting hypervelocity vehicle a combination of an initial entry at a high angle of attack using a pure ballistic mode, followed by a tip over to lower the angle-of-attack, and continued with a high lift-to-drag ratio gliding mode, looks promising from the standpoint of aerodynamic heating.

For manned flights, another factor to be considered is the peak deceleration. Along an entry trajectory we consider the points where the quantities $\bar{q}_s$ , $\bar{q}_{av}$ and $(a/g)$ reach their respective maximum values. The solutions obtained in Chapter 7 and in the present Chapter are summarized in Table 9-1.

Table 9-1. Points of maximum $\bar{q}_s$ , $\bar{q}_{av}$ and $(a/g)$ .

| | $(\bar{q}_s)_{max}$ | $(\bar{q}_{av})_{max}$ | $(\frac{a}{g})_{max}$ |
|---|---|---|---|
| Ballistic | $\eta = -\frac{1}{6}\sin\gamma_o$ | $\eta = -\frac{1}{3}\sin\gamma_o$ | $\eta = -\frac{1}{2}\sin\gamma_o$ |
| Skip | $\tan\frac{\gamma}{2} = -\frac{6\sin^2\frac{\gamma_o}{2}}{(C_L/C_D)}$ | $\tan\frac{\gamma}{2} = -\frac{3\sin^2\frac{\gamma_o}{2}}{(C_L/C_D)}$ | $\tan\frac{\gamma}{2} = -\frac{2\sin^2\frac{\gamma_o}{2}}{(C_L/C_D)}$ |
| Glide | $\frac{V}{\sqrt{g_o r_o}} = \frac{\sqrt{6}}{3}$ | $\frac{V}{\sqrt{g_o r_o}} = \frac{\sqrt{3}}{3}$ | $\frac{V}{\sqrt{g_o r_o}} \approx 0$ |

In the ballistic mode at nearly constant angle $\gamma$ , the maximum of $\bar{q}_s$ occurs first, at the lowest value of $\eta$ , (hence at the highest altitude), then comes the maximum of $\bar{q}_{av}$ , and finally the maximum of $(a/g)$ .

In the skip mode the negative flight path angle increases from the initial value $\gamma_o$ to $\gamma = 0$ when the vehicle reaches the lowest point. From the Table, the three maxima occur in the same order.

Finally in the glide mode, as the speed decreases continuously along the flight trajectory, again the vehicle reaches $(\bar{q}_s)_{max}$ first, and then $(\bar{q}_{av})_{max}$ . In the meantime the deceleration builds up to reach its maximum at the final time.

The respective maximum values of $\bar{q}_s$ , $\bar{q}_{av}$ and $(a/g)$ are summarized in Table 9-2.

Table 9-2. Maximum values of $\bar{q}_s$ , $\bar{q}_{av}$ and $(a/g)$ .

| | $(\bar{q}_s)_{max}$ | $(\bar{q}_{av})_{max}$ | $(\frac{a}{g})_{max}$ |
|---|---|---|---|
| Ballistic | $u_o^{3/2}\sqrt{-\frac{\sin\gamma_o}{6e}}$ | $-\frac{u_o^{3/2}\sin\gamma_o}{3e}$ | $-\frac{\beta r_o u_o \sin\gamma_o}{e}$ |
| Skip | $\frac{u_o^{3/2}\gamma_o}{\sqrt{2(C_L/C_D)}}\exp\frac{3\gamma_o}{C_L/C_D}$ | $\frac{u_o^{3/2}\gamma_o^2}{2(C_L/C_D)}\exp\frac{3\gamma_o}{C_L/C_D}$ | $\frac{\beta r_o u_o \gamma_o^2}{(C_L/C_D)}\exp\frac{2\gamma_o}{C_L/C_D}$ |
| Glide | $\frac{1}{3\sqrt{6\beta r_o (C_L/C_D)}}$ | $\frac{1}{3\sqrt{6\,\beta r_o (C_L/C_D)}}$ | $\frac{1}{(C_L/C_D)}$ |

From the formulas, it is seen that using a high lift-to-drag ratio, $C_L/C_D$ , has the effect of decreasing $(\bar{q}_s)_{max}$ , and also decreasing the peak deceleration for both ballistic and glide entries. Then, for entry trajectories with an upper constraint on the peak deceleration, it is suggested that high lift be used to reduce the deceleration. Unfortunately, because of the lift-drag relationship and because of heating considerations, the high drag portion of the drag polar is generally employed so that when the lift-to-drag ratio increases, the drag coefficient decreases (Fig. 9-3) and from the expression (9-63) for total heat transferred by convection, the heat absorbed increases. These effects, which work at cross purposes, will be discussed again in Chapter 12 in connection with the concept of the entry corridor.

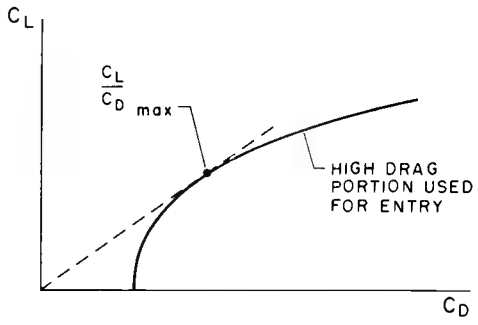


Fig. 9-3. Drag polar for a lifting hypervelocity vehicle.

## References

1. Allen, H. J., and Eggers, A. J., Jr., "A Study of the Motion and and Aerodynamic Heating of Missiles Entering the Earth's Atmosphere at High Supersonic Speeds," NACA TR 1381, 1958.

2. Lees, L., and Probstein, R. F., "Hypersonic Viscous Flow Over a Flat Plate," Princeton University Aeronautical Engineering Laboratory, Report No. 195, 1952.

3. Li, Ting-Yi, and Nagamatsu, H. T., "Shock Wave Effects on the Laminar Skin Friction of an Insulated Flat Plate at Hypersonic Speeds," GALCIT Memorandum, No. 9, 1952.

4. Eggers, A. J., Jr., Allen, H. J., and Neice, S. E., "A Comparative Analysis of the Performance of Long-Range Hypervelocity Vehicles," NACA TN-4046, 1957.

5. Miele, A., Flight Mechanics, Vol. I, Theory of Flight Paths, Addison-Wesley Publishing Company, Inc., Reading, Massachusetts, 1962.

6. Lees, L., "Laminar Heat Transfer Over Blunt-Nosed Bodies at Hypersonic Flight Speeds," Jet Propulsion, Vol. 26, No. 4, pp. 259-269, April 1956.

# Chapter 10

# Yaroshevskii's Theory for Entry into Planetary Atmospheres

## 10-1. INTRODUCTION

The analytical development in Chapters 7, 8 and 9 presents the classical theories for entry into a planetary atmosphere. The simple results given are adequate for the purpose of a preliminary estimate of the variations of the trajectory variables along an entry flight path and the different physical characteristics expressed as functions of these entry variables. Beginning in this chapter, we shall present various modern theories for planetary entry.

First, with the physical understanding of the phenomena associated with an entry trajectory as presented in the previous chapters, scientists and engineers are led to formulating very general assumptions which are valid for nearly all types of entry trajectories. This results in a set of equation of motion valid for all types of entry trajectories of practical interests. Furthermore, if these equations can be presented in dimensionless form, in the same way as has been done in the previous chapters for first-order analysis, the results obtained can be applied to any entry vehicle regardless of its physical characteristics. This type of approach is illustrated by Yaroshevskii's theory presented in this chapter, and Chapman's theory in Chapters 11 and 12.

Next, if the restrictive assumptions introduced are removed while the universal character of the entry equations is still preserved, the exact dimensionless equations of motion for planetary entry are obtained and they are valid for all types of entry trajectories of any entry vehicle regardless of its mass, size and aerodynamic characteristics. Furthermore, the trajectory considered can be completely immersed inside the atmosphere or can be partly outside of it in the form of Keplerian arcs. This also will include orbital motion of satellites at very high altitude subject to Newtonian gravitational attraction and infinitesimally small atmospheric drag. This analysis will be considered in the following chapters.

Finally, one may consider the case where the aerodynamic controls in the form of the lift-to-drag ratio and the bank angle are not constant but can be modulated according to a certain law in order to achieve a specific purpose. This type of trajectories will be analyzed in the last chapters.

Yaroshevskii's theory for entry trajectory is a semi-analytical theory. Using some simplifying assumptions, he derived a nonlinear, second-order differential equation which can be integrated analytically by using series expansions. To some extent, Yaroshevskii's theory is a special case (Refs. 1,2) of a more sophisticated theory developed by Chapman (Ref. 3). Because his theory has some features of merit, we shall present it in this chapter. Chapman's theory will be developed in the next chapter, and the connection between the two theories will be examined.

## 10-2. SECOND-ORDER NONLINEAR DIFFERENTIAL EQUATION FOR ENTRY TRAJECTORY

Consider the basic equations for planar entry derived in Chapter 2

$$\frac{dV}{dt} = -\frac{\rho S C_D V^2}{2m} - g \sin\gamma$$

$$V\frac{d\gamma}{dt} = \frac{\rho S C_L V^2}{2m} - \left(g - \frac{V^2}{r}\right)\cos\gamma$$

$$\frac{dr}{dt} = V \sin\gamma \qquad (10\text{-}1)$$

Strictly speaking, as was mentioned in Section 6-2, the lift and the drag coefficients are functions of the angle of attack $\alpha$, of the Mach number $M$, and the Reynolds number $R_e$. For constant angle of attack, Yaroshevskii assumed that the lift coefficient $C_L$, and the drag coefficient $C_D$ are functions of the Mach number. For an isothermal atmosphere, this is just a function of the speed, $V$.

If, in the equation for $V$, we neglect the tangential component of the gravity force, and in the equation for $\gamma$ and $r$ we use the approximation of small flight path angle, we can write the Eqs. (10-1) as

$$\frac{dV}{dt} = -\frac{\rho S C_D(V)\, V^2}{2m}$$

$$V\frac{d\gamma}{dt} = \frac{\rho S C_L(V)\, V^2}{2m} - g + \frac{V^2}{r}$$

$$\frac{dr}{dt} = V\gamma \qquad (10\text{-}2)$$

The first of these equations can be used to change the independent variable to $V$:

$$\frac{dr}{dV} = - \frac{\gamma}{\frac{\rho S C_D(V)\, V}{2m}}$$

$$V \frac{d\gamma}{dV} = - \frac{C_L}{C_D} + \frac{g - \frac{V^2}{r}}{\frac{\rho S C_D(V)\, V^2}{2m}} \qquad (10\text{-}3)$$

To derive his second-order nonlinear differential equation for entry into a planetary atmosphere, Yaroshevskii used an independent variable $x$, and a dependent variable $y$ defined as

$$x \equiv - \int_1^{\overline{V}} \frac{C_D(1)\, d\overline{V}}{C_D(\overline{V})\, \overline{V}}$$

$$y \equiv \frac{C_D(1)\, S}{2m} \sqrt{\frac{r_o}{\beta}}\, \rho \qquad (10\text{-}4)$$

where $r_o$ is the radius of the planet and $\overline{V}$ is the dimensionless speed

$$\overline{V} \equiv \frac{V}{\sqrt{g r_o}} \qquad (10\text{-}5)$$

At this point the following remarks are in order:

a/ The altitude $h$ is small compared to the radius $r_o$ of the planet. Hence, $g$ is approximately constant.

b/ For the same reason, $\sqrt{g r_o}$ can be considered as the circular speed at the entry altitude. Hence, if the entry is from circular speed, the initial value of $\overline{V}$ is unity, and from the definition (10-4) of the independent variable $x$, this variable increases monotonically from the initial value $x = 0$.

If a strictly exponential atmosphere is used, then

$$\frac{d\rho}{\rho} = - \beta dr \qquad (10\text{-}6)$$

where $\beta$ is constant. Hence, from the definition of $y$

$$\frac{dy}{y} = - \beta dr \qquad (10\text{-}7)$$

On the other hand

$$dx = - \frac{C_D^{(1)}}{C_D(\bar{V})} \frac{d\bar{V}}{\bar{V}} = - \frac{C_D^{(1)}}{C_D(\bar{V})} \frac{dV}{V} \tag{10-8}$$

With these differential relations, and the definition (10-4) of $x$ and $y$, the Eqs. (10-3) are

$$\frac{dy}{dx} = - \sqrt{\beta r_o}\ \gamma$$

$$\frac{d\gamma}{dx} = \frac{C_L[\bar{V}(x)]}{C_D^{(1)}} - \frac{1 - \bar{V}^2(x)}{\sqrt{\beta r_o}\ y \bar{V}^2(x)} \tag{10-9}$$

where in the equation for $\gamma$, the approximation of small altitude, $r = r_o$, has been used.

Eliminating $\gamma$ between the two equations above, we obtain a single equation of the second-order

$$\frac{d^2y}{dx^2} = - \sqrt{\beta r_o} \left\{ \frac{C_L[\bar{V}(x)]}{C_D^{(1)}} + \frac{\frac{1}{\bar{V}^2(x)} - 1}{y} \right\} \tag{10-10}$$

This equation is Yaroshevskii's nonlinear, second-order differential equation for studying entry into a planetary atmosphere. The quantity $\beta r_o$ is constant, and for the Earth's atmosphere we can take $\beta r_o$ as about 900. The equation takes into account the effect of the Mach number on the lift and the drag coefficients at constant angle of attack. In general, this equation has to be integrated numerically. In the special case where $C_L$ and $C_D$ are independent of the Mach number, the equation can be integrated using some appropriate series expansions, depending on the type of entry trajectory.

Once the variable $y$ is known as a function of the independent variable $x$, other quantities of interest can be evaluated.

First, the flight path angle is given by the first of the Eqs. (10-9)

For the time of flight, we write the first of the Eqs. (10-2) in terms of $x$ and $y$

$$\frac{dx}{dt} = \sqrt{\beta g}\ y\ \bar{V}(x) \tag{10-11}$$

Hence, the time is obtained by performing the quadrature

$$\sqrt{\beta g}\ t = \int_{x_i}^{x} \frac{dx}{y \bar{V}(x)} \tag{10-12}$$

where $x_i$ is the initial value of $x$. The distance travelled, $s$, as projected on the surface of the planet, is given by the kinematic relation

$$\frac{ds}{dt} = r_o \frac{d\theta}{dt} = \frac{r_o}{r} V \cos\gamma$$

Hence, for small flight path angles, and with the approximation of small flight altitude relative to $r_o$, we have

$$\frac{ds}{dt} = \sqrt{g r_o}\ \overline{V}(x) \tag{10-13}$$

Using Eq. (10-11), it is seen that the distance travelled is given by the integral

$$\sqrt{\frac{\beta}{r_o}}\ s = \int_{x_i}^{x} \frac{dx}{y} \tag{10-14}$$

The deceleration along the trajectory, during entry, is $-(dV/dt)$. Using the first of the Eqs. (10-2), and the definitions (10-4) and (10-5), we have

$$-\left(\frac{dV}{dt}/g\right) = \sqrt{\beta r_o}\ \frac{C_D[\overline{V}(x)]}{C_D(1)}\, y\, \overline{V}^2(x) \tag{10.15}$$

Other physical quantities of interest, such as the heating rate and the total heat absorbed, will be given in the immediately following section when we consider entry at constant lift-to-drag ratio.

## 10-3. ATMOSPHERIC ENTRY AT CONSTANT LIFT-TO-DRAG RATIO

In practice, the simplest and most interesting case is that obtained for constant lift and drag coefficients. This case is commonly encountered along the main part of the entry trajectory where, at high Mach number, the lift and the drag coefficients are independent of $M$. It is also along this portion of the trajectory that the deceleration and the heating rate reach their maxima.

From the definition of $x$, Eq. (10-4), it is seen that when $C_D$ is independent of the Mach number

$$x = \log \frac{\sqrt{g r_o}}{V}, \qquad \overline{V} = e^{-x} \tag{10-16}$$

The basic nonlinear differential equation, Eq. (10-10), is reduced to

$$\frac{d^2y}{dx^2} = -\sqrt{\beta r_o}\ \frac{C_L}{C_D} + \frac{e^{2x} - 1}{y} \tag{10-17}$$

This equation can be integrated by using an appropriate series expansion, depending on the type of trajectory.

While the distance travelled, Eq. (10-14), remains the same, in the case of constant lift-to-drag ratio entry, the expression for the time of flight and the deceleration, Eqs. (10-12) and (10-15) become

$$\sqrt{\beta g}\ t = \int_{x_i}^{x} \frac{e^x dx}{y} \tag{10-18}$$

and

$$\bar{a} = -\left(\frac{dV}{dt}/g\right) = \sqrt{\beta r_o}\ y e^{-2x} \tag{10-19}$$

In the numerical computation, we can use the following approximate characteristic values of the Earth

$$\frac{1}{\beta} \approx 7000 \text{ m}, \quad \sqrt{\beta r_o} \approx 30$$

$$\frac{1}{\sqrt{\beta g}} \approx 26.5 \text{ sec}, \quad \sqrt{\frac{r_o}{\beta}} \approx 212 \text{ km}$$

$$V_{circular} = \sqrt{g r_o} \approx 7850 \text{ m/sec} \tag{10-20}$$

For a strictly exponential atmosphere, the dependent variable $y$ is simply proportional to the atmospheric density $\rho$. With the approximate value given above,

$$y \approx 1.04 \times 10^6 B\rho \tag{10-21}$$

where $B$ is the drag parameter

$$B \equiv \frac{SC_D}{mg}\ m^2/\text{kg} \tag{10-22}$$

The aerodynamic heating rate per unit area on a body reaches its maximum at a stagnation point of radius of curvature $R$, and is given by (Refs. 4-6)

$$q_s = \frac{C}{\sqrt{R}} \rho^n V^m \tag{10-23}$$

where the constants $C$, $n$ and $m$ depend on the type of boundary layer. For laminar flow, $n = 1/2$, and the value of $m$ has been given by various authors as $3.1 \leq m \leq 3.25$. For his numerical computation Yaroshevskii adopted the following formula as given by

Kemp and Riddell, (Ref. 7), for the stagnation point heat transfer rate:

$$q_s = \frac{8.8 \times 10^4}{\sqrt{R}} \rho^{1/2} \left( \frac{V}{\sqrt{g r_o}} \right)^{3.25} \frac{\text{kcal}}{\text{m}^2 \text{sec}} \qquad (10\text{-}24)$$

For a constant drag coefficient, for which the relations (10-16) and (10-21) apply, this formula becomes

$$q_s = \frac{85 y^{0.5} e^{-3.25x}}{R^{0.5} B^{0.5}} \frac{\text{kcal}}{\text{m}^2 \text{sec}} \qquad (10\text{-}25)$$

If there is a turbulent boundary layer, the aerodynamic heating rate per unit area reaches its maximum at the section where the transition through the speed of sound takes place, (Ref. 8). The formula (10-25) for laminar flow is replaced by, (Ref. 1),

$$q_t = \frac{25 y^{0.8} e^{-3.19x}}{R^{0.2} B^{0.8}} \frac{\text{kcal}}{\text{m}^2 \text{sec}} \qquad (10\text{-}26)$$

for the heat transfer rate at the turbulent sonic point.

Another quantity of interest in aerodynamic heating is the total heat absorbed per unit area

$$\frac{Q}{A} = \int q \, dt \qquad (10\text{-}27)$$

where $A$ is the whole surface wetted by the boundary layer, and $q$ is given by Eq. (10-25) for laminar flow, and Eq. (10-26) for turbulent flow. The integration with respect to $t$ can be changed into the integration with respect to $x$, by the use of Eq. (10-18),

$$\frac{Q_s}{A} = \frac{2250}{R^{0.5} B^{0.5}} \int_{x_i}^{x} \frac{e^{-2.25x}}{y^{0.5}} dx \frac{\text{kcal}}{\text{m}^2} \qquad (10\text{-}28)$$

and

$$\frac{Q_t}{A} = \frac{665}{R^{0.2} B^{0.8}} \int_{x_i}^{x} \frac{e^{-2.19x}}{y^{0.2}} dx \frac{\text{kcal}}{\text{m}^2} \qquad (10\text{-}29)$$

It is seen that, if the basic nonlinear differential equation for constant lift-to-drag ratio entry, Eq. (10-17), can be integrated, the variable $y$ is obtained as function of the independent variable $x$. The deceleration during entry is given by Eq. (10-19), while the time of flight, the heating rate and the heat absorbed are obtained explicitly or by quadratures through Eqs. (10-18), (10-25) - (10. 26), and (10-28) - (10-29), respectively.

## 10-4. SERIES SOLUTIONS OF THE BASIC NONLINEAR DIFFERENTIAL EQUATION

The basic nonlinear differential equation for constant lift-to-drag ratio entry, Eq. (10-17), can be integrated approximately by using series solutions. We shall integrate this equation in the following cases.

### 10-4.1. Ballistic Decay From Satellite Orbits

For ballistic entry trajectory, $C_L / C_D = 0$ , and Eq. (10-17) is reduced to

$$\frac{d^2y}{dx^2} = \frac{e^{2x} - 1}{y} \tag{10-30}$$

Under the action of atmospheric drag, acting primarily at periapsis, a high altitude satellite orbit tends to a circular orbit before effective entry. Hence, in this case, for the portion of the trajectory where effective entry is achieved, Eq. (10-30) is integrated with the initial conditions

$$x_i = 0 \quad , \quad y(0) = 0 \quad , \quad y'(0) = 0 \tag{10-31}$$

where the prime denotes the derivative taken with respect to $x$ . The differential equation (10-30) has a singularity at $y = 0$ . To remove this singularity, we notice that, in the neighborhood of $x = 0$ , the equation becomes

$$yy'' = 2x \tag{10-32}$$

This equation has the solution

$$y = \sqrt{\frac{8}{3}}\, x^{3/2} \tag{10-33}$$

satisfying the initial condition (10-31). Hence, we can seek a solution of the differential equation (10-30) in the form

$$y = \sqrt{\frac{8}{3}}\, x^{3/2} (a_0 + a_1 x + a_2 x^2 + a_3 x^3 + \dots) \tag{10-34}$$

Writing Eq. (10-30)

$$yy'' = 2x + 2x^2 + \frac{4}{3} x^3 + \frac{2}{3} x^4 + \dots \tag{10-35}$$

substituting the series (10-34), and equating coefficients of like powers in $x$ , we obtain for the coefficients $a_k$

$$a_0 = 1 \quad , \quad a_1 = \frac{1}{6} \quad , \quad a_2 = \frac{1}{24} \quad , \quad a_3 = \frac{47}{4752} \quad , \quad \ldots \tag{10-36}$$

The recurrence formula for computing the coefficients $a_k$ is

$$a_k = \frac{\dfrac{2^k}{(k+1)!} - \dfrac{1}{3} \displaystyle\sum_{m=1}^{k-1} (2m+1)(2m+3)\, a_m a_{k-m}}{1 + \dfrac{(2k+1)(2k+3)}{3}} \tag{10-37}$$

It can be seen that

$$|a_k| \leq 1/(k+1)^2 (1.5)^k \tag{10-38}$$

Therefore, the radius of convergence of the series is not less than $1.5$ . The series solution is sufficiently accurate to evaluate the maximum deceleration and heat transfer rate which occurs during the fundamental part of the entry trajectory where the main assumptions used for the derivation of the nonlinear differential equation are valid.

For $x < 1$ , we need only three terms of the series, and the truncated $y$ function for ballistic entry from circular orbit is

$$y = \sqrt{\frac{8}{3}} \left(1 + \frac{x}{6} + \frac{x^2}{24}\right) x^{3/2} \tag{10-39}$$

From Eq. (10-19), the deceleration is

$$-\left(\frac{dV}{dt}/g\right) = \sqrt{\frac{8\beta r_o}{3}} \left(x^{3/2} + \frac{x^{5/2}}{6} + \frac{x^{7/2}}{24}\right) e^{-2x} \tag{10-40}$$

The peak deceleration is obtained by taking the derivative of this equation with respect to $x$ and setting it equal to zero. The resulting equation is

$$4x^3 + 9x^2 + 76x - 72 = 0 \tag{10-41}$$

The solution of this equation gives the conditions at maximum deceleration:

$$x = 0.835 \quad , \quad \frac{V}{\sqrt{g r_o}} = 0.434$$

$$y = 1.45 \quad , \quad -(a/g)_{max} = 0.277 \sqrt{\beta r_o} \tag{10-42}$$

Substitution of the solution (10-39) into Eqs. (10-25) and (10-26) yields the expression for the aerodynamic heating rate per unit area for laminar flow, (at the stagnation point), and turbulent flow, (at the sonic point), respectively. The maximization of these functions provides:

The maximum heating rate along the trajectory under laminar flow conditions is characterized by:

$$x = 0.237 \quad , \quad \frac{V}{\sqrt{gr_o}} = 0.789$$

$$y = 0.197 \quad , \quad q_{s_{max}} = \frac{17.4}{R^{0.5} B^{0.5}} \quad \frac{kcal}{m^2 sec} \tag{10-43}$$

The maximum heating rate along the trajectory under turbulent flow conditions is characterized by:

$$x = 0.4 \quad , \quad \frac{V}{\sqrt{gr_o}} = 0.670$$

$$y = 0.444 \quad , \quad q_{t_{max}} = \frac{3.65}{R^{0.2} B^{0.8}} \quad \frac{kcal}{m^2 sec} \tag{10-44}$$

10-4.2. Ballistic Entry With Various Initial Flight Path Angles.

The basic equation for ballistic entry, Eq. (10-30), is now integrated with nonzero initial flight path angle. For entry from circular speed, the initial conditions are

$$x_i = 0 \quad , \quad y(0) = 0 \quad , \quad y'(0) = c_1 \tag{10-45}$$

where, from the first of the Eqs. (10-9)

$$c_1 = - \sqrt{\beta r_o} \, \gamma_i > 0 \tag{10-46}$$

First, we consider the case of small values of $c_1$. The case $c_1 = 0$ has been considered in the previous section. For small values of $x$, we have approximately the same Eq. (10-32). We rescale the initial conditions (10-45) by using the transformation of variables

$$\eta = \frac{x}{c_1^2} \quad , \quad y = c_1^3 g(\eta) \tag{10-47}$$

Thus, Eq. (10-32) becomes

$$\frac{d^2 g}{d\eta^2} = \frac{2\eta}{g} \tag{10-48}$$

It has the same form as before, but with the new standard initial

condition

$$\eta_i = 0 \quad , \quad g(0) = 0 \quad , \quad \frac{dg}{d\eta} = 1 \tag{10-49}$$

Hence, Eq. (10-48) with the initial conditions (10-49) can be integrated numerically once for all, and by the transformation (10-47), the result obtained can be used for any small value of $c_1 = -\sqrt{\beta r_o}\,\gamma_i$ . Fig. 10-1 plots this solution as a solid line, while the dashed line is the exact analytical solution of the Eq. (10-48) with the initial conditions $g(0) = 0$ , $dg/d\eta = 0$ .

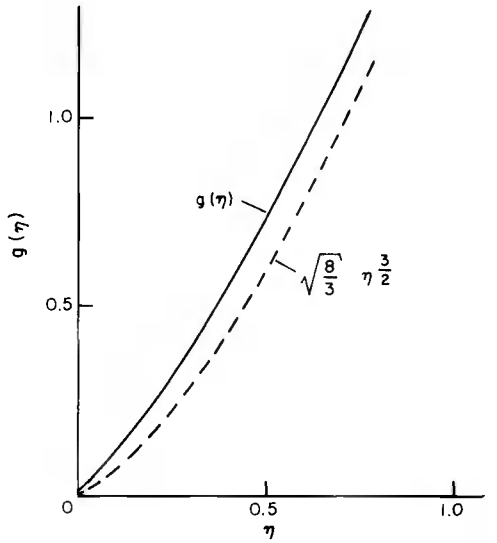


Fig. 10-1. Solution for ballistic entry from circular speed at small initial flight path angle.

For large values of $c_1$ , we consider Eq. (10-30) , or rather its expanded form, Eq. (10-35). Based on the initial conditions (10-45), we seek its series solution in the form

$$y = \sum_{m=1}^{\infty} c_m x^m \tag{10-50}$$

Substituting this series into Eq. (10-35) and equating coefficients of like powers in $x$ , we have for the coefficients $c_m$

$$c_2 = \frac{1}{c_1}, \quad c_3 = \left(1 - \frac{1}{c_1^2}\right)\frac{1}{3c_1}$$

$$c_4 = \left(1 - \frac{2}{c_1^2} + \frac{2}{c_1^4}\right)\frac{1}{9c_1}, \quad c_5 = \left(3 - \frac{10}{c_1^2} + \frac{20}{c_1^4} - \frac{17}{c_1^6}\right)\frac{1}{90c_1} \tag{10-51}$$

It can be seen that the recurrence formula to evaluate $c_m$ is

$$m(m-1)c_1 c_m = \frac{2^{m-1}}{(m-1)!} - \sum_{k=2}^{m-1} k(k-1)c_k c_{m+1-k} \tag{10-52}$$

Figure 10-2 plots the numerical solution of Eq. (10-30) using the initial conditions (10-45) with various values of $c_1$, as solid lines. The analytical solution for entry at zero initial flight path angle, Eq. (10-34), and entry at various nonzero initial flight path angles, Eq. (10-50), using 4 terms of the series, are plotted as dashed lines.

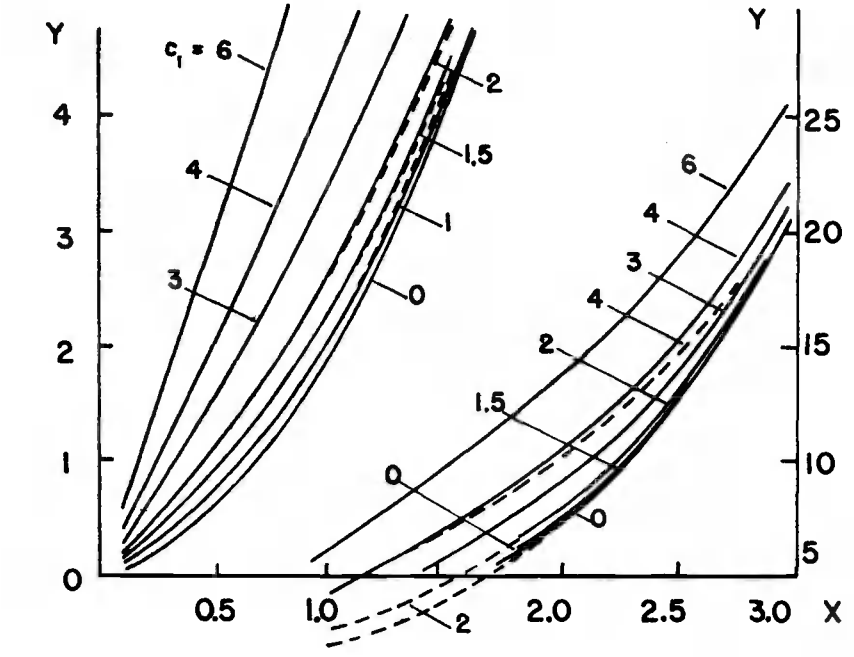


Fig. 10-2. Solutions for ballistic entry from circular speed at various initial flight path angles.

_____ Numerical solutions ------ 4 terms of the series

Figures 10-3 to 10-8 give the plots of the numerical integration of the equation for ballistic entry, Eq. (10-3), with various values for $c_1 = -\sqrt{\beta r_o}\ \gamma_i$ .

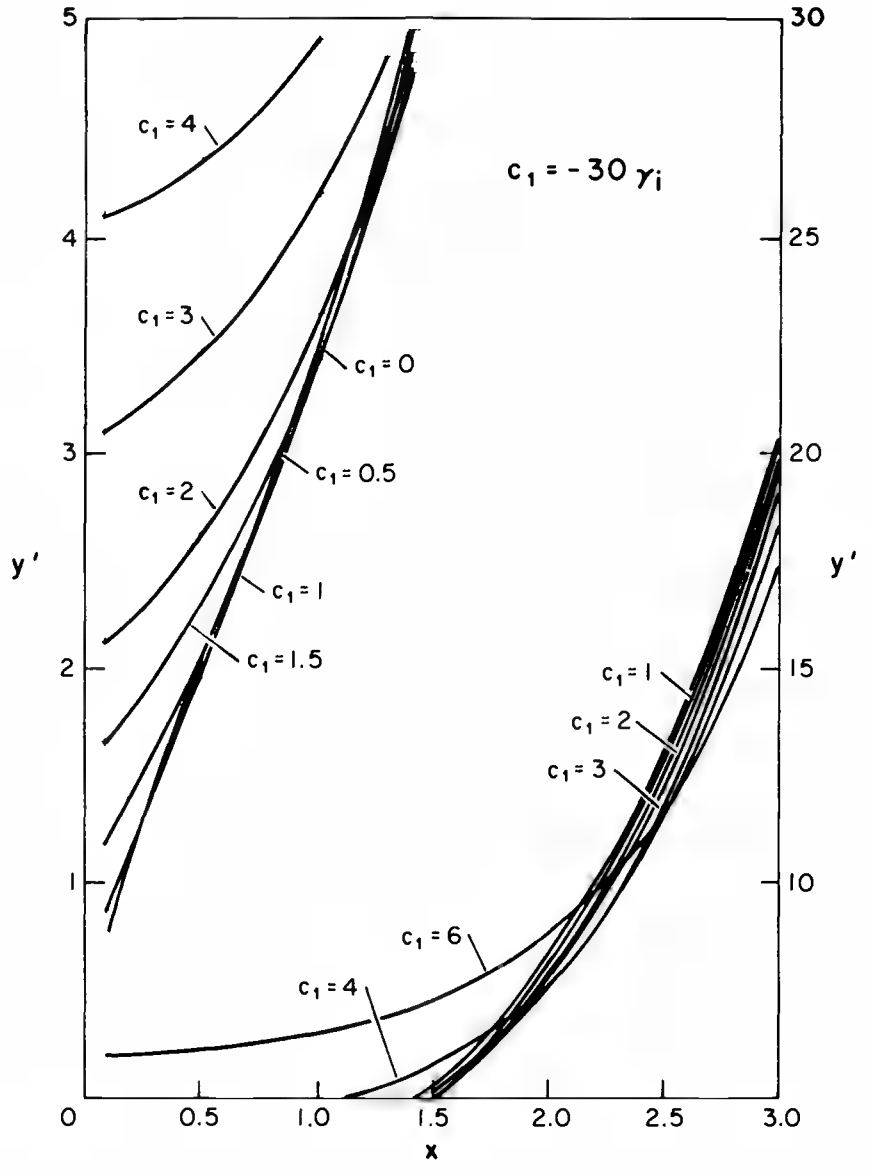


Fig. 10-3. Variations of $y' = -30\gamma$ versus $x$, for ballistic entry.

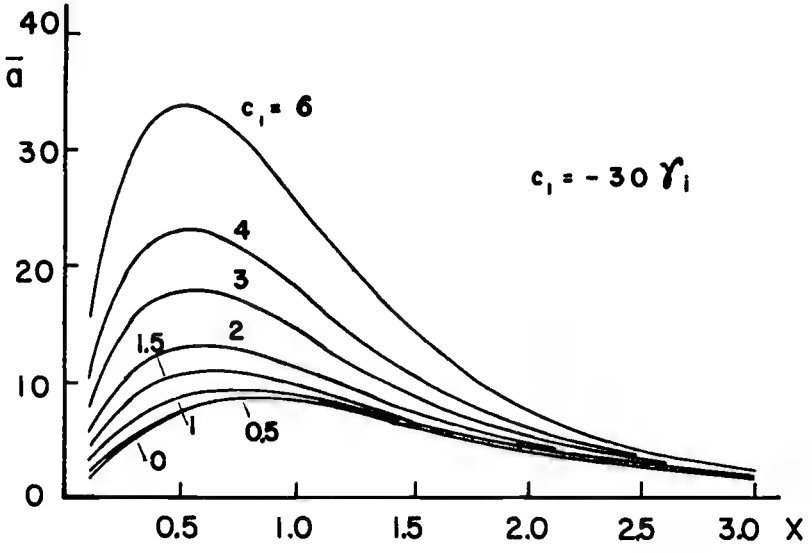


Fig. 10-4. Variation of the deceleration during ballistic entry from circular speed for various initial flight path angles.

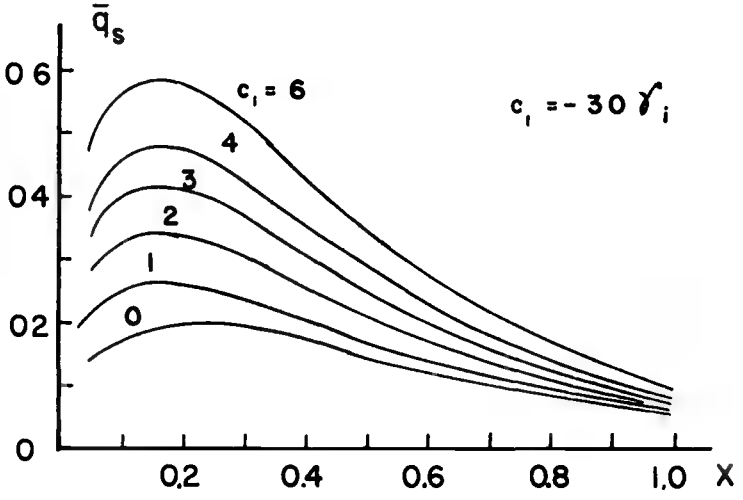


Fig. 10-5. Variation of the laminar heating rate during ballistic entry from circular speed.

Figure 10-3 plots $y' = -\sqrt{\beta r_o}\,\gamma$ versus $x$, and it can be used to evaluate the flight path angle during entry.

Figure 10-4 plots the deceleration during entry, as given by Eq. (10-19).

Figure 10-5 plots the variation of the heating rate at the stagnation point for laminar flow. As given by Eq. (10-25), the figure plots $\bar{q}_s$ versus $x$, where

$$\bar{q}_s = \frac{\sqrt{RB}}{85} q_s = y^{0.5} e^{-3.25x} \tag{10-53}$$

Figure 10-6 plots the variation of the heating rate for turbulent flow. As given by Eq. (10-26), the figure plots $\bar{q}_t$ versus $x$, where

$$\bar{q}_t = \frac{R^{0.2} B^{0.8}}{25} q_t = y^{0.8} e^{-3.19x} \tag{10-54}$$

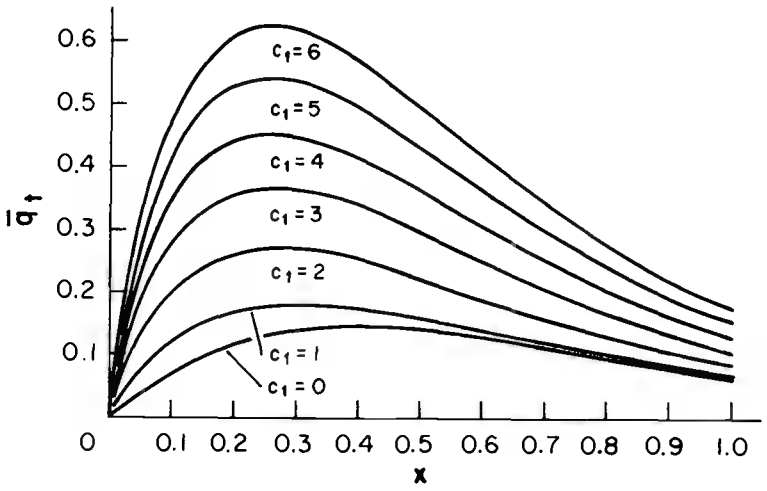


Fig. 10-6. Variation of the turbulent heating rate during ballistic entry from circular speed.

Finally, Fig. 10-7 plots the range versus $x$, as given by Eq. (10-14) and Fig. 10-8 plots the time of flight versus $x$ as given by Eq. (10-18).

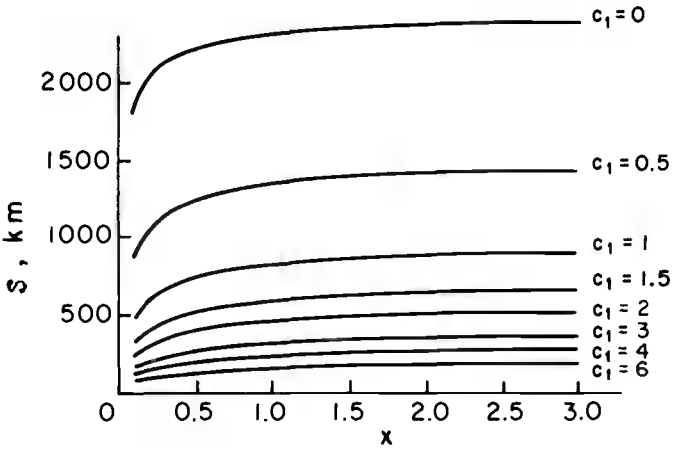


Fig. 10-7. Variation of the range for ballistic entry from circular speed.

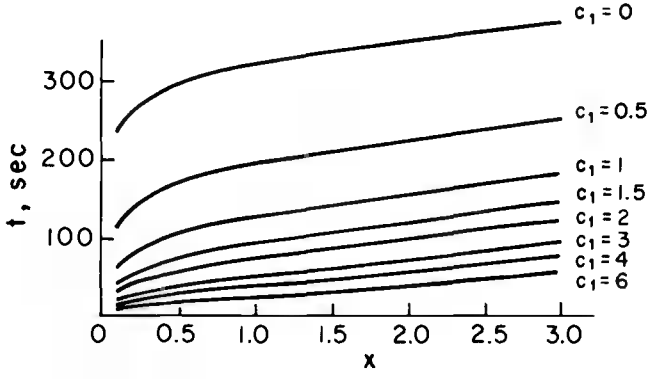


Fig. 10-8. Time of flight versus x for ballistic entry from circular speed.

## 10-4.3. Lifting Entry From Circular Speed

For entry with constant lift and drag coefficients, the flight parameter to be specified is $K = \sqrt{\beta r_o}\ (C_L/C_D)$. Hence, we write the basic nonlinear differential equation, Eq. (10-17)

$$y'' = -K + \frac{e^{2x} - 1}{y}, \quad K = \sqrt{\beta r_o}\ \frac{C_L}{C_D} \tag{10-55}$$

We first integrate this equation for small values of $K$. If $K$ is of the order of unity, the corresponding lift-to-drag ratio (for Earth's atmosphere) is of the order of $C_L/C_D \approx 1/30$.

For entry from circular speed with nearly zero initial flight path angle, that is, for the case of entry from orbit decay with small lift, we have the initial conditions

$$x_i = 0 \quad , \quad y(0) = 0 \quad , \quad y'(0) = 0 \tag{10-56}$$

The solution of Eq. (10-55) is sought as a power series in $x^{1/2}$. The solution which satisfies the initial conditions (10-56) is

$$y = \sqrt{\frac{8}{3}}\, x^{3/2} - \frac{4K}{11}\, x^2 + \sqrt{\frac{8}{3}}\left(\frac{1}{6} + \frac{K^2}{121}\right) x^{5/2}$$

$$+ \left(\frac{8K}{27 \cdot 11} + \frac{16K^3}{9 \cdot 1331}\right) x^3 + \sqrt{\frac{8}{3}}\left(\frac{1}{24} + \frac{13K^2}{6 \cdot 19 \cdot 121} + \frac{11K^4}{38 \cdot 11^4}\right) x^{7/2}$$

$$+ \ \ldots \tag{10-57}$$

For $|K| < 3$, which, in the case of the Earth's atmosphere, corresponds to the range of lift-to-drag ratio $|C_L/C_D| < 0.1$, the solution (10-57) is sufficiently accurate for the range of $x$ within the interval where the maximum deceleration and the maximum heating rate occur.

When the entry angle is not zero, we have the initial conditions

$$x_i = 0 \quad , \quad y(0) = 0 \quad , \quad y'(0) = c_1 \tag{10-58}$$

where $c_1 = -\sqrt{\beta r_o}\ \gamma_i$. The solution to Eq. (10-55) is sought as a power series in $x$

$$y = c_1 x + c_2 x^2 + c_3 x^3 + c_4 x^4 + \ldots \tag{10-59}$$

Substituting this series into Eq. (10-55) and equating like powers in $x$ yields for the coefficients $c_m$

$$c_2 = \left(\frac{1}{c_1} - \frac{K}{2}\right) \quad , \quad c_3 = \frac{1}{3c_1}\left(\frac{K}{2c_1} + 1 - \frac{1}{2c_1}\right)$$

$$c_4 = \frac{1}{12c_1}\left[\frac{4}{3} - \frac{1}{3c_1}\left(\frac{K}{2c_1} + 1 - \frac{1}{2c_1}\right)\left(\frac{8}{c_1} - 3K\right)\right] \tag{10-60}$$

The radius of convergence of this series is small and the solution is restricted to small values of $K$.

Numerical integration of Eq. (10-55) for entry from circular speed with different values of $c_1$ has been carried out by Yaroshevskii, and the results are plotted in Figs. 10-9 through 10-11. The dashed lines are the plots of the analytical solutions, Eqs. (10-57) and (10-59).

Figure 10-9 plots the function y versus x for entry at zero initial flight path angle from circular speed using K as parameter.

Figure 10-10 plots the function y versus x for entry with non-zero initial flight path angle from circular speed using K as parameter.

Figure 10-11 plots the maximum deceleration versus the initial flight path angle. It is seen that, as $c_1 = -\sqrt{\beta r_o}\,\gamma_i$ increases from zero, the maximum deceleration first slightly decreases, and then increases. Also, it is seen that the effect of positive lift in reducing the maximum deceleration is very powerful. Effects of the lift-to-drag ratio, $C_L/C_D$, on maximum deceleration and maximum heating rate during entry will be discussed in detail in Chapter 11 in the discussion of Chapman's theory for atmospheric entry, which is more accurate than Yaroshevskii's theory.

### 10-4.4. Gliding Trajectory

If the lift-to-drag ratio is large while the flight path angle remains small, we have the condition of equilibrium glide as first formulated by Sänger (Refs. 9, 10). In this case, in Eq. (10-55), the term $y''$, which represents the vertical acceleration, is nearly zero, and the equation is reduced to the equilibrium condition for gliding flight

$$y = \frac{e^{2x} - 1}{K} \tag{10-61}$$

When the speed becomes small, the assumption of small vertical acceleration is no longer valid. For small speed, we use the transformation

$$y \equiv \frac{e^{2x} - 1}{K} f(z) \tag{10-62}$$

where we define z as

$$z \equiv \frac{e^{x}}{K} \tag{10-63}$$

Hence, the relation between the derivatives is

$$\frac{d}{dx}(\;) = z\frac{d}{dz}(\;) \tag{10-64}$$

With this transformation, the basic equation, Eq. (10-55), becomes

$$z^2\left(z^2 - \frac{1}{K^2}\right)\frac{d^2f}{dz^2} + z\left(5z^2 - \frac{1}{K^2}\right)\frac{df}{dz} + 4z^2 f = -1 + \frac{1}{f} \tag{10-65}$$

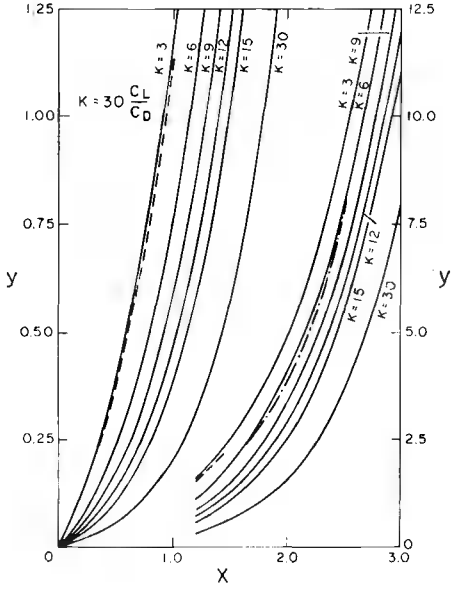


Fig. 10-9. Variations of y for lifting entry at zero initial flight path angle from circular speed

— — — Eq. (10-57) —·— Eq. (10-62)

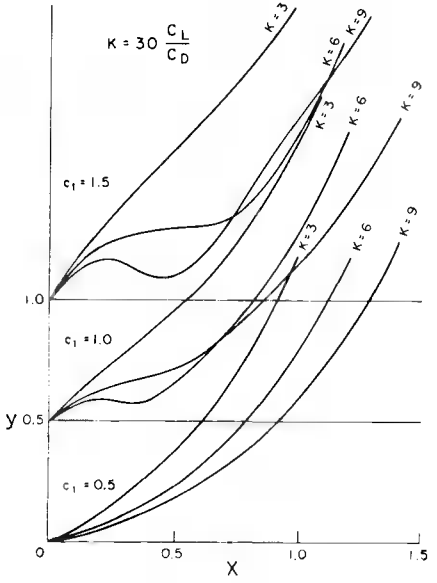


Fig. 10-10. Variations of y for lifting entry at various initial flight path angles from circular speed.

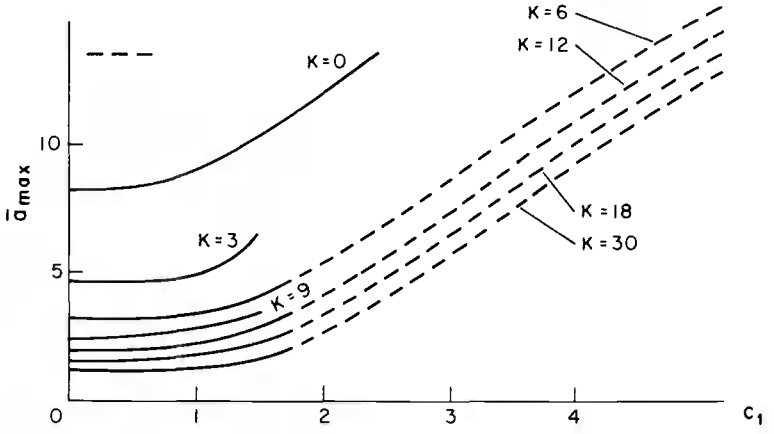


Fig. 10-11. Variations of the maximum deceleration as function of the initial flight path angle.

For $C_L/C_D > 1$ , $1/K^2 < (1/\beta r_o) << 1$ , and an approximation of this equation is

$$z^4 \frac{d^2f}{dz^2} + 5z^3 \frac{df}{dz} + 4z^2 f(z) = -1 + \frac{1}{f(z)} \tag{10-66}$$

The function $f(z)$ is constructed to extend the validity of the solution for small speed. Hence, for a trajectory beyond the validity of the solution (10-61), by the definition (10-62), we have the initial conditions

$$f(0) = 1 \ , \quad \frac{df}{dz} = 0 \tag{10-67}$$

to integrate Eq. (10-66).

For small $z$ , an approximate solution to the equation is

$$f(z) = 1 - 4z^2 \tag{10-68}$$

while for large $z$ , an approximate solution is

$$f(z) = \frac{1}{z} - \frac{1}{z^2} \tag{10-69}$$

Now, if we use the solution (10-61) in Eq. (10-14) to compute the range, we have

$$s = \sqrt{\frac{r_o}{\beta}} \int_{x_i}^{x} \frac{K dx}{e^{2x} - 1} = \frac{r_o}{2} \left( \frac{C_L}{C_D} \right) \log \frac{1 - \bar{V}^2}{1 - \bar{V}_i^2} \tag{10-70}$$

On the other hand, if the solution (10-61) for gliding flight is used in Eq. (10-18) to evaluate the time of flight, we have

$$t = \frac{1}{\sqrt{\beta g}} \int_{x_i}^{x} \frac{K e^{x} dx}{e^{2x} - 1} = \frac{1}{2}\sqrt{\frac{r_o}{g}} \left(\frac{C_L}{C_D}\right) \log \frac{[1 - \overline{V}]}{[1 + \overline{V}]} \frac{[1 + \overline{V}_i]}{[1 - \overline{V}_i]}$$

(10-71)

These are the first-order solutions for gliding entry obtained in Chapter 7 .

## References


1. Yaroshevskii, V. A., "The Approximate Calculation of Trajectories of Entry Into the Atmosphere. I", Translated from Kosmicheskie Issledovaniya, Vol. 2, No. 4, 1964.

2. Yaroshevskii, V. A., "The Approximate Calculation of Trajectories of Entry Into the Atmosphere. II" , Translated from Kosmicheskii Issledovaniya, Vol. 2, No. 5, 1964.

3. Chapman, D. R., "An Approximate Analytical Method for Studying Entry Into Planetary Atmospheres," NASA TR R-11, 1959.

4. Lees, L., "Laminar Heat Transfer Over Blunt-Nosed Bodies at Hypersonic Flight Speeds," Jet Propulsion, Vol. 26, No. 4, pp. 259-269, 1956.

5. Lees, L., "Recovery Dynamics - Heat Transfer at Hypersonic Speeds in a Planetary Atmosphere," Chapter 12 of Space Technology, ed. by H. S. Seifert, John Wiley and Sons, N. Y., 1959.

6. Fay, J. A., and Riddell, F. R., "Theory of Stagnation Point Heat Transfer in Dissociated Air," J. of Aeronautical Sciences, Vol. 25, No. 2, pp. 73-85, 1958.

7. Kemp, N. H., and Riddell, F. R., "Heat Transfer to Satellite Vehicles Reentering the Atmosphere," Jet Propulsion, Vol. 27, No. 2, 1957.

8. Sibulkin, M., "Estimation of Turbulent Heat Transfer at the Sonic Point of a Blunt-Nosed Body," Jet Propulsion, Vol. 28, No. 8, pp. 548-554, 1958.

9. Sänger, E., Raketen-Flugtechnik, R. Oldenbourg, Berlin, 1933.

10. Sänger, E., and Bredt, J., "A Rocket Drive for Long Range Bombers," Translation CGD-32, Technical Information Branch, Navy Department, 1944.

# Chapter 11

# Chapman's Theory for Entry into Planetary Atmospheres

## 11-1. INTRODUCTION

Compared with Yaroshevskii's theory for the entry trajectory, Chapman's theory offers a higher degree of sophistication. Using some simplifying assumptions, Chapman derived a relatively simple nonlinear differential equation of the second-order, free of the characteristics of the vehicle (Ref. 1). This is made possible by introducing a set of completely nondimensionalized variables. Chapman's reduced equation includes various terms, certain of which represent the gravity force, the centrifugal force and the lift force. If these particular terms are disregarded, the differential equation becomes linear and its integration yields precisely the solution of Allen and Eggers for ballistic entry at steep flight path angles. If, in the basic equation, the vertical acceleration is neglected according to the equilibrium glide assumption, the resulting truncated differential equation yields the solution of Sänger for equilibrium glide with relatively large lift-to-drag ratio.

In the general case, Chapman's equation has to be integrated numerically. For each prescribed lift-to-drag ratio, and initial speed and flight path angle, the integration of the equation generates a solution. Each of these solutions is universal in the sense that it can be used for any vehicle, of arbitrary weight, dimensions and shape, entering an arbitrary atmosphere. Only the lift-to-drag ratio, initial speed, and initial flight path angle serve as parameters of the solution.

## 11-2. DEVELOPMENT OF THE NONLINEAR DIFFERENTIAL EQUATION

In deriving his equation, Chapman used the set of the equations of equilibrium of the forces along the radial and the normal direction to the flight path. For the sake of uniformity, we shall use instead the equations in tangential coordinates as derived in Chapter 2.

For planar motion, the equations are

$$\frac{dV}{dt} = -\frac{\rho S C_D V^2}{2m} - g \sin\gamma$$

$$V\frac{d\gamma}{dt} = \frac{\rho S C_L V^2}{2m} - \left(g - \frac{V^2}{r}\right)\cos\gamma$$

$$\frac{dr}{dt} = V \sin\gamma \qquad (11\text{-}1)$$

The last equation may be used to make $r$ the independent variable.

$$\frac{dV}{dr} = -\frac{\rho S C_D V}{2m \sin\gamma} - \frac{g}{V}$$

$$\frac{d\gamma}{dr} = \frac{\rho S C_L}{2m \sin\gamma} + \left(1 - \frac{gr}{V^2}\right)\frac{\cos\gamma}{r \sin\gamma} \qquad (11\text{-}2)$$

We shall use Chapman's basic assumptions and his coordinate transformation to reduce this pair of equations of motion to a single, ordinary, nonlinear differential equation of the second-order.

In his theory, Chapman used two basic assumptions:

a/ In a given increment of time, the fractional change in distance from the planet center is small compared to the fractional change in the horizontal component of the velocity. Mathematically, this assumption is expressed as

$$\left|\frac{d(V\cos\gamma)}{V\cos\gamma}\right| >> \left|\frac{dr}{r}\right| \qquad (11\text{-}3)$$

b/ For a lifting vehicle, the flight path angle $\gamma$ is sufficiently small that the lift component in the horizontal direction is small compared to the drag component in the same direction. Mathematically, this assumption is expressed as

$$1 >> \left|\frac{C_L}{C_D}\tan\gamma\right| \qquad (11\text{-}4)$$

It is erroneous to think that these assumptions will restrict Chapman's analysis to entry trajectories with small flight path angles and small lift-to-drag ratios as many authors have believed. On the contrary, these assumptions, applied simultaneously, constitute a well-balanced set of hypotheses and make Chapman's theory applicable to a large family of entry trajectories. It is clear that assumption b/ is identically satisfied for ballistic entry. On the other hand, in this case, assumption a/ does not specifically restrict the flight path angle, since for ballistic entry, the flight path angle is nearly constant, and the left-hand side of inequality (11-3) simply represents the fractional change in the speed. Thus, the assumption is valid whenever the aerodynamic force becomes sensible enough to induce a rapid change in the speed, regardless of the magnitude of the flight path angle.

Chapman used an independent variable $\bar{u}$, and a dependent variable $\bar{Z}$ defined as

$$\bar{u} \equiv \frac{V \cos\gamma}{\sqrt{gr}} \quad , \quad \bar{Z} \equiv \frac{\rho S C_D}{2m}\sqrt{\frac{r}{\beta}}\ \bar{u} \tag{11-5}$$

It is convenient for subsequent derivations to express the basic assumption (11-3) in terms of the $\bar{u}$ and $\bar{Z}$ variables. We write this inequality with the aid of the Eqs. (11-2) and (11-5)

$$\left| \frac{d(V\cos\gamma)/V\cos\gamma}{dr/r} \right| = \left| -\frac{\sqrt{\beta r}\ \bar{Z}}{\bar{u}\sin\gamma}\left(1 + \frac{C_L}{C_D}\tan\gamma + \frac{\bar{u}\sin\gamma}{\sqrt{\beta r}\ \bar{Z}}\right) \right| >> 1$$

or

$$\left| 1 + \frac{C_L}{C_D}\tan\gamma + \frac{\bar{u}\sin\gamma}{\sqrt{\beta r}\ \bar{Z}} \right| >> \left| \frac{\bar{u}\sin\gamma}{\sqrt{\beta r}\ \bar{Z}} \right|$$

Hence, the basic assumption a/ is simply expressed as

$$\left| 1 + \frac{C_L}{C_D}\tan\gamma \right| >> \left| \frac{\bar{u}\sin\gamma}{\sqrt{\beta r}\ \bar{Z}} \right| \tag{11-3a}$$

Now, the derivative of $\bar{u}$, as defined by Eq. (11-5), with respect to $r$, is

$$\frac{d\bar{u}}{dr} = \frac{\cos\gamma}{\sqrt{gr}}\frac{dV}{dr} - \frac{V\sin\gamma}{\sqrt{gr}}\frac{d\gamma}{dr} + \frac{V\cos\gamma}{2r\sqrt{gr}}$$

where the assumption of an inverse square force field, $g = \mu/r^2$, has been used. From Eqs. (11-2) and definition (11-5), the exact equation for $\bar{u}$ can be written as

$$\frac{d\bar{u}}{dr} = -\frac{\bar{Z}}{\sin\gamma}\sqrt{\frac{\beta}{r}}\left(1 + \frac{C_L}{C_D}\tan\gamma + \frac{\bar{u}\sin\gamma}{2\sqrt{\beta r}\ \bar{Z}}\right) \tag{11-6}$$

Hence, if the basic assumptions a/ and b/, Eqs. (11-3a) and (11-4), are applied, the simplified equation for $\bar{u}$ is

$$\frac{d\bar{u}}{dr} = -\frac{\bar{Z}}{\sin\gamma}\sqrt{\frac{\beta}{r}} \tag{11-7}$$

To derive the equation in $\bar{Z}$, we consider the differential law for the atmospheric density

$$\frac{d\rho}{\rho} = -\beta dr \tag{11-8}$$

By taking the derivative of $\bar{Z}$, defined by Eq. (11-5), with respect to r and using Eqs. (11-7) and (11-8), we have

$$\frac{d\bar{Z}}{dr} = -\frac{\bar{Z}^2}{\bar{u}\sin\gamma}\sqrt{\frac{\beta}{r}} - \beta\bar{Z}\left(1 - \frac{1}{2\beta r} + \frac{1}{2\beta^2}\frac{d\beta}{dr}\right) \tag{11-9}$$

Concerning the last term of this equation, if a strictly exponential atmosphere is used, $\beta$ = constant and $d\beta/dr = 0$. On the other hand, if an isothermal atmosphere is used, $\beta/g$ = constant, and $(1/2\beta^2)(d\beta/dr) = -(1/\beta r)$. In both cases, since $\beta r$ is large, the last term of the equation can be taken as $-\beta\bar{Z}$ and this equation becomes

$$\frac{d\bar{Z}}{dr} = -\frac{\bar{Z}}{\sin\gamma}\sqrt{\frac{\beta}{r}}\left(\frac{\bar{Z}}{\bar{u}} + \sqrt{\beta r}\sin\gamma\right) \tag{11-10}$$

Finally, the second of Eq. (11-2) in terms of the $\bar{u}$ and $\bar{Z}$ variables is

$$\frac{d\gamma}{dr} = \frac{\bar{Z}}{\bar{u}\sin\gamma}\sqrt{\frac{\beta}{r}}\left[\frac{C_L}{C_D} + \frac{\bar{u}\cos\gamma}{\sqrt{\beta r}\,\bar{Z}}\left(1 - \frac{\cos^2\gamma}{\bar{u}^2}\right)\right] \tag{11-11}$$

Chapman used $\bar{u}$ as the independent variable. Hence, Eq. (11-7) is used to change the independent variable from r to $\bar{u}$, and the equations for $\bar{Z}$ and $\gamma$, Eqs. (11-10) and (11-11), become

$$\frac{d\bar{Z}}{d\bar{u}} - \frac{\bar{Z}}{\bar{u}} = \sqrt{\beta r}\sin\gamma \tag{11-12}$$

and

$$\frac{d\gamma}{d\bar{u}} = -\frac{1}{\bar{u}}\left[\frac{C_L}{C_D} + \frac{\bar{u}\cos\gamma}{\sqrt{\beta r}\,\bar{Z}}\left(1 - \frac{\cos^2\gamma}{\bar{u}^2}\right)\right] \tag{11-13}$$

Equation (11-12) is Chapman's first equation. It is used to evaluate the flight path angle. If we take the derivative of this equation with respect to $\bar{u}$, using Eq. (11-13) and considering $\beta r$ as constant, we have

$$\bar{u}\frac{d}{d\bar{u}}\left(\frac{d\bar{Z}}{d\bar{u}} - \frac{\bar{Z}}{\bar{u}}\right) + \frac{\cos^2\gamma\,(\bar{u}^2 - \cos^2\gamma)}{\bar{Z}\,\bar{u}} + \sqrt{\beta r}\frac{C_L}{C_D}\cos\gamma = 0 \tag{11-14}$$

This equation is equivalent to Chapman's second-order nonlinear differential equation with $\bar{Z}$ as the dependent variable and $\bar{u}$ as the independent variable. In this equation, $\cos\gamma = \sqrt{1 - \sin^2\gamma}$ can be expressed in terms of $\bar{u}$, $\bar{Z}$ and $d\bar{Z}/d\bar{u}$ through Eq. (11-12).

To obtain the equation in the form identical to the one given by Chapman in his classical paper (Ref. 1), we write it as

$$\bar{u}\,\frac{d^2\bar{Z}}{d\bar{u}^2} - \left(\frac{d\bar{Z}}{d\bar{u}} - \frac{\bar{Z}}{\bar{u}}\right) - \frac{(1-\bar{u}^2)\cos^4\gamma}{\bar{Z}\,\bar{u}} + \sqrt{\beta r}\,\frac{C_L}{C_D}\cos^3\gamma$$

$$+ \frac{\bar{u}\cos^2\gamma\sin^2\gamma}{\bar{Z}} + \sqrt{\beta r}\,\frac{C_L}{C_D}\cos\gamma\sin^2\gamma = 0 \qquad (11\text{-}15)$$

With the aid of Eq. (11-12), we consider the sum of the terms

$$-\left(\frac{dZ}{d\bar{u}} - \frac{\bar{Z}}{\bar{u}}\right) + \frac{\bar{u}\cos^2\gamma\sin^2\gamma}{\bar{Z}} + \sqrt{\beta r}\,\frac{C_L}{C_D}\cos\gamma\sin^2\gamma$$

$$= -\sqrt{\beta r}\,\sin\gamma\left[1 - \frac{C_L}{C_D}\cos^2\gamma\tan\gamma - \frac{\bar{u}\cos^2\gamma\sin\gamma}{\sqrt{\beta r}\,\bar{Z}}\right] \approx \sqrt{\beta r}\,\sin\gamma$$

The last step is a result of applying the basic assumptions a/ and b/, Eqs. (11-3a) and (11-4). This is equivalent to neglecting the terms containing $\sin^2\gamma$ in Eq. (11-15), yielding

$$\underbrace{\bar{u}\,\frac{d^2\bar{Z}}{d\bar{u}^2}}_{\text{Vertical acceleration}} - \underbrace{\left(\frac{d\bar{Z}}{d\bar{u}} - \frac{\bar{Z}}{\bar{u}}\right)}_{\text{Vertical component of drag force}} = \underbrace{\frac{(1-\bar{u}^2)}{\bar{Z}\,\bar{u}}\cos^4\gamma}_{\text{Gravity minus centrifugal force}} - \underbrace{\sqrt{\beta r}\,\frac{C_L}{C_D}\cos^3\gamma}_{\text{Lift force}} \qquad (11\text{-}16)$$

This equation is the second Chapman equation. Following Chapman, we have identified the different components of the force as labelled. Another form is

$$\bar{u}\,\frac{d}{d\bar{u}}\left(\frac{d\bar{Z}}{d\bar{u}} - \frac{\bar{Z}}{\bar{u}}\right) = \frac{(1-\bar{u}^2)}{\bar{Z}\,\bar{u}}\cos^4\gamma - \sqrt{\beta r}\,\frac{C_L}{C_D}\cos^3\gamma \qquad (11\text{-}16a)$$

In general, this nonlinear differential equation has to be integrated numerically. For a nonlifting vehicle, $C_L/C_D = 0$, the equation is applicable to large flight path angles, as well as small angles. For lifting vehicles, it is applicable when $(C_L/C_D)\tan\gamma$ is small.

## 11-3. THE $\bar{Z}$ FUNCTIONS AND RELATED QUANTITIES

As mentioned in the introductory section of this chapter, Chapman's equation, Eq. (11-16), is universal in the sense that it is free of the physical characteristics of the vehicle. Hence, it is applicable to any type of entry vehicle regardless of its weight, dimensions and shape.

For an entry trajectory, since $\bar{Z}_i \approx 0$, only initial conditions on $\bar{u}_i$ and $\gamma_i$ need be given. The flight parameter $C_L / C_D$ and the characteristic of the atmosphere, $\beta r$, must, of course, be specified.

For each planetary atmosphere, the average value for $\beta r$ is known to a greater or lesser degree of accuracy, as was discussed in Chapter 1. For Earth, $\sqrt{\beta r}$ is 30. Thus, Eq. (11-16) can be integrated numerically starting from the initial value $\bar{u}_i$ of the independent variable, using the initial conditions on $\bar{Z}_i$ and $d\bar{Z}/d\bar{u}_i$. For an entry trajectory,

$$\bar{Z}(\bar{u}_i) \approx 0 \tag{11-17}$$

Since the basic nonlinear equation has a singularity at $\bar{Z} = 0$, the first step in the numerical integration must be handled analytically by using an approximate value for $\bar{Z}$ in the initial portion of the trajectory, depending on the type of entry. Some approximate $\bar{Z}$ functions will be given in the next section. If $\gamma_i$ is given, the initial value for $d\bar{Z}/d\bar{u}_i$ is given by Eq. (11-12) as

$$\frac{d\bar{Z}}{d\bar{u}_i} = \sqrt{\beta r} \sin\gamma_i + \frac{\bar{Z}_i}{\bar{u}_i} \approx \sqrt{\beta r} \sin \gamma_i \tag{11-18}$$

For each flight program and entry condition, the resulting variation of $\bar{Z}$ as a function of $\bar{u}$ can be tabulated. These Tables, known as the Tables of the $\bar{Z}$ Functions (Ref. 2), can be used to analyze the entry of any arbitrary vehicle.

In some instances, these Tables, computed for entry into the Earth's atmosphere, can be extrapolated for use with other planetary atmospheres.

First, for a shallow entry at very small flight path angle, Eq. (11-16) is reduced to

$$\bar{u} \frac{d}{d\bar{u}} \left( \frac{d\bar{Z}}{d\bar{u}} - \frac{\bar{Z}}{\bar{u}} \right) - \frac{1 - \bar{u}^2}{\bar{Z}\,\bar{u}} + \sqrt{\beta r} \frac{C_L}{C_D} = 0 \tag{11-19}$$

with the initial condition for a prescribed $\bar{u}_i$

$$\bar{Z}(\bar{u}_i) = 0 \quad , \quad \frac{d\bar{Z}}{d\bar{u}_i} = 0 \tag{11-20}$$

Hence, in this case, Tables of the $\bar{Z}$ functions can be used for any planetary atmosphere, for entry with the same prescribed flight parameter $\sqrt{\beta r}\ (C_L/C_D)$, as far as the variations of $\bar{Z}$ and $\bar{u}$ are

concerned. For the flight path angle, using subscript e for the Earth, and subscript P for any other planet, from Eq. (11-12) comes

$$\gamma_P = k\gamma_e \quad , \quad k = \frac{\sqrt{(\beta r)_e}}{\sqrt{(\beta r)_P}} \tag{11-21}$$

where k is the conversion factor. The condition discussed above is, in particular, true for a decaying orbit for various lift-to-drag ratios. In this case, $\bar{u}_i = 1$ .

Next, the extrapolation can be extended to the cases of small entry angle. Equation (11-19) is still valid, but with the initial conditions

$$\bar{Z}(\bar{u}_i) = 0 \quad , \quad \frac{d\bar{Z}}{d\bar{u}_i} = \sqrt{\beta r}\ \gamma_i \tag{11-22}$$

Hence, the Tables can be used for any planetary atmosphere, for entry with the same $\sqrt{\beta r}\ (C_L/C_D)$ and $\sqrt{\beta r}\ \gamma_i$ . Under these conditions, the $\bar{Z}$ and $\bar{u}$ variations are the same, while the $\gamma$ variation is obtained from Eq. (11-21).

In all cases, the validity of the application is restricted to the part of the trajectory where the flight path angle remains small.

Several useful quantities during entry can be constructed from the Tables of the $\bar{Z}$ functions.

The first quantity of interest is the deceleration during entry. The deceleration along the flight trajectory is simply $dV/dt$ . The first of Eqs. (11-1), and definitions (11-5) of $\bar{u}$ and $\bar{Z}$ , yields

$$-\left(\frac{dV}{dt}/g\right) = \frac{\sqrt{\beta r}\ \bar{Z}\ \bar{u}}{\cos^2\gamma} + \sin\gamma \tag{11-23}$$

For small flight path angles,

$$-\left(\frac{dV}{dt}/g\right) \approx \sqrt{\beta r}\cdot\bar{Z}\ \bar{u} \tag{11-24}$$

and the deceleration is simply proportional to the product $\bar{Z}\,\bar{u}$ . Reference 1 gives several plots of $\sqrt{\beta r}\ \bar{Z}\ \bar{u}$ versus $\bar{u}$ for different types of entry. Some of these plots are reproduced in Section 11-5 of this chapter. They are useful in locating the speed $\bar{u}$ and the altitude $\bar{Z}$ where the deceleration reaches its maxima and minima during entry.

The deceleration due to the combined lift and drag forces, as felt by the pilot or an accelerometer during entry, is

$$\frac{a}{g} = \sqrt{\left(\frac{L}{mg}\right)^2 + \left(\frac{D}{mg}\right)^2} = \frac{\sqrt{\beta r}\ \bar{Z}\ \bar{u}}{\cos^2\gamma}\sqrt{1+\left(\frac{C_L}{C_D}\right)^2} \tag{11-25}$$

Hence, for entry at small angles, the deceleration due to aerodynamic force is obtained simply by multiplying the vehicle deceleration, given by Eq. (11-24), by the constant factor $\sqrt{1 + (C_L/C_D)^2}$ .

The $\bar{Z}$ function provides the flight altitude of the vehicle once the drag parameter $(SC_D/2m)$ is specified. For an arbitrary atmosphere, the altitude is most conveniently expressed in terms of the local atmospheric density $\rho$ . Let subscript $s$ denote the condition at sea level. From the definition (11-5) of $\bar{Z}$ , we have

$$\frac{\rho}{\rho_s} = \left(\frac{2m}{SC_D r_s \rho_s}\right) \frac{\sqrt{\beta r}\ \bar{Z}}{\bar{u}} \tag{11-26}$$

Hence, for a strictly exponential atmosphere, the altitude $h$ is given by

$$h = \frac{1}{\beta} \log \left[ \left(\frac{SC_D r_s \rho_s}{2m}\right) \frac{\bar{u}}{\sqrt{\beta r}\ \bar{Z}} \right] \tag{11-27}$$

Another quantity of interest is the dynamic pressure exerted on the vehicle.

$$\frac{1}{2}\rho V^2 = \left(\frac{mg}{SC_D}\right) \frac{\sqrt{\beta r}\ \bar{Z}\ \bar{u}}{\cos^2 \gamma} \approx \left(\frac{mg}{SC_D}\right) \sqrt{\beta r}\ \bar{Z}\ \bar{u} \tag{11-28}$$

Hence, the dynamic pressure is proportional to the deceleration of the vehicle.

The free-stream Reynolds number per unit length is

$$\frac{R_e}{\ell} = \frac{V\rho}{\mu} = \frac{2\sqrt{\beta g}}{\mu \cos\gamma} \left(\frac{m}{SC_D}\right) \bar{Z} \approx \frac{2\sqrt{\beta g}}{\mu} \left(\frac{m}{SC_D}\right) \bar{Z} \tag{11-29}$$

where $\mu$ is the atmospheric dynamic viscosity. Thus, the Reynolds number per unit length is proportional to the $\bar{Z}$ function.

Relatively simple expressions can also be obtained for the aerodynamic heating rate per unit area, $q$ , and the total heat absorbed per unit area, $Q/A$ .

According to the local similarity law of Lees, (Refs. 3,4), the heating rate $q$ at any point on a body is equal to a fraction of the heating rate $q_s$ at a stagnation point of radius of curvature $R$ . Thus, the local heating rate is expressed as

$$k_1 \equiv \frac{q}{q_s} \tag{11-30}$$

where the heating rate in hypersonic flow at a stagnation point, $q_s$ , can be expressed as

$$q_s = \frac{C}{\sqrt{R}} \left(\frac{\rho}{\rho_o}\right)^n \left(\frac{\bar{u}}{\cos\gamma}\right)^m \text{ k cal/m}^2 \text{ sec} \qquad (11\text{-}31)$$

where the constants $C$, $n$, and $m$ depend on the type of boundary layer flow. For laminar flow, $n = 1/2$. A simple power law, $m = 3$, for the speed, together with the expression (11-26) for the density ratio, gives the expression for the laminar convective heat transfer rate in terms of the $\bar{Z}$ and $\bar{u}$ variables

$$q = \left[C \sqrt[4]{\frac{\beta}{r_o \rho_o^2}}\right]\left[k_1 \sqrt{\frac{2m}{SC_D R}}\right]\left[\frac{\bar{q}}{\cos^3\gamma}\right] \frac{\text{k cal}}{\text{m}^2 \text{ sec}} \qquad (11\text{-}32)$$

where

$$\bar{q} = \bar{Z}^{1/2} \bar{u}^{5/2} \qquad (11\text{-}33)$$

The expression for the heat transfer rate has been written in the form of the product of three factors. The first factor represents the effect on heat flux of the particular planetary atmosphere. The second factor represents the effect of the physical characteristics of the vehicles, that is, the mass, dimensions and shape of the vehicle. The last factor, which for flight at small flight path angles is reduced to $\bar{Z}^{1/2}\bar{u}^{5/2}$ represents the effect of the particular type of entry trajectory.

Although Eq. (11-32) for heating rate is useful in studying vehicles designed to operate at radiation equilibrium temperatures, an equation for the total heat absorbed, $Q$, during entry is of more interest for heat-sink type vehicles. This is expressed in the form of an integral

$$Q = \int\int q\,dt\,dA = \int\int k_1 q_s\,dt\,dA \qquad (11\text{-}34)$$

where $A$ is the whole surface wetted by the boundary layer. Let

$$k_2 \equiv \frac{1}{A}\int k_1\,dA = \frac{1}{A}\int \frac{q}{q_s}\,dA \qquad (11\text{-}35)$$

where $k_2$ is the factor which takes into account the variations in heat flux over the whole surface $A$. For a hemisphere, we have then $k_2 \approx 0.5$.

$$Q = k_2 A \int q_s\,dt \qquad (11\text{-}36)$$

Using the expression (11-32) for $q_s = q/k_1$ in this integral, we have

$$Q = \left[C \sqrt[4]{\frac{\beta}{r_o \rho_o^2}}\right]\left[k_2 A \sqrt{\frac{2m}{SC_D R}}\right] \int \frac{\bar{Z}^{1/2}\bar{u}^{5/2}}{\cos^3\gamma}\,dt \qquad (11\text{-}37)$$

The integration with respect to the independent variable $\bar{u}$ can be accomplished if the simplified expression (11-7) for $d\bar{u}/dr$ is rewritten with respect to $t$,

$$\frac{d\bar{u}}{dt} = \frac{d\bar{u}}{dr}\frac{dr}{dt} = -\sqrt{\beta g}\,\frac{\bar{Z}\,\bar{u}}{\cos\gamma} \tag{11-38}$$

This equation gives the time of flight between $\bar{u}_1$ and $\bar{u}$ as

$$t = \frac{1}{\sqrt{\beta g}} \int_{\bar{u}}^{\bar{u}_1} \frac{\cos\gamma\, d\bar{u}}{\bar{Z}\,\bar{u}} \tag{11-39}$$

Substitution of (11-38) into (11-37), yields the expression for the total heat absorbed between $\bar{u}_1$ and $\bar{u}$

$$Q = \left[C\sqrt[4]{\frac{1}{\beta g^2 r_o \rho_o^2}}\right]\left[k_2 A\sqrt{\frac{2m}{SC_D R}}\right]\bar{Q}\ \text{kcal} \tag{11-40}$$

where

$$\bar{Q} = \int_{\bar{u}}^{\bar{u}_1} \frac{\bar{u}^{3/2}\, d\bar{u}}{\bar{Z}^{1/2}\cos^2\gamma} \tag{11-41}$$

## 11-4. SOME APPROXIMATE ANALYTICAL SOLUTIONS

The ultimate purpose of the Chapman formulation is the numerical integration and tabulation of the $\bar{Z}$ functions, as generated by Eq. (11-16), for use in the preliminary design of the entry vehicle and its mission planning. Although Chapman's equation is only approximate, the assumptions made are general enough so that the basic nonlinear equation, Eq. (11-16), contains all the principal effects of the forces acting on the vehicle during entry. Hence, under various assumptions to simplify this equation, Chapman's reduced equation should provide the other first-order solutions discussed previously. In this section, we shall consider several such cases.

### 11-4.1. Yaroshevskii's Solution

For constant lift-to-drag ratio entry, Yaroshevskii's second-order nonlinear differential equation, discussed in Chapter 10, is simply a case of Chapman's equation.

For constant lift and drag coefficients, Yaroshevskii's variables are (Ref. 5)

$$x \equiv \log\frac{\sqrt{g_o r_o}}{V}, \qquad y \equiv \frac{SC_D}{2m}\sqrt{\frac{r_o}{\beta}}\,\rho \tag{11-42}$$

where the subscript o denotes the condition at a reference level.

In the more sophisticated definition of Chapman's variables, Eqs. (11-5), if a constant reference value for r is used, and a very small flight path angle is assumed, then

$$\bar{u} = \frac{V}{\sqrt{g_o r_o}} \quad , \quad \bar{Z} = \frac{SC_D\rho}{2m}\sqrt{\frac{r_o}{\beta}}\,\bar{u} \tag{11-43}$$

Hence, the relations between the two sets of variables are

$$\frac{\bar{Z}}{\bar{u}} = y \quad , \quad \bar{u} = e^{-x} \tag{11-44}$$

The corresponding relation between the derivatives is

$$\frac{d}{d\bar{u}}(\;) = -e^{x}\frac{d}{dx}(\;) = -\frac{1}{\bar{u}}\frac{d}{dx}(\;) \tag{11-45}$$

Transformations (11-44) and (11-45) applied to Chapman's simplified equation for entry at very small flight path angles, Eq. (11-19), gives

$$\frac{d^2y}{dx^2} + \frac{1 - e^{2x}}{y} + \sqrt{\beta r_o}\,\frac{C_L}{C_D} = 0 \tag{11-46}$$

This equation is identical to Yaroshevskii's equation, Eq. (10-17), and its analytical solutions for various entry trajectories have been presented in Chapter 10.

### 11-4.2. Solution for Ballistic Entry

For ballistic entry, using Allen and Eggers assumption (Ref. 6), we disregard the gravity, centrifugal and lift force in Chapman's equation, Eq. (11-16), and write it as

$$\bar{u}\,\frac{d}{d\bar{u}}\left(\frac{d\bar{Z}}{d\bar{u}} - \frac{\bar{Z}}{\bar{u}}\right) = 0 \tag{11-47}$$

This, and Eq. (11-12), shows that the flight path angle remains constant. The integral of Eq. (11-47) can be written

$$\frac{d\bar{Z}}{d\bar{u}} - \frac{\bar{Z}}{\bar{u}} = \sqrt{\beta r}\,\sin\gamma_i \tag{11-48}$$

A second integration, along with the initial conditions, produces the solution for ballistic entry

$$\bar{Z}_I = \sqrt{\beta r}\, \sin\gamma_i\, \bar{u} \log \frac{\bar{u}}{\bar{u}_i} \tag{11-49}$$

The $\bar{Z}_I$ function provides an approximate solution for the motion and heating identical to the solution of Allen and Eggers for ballistic entry.

### 11-4.3. Solution for Glide Entry

For glide entry, using Sänger's assumption (Ref. 7), we neglect the vertical acceleration and vertical component of the drag force in Chapman's equation. Chapman's equation, along with Eq. (11-12), shows that this amounts to considering the glide angle as negligibly small, $\cos\gamma \approx 1$ . Hence, Eq. (11-16) is reduced to the condition for equilibrium glide

$$\bar{Z}_{II} = \frac{1 - \bar{u}^2}{\sqrt{\beta r}\left(\frac{C_L}{C_D}\right)\bar{u}} \tag{11-50}$$

The $\bar{Z}_{II}$ function corresponds to equilibrium gliding flight as discussed by Sänger and Bredt.

### 11-4.4. Solution for Skip Trajectory

For skip trajectories, using Eggers, Allen, and Neice's assumption (Ref. 8), we neglect the gravity and centrifugal force in Chapman's equation. Thus,

$$\bar{u}\,\frac{d}{d\bar{u}}\left(\frac{d\bar{Z}}{d\bar{u}} - \frac{\bar{Z}}{\bar{u}}\right) = -\sqrt{\beta r}\,\frac{C_L}{C_D}\cos^3\gamma \tag{11-51}$$

By using an average value $\bar{\gamma}$ for $\gamma$ on the right-hand side of this equation, and using Eq. (11-12), we may integrate this and apply the initial conditions to obtain

$$\sin\gamma = \sin\gamma_i - \frac{C_L}{C_D}\cos^3\bar{\gamma}\,\log\left(\frac{\bar{u}}{\bar{u}_i}\right) \tag{11-52}$$

This equation gives the flight path angle in terms of the flight speed. The $\bar{Z}$ function for skip trajectories may be obtained by combining Eqs. (11-52) and (11-12):

$$\frac{d\bar{Z}}{d\bar{u}} - \frac{\bar{Z}}{\bar{u}} = \sqrt{\beta r}\,\sin\gamma_i - \sqrt{\beta r}\,\frac{C_L}{C_D}\cos^3\bar{\gamma}\,\log\left(\frac{\bar{u}}{\bar{u}_i}\right) \tag{11-53}$$

This integrates to

$$\bar{Z}_{III} = \bar{u}\left[\frac{\bar{Z}_i}{\bar{u}_i} + \sqrt{\beta r}\,\sin\gamma_i \log\frac{\bar{u}}{\bar{u}_i} - \frac{\sqrt{\beta r}}{2}\left(\frac{C_L}{C_D}\right)\cos^3\bar{\gamma}\log^2\frac{\bar{u}}{\bar{u}_i}\right] \tag{11-54}$$

The $\bar{Z}_{III}$ function gives the solution for evaluating the altitude of a skip vehicle. In practice, since the flight path angle is small, the average value of $\cos^3\bar{\gamma}$ may be taken as unity.

## 11-5. NUMERICAL RESULTS

Several plots of the $\bar{Z}$ functions, obtained by numerically integrating the basic nonlinear equation, Eq. (11-16), for different types of entry, have been given in Ref. 1. The accuracy of Chapman's solution is remarkably good for entry at small flight path angles. The discussion of these graphs is enlightening since they provide all the interesting features for the variations of the deceleration and other physical quantities during entry.

### 11-5.1. Entry From a Decaying Orbit for Various Lift-to-Drag Ratios

Chapman's analysis is designed to investigate the atmospheric entry portion of the trajectory. It is not effective for analyzing the flight in the near vacuum since in this case the two basic assumptions are violated and the variable $\bar{u}$ no longer monotonically decreases, as shown in Chapter 13 in the development of the general theory for entry into a planetary atmosphere. Nevertheless, the behavior of a decaying orbit can be discussed qualitatively. For orbital flight at very high atmospheric altitude, the trajectory is a near-Keplerian orbit. Atmospheric drag is primarily effective near the lowest point, at the periapsis. The reduction of the speed near the periapsis behaves, during each passage, as an impulsive braking force, lowering the apoapsis of the orbit while leaving the periapsis altitude nearly unchanged. The orbit eventually becomes nearly circular. For the last revolution, when entry is effectively achieved, with $\gamma \approx 0$, Eq. (11-19) is valid. The initial conditions are

$$\bar{u}_i = 1\,, \quad \bar{Z}(\bar{u}_i) \approx 0\,, \quad \frac{d\bar{Z}}{d\bar{u}_i} = 0 \tag{11-55}$$

Figure 11-1 presents the plot of $\bar{Z}\,\bar{u}$ which is proportional to the deceleration versus $\bar{u}$ for the case $C_L/C_D = 0$ using the initial conditions (11-55). The peak deceleration occurs at the point where $\bar{u} \approx 0.43$. While this value is the same for any planetary atmosphere, the maximum deceleration varies from planet to planet. The maximum of $\bar{Z}\,\bar{u}$ is 0.278, and by Eq. (11-24), the maximum deceleration for ballistic entry from circular orbit into any particular

atmosphere is $0.278\sqrt{\beta r}$ , where $\beta r$ is the characteristic value of the specified atmosphere.

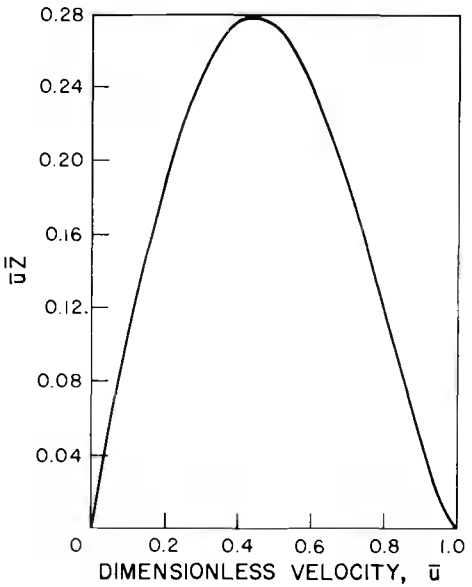


Fig. 11-1. Value of $\bar{Z}$ function for ballistic entry from decaying circular orbit.

Figure 11-2 plots the results of the numerical integration of the simplified equation, Eq. (11-19), with the initial conditions (11-55), for different values of $\sqrt{\beta r}(C_L / C_D)$ . The plots can be used for any planetary atmosphere. For high lift-to-drag ratios, the $\bar{Z}_{II}$ function, Eq. (11-50), is valid. It can be seen that this equilibrium glide solution, first derived by Sänger, is accurate up to the point where the speed is reduced to $\bar{u} \approx 0.2$ . The curves approach asymptotically the dashed line representing the $\bar{Z}_{II}$ function which can be seen as the exact solution for $C_L / C_D \to \infty$ .

### 11-5.2. Ballistic Entry From Circular Speed With Various Initial Flight Path Angles

If the initial speed $\bar{u}_i$ is given arbitrarily, for the case of ballistic entry, the basic equation, Eq. (11-16), is used with the value $C_L / C_D = 0$ , and the initial conditions

$$\bar{Z}(\bar{u}_i) \approx 0 \quad , \quad \frac{d\bar{Z}}{d\bar{u}_i} = \sqrt{\beta r} \sin \gamma_i \tag{11-56}$$

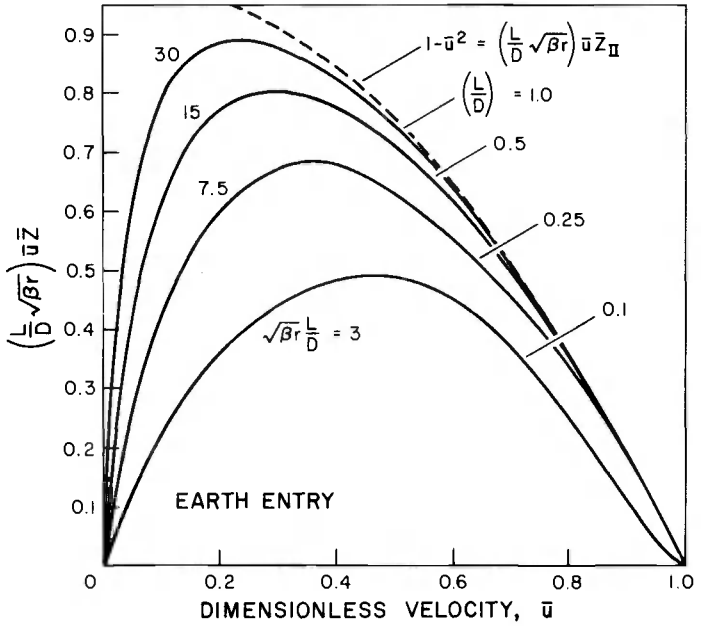


Fig. 11-2. Values of $\bar{Z}$ functions for a decaying circular orbit with various $C_L/C_D$ .

The integration generates a two-parameter family of solutions, with parameters $\bar{u}_i$ and $\sqrt{\beta r}\sin\gamma_i$ . Since in the reduced equation, the term $\cos^4\gamma$ has to be evaluated by using Eq. (11-12), which requires specifying separately the value of $\beta r$ , extrapolation of the numerical results for use with other planetary atmospheres is generally restricted to small flight path angles.

Figure 11-3 gives the plots of ballistic entry from $\bar{u}_i = 1$ for several values of the initial flight path angle $\gamma_i$ . The graphs plot $30\,\bar{Z}\,\bar{u}$ versus $\bar{u}$ . While the values of $\bar{u}$ for the peak deceleration read from the graphs are the same for all planetary atmospheres, the ordinates present the deceleration for the Earth. For other planets the values have to be evaluated proportionally according to the specified value of $\beta r$ . It can be seen that while generally the peak deceleration increases with increasing initial angle, the lowest peak deceleration occurs for an initial angle $\gamma_i$ somewhere between $0^\circ$ and $2^\circ$ . A detailed analysis, using the exact equations developed in Chapter 13, shows that this occurs for a small entry angle between $0^\circ$ and $1^\circ$ resulting in a minimum peak deceleration equal to 8.2g for the Earth's atmosphere.

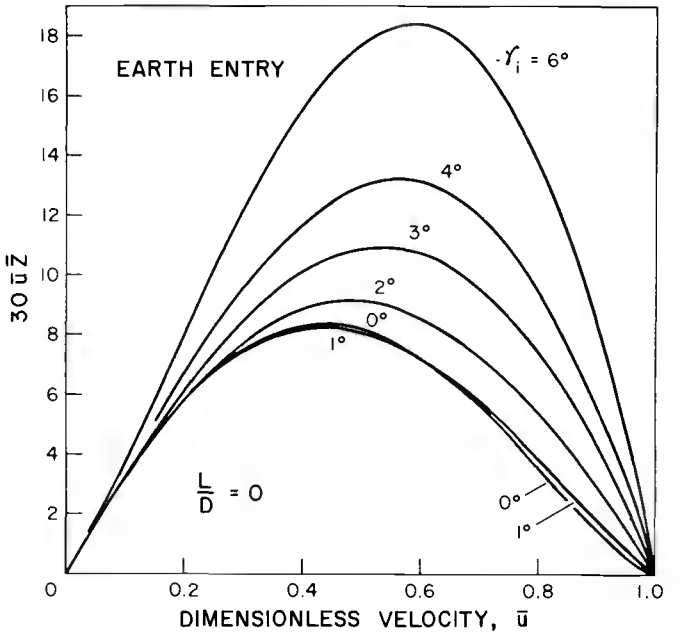


Fig. 11-3. Values of $\bar{Z}$ functions for ballistic entry from circular speed, at various initial angles.

11-5.3. Lifting Entry From Circular Speed With Various Initial Flight Path Angles

Figure 11-4 gives the plots for entry from $\bar{u}_i = 1$ for several values of the initial flight path angle, but with a positive lift-to-drag ratio, $C_L / C_D = 0.25$. For the integration, the basic equation (11-16) is used with the initial conditions (11-56) applied to $u_i = 1$. The graphs plot $30\,\bar{Z}\,\bar{u}$, which is the deceleration at small flight path angles for the Earth's atmosphere.

Comparing the two figures, Fig. 11-3 and Fig. 11-4, it is seen that lifting entry has the effect of decreasing the peak deceleration. Furthermore, for large initial flight path angles, there appear two peak decelerations of unequal magnitude. For low initial angles, the first peak is lower than the second peak, while for large initial angles, the first peak is higher.

The appearance of several peak decelerations is quite definite when the lift-to-drag ratio is increased, as can be seen in Fig. 11-5. Figure 11-5 presents the plots for entry from circular speed, $u_i = 1$, at various initial flight path angles, and with the value of the lift-to-drag ratio equal to 0.5, 0.7 and 1.0 respectively.

As the lift-to-drag ratio increases, the entry trajectory becomes more oscillatory with an oscillatory variation in the altitude (hence, also in the $\bar{Z}$ function) inducing an oscillatory variation in the product $\bar{Z}\,\bar{u}$.

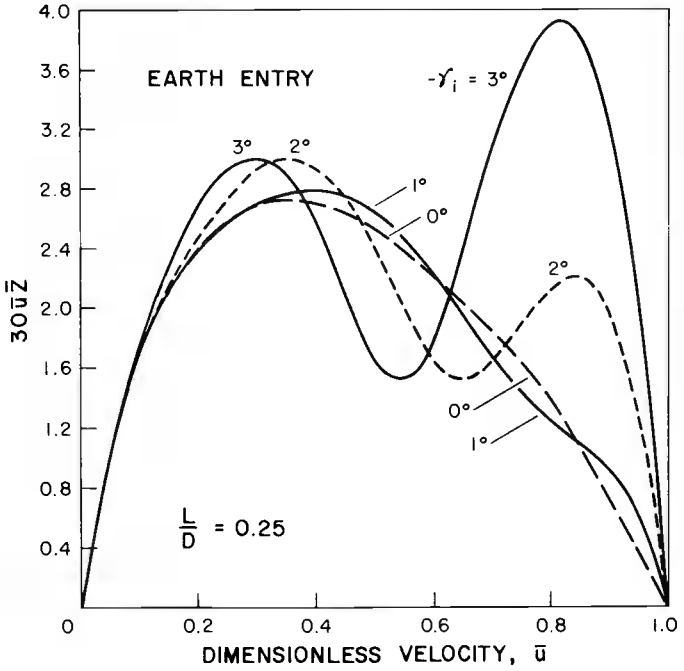


Fig. 11-4. Values of $\bar{Z}$ function for lifting entry from circular speed, at various initial angles.

## 11-5.4. Entry From Super Circular Speed

For entry from a high altitude orbit, the vehicle approaches the atmosphere along an elliptical orbit. Hence, the inital speed is generally $\bar{u}_i > 1$ .

Figure 11-6 presents the plots for ballistic entry, $C_L / C_D = 0$ , at $\bar{u}_i = 1.4$ , which is around parabolic speed when $\cos \gamma$ is near unity, with various initial angles.

When the initial flight path angle is small, which is the case for a high periapsis altitude of the initial Keplerian orbit, the vehicle passes through the sensible atmosphere for a short distance, and then exits into the vacuum. The integration is terminated whenever $\bar{Z}$ becomes small enough so that the vehicle is, at that time, essentially outside the sensible atmosphere. At that point, the speed has been reduced from the initial speed $\bar{u}_i$ to a final speed $\bar{u}_1$ , with an exit angle $\gamma_1$ . We say that the vehicle has made one passage through the atmosphere. Once outside the atmosphere, the vehicle continues its course, following a Keplerian orbit, with a lower apogee. Because of the symmetry of the Keplerian orbit, the following entry will be made at an inital speed equal to $\bar{u}_1$ with an initial angle equal to $-\gamma_1$ . This process can be repeated and we say that the entry is effected by several passages using atmospheric braking.

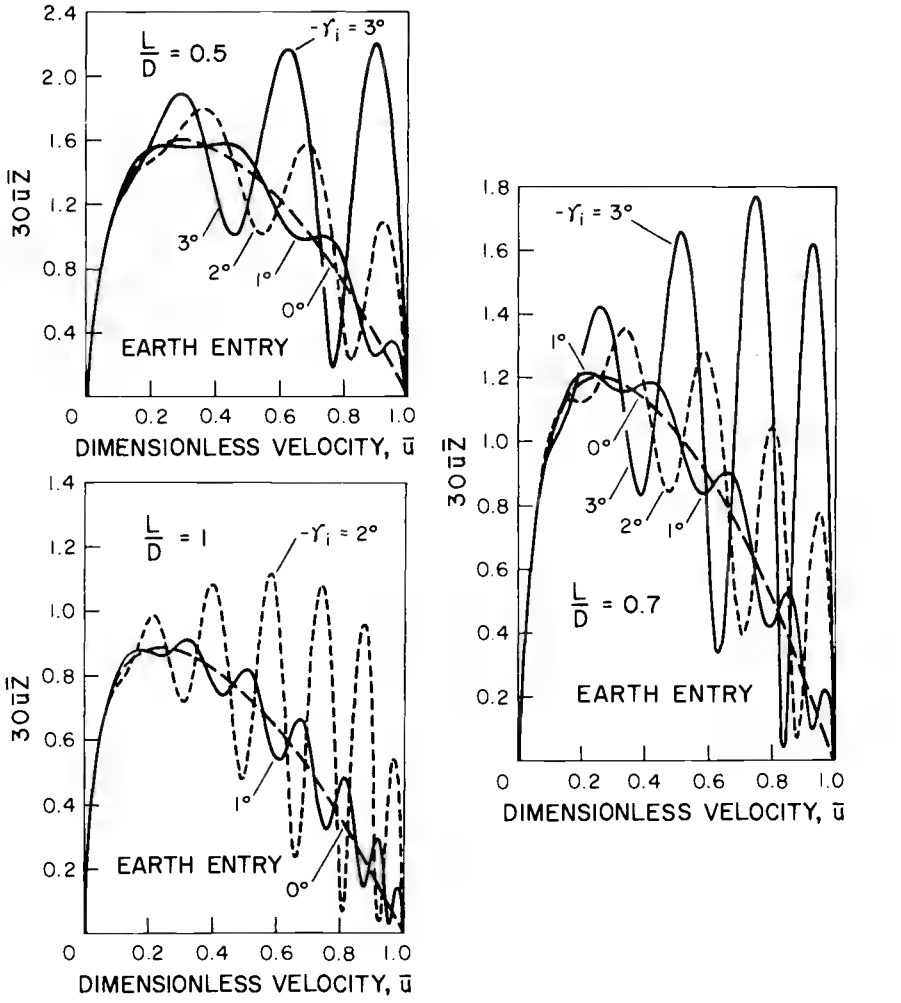


Fig. 11-5. Values of $\overline{Z}$ function for entry from circular speed at various initial angles.

Curve (a) in Fig. 11-6 presents an atmospheric braking with 6 passages.

If the initial flight path angle is increased by decreasing the periapsis altitude of the initial Keplerian orbit, the first passage is effected at lower altitude, resulting in a higher loss of speed during the passage. This is seen in curve (b) in Fig. 11-6. The greater loss in speed decreases the number of passages, Ultimately, a critical entry angle is reached when the complete entry is made in one passage. This occurs for an entry angle somewhere between curves (b) and (c). It can be seen that before obtaining curve (a), for initial entry at near zero initial flight path angles, which corresponds to a very high periapsis altitude of the initial Keplerian orbit, we have the condition of orbital decay. The number of passages is very large. Theoretically, it is infinite. The last passage, during which the entry is completed,

is initiated at $\bar{u}_n = 1$ , $\gamma_n = 0$ , where $n$ is the number of passages before effective entry.

We shall return for a more detailed discussion of these features in Chapter 13, with the development of an exact theory for planetary entry.

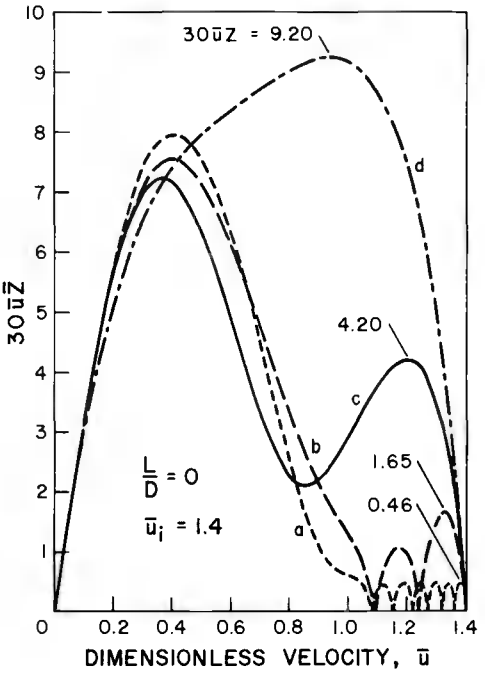


Fig. 11-6. Values of $\bar{Z}$ function for atmospheric braking of nonlifting vehicles starting from $\bar{u}_i = 1.4$.

## 11-6. EFFECT OF LIFT ON ENTRY

The physical quantities during entry, such as the deceleration, and heating, are functions of the $\bar{Z}$ function which, for a prescribed entry condition, depends on the lift-to-drag ratio. In this section, we shall examine the effect of the flight parameter $C_L / C_D$ on the deceleration, heating rate and total heat absorbed during entry. The effect, explicitly displayed, is of valuable assistance to preliminary design and mission planning purposes. To some extent, this question has been examined in Chapter 10, in connection with Yaroshevskii's theory for entry into a planetary atmosphere. In this section, the variables $\bar{Z}$ and $u$ are used in connection with Chapman's basic equation, Eq. (11-16), which is more accurate than Yaroshevskii's basic equation, Eq. (10-17).

First, we shall consider the case of lifting entry from a decaying orbit. That is, we shall first consider trajectories with various values of $C_L / C_D$ for an initial condition $\bar{u}_i = 1$ , $\gamma_i = 0$ .

### 11-6.1. Effect of Lift on Deceleration

A plot of the function $30\,\bar{Z}\,\bar{u}$ which, by Eq. (11-24), represents approximately the vehicle deceleration for entry at small angles into the Earth's atmosphere, is presented in Fig. 11-7, as a function of the dimenionless speed $\bar{u}$ for various lift-to-drag ratios.

It is seen that the effect of the lift-to-drag ratio, $C_L / C_D$, is very powerful. By increasing this flight parameter from 0 to 0.1, the peak deceleration is reduced from 8.38g to 4.9g, while by using a negative lift-to-drag ratio equal to -0.1, the peak deceleration increases to 12.8g.

For small lift-to-drag ratios, the peak deceleration occurs in the range of the dimensionless speed near $\bar{u} = 0.4$. When the lift-to-drag ratio increases, the peak deceleration occurs at lower speed. It should be noted that, due to Chapman's completely nondimensionalized formulation, the graphs apply to any type of vehicle, regardless of its weight, shape or size.

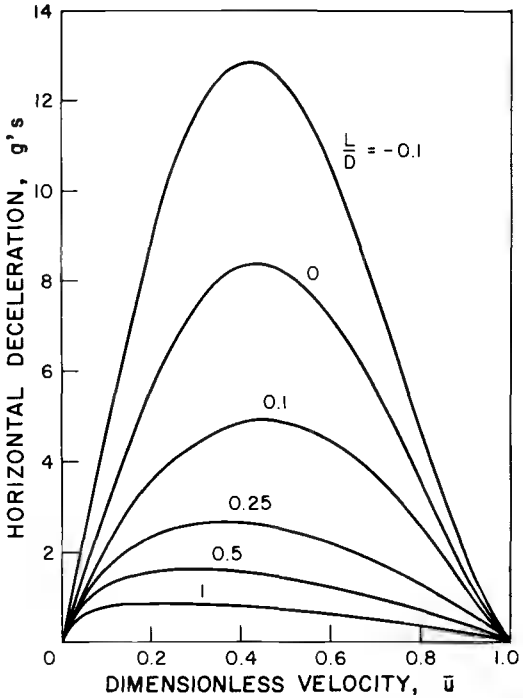


Fig. 11-7. Effect of $C_L / C_D$ on deceleration for entry into Earth's atmosphere from a decaying orbit.

Figure 11-7 plots the vehicle deceleration. If we consider the total deceleration, as felt by the pilot, then from Eq. (11-25), this deceleration at its maximum, which generally occurs at small flight path angles, is

$$\left(\frac{a}{g}\right)_{max} = \sqrt{\beta r}\ \left(\overline{Z}\,\overline{u}\right)_{max}\sqrt{1 + (C_L/C_D)^2} \qquad (11\text{-}57)$$

All the peak decelerations read from Fig. 11-7 must be increased by the factor $\sqrt{1 + (C_L/C_D)^2}$ to yield the maximum total deceleration as felt by the pilot.

Chapman gives the plot of Eq. (11-57) for different planetary atmospheres, as a function of the lift-to-drag ratio (Fig. 11-8). Included in this figure is a boundary representing human tolerance. It is seen that, from the human standpoint, an entry into Mars' atmosphere can be made with negative lift, while for an entry into the atmosphere of Jupiter, a positive lift is necessary to lower the peak deceleration to an allowable level.

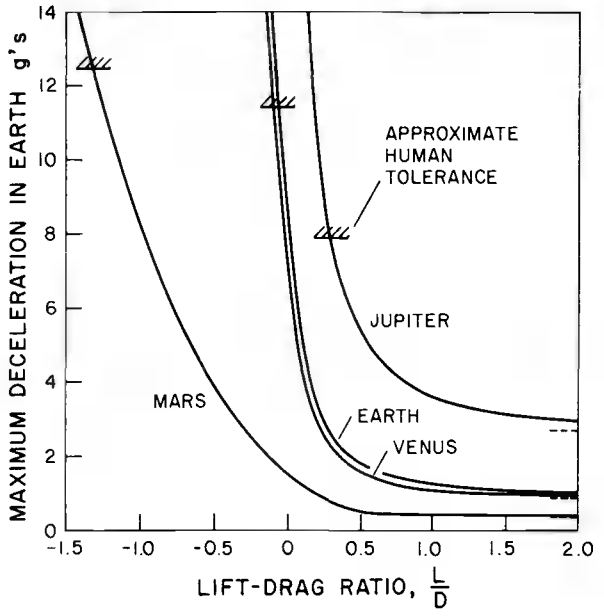


Fig. 11-8. Effect of $C_L/C_D$ on maximum deceleration for entry into various planetary atmospheres from decaying orbits.

## 11-6.2. Effect of Lift on Heating Rate

The use of the $\overline{Z}$ function also allows a general analysis of the heating for an arbitrary type of vehicle.

As given by Eq. (11-32), the heating rate per unit area for laminar flow at any point on a body is proportional to $\overline{q} = \overline{Z}^{1/2}\,\overline{u}^{5/2}$. Hence, as for the deceleration, the function $\overline{q}$ can be plotted versus $\overline{u}$, for different values of the lift-to-drag ratio, $C_L/C_D$ (Fig. 11-9). The initial condition used for the integration is also the one for a decaying orbit, while the value $\sqrt{\beta r} = 30$ is the characteristic value for the Earth atmosphere.

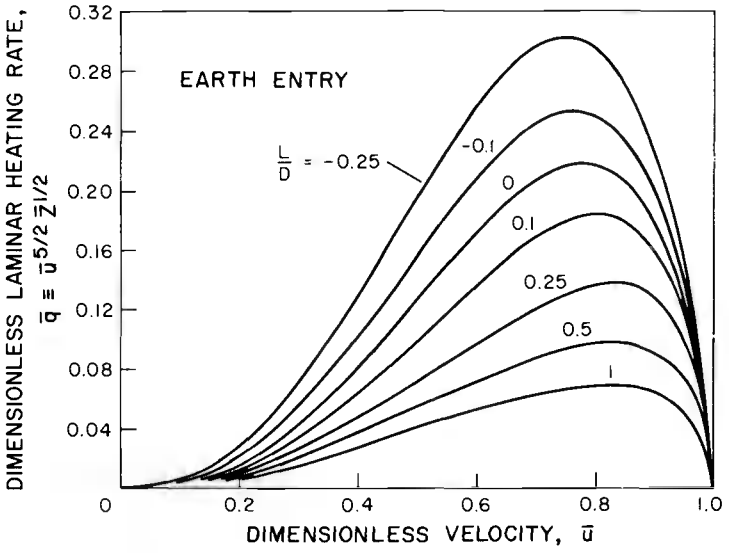


Fig. 11-9. Effect of $C_L / C_D$ on laminar heating rate for entry from decaying orbits.

As was discussed in Section 11-3, for small flight path angles, extrapolation can be used for other planetary atmospheres.

Let

$$k \equiv \frac{\sqrt{(\beta r)_e}}{\sqrt{(\beta r)_P}} \tag{11-58}$$

Since in the basic equation for the integration of entry into the Earth atmosphere, $\sqrt{(\beta r)_e}$ and $(C_L / C_D)_e$ enter as the product $\sqrt{(\beta r)_e}\,(C_L / C_D)_e$, and since for small flight path angles, the equation is nearly independent of $\gamma$, and hence does not require specifying the value of $\sqrt{(\beta r)_e}$ separately, then for entry into any planetary atmosphere, with a lift-to-drag ratio $(C_L / C_D)_P$ and characteristic value $\sqrt{(\beta r)_P}$, to use the same curve on Fig. 11-9, we must have

$$\left(\frac{C_L}{C_D}\right)_P = k \left(\frac{C_L}{C_D}\right)_e \tag{11-59}$$

From the figure, the maximum of $\bar{q}$ is seen to occur near the value $\bar{u} = 0.8$. As in the case of the deceleration, the heating rate decreases when $C_L / C_D$ is increased. The heating rate increases when negative lift is introduced.

For high lift-to-drag ratios, the $\bar{Z}$ function tends to the $\bar{Z}_{II}$ function as given by Eq. (11-50). Hence, when $C_L / C_D > 1$,

$$\bar{q} = \bar{Z}^{1/2}\,\bar{u}^{5/2} \approx \frac{\bar{u}^2(1-\bar{u}^2)^{1/2}}{(\beta r)^{1/4}(C_L/C_D)^{1/2}} \tag{11-60}$$

According to this approximation, $\bar{q}_{max}$ occurs when

$$\bar{u} = \sqrt{\frac{2}{3}} = 0.816 \tag{11-61}$$

and has the value

$$\bar{q}_{max} = \frac{2}{3\sqrt{3}(\beta r)^{1/4}\sqrt{C_L/C_D}} \tag{11-62}$$

### 11-6.3. Effect of the Initial Flight Path Angle

The initial flight path angle also has a strong effect on the deceleration and heating. It influences other kinematic quantities such as the total range and the time of flight as well. We shall consider the effect of the initial flight path angle for entries from circular speed, $\bar{u}_i = 1$, with various lift-to-drag ratios.

Figure 11-10 plots the maximum deceleration experienced during an entry from circular speed of a nonlifting vehicle, $C_L/C_D = 0$, into the Earth's atmosphere, as a function of the initial flight path angle, $\gamma_i$. The curves can be applied to other planets if the abscissa is regarded as being $-k\gamma_i$, and if the ordinate scale is multiplied by $kg_e/g_P$.

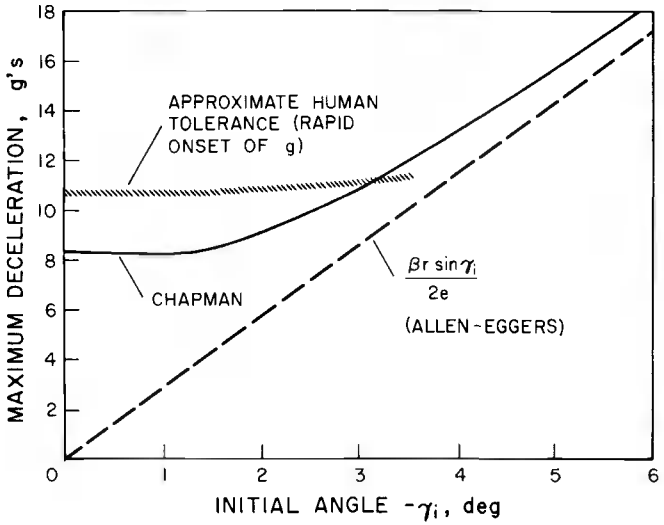


Fig. 11-10. Effect of the initial flight path angle on maximum deceleration.

It is seen from the figure that the deceleration first slightly decreases to a value of 8.2 g for an initial angle near $-1^{\circ}$, and then increases as $-\gamma_i$ increases. The dashed line plots the approximation of Allen and Eggers (Ref. 6). This corresponds to the function $\bar{Z}_I$ as given by Eq. (11-49). Hence, using this solution in Eq. (11-24), we have, with $\bar{u}_i = 1$

$$-\left(\frac{dV}{dt}/g\right) = \beta r \sin\gamma_i \bar{u}^2 \log \bar{u} \tag{11-63}$$

According to this approximate expression, the maximum deceleration occurs at

$$\bar{u} = \frac{1}{\sqrt{e}} = 0.606 \tag{11-64}$$

and has a value of

$$-\left(\frac{dV}{dt}/g\right)_{max} = -\frac{\beta r \sin\gamma_i}{2e} \tag{11-65}$$

Figure 11-11 plots the maximum of the dimensionless heating rate, $\bar{q}$, given by Eq. (11-33) for laminar flow, and the dimensionless total heat absorbed, $\bar{Q}$, given by the integral (11-41).

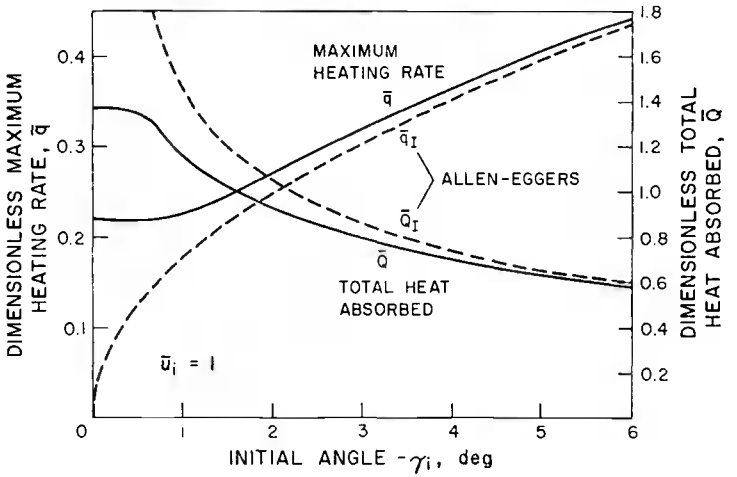


Fig. 11-11. Effect of the initial flight path angle on maximum laminar heating rate and total heat absorbed during entry.

The dashed lines are the plots using Allen and Eggers' approximate solution, the $\bar{Z}_I$ function as given by Eq. (11-49). Using this solution in Eq. (11-33), we have

$$\bar{q} = Z^{1/2} \bar{u}^{5/2} \approx \sqrt{\sqrt{\beta r} \sin(-\gamma_i)}\, \bar{u}^3 \log^{1/2}(1/\bar{u}) \tag{11-66}$$

According to this approximate formula, the maximum of $\bar{q}$ occurs at

$$\bar{u} = \frac{1}{e^{1/6}} \approx 0.8465 \tag{11-67}$$

This gives the maximum value for $\bar{q}$

$$\bar{q}_{max} = \frac{(\beta r)^{1/4}}{\sqrt{6e}} \sqrt{\sin(-\gamma_i)} \tag{11-68}$$

The function $\bar{Z}_I$ used in the integral (11-41), with an average value for $\cos\gamma$, yields the dimensionless heat absorbed, $\bar{Q}$, from $\bar{u}_i = 1$ to $\bar{u} = 0$,

$$\bar{Q} = \frac{1}{(\beta r)^{1/4} \cos^2\bar{\gamma} \sqrt{\sin(-\gamma_i)}} \int_0^1 \frac{\bar{u}\, d\bar{u}}{\log^{1/2}(1/\bar{u})}$$

$$= \frac{\sqrt{\pi}}{(\beta r)^{1/4} \cos^2\bar{\gamma} \sqrt{2\sin(-\gamma_i)}} \tag{11-69}$$

It is seen that the solution by Allen and Eggers for heat transfer in this case is quite accurate for initial flight path angles greater than about $2^\circ$.

Finally, Figs. 11-12 and 11-13 show the influence of the lift-to-drag ratio on the heating during entry at nonzero initial angles.

Figure 11-12 plots the maximum of the dimensionless heating rate, $\bar{q}_{max}$, versus the initial flight path angle, $\gamma_i$, for several values of the lift-to-drag ratio, $C_L/C_D$. For each $\gamma_i$, the maximum of $\bar{q}$ decreases as $C_L/C_D$ increases.

Figure 11-13 plots the dimensionless total heat absorbed, $\bar{Q}$, versus the initial flight path angle for different values of the lift-to-drag ratio. It is also seen that increasing the lift-to-drag ratio has the effect of decreasing the total heat absorbed for a prescribed initial flight path angle.

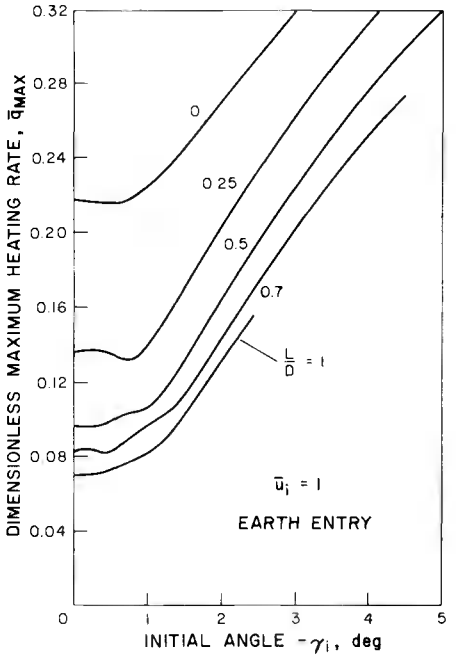


Fig. 11-12. Effect of initial flight path angle and lift-to-drag ratio on maximum heating rate.

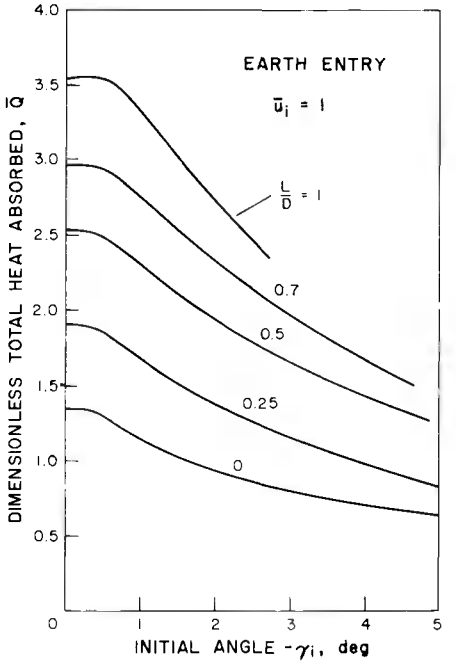


Fig. 11-13. Effect of the initial flight path angle and lift-to-drag ratio on total laminar heat absorbed.

## References

1. Chapman, D. R., "An Approximate Analytical Method for Studying Entry Into Planetary Atmospheres," NASA TR R-11, 1959.

2. Chapman, D. R., and Kapphahn, A. K., "Tables of Z Functions for Atmsopheric Entry Analyses," NASA TR R-106, 1961.

3. Lees, L., " Laminar Heat Transfer Over Blunt-Nosed Bodies at Hypersonic Flight Speeds," Jet Propulsion, Vol. 26, No. 4, pp. 259-269, 1956.

4. Lees, L., "Recovery Dynamics - Heat Transfer at Hypersonic Speeds in a Planetary Atmosphere," Chapter 12 of Space Technology, ed. by H. S. Seifert, John Wiley and Sons, N. Y., 1959.

5. Yaroshevskii, V. A., "The Approximate Calculation of Trajectories of Entry Into the Atmosphere. I", Translated from Kosmicheskie Issledovaniya, Vol. 2, No. 4, 1964.

6. Allen, H. J., and Eggers, A. J., Jr., "A Study of the Motion and Aerodynamic Heating of Missile Entering the Earth's Atmosphere at High Supersonic Speeds," NACA Report No. 1381, 1958.

7. Sänger, E., and Bredt, J., "A Rocket Drive For Long Range Bomber," Translation No. CGD-32, Technical Information Branch, Navy Department, 1944.

8. Eggers, A. J., Jr., Allen, H. J., and Neice, S. E., "A Comparative Analysis of the Performance of Long-Range Hypervelocity Vehicles," NACA TN 4046, 1957.

# Chapter 12

# Entry Corridor

## 12-1. INTRODUCTION

In Chapter 5, the analysis of the descent from orbit before entry into the atmosphere of a vehicle was presented. In the vacuum of space, any maneuver for changing orbit must be effected by the application of power. After the last thrusting maneuver has been carried out, the descending vehicle is in free flight and approaches the atmosphere on a Keplerian orbit. When the aerodynamic force becomes sensible, the vehicle begins to deviate from its Keplerian orbit. This marks the beginning of the atmospheric entry phase.

At the initial altitude where it is considered that the entry phase begins, the vehicle possesses a certain velocity $\vec{V}_i$, of magnitude $V_i$ and directed at an angle $\gamma_i$ (Fig. 12-1). The entry trajectory, for any specified vehicle, depends on these entry conditions. They can be evaluated from the elements of the approaching Keplerian orbit if the altitude for entry is given.

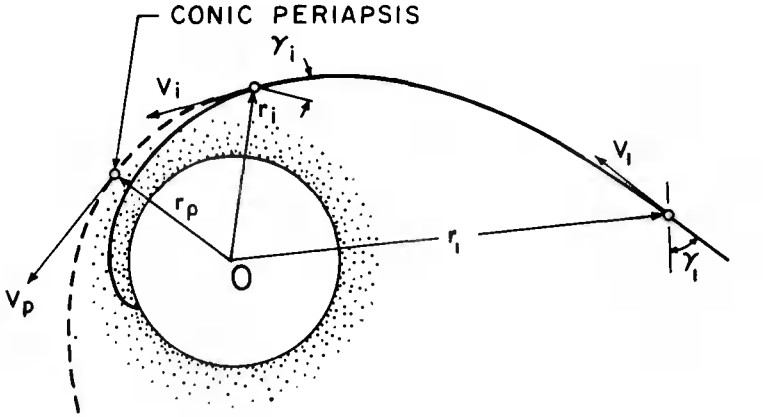


Fig. 12-1. Geometry of the entry trajectory.

In outer space, a Keplerian orbit is completely defined by the position vector $\vec{r}$ and the velocity vector $\vec{V}$ at any instant $t$. In the plane of motion, with the direction of $\vec{r}$ as the reference direction,

the three scalar quantities $r$, $V$ and $\gamma$ suffice to specify the orbit. This has been studied in detail in Chapter 3. In the following, we shall consider three particular positions for defining the approaching Keplerian orbit:

i/ The first point is an arbitrary point on the orbit, at very high altitude where the vehicle is still in the vacuum (Fig. 12-1). The quantities associated with this point are $r_1$, $V_1$ and $\gamma_1$.

ii/ The second point is the entry point and the quantities associated with this point are $r_i$, $V_i$ and $\gamma_i$. Theoretically, the definition of this point involves a certain degree of arbitrariness. One may consider the distance $r_i$ as the distance to the top of the sensible atmosphere. Another definition of the entry point is that point where the deceleration due to atmospheric force has reached a certain fraction, say one per cent, of the local gravitational force so that the vehicle has just begun its nonKeplerian trajectory. Obviously, in this case the corresponding initial distance $r_i$ depends on the drag coefficient $SC_D/m$ of the vehicle, the initial speed $V_i$ and the initial flight path angle $\gamma_i$. We shall return to this question in Chapter 13. Whatever the definition used, for all practical computation, the entry point will be considered the last point on the approaching Keplerian orbit.

iii/ The third point to be used for the definition of the Keplerian trajectory is its pericenter. This point is the lowest point on the nominal Keplerian trajectory. It is the pericenter of the conic trajectory which the vehicle would have followed had there been no atmosphere around the planet. In the case where the Keplerian orbit intersects the planet, the trajectory is extended to lead to a pericenter inside the planet. The quantities associated with this point are $r_p$, $V_p$ and $\gamma_p = 0$.

The entry speed from a close orbit is near circular speed at the entry altitude, while entry from a high altitude orbit is effected at supercircular speed. In particular, for a moon flight return to the Earth's atmosphere, the entry speed is near parabolic speed. In the case of an entry following an interplanetary flight, the vehicle enters the planetary atmosphere at hyperbolic speed. For a safe recovery of a ballistic vehicle, one must select the entry conditions, the speed $V_i$ and the flight path angle $\gamma_i$ at the distance $r_i$, such that the subsequent trajectory generates deceleration and heating conditions within acceptable limits. For a lifting hypervelocity vehicle, the entry position must also be selected such that, near the end of the atmospheric entry trajectory, the vehicle is in the correct presentation in the position vector and the velocity vector for effectively performing the last aerodynamic and thrusting maneuver phase for making a safe approach and landing at the previously selected airfield.

While thrusting maneuvers in space can always be programmed to bring the vehicle to a prescribed entry condition, the resulting fuel consumption may become prohibitive. Savings in fuel consumption will increase the useful payload, cargo, life support equipment and manpower onboard the vehicle, thus providing more flexibility in mission planning.

On the other hand, there exist constraints on the entry condition as illustrated in Fig. 12-2. Let us assume that a physical constraint, say the maximum deceleration, has been advanced in the selection of an entry trajectory. This is obviously one of the constraints in manned flights. For a given vehicle, with a certain ballistic coefficient, using a prescribed lift-to-drag ratio, all approach orbits, having a prescribed periapsis speed $V_p$ at the fictitious pericenter, can be divided into two families. In one family, the resulting atmospheric entry trajectories generate a peak deceleration exceeding the prescribed maximum deceleration. The boundary of this family will be referred to as the undershoot boundary and the resulting periapsis distance is $r_{p_{un}}$ (Fig. 12-2). In general an undershoot trajectory, that is a trajectory leading to an unacceptable peak deceleration, has its periapsis distance less than this minimum acceptable periapsis distance.

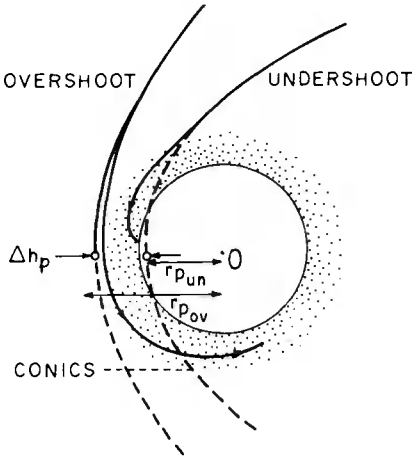


Fig. 12-2. The entry corridor.

On the other hand, among the trajectories of the remaining family of Keplerian orbits, not all can be considered as entry trajectories. This is because if the periapsis distance of the nominal Keplerian conic considered is too large, the atmospheric force encountered is too small and after a short flight inside the atmosphere the vehicle will escape into space and entry is not completed during the first pass. The boundary of these escaping trajectories is called the overshoot boundary and the resulting periapsis distance is $r_{p_{ov}}$. In general, an overshoot trajectory, that is a trajectory leading to an exit into space, has a periapsis distance larger than this maximum periapsis distance.

The portions representing excessive overshoot and undershoot in the figure are excluded as not representing the intended maneuver. This leads to a narrow corridor through which the vehicle must be guided. The difference $\Delta h_p = r_{p_{ov}} - r_{p_{un}}$ will be referred to as the

corridor width. For a successful entry during the first pass, within the limit of the physical constraint imposed upon the trajectory, the vehicle must be guided during its Keplerian phase into this narrow corridor. Flight from circular or elliptical orbit is somewhat tolerant of guidance errors. An undershoot trajectory can be readily corrected by application of a thrust at a large distance before entry. An overshoot trajectory can be similarly corrected. If necessary, one can use an aerodynamic maneuver during the skipping phase to have a correct presentation on the next return.

In contrast, entry at hyperbolic speed from outer space is unforgiving of guidance errors. For an undershoot trajectory, because of the high approach speed, thrusting correction may be prohibitive because of the fuel consumption, and an insufficiently corrected undershoot trajectory may cause destruction of the vehicle during entry. On the other hand, an overshoot trajectory, if inadequately corrected, may result in a hyperbolic departure leading the vehicle into a homeless exit into space, or a highly elliptic ejection prolonging dangerously the lapse time until the next return.

The concept of an entry corridor was first formulated by Chapman (Ref. 1). Before we continue with the presentation of this outstanding formulation, one fundamental comment is in order.

The introductory notion given above is related to a prescribed vehicle, with a given ballistic coefficient following different Keplerian trajectories, all leading to the same fictitious periapsis speed $V_p$. More clearly, for a given ballistic coefficient, with the same conic periapsis speed $V_p$, for the entry to be accomplished during the first pass, within the prescribed maximum deceleration, the periapsis distance of the approaching Keplerian orbit should be aimed between $r_{p_{un}}$ and $r_{p_{ov}}$.

A novel feature introduced in Chapman's original paper (Ref. 1) is a dimensionless periapsis parameter combining certain characteristics of the vehicle with certain quantities associated with the conic pericenter. With this parameter, the analysis can be applied to a vehicle of arbitrary weight, shape and size, entering an arbitrary planetary atmosphere.

## 12-2. BASIC DIFFERENTIAL EQUATIONS

Chapman developed his theory of the entry corridor for small flight path angles. Hence, the fundamental second-order nonlinear differential equation to be used is Eq. (11-19) written as

$$\bar{u}\,\frac{d^2\bar{Z}}{d\bar{u}^2} - \left(\frac{d\bar{Z}}{d\bar{u}} - \frac{\bar{Z}}{\bar{u}}\right) = \frac{1-\bar{u}^2}{\bar{u}\bar{Z}}\,\sqrt{\beta r}\,\frac{C_L}{C_D} \qquad (12\text{-}1)$$

where

$$\bar{u} = \frac{V \cos \gamma}{\sqrt{gr}}$$

$$\bar{Z} = \frac{\rho S C_D}{2m} \sqrt{\frac{r}{\beta}}\, \bar{u} \qquad (12\text{-}2)$$

The integration of the equation requires two initial conditions on $\bar{Z}$ and $\bar{Z}' = d\bar{Z}/d\bar{u}$ at the initial time, $\bar{u} = \bar{u}_i$ .

$$\bar{Z}(\bar{u}_i) = \bar{Z}_i \quad , \quad \bar{Z}'(\bar{u}_i) = \bar{Z}_i' \qquad (12\text{-}3)$$

To evaluate $\bar{Z}'$ , we use Eq. (11-12) reproduced here for convenience

$$\frac{d\bar{Z}}{d\bar{u}} - \frac{\bar{Z}}{\bar{u}} = \sqrt{\beta r}\, \sin \gamma \qquad (12\text{-}4)$$

Hence, the initial conditions are

$$\bar{Z}(\bar{u}_i) = \bar{Z}_i \quad , \quad \bar{Z}'(\bar{u}_i) = \frac{\bar{Z}_i}{\bar{u}_i} + \sqrt{\beta_i r_i}\, \sin \gamma_i \qquad (12\text{-}5)$$

The kinematic elements at entry are $r_i$ , $V_i$ and $\gamma_i$ . Hence, we can form the dimensionless entry speed $\bar{V}_i = V_i / \sqrt{g_i r_i}$ . Then $\bar{u}_i = \bar{V}_i \cos \gamma_i$ , $\gamma_i$ and the additional prescribed value $\bar{Z}_i$ will provide sufficient initial conditions for the integration of the nonlinear equation (12-1). Subsequently, the flight path angle is given by Eq. (12-4) and the deceleration, the heating rate or any other physical quantity at any instant can be obtained from $\bar{Z}$ , $\bar{u}$ , and $\gamma$ as has been presented in Chapter 11.

Now, since $\bar{Z}_i$ can be taken as approximately zero, or analytically by using the first-order solutions, it is seen that only $\bar{V}_i$ and $\gamma_i$ need be prescribed. Then, the analysis of the deceleration, or whatever physical quantity is considered, determines whether or not the trajectory is an undershoot trajectory while the corresponding $\bar{Z}$ function is used to assess if a trajectory is a skip trajectory, $\bar{Z}_f = \bar{Z}_i$ , or a descending trajectory, $\bar{Z} > \bar{Z}_i$ . Several hundred solutions for different entry trajectories were computed by Chapman and the results presented in his report (Ref. 1). A very convenient parameter, the periapsis parameter, was introduced to present the results in a completely dimensionless form applicable to any type of vehicle, of arbitrary weight, shape and size, entering an arbitrary planetary atmosphere.

## 12-3. THE PERIAPSIS PARAMETER

It was explained in Chapter 11 that the use of Chapman's variables $\overline{Z}$ and $\overline{u}$ has the advantage of eliminating the specification of the entry altitude $h_i$ and the ballistic coefficient $SC_D/m$. The characteristics of the planet's atmosphere enter the basic equation (12-1) in the dimensionless parameter $\sqrt{\beta r}$. From Eq. (12-5), it follows that, for shallow entry at a high altitude, where the initial values of $\overline{Z}$ are negligible compared to subsequent values during entry, the second initial condition can be written as

$$\overline{Z}'(\overline{u}_i) = \sqrt{\beta_i r_i}\,\gamma_i \tag{12-6}$$

The initial flight path angle $\gamma_i$ should be taken at the beginning of the sensible atmosphere. Theoretically, from Fig. 12-1, it is seen that, once the Keplerian approach orbit is known, this angle $\gamma_i$ can be evaluated for any distance $r_i$ chosen as the radius of the sensible atmosphere. But this distance $r_i$ is not well-defined. From a physical standpoint, if the entry altitude is defined as the altitude where aerodynamic force begins to take effect, then this altitude obviously depends on the drag parameter $SC_D/m$, the entry speed $V_i$ and the angle $\gamma_i$ itself. For very shallow trajectories grazing the edge of the atmosphere, a precise evaluation of $\gamma_i$ is therefore cumbersome.

A convenient parameter for the analysis of the entry corridor, the periapsis parameter, was introduced by Chapman. This parameter is associated with the hypothetical periapsis distance of the approach conic orbit (Fig. 12-1). The relation between this periapsis distance $r_p$, and the elements $r$, $V$ and $\gamma$ at any arbitrary point on the Keplerian orbit was given in Chapter 3, Eq. (3-70). This equation can be rewritten in the current notation as

$$\frac{r_p}{r} = \frac{1 - \sqrt{(\overline{V}^2 - 1)^2 + \overline{V}^2(2 - \overline{V}^2)\sin^2\gamma}}{2 - \overline{V}^2} \tag{12-7}$$

where

$$\overline{V} = \frac{V}{\sqrt{gr}} = \frac{\overline{u}}{\cos\gamma} \tag{12-8}$$

For shallow entries for which the flight path angle is small,

$$\frac{\overline{V}^2(2 - \overline{V}^2)\sin^2\gamma}{(\overline{V}^2 - 1)^2} \ll 1$$

and Eq. (12-7) for supercircular entries $(\overline{V}_i^2 - 1) > 0$, with the arbitrary point taken as the entry point, can be approximated as

$$\frac{r_p}{r_i} \approx 1 - \frac{\bar{V}_i^2 \sin^2 \gamma_i}{2(\bar{V}_i^2 - 1)}$$

Hence,

$$\frac{r_i - r_p}{r_i} \approx \frac{\bar{V}_i^2 \gamma_i^2}{2(\bar{V}_i^2 - 1)} \tag{12-9}$$

Chapman introduced a periapsis parameter defined as

$$F_p = \frac{\rho_p S C_D}{2m} \sqrt{\frac{r_p}{\beta}} \tag{12-10}$$

where $r_p$ is the hypothetical periapsis distance and $\rho_p$ is the atmospheric density evaluated at this distance. For an atmosphere which is strictly exponential between the initial point and the pericenter,

$$\rho_p = \rho_i e^{-\beta(h_p - h_i)} = \rho_i e^{\beta(r_i - r_p)} \tag{12-11}$$

On the other hand, from the definition (12-2) of the $\bar{Z}$ function

$$\bar{Z}_i = \frac{\rho_i S C_D}{2m} \sqrt{\frac{r_i}{\beta}}\, \bar{u}_i \tag{12-12}$$

so that,

$$F_p = \frac{\bar{Z}_i}{\bar{u}_i} \sqrt{\frac{r_p}{r_i}}\, e^{\beta(r_i - r_p)} \tag{12-13}$$

For shallow entries, $\bar{u}_i^2 = \bar{V}_i^2 \cos^2 \gamma_i \approx \bar{V}_i^2$, and the ratio $r_p / r_i$ can be set equal to unity, consistent with the approximation made in deriving Eq. (12-9). Hence, the approximate expression for $F_p$ is

$$F_p = \frac{\bar{Z}_i}{\bar{V}_i} \exp\left[\frac{\bar{V}_i^2 (\sqrt{\beta_i r_i}\ \gamma_i)^2}{2(\bar{V}_i^2 - 1)}\right] \tag{12-14}$$

This is the form given by Chapman (Ref. 1). For the case of shallow entry

$$(\sqrt{\beta_i r_i}\ \gamma_i)^2 = \frac{2(\bar{V}_i^2 - 1)}{\bar{V}_i^2} \log\left(\frac{\bar{V}_i}{\bar{Z}_i} F_p\right) \tag{12-15}$$

That is, $\sqrt{\beta_i r_i}\ \gamma_i$ is a function only of $\overline{V}_i$, $\overline{Z}_i$ and $F_p$. Consequently, the two initial conditions $\overline{Z}_i$ and $\overline{Z}_i' = \sqrt{\beta_i r_i}\ \gamma_i$, imposed at $\overline{u}_i$ on the basic nonlinear second-order differential equation, Eq. (12-1), can be replaced by the equivalent two, $\overline{Z}_i$ and $F_p$, imposed at $\overline{V}_i$.

To explain the usefulness and generality of the periapsis parameter $F_p$ in a clear and satisfactory way, let us consider the case of ballistic entry, $C_L / C_D = 0$, at parabolic speed, $\overline{V}_i = 1.4$, into the Earth's atmosphere. The basic equation to be integrated is

$$\overline{u}\,\frac{d^2\overline{Z}}{d\overline{u}^2} - \left(\frac{d\overline{Z}}{d\overline{u}} - \frac{\overline{Z}}{\overline{u}}\right) = \frac{1 - \overline{u}^2}{\overline{u}\,\overline{Z}} \qquad (12\text{-}16)$$

The initial conditions required for the integration are

$$\overline{u}_i = \overline{V}_i = 1.4\ ,\quad \overline{Z}(\overline{u}_i) = \overline{Z}_i\ ,\quad \overline{Z}_i' = \sqrt{\beta_i r_i}\ \gamma_i \qquad (12\text{-}17)$$

A nonzero value $\overline{Z}_i$ is obtained analytically as explained in Chapman's Ref. 2, while, instead of $\sqrt{\beta_i r_i}\ \gamma_i$ as a scanning parameter to generate different entry trajectories, $F_p$ is used as an arbitrary scanning parameter and $\sqrt{\beta_i r_i}\ \gamma_i$ is obtained from Eq. (12-15) to be used in the second initial condition (12-17). For each parabolic entry trajectory into the Earth's atmosphere, the peak deceleration is plotted versus the corresponding value $F_p$ in Fig. 12-3. The curve ends at the value $F_p = 0.06$. For $F_p$ smaller than this value, the vehicle will pass through the atmosphere, exit into space, and then return for at least a second pass before the entry is completed. Hence, this value of $F_p$ corresponds to the overshoot boundary for single-pass entries. Now, let us assume that 10 g is the maximum deceleration allowed for this particular case of parabolic entry into the Earth's atmosphere. From the graph, the corresponding value for $F_p$ is $F_p = 0.31$. Hence, for single-pass entries limited at 10 g, the range for $F_p$ is

$$0.06 < F_p \leq 0.31$$

The result thus obtained is independent of the entry vehicle. In practice, when the drag parameter of the vehicle and the characteristics of the atmosphere have been specified, with $F_p = 0.06$, and $F_p = 0.31$, the equation (12-10) can be solved for a maximum and a minimum value of the periapsis distance. For a successful entry, the parabolic returning trajectory should be aimed so that its periapsis distance is between these limits.

In general, let us consider the ratio $\rho_{p_{un}} / \rho_{p_{ov}}$ of the values of the atmospheric density at the two limiting periapsis distances

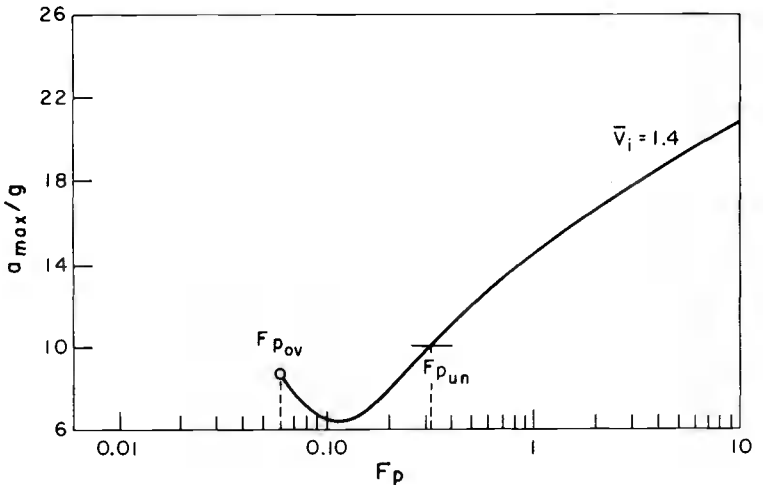


Fig. 12-3. Maximum deceleration during ballistic parabolic entry into the Earth's atmosphere.

$$\frac{\rho_{p_{un}}}{\rho_{p_{ov}}} = e^{\beta(h_{ov} - h_{un})} = \frac{(F_p m/SC_D)_{un}}{(F_p m/SC_D)_{ov}} \sqrt{\frac{r_{ov}}{r_{un}}} \qquad (12\text{-}18)$$

The difference $\Delta h_p = h_{ov} - h_{un}$ between the two conic periapsis altitudes is defined as the corridor width as illustrated in Fig. 12-2. This difference is small, $r_{ov}/r_{un} \approx 1$, so that the expression for the corridor width is approximately

$$\Delta h_p = \frac{1}{\beta} \log \left[ \frac{(F_p m/SC_D)_{un}}{(F_p m/SC_D)_{ov}} \right] \qquad (12\text{-}19)$$

For the special case wherein the ballistic coefficient $SC_D/m$ is the same along the two boundaries, we have

$$\Delta h_p = \frac{1}{\beta} \log \frac{F_{p_{un}}}{F_{p_{ov}}} \qquad (12\text{-}20)$$

For the case considered above, for the Earth's atmosphere with $1/\beta = 7,162$ m, the corridor width is $\Delta h_p = 7,162 \times \log 5.16 = 11,746$ m. From Eq. (12-20), it is apparent that, if the ballistic coefficient is the same for the two boundaries, a condition which is especially true when there is no deformation of the entry vehicle, then the corridor width for a given exponential atmosphere, (constant $\beta$), depends only on the ratio $F_{p_{un}}/F_{p_{ov}}$. Hence, the corridor width, for for a prescribed $\bar{V}_i$, is the same for all vehicles. However, the periapsis altitudes of the corridor boundaries, $h_{p_{un}}$ and $h_{p_{ov}}$ are functions of the ballistic coefficient through Eq. (12-10).

## 12-4. CHAPMAN'S RESULTS FOR THE ENTRY CORRIDOR

To ease the discussion, Fig. 12-3 has been presented for parabolic entry into the Earth's atmosphere. With the purpose of presenting his results in a completely dimensionless form, applicable to any arbitrary vehicle regardless of its weight, size and shape, entering an arbitrary planetary atmosphere, Chapman used a normalization technique.

From Eq. (11-25) of Chapter 11, the dimensionless deceleration for a shallow entry is

$$\frac{a}{g} = \sqrt{\beta r}\ \bar{Z}\ \bar{u}\ \sqrt{1 + (C_L/C_D)^2} \qquad (12\text{-}21)$$

Now, in integrating Eq. (12-1), instead of specifying the two values $\sqrt{\beta r}$ and $(C_L/C_D)$ separately, one can specify only the single parameter $\sqrt{\beta r}\,(C_L/C_D)$. Then, for any specified planetary atmosphere (i.e., given $\sqrt{\beta r}$) the actual lift-to-drag ratio flown can be deduced. Next, let us assume that for a prescribed value $\lambda = \sqrt{\beta r}\ (C_L/C_D)$, and for a certain prescribed condition on entry, a function $\bar{Z}$ has been generated with the corresponding value $\bar{u}$. Then we can evaluate the deceleration for the case of the Earth (subscript e) and the deceleration for the case of an arbitrary planet (no subscript) as

$$\frac{a_e}{g_e} = \sqrt{(\beta r)_e}\ \bar{Z}\ \bar{u}\ \sqrt{1 + \frac{\lambda^2}{(\beta r)_e}}$$

$$\frac{a}{g} = \sqrt{\beta r}\ \bar{Z}\ \bar{u}\ \sqrt{1 + \frac{\lambda^2}{\beta r}} \qquad (12\text{-}22)$$

Since $\lambda$ is prescribed for the computation of the $\bar{Z}$ function, we can construct the dimensionless deceleration function

$$\bar{G} = 30\ \bar{Z}\ \bar{u}\ \sqrt{1 + \frac{\lambda^2}{900}} \qquad (12\text{-}23)$$

Since for the Earth's atmosphere $(\beta r)_e = 900$, it is seen that this function is simply the dimensionless deceleration, in Earth g's, for entry into the Earth's atmosphere. From the Eqs. (12-22) and (12-23), it is seen that, through the use of the dimensionless universal function $\bar{Z}$, all the decelerations reach their respective maximum values at the same values for $\bar{Z}$, and $\bar{u}$. Hence, if the function $\bar{G}_{max}$ is used for the diagram, $\bar{G}_{max}$ versus $F_p$, for different values of the dimensionless entry speed $\bar{V}_i$, it represents the point of peak deceleration for entry of any arbitrary vehicle into any arbitrary planetary atmosphere. The diagram can be used directly for evaluation of the entry corridor for entry into the Earth's atmosphere. For entry into any other planetary atmosphere, from Eq. (12-22), the

deceleration normalized with respect to the Earth gravity will be

$$\frac{a}{g_e} = \frac{g\sqrt{\beta r}}{g_e} \bar{Z}\,\bar{u}\sqrt{1+\frac{\lambda^2}{\beta r}}$$

or, in terms of $\bar{G}$ as defined in Eq. (12-23)

$$\frac{a}{g_e} = \frac{g}{g_e}\frac{\sqrt{\beta r}}{\sqrt{(\beta r)_e}}\bar{G}\frac{\sqrt{1+(\lambda^2/\beta r)}}{\sqrt{1+(\lambda^2/900)}} \qquad (12\text{-}24)$$

In the notation of Chapman

$$\frac{g}{g_e} = g_\oplus\,, \quad \frac{\sqrt{\beta r}}{\sqrt{(\beta r)_e}} = \sqrt{(\beta r)_\oplus} \qquad (12\text{-}25)$$

this is

$$G = \frac{a}{g_e} = g_\oplus\sqrt{(\beta r)_\oplus}\,\bar{G}\,\frac{\sqrt{1+(C_L/C_D)^2}}{\sqrt{1+[\sqrt{(\beta r)_\oplus}(C_L/C_D)]^2}} \qquad (12\text{-}26)$$

Hence, for any other planetary entry, with the constraint $G_{max} = a_{max}/g_e$ prescribed, Eq. (12-26) must be used to evaluate the corresponding $\bar{G}_{max}$ before referring to the diagram $\bar{G}_{max}$ versus $F_p$.

The results of Chapman's investigation are presented in Figs. 12-4, 12-5 and 12-6 for ballistic entry, $C_L/C_D = 0$, for different dimensionless entry speeds.

Figure 12-4 plots the dimensionless maximum deceleration $\bar{G}_{max}$ versus the periapsis parameter $F_p$. For entry into the Earth's atmosphere, the maximum deceleration in Earth's g's is given directly by the ordinate. As mentioned above, for parabolic entry, $\bar{V}_i = 1.4$, the overshoot boundary corresponds to $F_{p_{ov}} = 0.06$, while, if the maximum deceleration is limited to 10 g, the corresponding value for $F_p$ is $F_{p_{un}} = 0.31$. Consider now a parabolic entry into another planetary atmosphere, for example, the atmosphere of Jupiter. The value for $F_{p_{ov}}$ is the same for any planet. But to have the same value for $F_{p_{un}}$, and hence the same $\bar{G}_{max} = 10$, since for Jupiter $g_\oplus\sqrt{(\beta r)_\oplus} = 5.3$, from Eq. (12-26) one must have the maximum allowable deceleration equal to an unrealistic 53 Earth g's. With this maximum deceleration, for Jupiter we take $1/\beta = 18,288$ m, and by Eq. (12-20) the corridor width on Jupiter is $\Delta h_p = 29,992$ m.

More realistically, if we want to keep the maximum deceleration for ballistic entry into Jupiter's atmosphere at 10 Earth g's, the corresponding $\bar{G}_{max}$ would be $\bar{G}_{max} = 10/5.3 = 1.89$. But the smallest possible maximum deceleration for a nonlifting vehicle entering any planetary atmosphere corresponds to $\bar{G}_{max} = 6.5$ for a hyperbolic entry, $\bar{V}_i \approx 1.48$, as may be seen on Fig. 12-4. Hence, for entry into Jupiter's atmosphere the 10 Earth g corridor width would be nonexistent. The smallest value of the peak deceleration for nonlifting entry into Jupiter's atmosphere is $G = 6.5 \times 5.3 = 34$ Earth g's.

Figure 12-5 plots the dimensionless heating rate $\bar{q}_{max}$ versus $F_p$ for ballistic entry at different speeds, while Fig. 12-6 plots the dimensionless total heat absorbed $\bar{Q}$ versus $F_p$. The definitions of $\bar{q}$ and $\bar{Q}$ are given in Eqs. (11-33) and (11-41) in Chapter 11. The results are presented for the entry of a nonlifting vehicle.

Before discussing the influence of aerodynamic lift on the corridor boundaries we conclude this section with some remarks of interest.

First, the relationship (12-14) between $\sqrt{\beta_i r_i}\,\gamma_i$ and $F_p$ is derived based on the assumption of small entry flight path angles such that

$$\frac{\bar{V}_i^2 (2 - \bar{V}_i^2) \sin^2 \gamma_i}{(\bar{V}_i^2 - 1)^2} << 1 \qquad (12\text{-}27)$$

Hence, it will require that $\bar{V}_i$ is not near the circular speed. The assumption is good if

$$\bar{V}_i^2 - 1 > -\gamma_i$$

Since $-\gamma_i$ is the order of 0.1, the use of $F_p$ as a similarity parameter for entry into different planetary atmospheres is restricted to about $\bar{V}_i^2 > 1.1$, or $\bar{V}_i > 1.05$.

Next, although theoretically a skip trajectory is a trajectory leading to $\bar{Z}_f = \bar{Z}_i \approx 0$, in constructing the diagrams Chapman qualified an overshoot trajectory such that the exit speed exceeds the circular speed, that is, a trajectory such that $\bar{V}_f \geq 1$ at the exit point.

Finally, an interesting, and possibly unexpected, result for the entry of nonlifting vehicles, is exhibited by the curves for maximum deceleration in Fig. 12-4, and also by the curves for maximum rate of laminar heating in Fig. 12-5. The absolute minimum value of $\bar{G}_{max}$, and the absolute minimum value of $\bar{q}_{max}$ do not occur at the lowest supercircular entry speed as might be expected. The absolute minimum $\bar{G}_{max}$ occurs for entry at slightly hyperbolic speed and the absolute minimum $\bar{q}_{max}$ occurs for entry at slightly supercircular speed.

A cross plot is presented in Fig. 12-7. From this figure, it is seen that the lowest possible maximum deceleration for ballistic entry into a planetary atmosphere is experienced when entering at the hyperbolic speed $\bar{V}_i = 1.48$ and aiming at a periapsis parameter of $F_p = 0.12$. This results in a minimum $\bar{G}_{max} = 6.5$ as compared

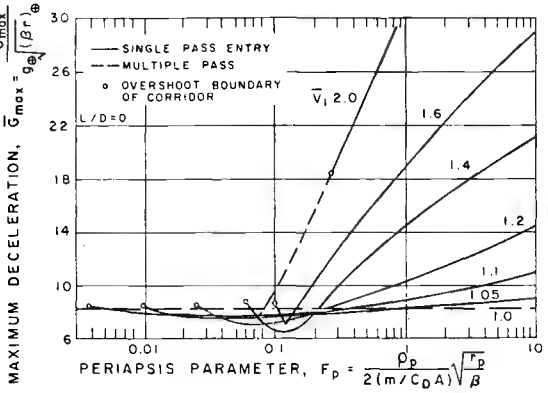


Fig. 12-4. Maximum deceleration

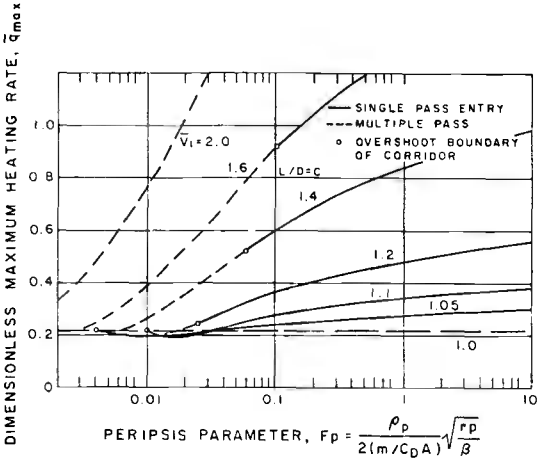


Fig. 12-5. Maximum laminar heating rate

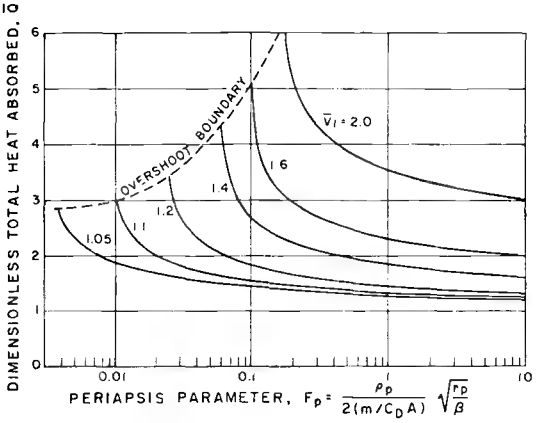


Fig. 12-6. Total laminar heat absorbed

Figs. 12-4, 12-5, 12-6. Ballistic entry at supercircular speed.

to $\bar{G}_{max} = 8.3$ for circular orbital decay. The lowest possible maximum heating rate for ballistic entry occurs at $\bar{V}_i = 1.12$ and at $F_p = 0.018$. This results in a minimum $\bar{q}_{max} = 0.19$ as compared to $\bar{q}_{max} = 0.22$ for circular orbital decay. An enlightening physical reason to explain the phenomena has been provided by Chapman in Ref. 1.

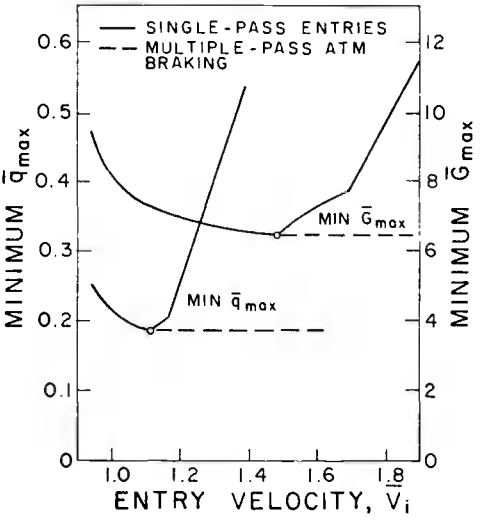


Fig. 12-7. Minimum values of $\bar{G}_{max}$ and $\bar{q}_{max}$ as functions of entry speed for nonlifting vehicles.

Also, as seen in Fig. 12-6, the normalized curves for the total heat absorbed during ballistic entry do not exhibit minima. For any entry speed, the lowest possible total heat is absorbed by entering at the largest possible value of $F_p$ which, as shown by Eq. (12-15) and Fig. 12-4, corresponds to the steepest possible entry and to the greatest possible deceleration.

## 12-5. INFLUENCE OF AERODYNAMIC LIFT ON THE CORRIDOR BOUNDARIES

One of the most interesting aspects of hypersonic flight is the use of the lifting capability of hypervelocity vehicles to effect maneuvers in an advantageous way. A complete analysis of the modulation of the lift, and possibly the bank angle, as functions of time, to achieve the maximization of a certain quantity, called the performance index, would require the tools of modern optimization theory. Such a subject will be discussed in a forthcoming text entitled, "Optimal Trajectories in Atmospheric Flight."

Since here we are mainly concerned with entry at constant angle-of-attack, or equivalently constant lift-to-drag ratio, we shall restrict ourselves to the discussion of the lift-to-drag ratio, considered as a parameter, and its influence on the boundaries of the entry corridor.

Referring to Fig. 12-2, let us assume that the overshoot boundary and the undershoot boundary correspond to ballistic entry, $C_L/C_D = 0$, of a certain vehicle. Now, if for a range of angle of attack, the vehicle can generate lifting forces, then it is reasonable to infer that, by using negative lift, the lifting vehicle, starting on the trajectory of the ballistic overshoot boundary, can be curved inward holding the trajectory inside the atmosphere. Thus, this incoming Keplerian trajectory is no longer an overshoot trajectory. That is to say, with lifting capability the overshoot boundary for the lifting vehicle will be higher than that of the ballistic vehicle, providing a larger $r_{p_{ov}}$.

Similarly, for the undershoot boundary, positive lift can be used to decrease the flight path angle and reduce the peak deceleration. The ultimate effect is to lower the lifting vehicle's undershoot boundary, providing a lower $r_{p_{un}}$.

Through these heuristic considerations, it may be concluded that the use of aerodynamic lift can have the effect of increasing the corridor width. The actual mechanism is more complicated because of the coupling between the lift-to-drag ratio, $C_L/C_D$, and the drag coefficient $C_D$. We shall study in some detail this coupling effect in the following sections.

## 12-5.1. Overshoot Boundary with Lift

If a vehicle entered the atmosphere along an overshoot trajectory it would pass through the atmosphere and exit into space at a point where $\overline{Z}_f = \overline{Z}_i \approx 0$. If the exit speed is large but less than the escape speed, the vehicle will return to the atmosphere for at least another pass. If the exit speed is small, the vehicle will follow a free flight trajectory outside the atmosphere for a short distance and re-enter the atmosphere to complete the entry. For small flight path angles, with small and moderate lift-to-drag ratios, if the exit speed is less than the local circular speed the vehicle will stay near the edge of the sensible atmosphere before finally descending. Hence, we can use Chapman's definition in considering the overshoot boundary as the trajectory such that the exit speed is the circular speed, that is, $\overline{V}_f = 1$. Using this definition, Chapman computed the overshoot boundaries for different lift-to-drag ratios using the entry speed $\overline{V}_i$ as the scanning parameter. His results are presented in Fig. 12-8. The figure plots the parameter $\sqrt{(\beta r)_\oplus}\,(C_L/C_D)$ versus the periapsis parameter $F_p$ for different values of the initial entry speed.

As anticipated, the curves in the figure show that, relative to the case of $C_L/C_D = 0$, for each entry speed $\overline{V}_i$, the overshoot boundary is extended upward, that is to lower $F_p$ (hence to lower $\rho_p$), if negative lift (lift directed toward the center of the planet) is employed. This is rigorously true when, while varying $C_L/C_D$, we can maintain $C_D$ constant. But, for a given vehicle aerodynamic configuration, when we vary the angle-of-attack both the lift and the drag coefficients vary. That is, there exists a relationship between the lift and the drag coefficients, or, referring to the drag polar, there

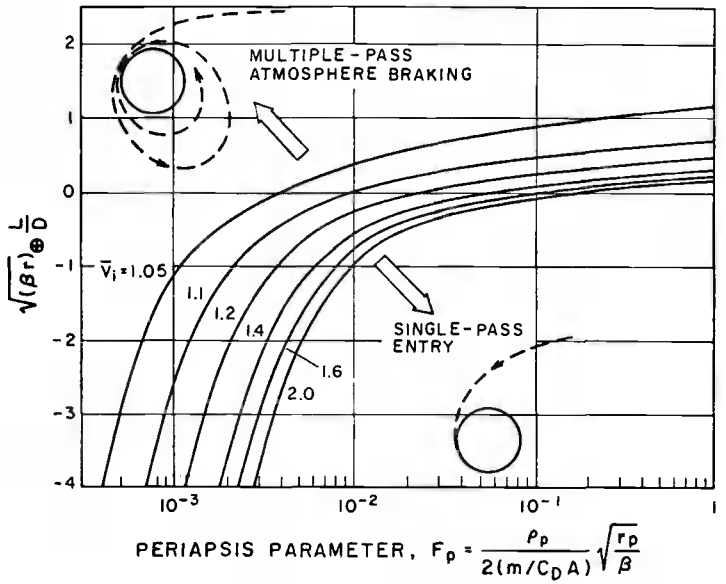


Fig. 12-8. Overshoot boundaries for single-pass entry of a lifting vehicle.

exists a relationship between the lift-to-drag ratio and the drag coefficient.

Typical relationships between $C_L/C_D$ and $C_D$ using Newtonian theory for hypersonic flow over a flat plate are presented in Fig. 12-9 taken from Chapman's Ref. 1. Along each drag polar, the lift-to-drag ratio increases from the value zero at $0^o$ angle-of-attack to a maximum, then decreases to zero at $90^o$ angle of attack when the drag coefficient reaches its maximum value. For each lift-to-drag ratio, there exist two values of $C_D$, one corresponds to low drag flight and one corresponds to high drag flight. Since high drag minimizes the aerodynamic heating, the high drag portion is used in connection with the attempt to widen the entry corridor. But the use of this portion will have a reverse effect. This can be seen in the Figs. 12-8 and 12-9 and from the definition (12-10) of the periapsis parameter written as

$$\frac{F_p}{C_D} = \frac{\rho_p S}{2m}\sqrt{\frac{r_p}{\beta}} \tag{12-28}$$

With a higher negative lift-to-drag ratio, the periapsis parameter $F_p$ decreases. But this does not induce automatically a decrease in $\rho_{p_{ov}}$, and hence an increase in $r_{p_{ov}}$, since the drag coefficient $C_D$ also decreases. In general, let $(F_{p_1}, C_{D_1})$ and $(F_{p_2}, C_{D_2})$ be the corresponding values for $F_p$ and $C_D$ for two

entries with lift-to-drag ratios $C_{L_1}/C_{D_1}$ and $C_{L_2}/C_{D_2}$. Since $r_{p_1} \approx r_{p_2}$,

$$\frac{F_{p_1}/C_{D_1}}{F_{p_2}/C_{D_2}} = e^{\beta(h_2 - h_1)} \tag{12-29}$$

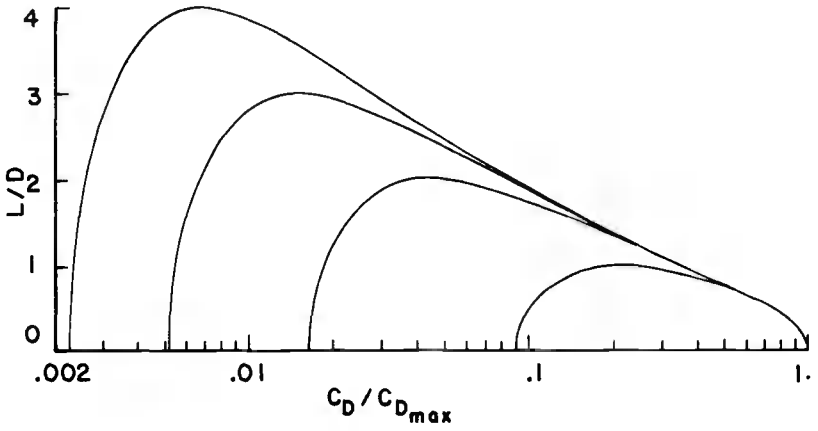


Fig. 12-9. Lift-drag polars for lifting surfaces in hypersonic Newtonian flow.

The change in the periapsis altitude of the overshoot boundary, when we change from $C_{D_1}$ to $C_{D_2}$, is

$$h_2 - h_1 = \Delta h_{p_{ov}} = \frac{1}{\beta} \log \left[ \frac{F_{p_1}/C_{D_1}}{F_{p_2}/C_{D_2}} \right] \tag{12-30}$$

The extension is upward, if and only if

$$\frac{F_{p_1}}{C_{D_1}} > \frac{F_{p_2}}{C_{D_2}} \tag{12-31}$$

A simple graphical evaluation of parabolic entry, $\bar{V}_i = 1.4$ on Fig. 12-8, using the $(C_L/C_D)_{max} = 4$ drag polar of Fig. 12-9, shows that, compared with ballistic entry, $C_L/C_D = 0$, between $C_L/C_D = 0$ and $C_L/C_D = -0.5$ the extension of the overshoot boundary is upward, reaching a maximum of 9.7 km for $C_L/C_D = -0.5$. Between $C_L/C_D = -0.5$ and $C_L/C_D = -4$ the extension of the overshoot boundary is downward producing a maximum narrowing of the corridor of 11.3 km when $C_L/C_D = -4$.

In practice, a more effective method of extending the overshoot

boundary would be to deploy a large, light, high-drag device to increase the drag coefficient $C_D$ while keeping $C_L = 0$ .

In addition to specifying the overshoot boundary $\overline{V}_f = 1$ , it is of interest for hyperbolic entry to specify the nonreturn boundary $\overline{V}_f = \sqrt{2}$ . Both boundaries are illustrated in Fig. 12-10 for two hyperbolic entries at $\overline{V}_i = 1.6$ and $\overline{V}_i = 2.0$ respectively. For moderate and high negative lift-to-drag ratios, $\sqrt{(\beta r)}_\oplus (C_L/C_D) < -0.05$ , the difference between the overshoot boundary and the nonreturn boundary is indistinguishable on this figure.

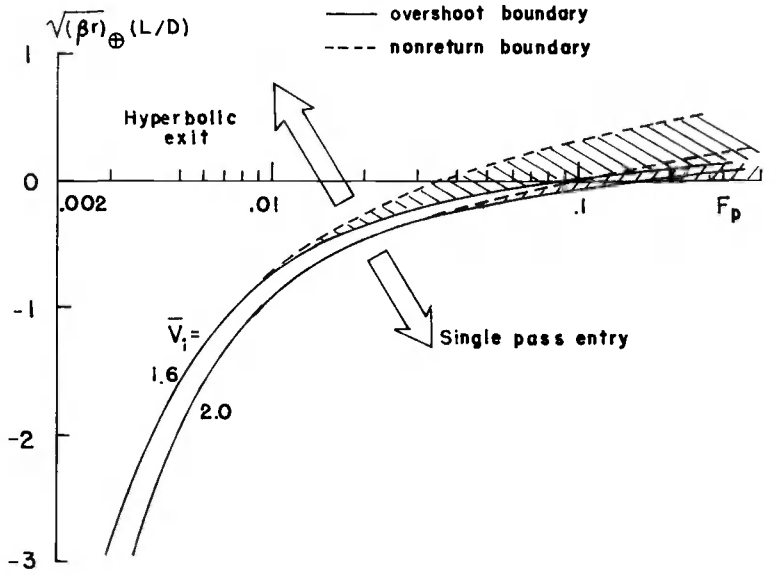


Fig. 12-10. Overshoot boundary and nonreturn boundary for hyperbolic entry.

## 12-5.2. Undershoot Boundary With Lift

For a prescribed entry speed $\overline{V}_i$ , a deceleration-limited undershoot boundary depends on the value $\overline{G}_{max}$ prescribed and the constant lift-to-drag ratio, $C_L/C_D$ , selected. As in the case of the overshoot boundary, an undershoot boundary can be extended downward, hence widening the entry corridor, by a proper selection of the constant lift-to-drag ratio. It is obvious that a better way to achieve an optimum extension of the undershoot boundary is to modulate the ratio $C_L/C_D$ as a function of time. A rigorous treatment of the problem would require the tools of modern optimization theory. Also a new definition of the $\overline{Z}$ function is in order since as $C_L/C_D$ varies, the coefficient $C_D$ , which is contained explicitly in $\overline{Z}$ , also varies.

Lees, Hartwig and Cohen (Ref. 3) have studied the effect of the modulation of $C_L/C_D$ , under the assumption of constant $C_D$ , on

the maximum deceleration during entry. They show that by modulating $C_L / C_D$ in a manner such that large $C_L / C_D$ values are employed in the first portion of the entry trajectory where the longitudinal deceleration is small, the resultant deceleration can build up to its maximum under conditions where the transverse component is dominant. Then, by maintaining this constant resultant value $G$ through decreasing the transverse component while increasing the longitudinal component, the entry with modulated lift can be completed without requiring large negative $C_L / C_D$ at any stage. In this way, the undershoot boundary for modulated $C_L / C_D$ can be extended considerably from the value for constant $C_L / C_D$, provided the value of $C_L / C_D$ at entry is relatively high. They found that the ratio of $\overline{G}_{max}$ for modulated lift to $\overline{G}_{max}$ for constant lift was essentially independent of $V_i$ and $\gamma_i$, and dependent only on the initial value of $C_L / C_D$ at entry. Their result is presented in Fig. 12-11.

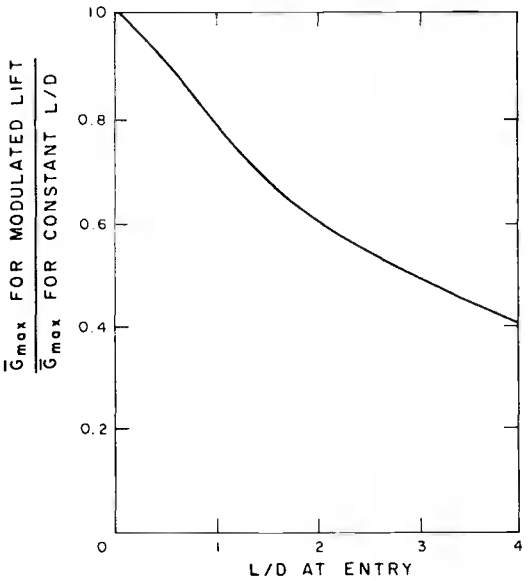


Fig. 12-11. Effect of modulated lift in reducing peak deceleration.

On the other hand, Chapman studied the effect of constant $C_L / C_D$ on the undershoot boundary for deceleration-limited entry. A typical diagram showing his results is presented in Fig. 12-12 for parabolic entry, $\overline{V}_i = 1.4$. The diagram plots the normalized maximum deceleration, $\overline{G}_{max}$, versus $\log_{10} F_p$. From the figure, it is apparent that an increase in $C_L / C_D$ up to about 2 can extend considerably the undershoot boundary for a given $\overline{G}_{max}$ since it leads to higher $F_p$, hence lower $r_p$ for constant $C_D$. It should be noted that a constant high lift-to-drag ratio may lead to a skip trajectory. Hence, the constant $C_L / C_D$ program used is only maintained until the flight path is essentially horizontal, $\gamma \approx 0$,

near the point where maximum deceleration is reached. After this point the lift-to-drag ratio is modulated to maintain the flight inside the atmosphere in order to complete entry in a single pass.

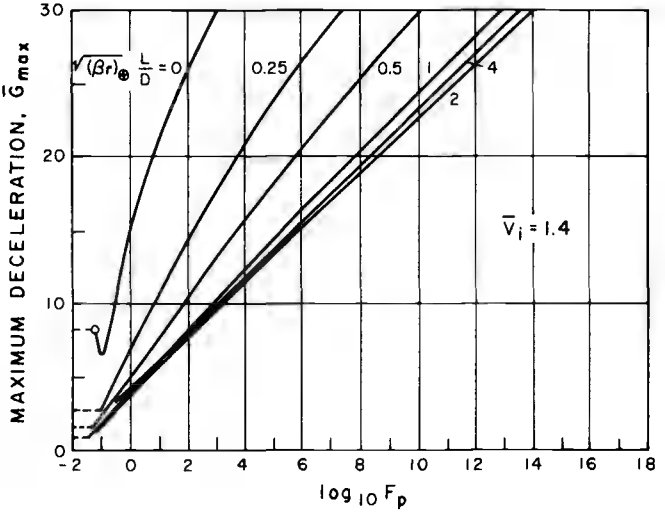


Fig. 12-12. Normalized maximum deceleration for various lift-to-drag ratio entries at parabolic speed.

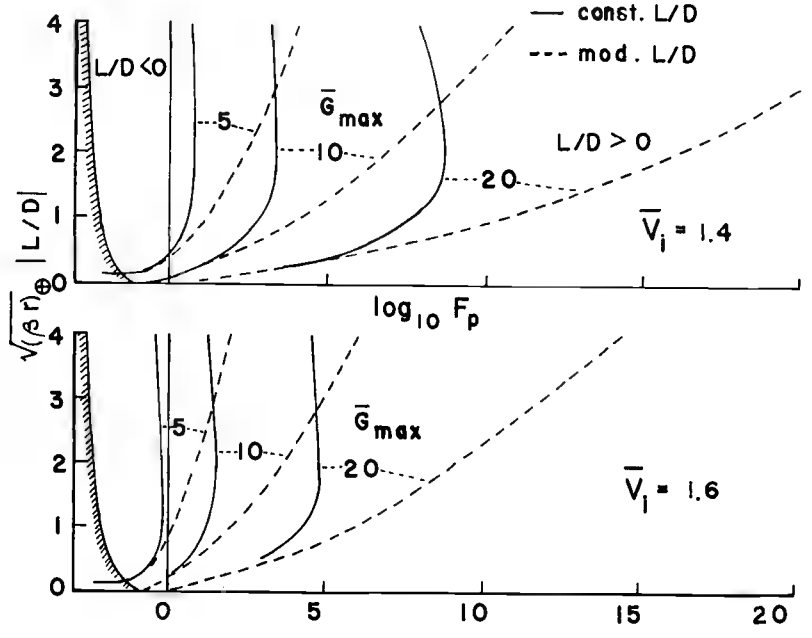


Fig. 12-13. Overshoot and undershoot boundaries as function of lift-to-drag ratio and maximum deceleration.

The overshoot boundary with negative lift, and the undershoot boundary with positive lift for various prescribed $\overline{G}_{max}$ are plotted in Fig. 12-13 for entry at parabolic speed, $\overline{V}_i = 1.4$, and entry at slightly hyperbolic speed, $\overline{V}_i = 1.6$. The curve in Fig. 12-11 is used for obtaining the extension of the undershoot boundaries for modulated $C_L / C_D$ from curves calculated for constant $C_L / C_D$. With a given $\overline{G}_{max}$ the improvement using modulated $C_L / C_D$ is insignificant in the range of $C_L / C_D$ less than about 0.5. At $C_L / C_D$ greater than about 1, the undershoot boundaries with modulated $C_L / C_D$ are considerably extended beyond those for constant $C_L / C_D$. Since a constant $C_D$ has been assumed and the abscissa is plotted in $\log_{10} F_p$, the corridor width is proportional to the horizontal spacing between the overshoot boundary and the undershoot boundary.

## References

1. Chapman, D. R., "An Analysis of the Corridor and Guidance Requirements for Supercircular Entry into Planetary Atmospheres," NASA Technical Report R-55, 1960.

2. Chapman, D. R., "An Approximate Analytical Method for Studying Entry into Planetary Atmospheres," NASA Technical Report R-11, 1959.

3. Lees, L., Hartwig, F. W., and Cohen, C. B., "The Use of Aerodynamic Lift During Entry Into the Earth's Atmosphere," STL Report GM-TR-0165-00519, 1958.

# Chapter 13

# Unified Theory for Entry into Planetary Atmospheres

## 13-1. INTRODUCTION

The classical theories for planar entry into planetary atmospheres have been presented in Chapters 6 through 12. Except for Loh's second-order theory which gives a high degree of accuracy, the application of all theories is severely restricted. Each theory is applicable to one particular type of entry trajectory because of the assumptions introduced to facilitate the integration of the equations of motion. Loh's theory itself is empirical. To alleviate this heuristic aspect, in Chapter 8 we offered a physical explanation to justify his theory.

This book is designed primarily as a textbook. However, it is also intended to present a complete account of the present state of the art of the problem of evaluating the performance of a lifting hypervelocity vehicle entering a planetary atmosphere along a three-dimensional path.

Up to this point, the first objective has been fulfilled. Entry theories have been presented with their appropriate simplifications to render explicit the dynamic characteristics of each type of entry trajectory. Simple but accurate first-order solutions have been obtained. They are of valuable assistance in analyzing the effect of the gravity force and the aerodynamic force, the two main forces considered in this volume, on the entry trajectories. Furthermore, the closed form solutions obtained lead to explicit forms for physical quantities of interest during entry, such as the deceleration and the heating rate. These data are of utmost importance for the preliminary design or mission planning of entry vehicles.

In the last quarter of this century, a new direction for space exploration is formulated. Frequent flights weekly or even daily to Earth orbit are planned. This introduces a new generation of space vehicles, a versatile lifting hypervelocity vehicle used both as a satellite and as a winged atmospheric vehicle with airplane aerodynamic maneuverability. This requires a unified theory for studying atmospheric entry, a theory that is applicable to all types of entry even with lift and bank modulation. The second objective of this book is the formulation of such a theory and the presentation of it in a complete

but readable form to assist engineers and scientists working on the space program in understanding the complexity associated with hypervelocity flight.

A unified theory that enables one to study the performance of a general type of lifting vehicle, regardless of its weight, shape and size, entering an arbitrary planetary atmosphere, would require a set of universal equations. In turn, this requires universal variables, free of the physical characteristics of the vehicle. In this respect, the best theory available is undoubtedly Chapman's theory for analysis of planetary entry (Ref. 1-2). Chapman's theory for planetary entry was presented in Chapters 11 and 12. Just as most other first-order theories, it is restricted to planar entries. This restriction is of minor inconvenience since it can be easily removed. A major deficiency in Chapman's theory is that, because of his two main assumptions, the equations are only approximate and the applications are restricted to entry trajectories with small flight path angles, or small lift-to-drag ratios.

In this chapter, Chapman's restrictive assumptions are removed and the results extended to three-dimensional entry trajectories, while all the distinctive features in Chapman's classical analysis are conserved. Furthermore, it will be shown that, from the exact equations, all the known first and second-order solutions can be obtained, thus displaying a certain universality for the present theory.

## 13-2. UNIVERSAL EQUATIONS FOR THREE-DIMENSIONAL ENTRY TRAJECTORIES

The equations of motion of a nonthrusting, lifting vehicle, entering a planetary atmosphere were derived in Chapter 2:

$$\begin{aligned}
\frac{dr}{dt} &= V \sin\gamma \\
\frac{d\theta}{dt} &= \frac{V \cos\gamma \cos\psi}{r \cos\phi} \\
\frac{d\phi}{dt} &= \frac{V \cos\gamma \sin\psi}{r} \\
\frac{dV}{dt} &= -\frac{\rho S C_D V^2}{2m} - g \sin\gamma \\
V\frac{d\gamma}{dt} &= \frac{\rho S C_L V^2}{2m} \cos\sigma - \left(g - \frac{V^2}{r}\right)\cos\gamma \\
V\frac{d\psi}{dt} &= \frac{\rho S C_L V^2}{2m\cos\gamma} \sin\sigma - \frac{V^2}{r}\cos\gamma\cos\psi\tan\phi
\end{aligned} \qquad (13\text{-}1)$$

The first three equations are simply the kinematic relations. The last three equations are the momentum equations. The planet and its atmosphere are assumed to be spherical and nonrotating. The

initial plane is taken as the reference plane which shall be referred to as the equatorial plane without loss of generality. The flight path angle $\gamma$ is measured positive upward from the local horizontal plane, and the heading angle $\psi$ is measured positive to the left of the initial trajectory in the direction of the North pole (Fig. 13-1). The bank angle $\sigma$ is taken such that, for positive $\sigma$, the vehicle is turning to the left. This angle is defined as the angle between the local vertical plane, the $(\vec{r}, \vec{V})$ plane, and the plane containing the aerodynamic force $\vec{A}$ and the velocity $\vec{V}$, the $(\vec{A}, \vec{V})$ plane.

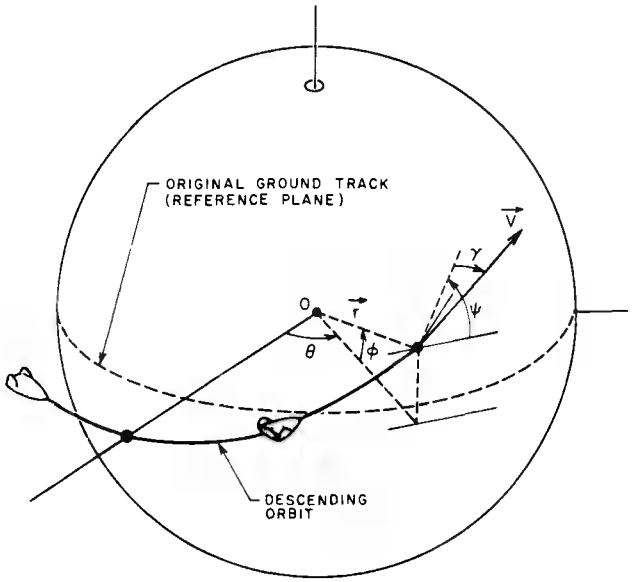


Fig. 13-1. Coordinate systems.

The gravitational field is taken to be a central, inverse square field, with the acceleration $g(r)$ given by

$$g(r) = \frac{\mu}{r^2} \tag{13-2}$$

where $\mu$ is the gravitational constant.

The atmospheric density, $\rho$, is a strong function of the altitude. It shall be assumed to be locally exponential in that it varies according to the differential law

$$\frac{d\rho}{\rho} = -\beta \, dr \tag{13-3}$$

where the local scale height, $1/\beta$, for any specified planetary atmosphere, is a function of the radial distance $r$.

In his classical paper (Ref. 1), Chapman introduced two dimensionless variables, $\bar{u}$ and $\bar{Z}$, defined as

$$\bar{u} \equiv \frac{V \cos\gamma}{\sqrt{gr}} \quad , \quad \bar{Z} \equiv \frac{\rho S C_D}{2m}\sqrt{\frac{r}{\beta}}\ \bar{u} \tag{13-4}$$

It has been found more convenient for the present theory to use the modified variables

$$u \equiv \frac{V^2\cos^2\gamma}{gr} \quad , \qquad Z \equiv \frac{\rho S C_D}{2m}\sqrt{\frac{r}{\beta}} \tag{13-5}$$

Chapman used the variable $\bar{u}$ as the independent variable. Under Chapman s assumption this variable is monotonically decreasing. It will be shown later that, at high altitude, $\bar{u}$ is purely periodic. To avoid this difficulty, in deriving the exact three-dimensional entry equations, we shall use the following dimensionless variable as the independent variable

$$s \equiv \int_0^t \frac{V}{r}\cos\gamma\, dt \tag{13-6}$$

This variable is strictly increasing as long as $\cos\gamma > 0$, a condition which is always satisfied for entry with constant lift and drag coefficients. With this independent variable Eqs. (13-1) become

$$\begin{aligned}
\frac{d\theta}{ds} &= \frac{\cos\psi}{\cos\phi} \\
\frac{d\phi}{ds} &= \sin\psi \\
\frac{dV^2}{ds} &= -\frac{r\rho S C_D V^2}{m\cos\gamma} - 2gr\tan\gamma \\
\frac{d\gamma}{ds} &= \frac{r\rho S C_L \cos\sigma}{2m\cos\gamma} + \left(1 - \frac{gr}{V^2}\right) \\
\frac{d\psi}{ds} &= \frac{r\rho S C_L \sin\sigma}{2m\cos^2\gamma} - \cos\psi\tan\phi
\end{aligned} \tag{13-7}$$

The differential relation between $r$ and $s$ is

$$\frac{dr}{ds} = r\tan\gamma \tag{13-8}$$

As in Chapman's theory, the variable $V^2$ is replaced by $u$, while the radial distance $r$, or equivalently the altitude, is replaced by the variable $Z$.

The derivative of $u$ with respect to $s$, with $u$ as defined in Eq. (13-5), is

$$\frac{du}{ds} = -\frac{2\sqrt{\beta r}\, Zu}{\cos\gamma}\left[1 + \frac{C_L}{C_D}\cos\sigma\tan\gamma + \frac{\sin\gamma}{2\sqrt{\beta r}\, Z}\right] \quad (13\text{-}9)$$

The derivative of $Z$ with respect to $s$, with the differential law for $\rho$, Eq. (13-3), is

$$\frac{dZ}{ds} = -\beta r\left(1 - \frac{1}{2\beta r} + \frac{1}{2\beta^2}\frac{d\beta}{dr}\right) Z\tan\gamma \quad (13\text{-}10)$$

Finally, the differential equations for $\gamma$ and $\psi$, written in terms of the dimensionless variables, are

$$\frac{d\gamma}{ds} = \frac{\sqrt{\beta r}\, Z}{\cos\gamma}\left[\frac{C_L}{C_D}\cos\sigma + \frac{\cos\gamma}{\sqrt{\beta r}\, Z}\left(1 - \frac{\cos^2\gamma}{u}\right)\right] \quad (13\text{-}11)$$

and

$$\frac{d\psi}{ds} = \frac{\sqrt{\beta r}\, Z}{\cos^2\gamma}\left[\frac{C_L}{C_D}\sin\sigma - \frac{\cos^2\gamma\cos\psi\tan\phi}{\sqrt{\beta r}\, Z}\right] \quad (13\text{-}12)$$

These dimensionless equations are exact. In particular, they reduce to the equations for Keplerian motion when $Z \to 0$.

In Eq. (13-10) for $Z$, if a strictly exponential atmosphere is used $\beta$ = constant, and $d\beta/dr = 0$. On the other hand, if an isothermal atmosphere is considered, $\beta/g$ = constant, and $(1/2\beta^2)(d\beta/dr) = -1/\beta r$. In both cases, in the equations of motion, the variables $\beta$ and $r$ enter as the product $\beta r$. For the Earth, for altitudes below 120 kilometers, the mean value is large. In this same region $\beta r$ varies from a low of about 750 to a high of about 1300. It is, however, a better assumption to use a mean value for $\beta r$ than simply to put $\beta$ constant and use the simple exponential atmosphere in the computation. This development will follow Chapman's lead and put $\beta r$ constant. Also, because of the large value for $\beta r$, the quantity inside the brackets in Eq. (13-10) is practically unity. This minor assumption concerning the product $\beta r$ does not alter the asymptotic behavior of the trajectory at very high altitudes where the equation in $Z$ becomes inoperative.

In summary, the equations of motion for three-dimensional entry trajectories are

$$\frac{dZ}{ds} = -\beta r\, Z \tan\gamma$$

$$\frac{du}{ds} = -\frac{2\sqrt{\beta r}\, Zu}{\cos\gamma}\left[1 + \lambda\tan\gamma + \frac{\sin\gamma}{2\sqrt{\beta r}\, Z}\right]$$

$$\frac{d\gamma}{ds} = \frac{\sqrt{\beta r}\, Z}{\cos\gamma}\left[\lambda + \frac{\cos\gamma}{\sqrt{\beta r}\, Z}\left(1 - \frac{\cos^2\gamma}{u}\right)\right]$$

$$\frac{d\theta}{ds} = \frac{\cos\psi}{\cos\phi}$$

$$\frac{d\phi}{ds} = \sin\psi$$

$$\frac{d\psi}{ds} = \frac{\sqrt{\beta r}\, Z}{\cos^2\gamma}\left[\delta - \frac{\cos^2\gamma\cos\psi\tan\phi}{\sqrt{\beta r}\, Z}\right] \qquad (13\text{-}13)$$

where

$$\lambda \equiv \frac{C_L}{C_D}\cos\sigma\,, \qquad \delta \equiv \frac{C_L}{C_D}\sin\sigma \qquad (13\text{-}14)$$

The equations (13-13) were first derived by Vinh and Brace (Ref. 3). In view of the definition (13-5) of $Z$, they are restricted to flight at constant lift-to-drag ratio, $C_L/C_D$ = constant, and for flight with a completely free modulation in the bank angle. Extension of these equations to the case of free modulation in the coefficients $C_D$ and $C_L$ and in the bank angle $\sigma$ for the study of three-dimensional optimal trajectories in atmospheric, hypervelocity flight has been obtained by Vinh, Busemann and Culp (Ref. 4).

The equations derived can be considered as the exact equations for entry into a planetary atmosphere. Just as Chapman's simplified equations, they are completely free of the characteristics of the vehicle. Hence, they can be used to analyze the motion of an arbitrary vehicle regardless of its weight, size and shape. The characteristics of the atmosphere enter the equations in the form of the parameter $\beta r$.

Once the atmosphere has been specified through $\beta r$, for any prescribed lift-to-drag ratio, $C_L/C_D$, and bank angle, $\sigma$, and with a prescribed set of initial conditions, the universal function $Z$ can be generated, and different physical quantities during entry can be evaluated and analyzed exactly as in Chapman's theory, described in Chapters 11 and 12. It may be thought at first glance that, to integrate Chapman's simplified equation, Eq. (11-16) of Chapter 11, only the product $\sqrt{\beta r}\,(C_L/C_D)$ need be prescribed and not $\beta r$ and $(C_L/C_D)$ separately. That is, Chapman's analysis appears to apply to any arbitrary atmosphere. But this is not rigorously true since in evaluating the flight path angle $\gamma$, using Chapman's first equation,

Eq. (11-12) of Chapter 11, the parameter $\sqrt{\beta r}$ needs to be prescribed. A normalizing technique to obtain a similarity solution for an arbitrary atmosphere requires sacrificing the accuracy in evaluating the universal $Z$ function and the flight path angle $\gamma$, and restricting the analysis to a small class of entry trajectories.

## 13-3. REDUCTION TO CLASSICAL SOLUTIONS

The equations derived are the universal equations in the sense of Chapman since they produce the universal $Z$ functions for analyzing the motion, deceleration and heating of an arbitrary vehicle. Furthermore, they are the exact equations for flight of a vehicle in a Newtonian gravitational field subject to aerodynamic force. In particular, they provide the Keplerian solution for flight in a vacuum and all other classical solutions when appropriate assumptions are introduced. These particuiar solutions can be obtained as follows.

### 13-3.1. Keplerian Solution

For flight in the vacuum, let $Z \to 0$. The first of Eqs. (13-13) is inoperative. It is replaced by Eq. (13-8). Using this equation to change the independent variable from $s$ to $r$, we rewrite the other Eqs. (13-13)

$$\frac{du}{dr} = -\frac{u}{r}$$

$$\frac{d\gamma}{dr} = \frac{1}{r \tan\gamma}\left(1 - \frac{\cos^2\gamma}{u}\right)$$

$$\frac{d\theta}{dr} = \frac{\cos\psi}{r \tan\gamma \cos\phi}$$

$$\frac{d\phi}{dr} = \frac{\sin\psi}{r \tan\gamma}$$

$$\frac{d\psi}{dr} = -\frac{\cos\psi \tan\phi}{r \tan\gamma} \qquad (13\text{-}15)$$

Integrating the first of these equations yields

$$u = \frac{p}{r} \qquad (13\text{-}16)$$

where $p$ is a constant of integration. Next, combining the first two equations to eliminate $r$ gives

$$\frac{d\gamma}{du} = -\frac{1}{u \tan\gamma}\left(1 - \frac{\cos^2\gamma}{u}\right) \qquad (13\text{-}17)$$

By the change of variable

$$\Gamma \equiv \frac{1}{\cos^2 \gamma} \tag{13-18}$$

this becomes the linear equation

$$\frac{d\Gamma}{du} + \frac{2}{u}\Gamma = \frac{2}{u^2} \tag{13-19}$$

which integrates to

$$\Gamma = \frac{2u + \text{constant}}{u^2}$$

For reasons that will be clear later this solution is written

$$\cos^2 \gamma = \frac{u^2}{2u - (1 - e^2)} \tag{13-20}$$

where $e$ is a constant of integration.

Combining the last two equations (13-15), we obtain

$$\frac{d\phi}{d\psi} = -\frac{\tan \psi}{\tan \phi} \tag{13-21}$$

The integration is immediate:

$$\cos \phi \cos \psi = \cos I \tag{13-22}$$

where $I$ is a new constant of integration.

The equation for $\theta$ can be written with $\psi$ as the independent variable.

$$\frac{d\theta}{d\psi} = -\frac{1}{\sin \phi} \tag{13-23}$$

Using the solution (13-22) for $\phi$ :

$$\frac{d\theta}{d\psi} = -\frac{\cos \psi}{\sqrt{\cos^2 \psi - \cos^2 I}} \tag{13-24}$$

The quadrature gives

$$\sin \psi = \sin I \cos (\theta - \Omega) \tag{13-25}$$

where $\Omega$ is another constant of integration.

Finally, we define a new variable $\alpha$ by the relation

$$\cos \alpha \equiv \cos \phi \cos (\theta - \Omega) \tag{13-26}$$

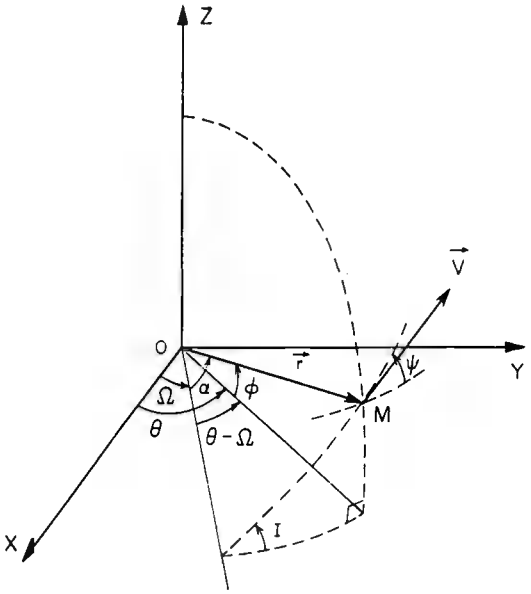


Fig. 13-2. The osculating plane and the orbital elements.

Figure 13-2 displays the geometric relationship among the angles $\theta$, $\phi$, $\psi$ and $I$, $\Omega$, $\alpha$. The angle $I$ is the inclination, and the angle $\Omega$ is the longitude of the ascending node. They are constants of the motion for a Keplerian orbit. The new variable $\alpha$, introduced to replace the angle $\theta$, is simply the polar angle, measured in the plane of motion from the line of the ascending node. From relations in spherical trigonometry we have also

$$\begin{aligned} \sin \phi &= \sin I \sin \alpha \\ \sin \psi &= \tan \phi \cot \alpha \\ \sin(\theta - \Omega) &= \tan \phi \cot I \end{aligned} \tag{13-27}$$

The derivative of Eq. (13-26) with respect to $r$, with Eqs. (13-15), (13-22), (13-25) and (13-27) used for simplification, results in

$$\frac{d\alpha}{dr} = \frac{1}{r \tan \gamma} \tag{13-28}$$

If $u$ is taken as the independent variable, and if the solution (13-20) is used to evaluate $\tan \gamma$ in terms of $u$, then .

$$\frac{d\alpha}{du} = - \frac{1}{\sqrt{- u^2 + 2u - (1 - e^2)}} \tag{13-29}$$

This integrates to

$$u = 1 + e \cos (\alpha - \omega) \tag{13-30}$$

where $\omega$ is the last constant of integration. It defines the argument of periapsis. From the solutions (13-16) and (13-30) we can identify $e$ as the eccentricity of the orbit and $p$ as the conic parameter.

For subsequent discussions, for Keplerian motion, we will take the plane of motion as the reference plane, with the reference direction along the pericenter. Then the equations of interest become

$$u = 1 + e \cos \theta = \frac{p}{r} \tag{13-31}$$

and

$$\cos^2 \gamma = \frac{u^2}{2u - (1 - e^2)} \tag{13-32}$$

We see that, outside the atmosphere, $u$ varies periodically between $u = 1 - e$ and $u = 1 + e$. Hence, for flight with atmospheric drag involving several passages through the atmosphere, the variable $u$, and hence Chapman's variable $\bar{u} \equiv u^{1/2}$, is oscillatory. It is, therefore, more convenient to replace it as independent variable by the dimensionless variable $s$ as defined by Eq. (13-6).

## 13-3.2. Chapman's Equations

In deriving his equations, Chapman introduced two basic assumptions as has been explained in Chapter 11.

a/ The percentage change in the radial distance is small compared to the percentage change in the horizontal component of the velocity.

$$\left| \frac{d(V \cos \gamma)}{V \cos \gamma} \right| >> \left| \frac{dr}{r} \right|$$

In terms of the variables $u$ and $Z$, this basic assumption is expressed as

$$\left| 1 + \frac{C_L}{C_D} \tan \gamma \right| >> \left| \frac{\sin \gamma}{\sqrt{\beta r}\, Z} \right| \tag{13-33}$$

b/ For lifting vehicles, the flight path angle $\gamma$ is sufficiently small that the lift component in the horizontal direction is small compared to the drag component in the same direction.

$$1 >> \left| \frac{C_L}{C_D} \tan \gamma \right| \tag{13-34}$$

Before we continue with the derivation of Chapman's equations from our formulation, the following remark is pertinent.

Most of the published analytical works on the theory concern planar entry. For nonplanar entry, as far as the altitude, speed and flight path angle are concerned, we only need to consider the first three of Eqs. (13-13). These equations govern the three-dimensional variation of $Z$, $u$, and $\gamma$, upon specification of the initial conditions for these variables, and the three-dimensional flight parameter $\lambda \equiv (C_L / C_D) \cos \sigma$. Hence, throughout the rest of this chapter, we shall consider only the three equations

$$\begin{aligned}
\frac{dZ}{ds} &= -\beta r \, Z \tan \gamma \\
\frac{du}{ds} &= -\frac{2\sqrt{\beta r}\, Zu}{\cos \gamma} \left(1 + \lambda \tan \gamma + \frac{\sin \gamma}{2\sqrt{\beta r}\, Z}\right) \\
\frac{d\gamma}{ds} &= \frac{\sqrt{\beta r}\, Z}{\cos \gamma} \left[\lambda + \frac{\cos \gamma}{\sqrt{\beta r}\, Z} \left(1 - \frac{\cos^2 \gamma}{u}\right)\right]
\end{aligned} \tag{13-35}$$

They are valid for three-dimensional entry at constant lift-to-drag ratio, and constant bank angle. For comparison with the classical solutions for planar entry we simply consider $\lambda$ as being $C_L / C_D$.

Now, applying Chapman's basic assumptions, Eqs. (13-33) and (13-34), to the equation for $u$, we have the reduced equation

$$\frac{du}{ds} = -\frac{2\sqrt{\beta r}\, Zu}{\cos \gamma} \tag{13-36}$$

These assumptions automatically restrict the validity of Chapman's theory to the portion of trajectory where $u$ is monotonically decreasing. Using this equation to change the independent variable from $s$ to $u$, we rewrite the equations for $Z$ and $\gamma$

$$\frac{dZ}{du} = \frac{\sqrt{\beta r} \sin \gamma}{2u} \tag{13-37}$$

and

$$\frac{d\gamma}{du} = -\frac{1}{2u} \left[\lambda + \frac{\cos \gamma}{\sqrt{\beta r}\, Z} \left(1 - \frac{\cos^2 \gamma}{u}\right)\right] \tag{13-38}$$

It is convenient for concordance to return to Chapman's original variables $\bar{u}$ and $\bar{Z}$ . From definitions (13-4) and (13-5),

$$u \equiv \bar{u}^2 \quad , \quad Z \equiv \frac{\bar{Z}}{\bar{u}} \tag{13-39}$$

Hence, in terms of Chapman's variables, Eqs. (13-37) and (13-38) become

$$\frac{d\bar{Z}}{d\bar{u}} - \frac{\bar{Z}}{\bar{u}} = \sqrt{\beta r} \sin\gamma \tag{13-40}$$

and

$$\frac{d\gamma}{d\bar{u}} = -\frac{1}{\bar{u}}\left[\lambda + \frac{\bar{u}\cos\gamma}{\sqrt{\beta r}\,\bar{Z}}\left(1 - \frac{\cos^2\gamma}{\bar{u}^2}\right)\right] \tag{13-41}$$

Equation (13-40) is Chapman's first equation. It is used to evaluate the flight path angle. If we take the derivative of this equation with respect to $\bar{u}$ , using Eq. (13-41), we have

$$\bar{u}\,\frac{d}{d\bar{u}}\left(\frac{d\bar{Z}}{d\bar{u}} - \frac{\bar{Z}}{\bar{u}}\right) + \frac{\cos^2\gamma(\bar{u}^2 - \cos^2\gamma)}{\bar{Z}\,\bar{u}} + \sqrt{\beta r}\,\lambda\cos\gamma = 0 \tag{13-42}$$

This equation is equivalent to Chapman's second-order nonlinear differential equation with $\bar{Z}$ as the dependent variable and $\bar{u}$ as the independent variable. To obtain the equation in the form identical to the one given by Chapman in his classical paper (Ref. 1), we write it as

$$\bar{u}\,\frac{d^2\bar{Z}}{d\bar{u}^2} - \left(\frac{d\bar{Z}}{d\bar{u}} - \frac{\bar{Z}}{\bar{u}}\right) - \frac{(1-\bar{u}^2)\cos^4\gamma}{\bar{Z}\,\bar{u}} + \sqrt{\beta r}\,\lambda\cos^3\gamma + \frac{\bar{u}\cos^2\gamma\sin^2\gamma}{\bar{Z}} + \sqrt{\beta r}\,\lambda\cos\gamma\sin^2\gamma = 0 \tag{13-43}$$

With the aid of Eq. (13-40), we consider the sum of the terms

$$-\left(\frac{d\bar{Z}}{d\bar{u}} - \frac{\bar{Z}}{\bar{u}}\right) + \frac{\bar{u}\cos^2\gamma\sin^2\gamma}{\bar{Z}} + \sqrt{\beta r}\,\lambda\cos\gamma\sin^2\gamma$$

$$= -\sqrt{\beta r}\sin\gamma\left[1 - \lambda\cos^2\gamma\tan\gamma - \frac{\bar{u}\cos^2\gamma\sin\gamma}{\sqrt{\beta r}\,\bar{Z}}\right]$$

$$\approx \sqrt{\beta r}\sin\gamma$$

The last step is obtained by applying Chapman's basic assumptions, Eqs. (13-33) and (13-34). We see that this is equivalent to neglecting the terms containing $\sin^2 \gamma$ in Eq. (13-43). Thus,

$$\bar{u} \frac{d^2\bar{Z}}{d\bar{u}^2} - \left(\frac{d\bar{Z}}{d\bar{u}} - \frac{\bar{Z}}{\bar{u}}\right) = \frac{1 - \bar{u}^2}{\bar{Z}\,\bar{u}} \cos^4\gamma - \sqrt{\beta r}\ \lambda \cos^3\gamma \tag{13-44}$$

Chapman derived this same equation for planar entry by repeatedly applying his two basic assumptions.

### 13-3.3. Yaroshevskii's Equation

Yaroshevskii's theory, (Ref. 5), is closely related to Chapman's theory. It can be shown that, for constant lift-to-drag ratio entry, Yaroshevskii's second-order nonlinear differential equation is a special case of Chapman's equation.

Yaroshevskii used an independent variable, $x$, and a dependent variable, $y$, defined as

$$x \equiv \log \frac{\sqrt{g_o r_o}}{V}, \qquad y \equiv \frac{SC_D}{2m}\sqrt{\frac{r_o}{\beta}}\ \rho \tag{13-45}$$

where the subscript zero denotes the condition at a reference level.

In the more sophisticated definition of Chapman's variables, Eq. (13-4), if we use a constant value for $r$, and the assumption of a very small flight path angle, $\cos\gamma \approx 1$, we have

$$\bar{u} = \frac{V}{\sqrt{g_o r_o}}, \qquad \bar{Z} = \frac{SC_D\rho}{2m}\sqrt{\frac{r_o}{\beta}}\,\bar{u} \tag{13-46}$$

Hence, we have the relations between the two sets of variables

$$\frac{\bar{Z}}{\bar{u}} = y, \qquad \bar{u} = e^{-x} \tag{13-47}$$

The corresponding relation in the derivatives is

$$\frac{d}{d\bar{u}}(\ ) = -e^{x}\frac{d}{dx}(\ ) = -\frac{1}{\bar{u}}\frac{d}{dx}(\ ) \tag{13-48}$$

On the other hand, for very small flight path angles, Chapman's equation, Eq. (13-44), is reduced to

$$\bar{u}\frac{d}{d\bar{u}}\left(\frac{d\bar{Z}}{d\bar{u}} - \frac{\bar{Z}}{\bar{u}}\right) - \frac{1 - \bar{u}^2}{\bar{Z}\,\bar{u}} + \sqrt{\beta r_o}\ \lambda = 0 \tag{13-49}$$

Using the transformations (13-47) and (13-48) in this equation, we have Yaroshevskii's equation

$$\frac{d^2y}{dx^2} + \frac{1 - e^{2x}}{y} + \sqrt{\beta r_o}\ \lambda = 0 \qquad (13\text{-}50)$$

13-3.4. Loh's Second-Order Solution

There exist several first-order solutions. The assumptions introduced concern the equation for $\gamma$, the third of the basic Eqs. (13-35). We write it as

$$\frac{d\gamma}{ds} = \frac{\sqrt{\beta r}\ Z}{\cos\gamma}\ (\lambda + G) \qquad (13\text{-}51)$$

where

$$G \equiv \frac{\cos\gamma}{\sqrt{\beta r}\ Z}\left[\ 1 - \frac{\cos^2\gamma}{u}\ \right] \qquad (13\text{-}52)$$

represents the combined gravity and centrifugal acceleration along the normal to the flight path.

For skip trajectories, Eggers, Allen and Neice neglect the G term compared to the lift $\lambda$, (Ref. 6). For equilibrium glide with nearly zero flight path angle, the correct assumption by Sänger yields $\lambda + G \approx 0$ (Ref. 7). This leads Loh to conjecture, based on extensive numerical analysis, that the G term is nearly constant during the integration (Ref. 8).

The equations for $\gamma$ and $u$, written with $Z$ as the independent variable, are

$$\frac{d\gamma}{dZ} = -\frac{(\lambda + G)}{\sqrt{\beta r}\ \sin\gamma} \qquad (13\text{-}53)$$

and

$$\frac{du}{dZ} = \frac{2u}{\sqrt{\beta r}\ \sin\gamma}\ (1 + \lambda\ \tan\gamma + \frac{\sin\gamma}{2\sqrt{\beta r}\ Z}) \qquad (13\text{-}54)$$

With Loh's assumption of constant G, the integration of Eq. (13-53) is immediate. We have

$$\cos\gamma - \cos\gamma_i = \frac{(\lambda + G)}{\sqrt{\beta r}}\ (Z - Z_i) \qquad (13\text{-}55)$$

where subscript i denotes the initial condition. To assess the effect of each of the entry variables, in the final equation, Eq. (13-55), G is to be replaced by its definition, Eq. (13-52).

Equation (13-54) for $u$ has a singularity for $Z = 0$. To avoid this difficulty, we rewrite it as

$$\frac{d}{dZ}\left[\log u - \frac{1}{\beta r}\log Z\right] = \frac{2}{\sqrt{\beta r}\sin\gamma}(1 + \lambda\tan\gamma) \qquad (13\text{-}56)$$

Dividing this equation by Eq. (13-53), we have

$$\frac{(\lambda + G)}{2}\frac{d}{d\gamma}\left[\log u - \frac{1}{\beta r}\log Z\right] = -(1 + \lambda\tan\gamma) \qquad (13\text{-}57)$$

Integrating and using the initial conditions, we have

$$\gamma - \gamma_i = \lambda\log\frac{\cos\gamma}{\cos\gamma_i} - \frac{(\lambda + G)}{2}\log\frac{u}{u_i} + \frac{(\lambda + G)}{2\beta r}\log\frac{Z}{Z_i} \qquad (13\text{-}58)$$

Equations (13-55) and (13-58), derived with the present dimensionless variables, constitute what Loh has called the unified solution of entry dynamics (Ref. 8). The last term in Eq. (13-58) is the higher-order effect term. It has been given only in approximate form by Loh. Furthermore, the equations used in Loh's analysis assume constant gravity. Neglecting the last term in Eq. (13-58) we have Loh's second-order solution.

$$\gamma - \gamma_i = \lambda\log\frac{\cos\gamma}{\cos\gamma_i} - \frac{(\lambda + G)}{2}\log\frac{u}{u_i} \qquad (13\text{-}59)$$

For ballistic entry, $\lambda = 0$. Thus, to the first order, by neglecting the gravity and centrifugal force, we have from this equation $\gamma \approx \gamma_i$. Keeping the $G$ term, we combine this equation with Eq. (13-55) to obtain

$$\frac{(Z - Z_i)}{\sqrt{\beta r}}\Big/\log\frac{u}{u_i} = -\frac{\cos\gamma - \cos\gamma_i}{2(\gamma - \gamma_i)} \approx \frac{\sin\gamma_i}{2}$$

The last simplifying step has been shown in Section 8-4.1. This gives the classical first-order solution for ballistic entry (Refs. 1, 9)

$$Z_I = Z_i + \frac{\sqrt{\beta r}}{2}\sin\gamma_i\log\frac{u}{u_i} \qquad (13\text{-}60)$$

For gliding entry the flight path angle is small and nearly constant and hence $\lambda + G \approx 0$, $\cos\gamma \approx 1$. Thus, from the definition (13-52) of $G$,

$$Z_{II} = \frac{1 - u}{\sqrt{\beta r}\ \lambda u} \qquad (13\text{-}61)$$

This is the first-order solution originally derived by Sänger (Ref. 7). For skip entry, $G \approx 0$, and Eq. (13-59) is reduced to

$$\frac{u^{1/2}}{\cos\gamma} = \frac{u_i^{1/2}}{\cos\gamma_i} \exp\left(\frac{\gamma_i - \gamma}{\lambda}\right) \tag{13-62}$$

while, from Eq. (13-55), we have the solution for $Z$

$$Z_{III} = Z_i + \frac{\sqrt{\beta r}\ (\cos\gamma - \cos\gamma_i)}{\lambda} \tag{13-63}$$

For small flight path angles the equations become

$$\gamma_i - \gamma = \frac{\lambda}{2} \log \frac{u}{u_i} \tag{13-64}$$

and

$$Z_{III} = Z_i + \frac{\sqrt{\beta r}}{2\lambda} (\gamma_i^2 - \gamma^2) \tag{13-65}$$

Using Eq. (13-64) we can rewrite this solution

$$Z_{III} = Z_i + \frac{\sqrt{\beta r}}{2} \gamma_i \log \frac{u}{u_i} - \frac{\sqrt{\beta r}}{8} \lambda \log^2 \frac{u}{u_i} \tag{13-66}$$

This is the solution for skip trajectories obtained by Chapman (Ref. 1).

The analysis in this section has shown that all the known first-order and second-order solutions for entry dynamics can be obtained from the present formulation including the exact limiting case for orbital flight outside the atmosphere. Another second-order theory can be constructed by matching the Keplerian solution with one of the first-order solutions as has been done by Shi and Pottsepp for planar trajectories (Ref. 10). Such a matched asymptotic solution for three-dimensional entry trajectories using the present formulation will be presented in Chapter 14.

## 13-4. NUMERICAL RESULTS

One outstanding feature of Chapman's approach is the construction of the $\bar{Z}$ - Tables for atmospheric entry (Ref. 11). For each initial speed $u_i$, entry angle $\gamma_i$ and lift-to-drag ratio $C_L / C_D$, these tables give the correspondence among the variables $\gamma$, $u$ and $\bar{Z}$ during entry. From these we can calculate other physical quantities of interest. The tabulation is valid for any entry vehicle. The only difference is the actual altitude which also can be calculated for any specified drag parameter $SC_D / m$.

But there are restrictions to the use of Chapman's tables due to his two basic assumptions. In the present analysis, we have removed these two restrictive assumptions and the basic equations (13-35) can be integrated using the same entry data $u_i$, $\gamma_i$ and $(C_L / C_D) \cos\sigma$ to generate more accurate tables. One additional benefit is that the data obtained are also valid for three-dimensional entry at constant lift-to-drag ratio and bank angle since they are tabulated in terms of the flight parameter $\lambda = (C_L / C_D) \cos\sigma$. Several $\bar{Z}$ functions, using the exact equations, have been computed by Brace (Ref. 12). Some selected trajectories are reproduced here and compared with Chapman's computed $\bar{Z}$ functions. They are chosen to display the quantitative aspect of Chapman's assumptions.

In order to meaningfully compare Chapman's original results with the results of the numerical integration of the exact equations the same value $\beta r = 900$ has been used. Furthermore, the same integration program and the same method for selecting the initial value $\bar{Z}_i$ have been used. The results for $Z$ and $u$ are converted into $\bar{Z}$, $\bar{u}$, through Eq. (13-39), and the diagrams are presented in terms of the deceleration $\sqrt{\beta r}\ \bar{Z}\ \bar{u}$ versus $\bar{u}$ as in Chapman's Ref. 1 for easy comparison.

Chapman's basic assumptions concern the coefficient $A$, the quantity in parentheses in Eq. (13-35) for $u$.

$$A = 1 + A_1 + A_2 \tag{13-67}$$

where

$$A_1 \equiv \lambda \tan\gamma \tag{13-68}$$

$$A_2 \equiv \frac{\bar{u} \sin\gamma}{2\sqrt{\beta r}\ \bar{Z}} \tag{13-69}$$

As has been shown in Eqs. (13-35) and (13-36), Chapman's assumptions consist of taking $A = 1$. Hence, Chapman's theory is accurate whenever $|A_1| << 1$ and $|A_2| << 1$, or more generally whenever $|A_1 + A_2| << 1$. It is therefore informative, for each comparison, to also plot the functions $A_1$, $A_2$ and $A$. In every case, the results of the numerical integration support the hypotheses regarding the accuracy of Chapman's solution. Along trajectories where $A_1$ and $A_2$ remain reasonably close to zero, Chapman's solution follows the exact solution. Along trajectories where $A$ is either discontinuous or does not remain close to unity, there are discrepancies between Chapman's theory and the present exact theory.

The best agreement between the exact analysis and Chapman's results is evidenced in the case of steep angle ballistic entry as shown in Fig. 13-3. $A_1$ is identically zero since $C_L = 0$, and $A_2$ remains close to zero over most of the trajectory. This can be predicted by inspection of Eq. (13-69). For steep ballistic entry, $\sin\gamma$ is nearly constant while $\sqrt{\beta r}\ \bar{Z}/\bar{u}$, which is proportional to $\rho$, quickly becomes finite and large. This leads to near zero value for $A_2$.

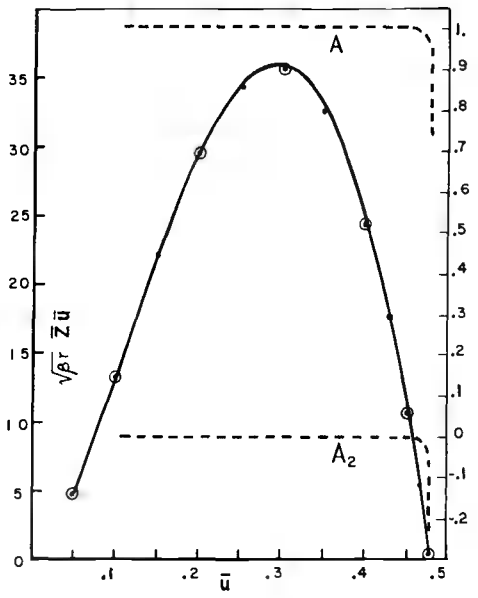


Fig. 13-3. $\sqrt{\beta r}\ \bar{Z}\ \bar{u}$ versus $\bar{u}$ for steep angle ballistic entry
$\lambda = 0$ , $\bar{V}_i = 1.4$ , $\gamma_i = -70^o$ , $\bar{u}_i = 0.478$, $\bar{Z}_i = 0.02819$
O - Chapman's results. —— Exact equations.

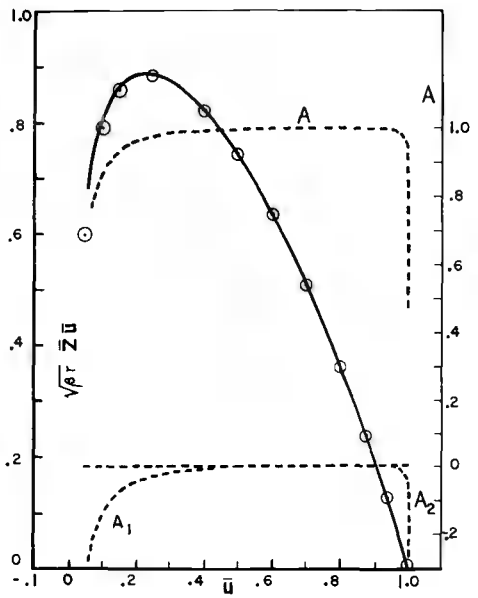


Fig. 13-4. $\sqrt{\beta r}\ \bar{Z}\ \bar{u}$ versus $\bar{u}$ for equilibrium glide entry
$\lambda = 1$ , $\bar{V}_i = 1$ , $\gamma_i = -0.13^o$ , $\bar{u}_i = 0.999$ , $\bar{Z}_i = 0.00007$
O - Chapman's results. —— Exact equations.

Figure 13-4 presents another favorable case for Chapman's theory, namely the equilibrium glide entry. Although $\lambda = 1$, $A_1 = \lambda \tan\gamma$ remains small for equilibrium glide along most of the trajectory except at lower altitude when $\gamma$ becomes large. On the other hand, although $A_2$, as given by Eq. (13-69) is negatively large at high altitude, as for all entry trajectories from high altitude where $\bar{Z} \approx 0$, as soon as the vehicle reaches the denser layer of the atmosphere $\sqrt{\beta r}\,\bar{Z}/\bar{u}$ again becomes finite and large so that $A_2$ tends to zero. It is seen from Fig. 13-4 that whenever A remains close to unity, Chapman's result is accurate.

Figure 13-5 presents a trajectory where the basic assumptions of Chapman may be valid but his selection of the variable $\bar{u}$ as independent variable renders his results inaccurate. This is a case of ballistic entry, hence $A_1$ is identically zero. But at parabolic speed $\bar{V}_i = 1.4$, and with a shallow entry, $\gamma_i = -3.75^\circ$, the trajectory is an overshoot trajectory. The trajectory makes a pass through the atmosphere, returns to a Keplerian orbit at $\bar{u} = 0.98$, and the entry is completed during the next passage. In the vicinity of $\bar{u} = 0.98$ not only is A not near unity, but A is discontinuous and reaches large negative values. Although not shown on the graphs, exact values of $\bar{u}$ produced by numerical integration using $\bar{s}$ as the independent variable show an oscillation in the variable $\bar{u}$ as predicted by the present theory. The result is a large discrepancy between the exact theory and Chapman's theory as can be seen in Fig. 13-5. From the figure, it should not be inferred that Chapman's result becomes accurate again at lower speed. The fact that the ordinate is $\sqrt{\beta r}\,\bar{Z}\,\bar{u}$, automatically sends both the exact solution and Chapman's solution to zero as $\bar{u}$ tends to zero.

Finally, the entry trajectory presented in Fig. 13-6 is a clearly unfavorable case for applying Chapman's theory. This is the case of a grazing circular entry, $\bar{V}_i = 1$, $\gamma_i = -0.2^\circ$, but with high negative lift, $\lambda = -4$. With high negative lift, the vehicle will dive steeper and steeper and the flight path angle will quickly reach large negative values. From Eqs. (13-67) - (13-69), it is seen that although $A_2$ tends to zero, $A_1$ will increase indefinitely providing values for A much larger than unity as shown in Fig. 13-6.

Although Chapman's theory was never designed to be used in the high-lift entry case, the $\bar{Z}$ Tables (Ref. 11) contain many such cases. Therefore, with the advent of a new generation of entry vehicles having high lift capability, the need for a revised set of data obtained by using the exact equations is clearly indicated.

## 13-5. THE ENTRY CORRIDOR

Chapman's theory of the entry corridor has been presented in detail in the previous chapter. Whenever his two basic assumptions are valid, the results are accurate. In any case, the basic conception, through the use of the periapsis parameter $F_p$, is an outstanding conception and should be retained for any future, more accurate analysis. The notion of the periapsis parameter is closely related to the

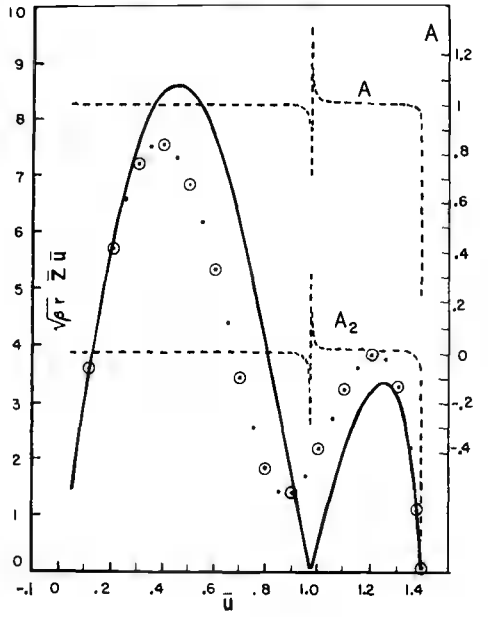


Fig. 13-5. $\sqrt{\beta r}\ \bar{Z}\ \bar{u}$ versus $\bar{u}$ for shallow angle ballistic entry.
$\lambda = 0$ , $\bar{V}_i = 1.4$ , $\gamma_i = -3.75^\circ$ , $\bar{u}_i = 1.396$ , $\bar{Z}_i = 0.00196$
O - Chapman's results. —— Exact equations.

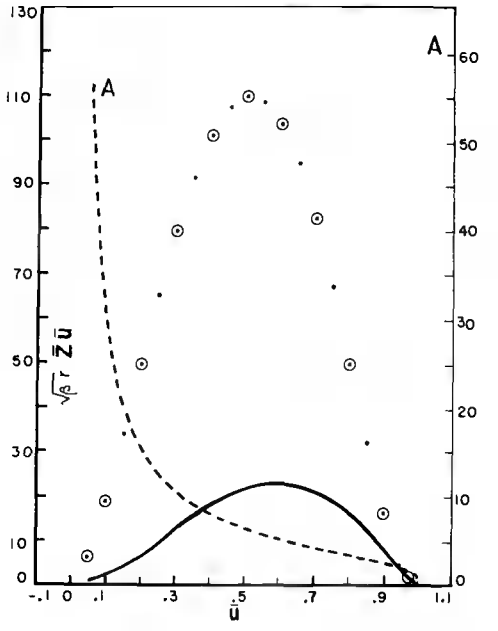


Fig. 13-6. $\sqrt{\beta r}\ \bar{Z}\ \bar{u}$ versus $\bar{u}$ for negative lift entry
$\lambda = -4$ , $\bar{V}_i = 1$ , $\gamma_i = -0.2^\circ$ , $\bar{u}_i = 0.999$, $\bar{Z}_i = 0.00016$
O - Chapman's results. —— Exact equations.

definition of the entry altitude which, in turn, is the basis for the computation of the overshoot and undershoot boundaries. These notions are revised in this section, in light of the exact equations as a tool for computing accurate entry trajectories.

### 13-5.1. Definition of the Entry Point

To some extent, any definition of an entry point is arbitrary, since from a strictly mathematical standpoint, the process of changing from a Keplerian orbit to an atmospheric flight orbit is a continuously varying process.

For the numerical integration of his equation, Chapman chose the starting value of $\gamma$ as the initial value of $\gamma$, and the starting value of $u$ for the first point as $0.995\, u_i$. Then, since the equation has a singularity at $Z = 0$, the starting value of $Z$ is obtained by an approximate method. This choice of the starting value of $u$ clearly assumes that $u$ is decreasing at the entry point. If we are interested in effective entry trajectories, along which the heating rate and the deceleration build up, then we can use Chapman's definition of an entry point as the point where $u$ starts to decrease. In this case, the initial value of $Z$ can be obtained from the equation

$$A = 1 + \lambda \tan \gamma_i + \frac{\sin \gamma_i}{2\sqrt{\beta r}\, Z_i} = 0 \qquad (13\text{-}70)$$

since with this value $du/ds = 0$.

If a broader class of trajectories is considered, especially trajectories with several passages through the atmosphere, then it is natural to consider the point where atmospheric flight is initiated as the point where the acceleration caused by the aerodynamic force has reached a selected small fraction, $f$, of the local gravity force. The expression for the acceleration due to aerodynamic force is

$$\bar{a} = \frac{a}{g} = \frac{\sqrt{\beta r}\, Z\, u}{\cos^2 \gamma} \sqrt{1 + (C_L / C_D)^2} \qquad (13\text{-}71)$$

Hence, for a given $u_i$ and $\gamma_i$, $Z_i$ is obtained from

$$\frac{a_i}{g_i} = \frac{\sqrt{\beta r}\, Z_i\, u_i}{\cos^2 \gamma_i} \sqrt{1 + (C_L / C_D)^2} = f \qquad (13\text{-}72)$$

The manner in which $f$ is chosen determines the accuracy with which the atmospheric portion of a trajectory may be interfaced with the Keplerian portion. As $f$ becomes smaller, the entry point moves backward along the trajectory, and the two portions of the trajectory are more accurately matched. However, a too small value of $f$

renders the entry portion too long and the tabulation of the numerical results unnecessarily cumbersome. A reasonable range for $f$ is from 0.005 to 0.05 . With regard to the tabulation of noncoplanar trajectories, since we specify $\lambda \equiv (C_L / C_D) \cos\sigma$ for economy of parameters, the definition (13-72) of the entry point, with $C_L / C_D$ replaced by $\lambda$ can still be used without interfering with the accuracy if a small enough value of $f$ is selected.

## 13-5.2. Trajectories With Several Passes

For this discussion, we adopt the definition of the entry point using Eq. (13-72). Numerical results presented here were obtained with the value $f = 0.05$ . We first consider the case where there is no interference with atmospheric force. The trajectory is Keplerian and the relation between the variables $u$ and $\gamma$ is given by Eq. (13-20) reproduced here for convenience

$$\cos^2\gamma = \frac{u^2}{2u - (1 - e^2)} \tag{13-73}$$

The constant $e$ is the eccentricity of the orbit. As discussed in Chapter 12 and shown in Fig. 12-1, this element, even for a reentry trajectory can be calculated by taking a point on the orbit at very high altitude where the motion is still Keplerian. With a known value of $e$, we can plot the Keplerian trajectory, Eq. (13-73), using a polar coordinate system $(u , \gamma)$ as shown in Fig. 13-7. In this $(u , \gamma)$ plane, the polar angle $\gamma$ is negative in the clock-wise direction. If there is no entry, the Keplerian trajectory is a closed curve symmetric with respect to the $\gamma = 0$ axis. In the case where the trajectory intersects the atmosphere, the Keplerian trajectory will be perturbed starting from a certain point $i_1$ representing the initial point for the first atmospheric passage (Fig. 13-7) . To calculate this point, we first notice that, following the Keplerian trajectory to a distance $r_i$ where a sensible atmosphere is likely to be present, the initial value $u_i = V_i^2 / g_i r_i$ (Fig. 12-1) can be evaluated accurately. Then, with this value of $u_i$ , Eq. (13-72) with $f = 0.05$ , and Eq. (13-73) with subscript $i$ can be solved for the remaining initial values $\gamma_i$ and $Z_i$ . The integration of the exact equations (13-35) can be started. If the trajectory leads to an exit into the vacuum, the deceleration as given in Eq. (13-71) will first increase from the value $f$ and then decrease to return to this same value. This portion of the "atmospheric fly through" is shown in Fig. 13-7 from the initial point $i_1$ to the exit point $e_1$ . Let $u_1$ , $\gamma_1$ and $Z_1$ be the values of the variables at the first exit. From this point on the trajectory is again Keplerian. The next return to the atmosphere occurs at the point $i_2$ where by spherical symmetry, we have the value $u_1$ , $-\gamma_1$ and $Z_1$ to start again the integration of the equations for atmospheric flight.

If the integration of the second atmospheric portion of the trajectory leads again to an exit point $e_2$ , the conditions for the third entry point $i_3$ are calculated in the same manner from the condition at the last exit point. The above procedure is repeated until final entry is effected.

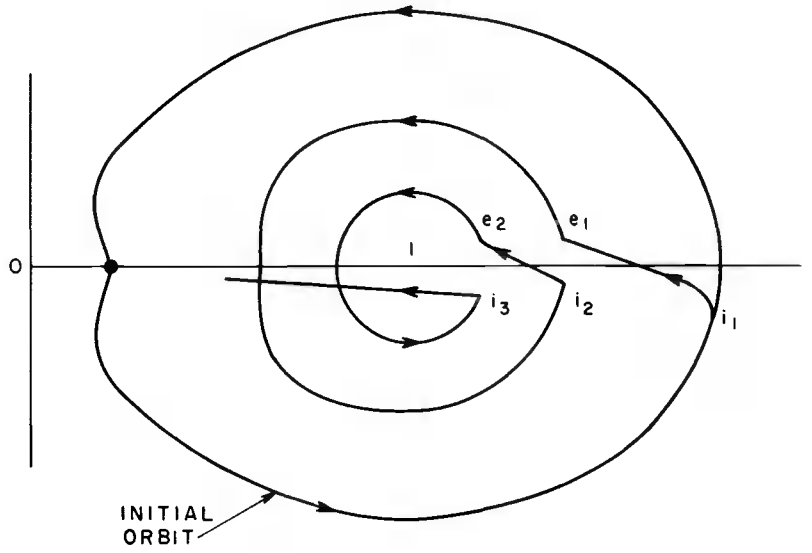


Fig. 13-7. Representation in the $(u, \gamma)$ plane of an entry trajectory with several passes.

13-5.3. Chapman's Periapsis Parameter, $F_p$

It has been shown in Chapter 12 that Chapman's periapsis parameter is used to define the entry condition.

He defined the periapsis parameter as

$$F_p \equiv \frac{\rho_p S C_D}{2m} \sqrt{\frac{r_p}{\beta}} \tag{13-74}$$

where $r_p$ is the hypothetical periapsis distance and $\rho_p$ is the atmospheric density evaluated at this periapsis altitude. For a very small entry angle $\gamma_i$, and for a supercircular speed $\overline{V}_i = V_i / \sqrt{g_i r_i} > 1.05$ an approximate relation between $\gamma_i$ and $F_p$ has been given by Chapman as

$$F_p \approx \frac{\overline{Z}_i}{\overline{V}_i} \exp\left[\frac{\overline{V}_i^2 (\sqrt{\beta_i r_i}\ \gamma_i)^2}{2(\overline{V}_i^2 - 1)}\right] \tag{13-75}$$

Hence $F_p$ can be used as an alternate parameter replacing $\gamma_i$. Before deriving a more accurate formula for $F_p$ for use in this chapter, we notice that, by the definition (13-5) of our $Z$ variable, we have $F_p = Z_p$. Hence, from now on, we shall use the notation $Z_p$ to replace $F_p$ to designate the periapsis parameter.

For an atmosphere which is essentially exponential between the initial entry point and the conic periapsis, we have

$$\frac{Z_p}{Z_i} = \sqrt{\frac{r_p}{r_i}}\, e^{-\beta (r_p - r_i)} \tag{13-76}$$

Now, if the value f in Eq. (13-72) is selected small enough, the entry point can be considered as a point on the initial Keplerian orbit (Fig. 13-7). Hence, Eqs. (13-31) and (13-32) apply. We have by evaluating the constant p and e at the entry point and hypothetical periapsis

$$\frac{r_p}{r_i} = \frac{u_i}{u_p} \tag{13-77}$$

and

$$\frac{u_i^2}{\cos^2 \gamma_i} - 2u_i = u_p^2 - 2u_p \tag{13-78}$$

Using Eq. (13-77) in Eq. (13-76), we obtain the expression for the periapsis parameter in terms of $Z_i$ and the ratio $u_i / u_p$.

$$Z_p = Z_i \sqrt{\frac{u_i}{u_p}}\, e^{\beta r_i (1 - \frac{u_i}{u_p})} \tag{13-79}$$

There are many possible computing schemes using the formulas just derived. For computation and tabulation of accurate Z functions we can follow Chapman using $\bar{V}_i$, $\gamma_i$ and $(C_L / C_D)$ as entry data, and $Z_p$ as an auxiliary parameter. For uniformity, a single value of f, say f = 0.05, is selected. Then, we have $u_i = \bar{V}_i^2 \cos^2 \gamma_i$. Then $u_p$ is obtained from Eq. (13-78), $Z_i$ from Eq. (13-72), and finally $Z_p$ from Eq. (13-79). The integration of the equations starts from the values $u_i$, $\gamma_i$ and $Z_i$. For tabulation we can use either the modified $(\bar{Z}, u)$ functions, or the original Chapman variables $(\bar{Z}, \bar{u})$.

In practical application, for a given vehicle with a prescribed drag parameter, approaching a planetary atmosphere, sometimes it is difficult to obtain an accurate evaluation of the entry angle $\gamma_i$, as has been pointed out by Chapman. In this case, since the Keplerian approach orbit is known, its drag-free periapsis distance $r_p$ can be easily evaluated. Hence, if the atmosphere is known, we also have $\rho_p$. For a prescribed drag parameter, $F_p$ is evaluated from Eq. (13-74). The entry speed $\bar{V}_i$ can be accurately evaluated from elements of the Keplerian orbit using a distance $r_i$ representing the radius of the atmosphere. This is because $\bar{V}_i$ is not as sensitive to variation of $r_i$ as is $\gamma_i$. Since the Z Tables have $\bar{V}_i$ and $Z_p$ as entry data, together with $C_L / C_D$, the entry trajectory can be identified.

Finally, Chapman used Eq. (13-75) to obtain an explicit formula for $\gamma_i$ in terms of $F_p$, $\bar{Z}_i$ and $\bar{V}_i$. Written in terms of $Z_p$, $Z_i$ and $\bar{V}_i$ this is

$$\beta r \gamma_i^2 = \frac{2(\bar{V}_i^2 - 1)}{\bar{V}_i^2} \log \left( \frac{Z_p}{Z_i} \right) \tag{13-80}$$

The use of this explicit formula is restricted to very small angles $\gamma_i$ and $\overline{V}_i > 1.05$. An informative derivation of an improved formula for $\gamma_i$ is as follows.

Let

$$y \equiv \frac{Z_p}{Z_i} , \quad x \equiv \frac{u_i}{u_p} \tag{13-81}$$

From Eq. (13-77) it may be seen that $(1 - x)$ is a very small positive quantity. Thus, Eq. (13-79), which is

$$y = x^{1/2} e^{\beta r(1-x)} \tag{13-82}$$

or

$$\log y = \frac{1}{2} \log x + \beta r(1 - x) \tag{13-83}$$

may be expanded for $x$ near unity as

$$\log x = \frac{x-1}{x} + \frac{1}{2}\left(\frac{x-1}{x}\right)^2 + \ldots$$

Thus,

$$\log y = (1 - x)\left[\beta r - \frac{1}{2x} + \frac{(1-x)}{4x^2} - \ldots\right] , \quad x \approx 1$$

That is, for large value of $\beta r$

$$1 - x = \frac{1}{\beta r} \log \left(\frac{Z_p}{Z_i}\right) \tag{13-84}$$

Now, since $u_p = u_i/x$, Eq. (13-78) becomes

$$u_i = \frac{2x(1-x)\cos^2\gamma_i}{\cos^2\gamma_i - x^2} = \overline{V}_i^2 \cos^2\gamma_i \tag{13-85}$$

Hence, solving for $\sin^2\gamma_i$ in terms of $x$ and $\overline{V}_i^2$

$$\sin^2\gamma_i = \frac{(1-x)[(1+x)\overline{V}_i^2 - 2x]}{\overline{V}_i^2} \tag{13-86}$$

where $x$ is given by (13-84). This formula may be written as

$$\beta r \sin^2 \gamma_i = \frac{1}{\bar{V}_i^2} [ (1+x) \bar{V}_i^2 - 2x ] \log \left( \frac{Z_p}{Z_i} \right) \quad (13\text{-}87)$$

Now it is apparent that if $x$ inside the square brackets is approximated by unity, Chapman's formula (13-80) is recovered.

### 13-5.4. The Entry Corridor

The theory of the Entry Corridor has been discussed in detail in Chapter 12. Here we shall present an accurate computing scheme for the calculation of the entry corridor, consistent with the new definition of the entry condition as given by Eq. (13-72). We shall consider only the undershoot boundary for deceleration-limited trajectories.

First, using the exact expression (13-71) for the deceleration due to aerodynamic force, by evaluating equation $d\bar{a}/ds = 0$ for maximum or minimum deceleration, we have, considering $\beta r$ as constant and using the basic equations (13-35)

$$2\sqrt{\beta r}\ Z + (\beta r - 1) \sin \gamma + \frac{2 \sin \gamma \cos^2 \gamma}{u} = 0 \quad (13\text{-}88)$$

It is interesting to notice that this condition does not depend explicitly on the lift-to-drag ratio although the trajectory depends on that parameter. Also, it is obvious that the condition can only be satisfied for negative flight path angles. When $a/g$ reaches an extremum, either a maximum or a minimum, the variables $Z$, $u$ and $\gamma$ satisfy condition (13-88) with the extremum $f_* \equiv a_*/g$ given by

$$f_* = \frac{\sqrt{\beta r}\ Zu}{\cos^2 \gamma} \sqrt{1 + (C_L/C_D)^2} \quad (13\text{-}89)$$

Hence, if $f = 0.05$ is used to define the entry condition, for entry trajectories to be completed during the first pass the minimum value for the deceleration $f_*$ should not be less than $0.05$. Then a systematic scanning of all the overshoot boundaries is as follows.

We use the two equations (13-88) and (13-89) as starting conditions, at the exit point, with $f_* = 0.05$ and integrate the trajectory backward until $f = 0.05$ again at the entry point. That is to say, for each prescribed $(C_L/C_D)$ we use the value of $Z$ at exit point $Z_e$ as a scanning parameter and obtain $\gamma_e$ and $u_e$ by solving the two Eqs. (13-88) and (13-89). The integration backward leads to the entry condition $\gamma_i$, $u_i$, $Z_i$ when $f = 0.05$. This will give a point for the overshoot boundary plotted on the diagram $\bar{V}_i$, $\gamma_i$, or in a better way, on the diagram $\bar{V}_i$, $Z_p$. The conversion from $\gamma_i$, $u_i$, $Z_i$ to $Z_p$ is obtained explicitly through Eqs. (13-78) and (13-79). The results are presented in Fig. 13-8 for ballistic entry giving the periapsis parameter $Z_p$ for overshoot boundary of any supercircular entry speed up to $\bar{V}_i = 2.2$.

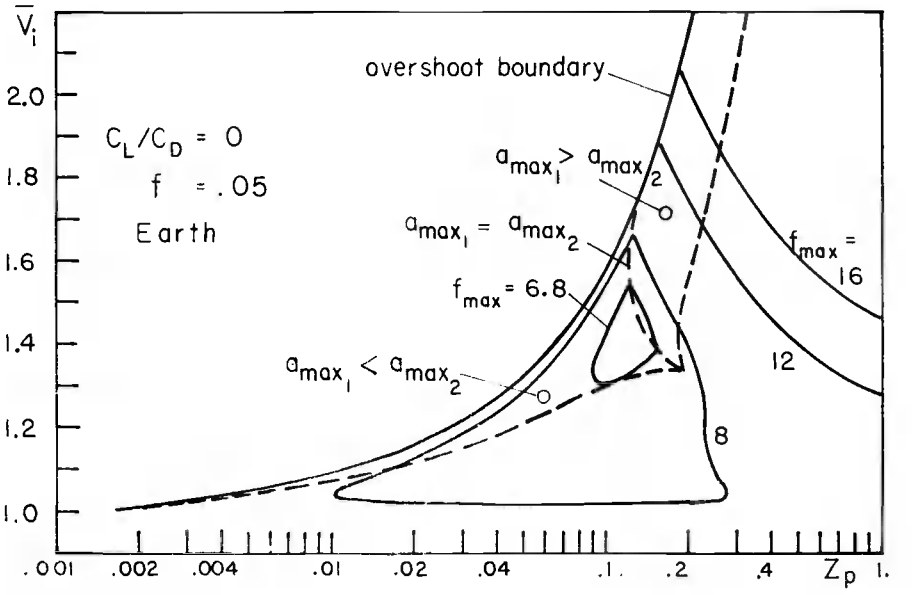


Fig. 13-8. Overshoot and undershoot boundaries for ballistic entries into the Earth's atmosphere.

Similarly, the undershoot boundary for any prescribed maximum deceleration $f_* = f_{max}$ can be obtained in the same way. The two equations (13-88) and (13-89) are used for the starting conditions at the point of peak deceleration, $f_* = f_{max}$. Then $Z$ is used as a scanning parameter for an integration backward to the entry point where $f = 0.05$. The resulting value $\gamma_i$, $u_i$ and $Z_i$ provides the entry condition for a peak deceleration $f_* = f_{max}$. It has been found that many ballistic entry trajectories have two peak decelerations. The region where they occur and a comparison of their magnitudes are shown in Fig. 13-8 depicting the undershoot boundaries for different values of $f_{max}$. As has been mentioned in Chapter 12, for ballistic entry at super-circular speed, there is a minimum value for the peak deceleration if the entry is completed during the first pass. Using the exact equations, it has been found that the smallest possible peak deceleration is 6.5 g which occurs for a slightly hyperbolic entry $\bar{V}_i = 1.466$ with $Z_p = 0.13$.

## References


1. Chapman, D. R., "An Approximate Analytical Method for Studying Entry Into Planetary Atmospheres," NASA TR-R-11, 1959.

2. Chapman, D. R., "An Analysis of the Corridor and Guidance Requirements for Supercircular Entry Into Planetary Atmospheres," NASA TR-R-55, 1960.

3. Vinh, N. X., and Brace, F. C., "Qualitative and Quantitative Analysis of the Exact Atmospheric Entry Equations Using Chapman's Variables," IAF paper No. 74-010, presented at the XXVth Congress of the International Astronautical Federation, Amsterdam, The Netherlands, October 1974.

4. Vinh, N. X., Busemann, A., and Culp, R. D., "Optimum Three-Dimensional Atmospheric Entry," Acta Astronautica, Vol. 2, pp. 593-611, 1975.

5. Yaroshevskii, V. A., "The Approximate Calculation of Trajectories of Entry into the Atmosphere I," translated from Kosmicheskie Issledovaniya, Vol. 2, No. 4, 1964.

6. Eggers, A. J., Jr., Allen, H. J., and Neice, S. E., "A Comparitive Analysis of the Performance of Long-Range Hypervelocity Vehicles," NACA TN 4046, 1957.

7. Sänger, E., Raketen-Flugtechnik, R. Odenbourg, Berlin, 1933.

8. Loh, W. H. T., Dynamics and Thermodynamics of Planetary Entry, Prentice-Hall, Inc., Englewood Cliffs, New Jersey, 1963.

9. Allen, H. J., and Eggers, A. J., Jr., "A Study of the Motion and Aerodynamic Heating of Missiles Entering the Earth's Atmosphere at High Supersonic Speed," NACA TN 4047, 1957.

10. Shi, Y. Y., and Pottsepp, L., "Asymptotic Expansion of a Hypervelocity Atmospheric Entry Problem," AIAA Journal, Vol. 7, No. 2, 1969.

11. Chapman, D. R., and Kapphahn, A. K., "Tables of Z Functions for Atmospheric Entry Analyses," NASA TR-R-106, 1961.

12. Brace, F. C., "An Improved Chapman Theory for Studying Entry Into Planetary Atmospheres," Ph. D. Thesis, The University of Michigan, 1974.

# Chapter 14

# Solution of the Exact Equations Using Directly Matched Asymptotic Expansions

## 14-1. INTRODUCTION

The dimensionless universal equations for atmospheric entry were derived in the previous chapter. The modified Chapman's variables were introduced primarily to generate numerically the Z functions appropriate for analyzing entries of arbitrary vehicles. First-order solutions were also obtained. As presented in Chapter 13, the theory is semi-analytical. In this chapter, a higher-order, analytical solution is presented. It is obtained by using the method of directly matched asymptotic expansions applied to the exact equations for three-dimensional entry. The two-regime approach of directly matched asymptotic expansions has proved to be feasible and effective in some restricted cases (Refs. 1 - 4). This chapter will follow the recent, complete integration of the exact universal equations, (Ref. 5).

## 14-2. THE DIMENSIONLESS EQUATIONS OF MOTION

If an isothermal atmosphere is used, the universal equations, derived in Chapter 13, have the form

$$\frac{dZ}{ds} = -\beta r\left(1 - \frac{3}{2\beta r}\right) Z \tan\gamma$$

$$\frac{du}{ds} = -\frac{2\sqrt{\beta r}\, Zu}{\cos\gamma}\left[1 + \lambda\tan\gamma + \frac{\sin\gamma}{2\sqrt{\beta r}\, Z}\right]$$

$$\frac{d\gamma}{ds} = \frac{\sqrt{\beta r}\, Z}{\cos\gamma}\left[\lambda + \frac{\cos\gamma}{\sqrt{\beta r}\, Z}\left(1 - \frac{\cos^2\gamma}{u}\right)\right]$$

$$\frac{d\theta}{ds} = \frac{\cos\psi}{\cos\phi}$$

$$\frac{d\phi}{ds} = \sin\psi \qquad (14\text{-}1)$$

$$\frac{d\psi}{ds} = \frac{\sqrt{\beta r}\ Z}{\cos^2\gamma}\left[\ \delta - \frac{\cos^2\gamma\cos\psi\tan\phi}{\sqrt{\beta r}\ Z}\ \right] \qquad \begin{matrix}(14\text{-}1)\\(con't)\end{matrix}$$

where

$$\lambda = \frac{C_L}{C_D}\cos\sigma \quad , \quad \delta = \frac{C_L}{C_D}\sin\sigma \qquad (14\text{-}2)$$

The nomenclature is displayed in Fig. 14-1. The flight program is specified by the lift-to-drag ratio, $C_L/C_D$, and the bank angle, $\sigma$, or equivalently, the flight parameters $\lambda$ and $\delta$. They are assumed constant for the flight. The $Z$ and $u$ variables are modified Chapman's variables.

$$Z \equiv \frac{\rho S C_D}{2m}\sqrt{\frac{r}{\beta}}$$

$$u \equiv \frac{V^2\cos^2\gamma}{gr} \qquad (14\text{-}3)$$

The dimensionless independent variable $s$ is related to the radial distance $r$ by the differential equation

$$\frac{ds}{dr} = \frac{1}{r\tan\gamma} \qquad (14\text{-}4)$$

The equations will be transformed to be more suitable for use in the method of directly matched asymptotic expansions.

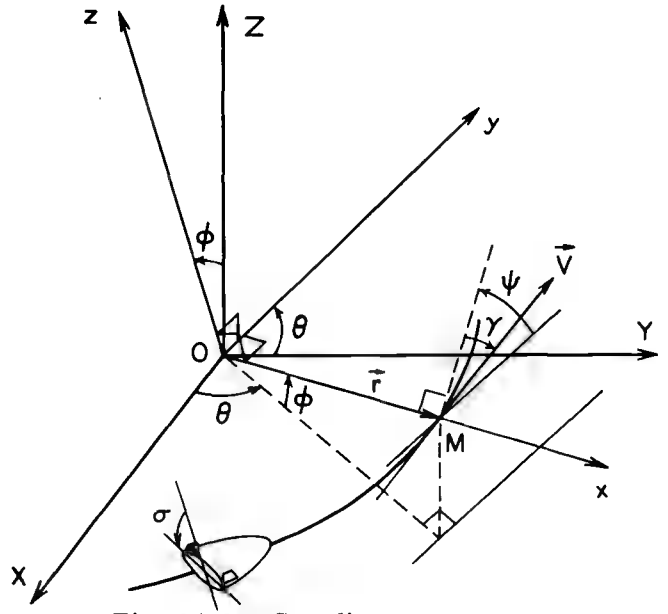


Fig. 14-1. Coordinate systems.

In this method, the solutions are obtained separately for an outer region, where the gravity force is predominant, and for an inner region, near the planetary surface, where the aerodynamic force is predominant. Hence, the altitude is the appropriate independent variable selected for the integration.

Let $y$ be the altitude and let subscript $s$ denote the reference altitude, for example, sea level. Then

$$r = r_s + y = r_s(1 + h) \tag{14-5}$$

where the dimensionless altitude $h$ is defined as

$$h = \frac{y}{r_s} \tag{14-6}$$

The differential relation between $s$ and $r$, Eq. (14-4), becomes

$$ds = \frac{dh}{(1 + h) \tan \gamma} \tag{14-7}$$

For the integration, we adopt a strictly exponential atmosphere, but the general method can be applied to any more realistic atmosphere such as, for example, the one proposed in Ref. 1. For an exponential atmosphere

$$\rho = \rho_s e^{-\beta y} = \rho_s e^{-h/\epsilon} \tag{14-8}$$

where

$$\epsilon = \frac{1}{\beta r_s} \tag{14-9}$$

Since the constant $\beta r_s$ is large, e.g., for the Earth atmosphere $\beta r_s \approx 900$, the parameter $\epsilon$ is a small quantity. By the definition (14-3) of $Z$

$$Z = \frac{\rho_s S C_D}{2m\beta} \sqrt{\frac{(1 + h)}{\epsilon}}\, e^{-h/\epsilon} \tag{14-10}$$

We define the ballistic coefficient

$$B \equiv \frac{S C_D \rho_s}{2m\beta} \tag{14-11}$$

For each vehicle, $B$ is specified and the variable $Z$ is obtained from

$$Z = B \sqrt{\frac{(1 + h)}{\epsilon}}\, e^{-h/\epsilon} \tag{14-12}$$

This relation can replace the first Eq. (14-1). The other equations, with the dimensionless altitude h as independent variable, can be written

$$\frac{du}{dh} = -\frac{u}{(1+h)} - \frac{2Bu(1+\lambda\tan\gamma)}{\epsilon\sin\gamma}\, e^{-h/\epsilon}$$

$$\frac{dq}{dh} = -\frac{q}{(1+h)}\left(1-\frac{q^2}{u}\right) - \frac{\lambda B}{\epsilon}\, e^{-h/\epsilon}$$

$$\frac{d\theta}{dh} = \frac{\cos\psi}{(1+h)\cos\phi\,\tan\gamma}$$

$$\frac{d\phi}{dh} = \frac{\sin\psi}{(1+h)\tan\gamma}$$

$$\frac{d\psi}{dh} = -\frac{\cos\psi\tan\phi}{(1+h)\tan\gamma} + \frac{B\delta\, e^{-h/\epsilon}}{\epsilon\sin\gamma\cos\gamma} \qquad (14\text{-}13)$$

where

$$q \equiv \cos\gamma \qquad (14\text{-}14)$$

The Eqs. (14-13) are in a suitable form for numerical integration for flight inside an atmosphere. For an analytical solution of the entry trajectory using the method of matched asymptotic expansions, we shall use a more convenient form using some elements of the orbit as introduced in celestial mechanics, since these elements are constants of the motion for flight in a vacuum.

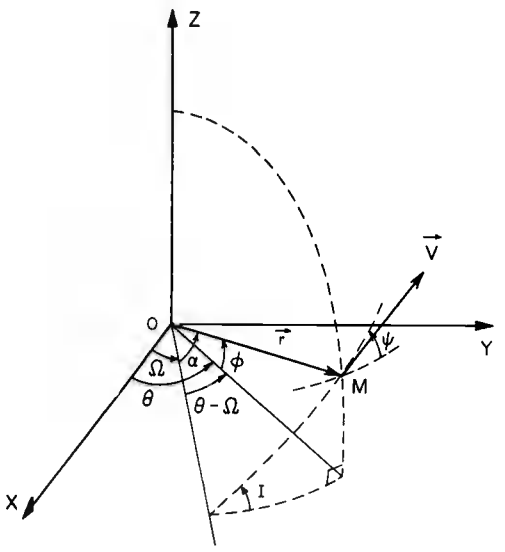


Fig. 14-2. The osculating plane and the orbital elements.

As seen in Fig. 14-2, if $I$ is the inclination of the plane of the osculating orbit, that is, the $(\vec{r}\ ,\ \vec{V})$ plane, $\Omega$ the longitude of the ascending node, and $\alpha$ the angle between the line of the ascending node and the position vector, the following pertinent relations from spherical trigonometry hold:

$$\begin{aligned} \cos\phi\ \cos\psi &= \cos I \\ \sin(\theta - \Omega) &= \frac{\tan\phi}{\tan I} \\ \cos\alpha &= \cos\phi\ \cos(\theta - \Omega) \end{aligned} \tag{14-15}$$

These relations are independent. We can easily deduce

$$\begin{aligned} \sin\phi &= \sin I \sin\alpha \\ \sin\psi &= \frac{\tan\phi}{\tan\alpha} \\ \sin\psi &= \sin I \cos(\theta - \Omega) \end{aligned} \tag{14-16}$$

Using these relations, we replace the variables $\theta$ , $\phi$ , and $\psi$ with the new variables $\alpha$ , $\Omega$ , and $I$ . The Eqs. (4-13) now become

$$\begin{aligned} \frac{du}{dh} &= -\frac{u}{(1+h)} - \frac{2Bu(1+\lambda\tan\gamma)}{\epsilon\sin\gamma}\, e^{-h/\epsilon} \\ \frac{dq}{dh} &= -\frac{q}{(1+h)}\left(1 - \frac{q^2}{u}\right) - \frac{\lambda B}{\epsilon}\, e^{-h/\epsilon} \\ \frac{d\alpha}{dh} &= \frac{1}{(1+h)\tan\gamma} - \frac{B\delta\ \sin\alpha}{\epsilon\tan I\sin\gamma\cos\gamma}\, e^{-h/\epsilon} \\ \frac{d\Omega}{dh} &= \frac{B\delta\ \sin\alpha}{\epsilon\ \sin I\sin\gamma\cos\gamma}\, e^{-h/\epsilon} \\ \frac{dI}{dh} &= \frac{B\delta\ \cos\alpha}{\epsilon\ \sin\gamma\cos\gamma}\, e^{-h/\epsilon} \end{aligned} \tag{14-17}$$

The Eqs. (14-17) are most suitable for an integration using the method of matched asymptotic expansions. We notice that, once the elements $\alpha$ , $\Omega$ , and $I$ are known, we obtain the original variables $\theta$ , $\phi$ , and $\psi$ from

$$\begin{aligned} \tan(\theta - \Omega) &= \cos I\tan\alpha \\ \sin\phi &= \sin I\sin\alpha \\ \tan\psi &= \cos\alpha\ \tan I \end{aligned} \tag{14-18}$$

## 14-3. INTEGRATION BY DIRECTLY MATCHED ASYMPTOTIC EXPANSIONS

### 14-3.1. Outer Expansions (Keplerian Region)

The Eqs. (14-17) are expressed in terms of the outer variables. The outer expansions are introduced to study the limiting conditions of the solution in the outer region where the gravitational force is predominant. They are obtained by repeated application of the outer limit, which is defined as the limit when $\epsilon \to 0$ with the variable $h$ and other dimensionless quantities held fixed.

We assume the following expansions

$$\begin{aligned} u &= u_0(h) + \epsilon u_1(h) + \ldots \\ q &= q_0(h) + \epsilon q_1(h) + \ldots \\ \alpha &= \alpha_0(h) + \epsilon \alpha_1(h) + \ldots \\ \Omega &= \Omega_0(h) + \epsilon \Omega_1(h) + \ldots \\ I &= I_0(h) + \epsilon I_1(h) + \ldots \end{aligned} \tag{14-19}$$

From Eqs. (14-17), the differential equations with zero order of $\epsilon$ are

$$\begin{aligned} \frac{du_0}{dh} &= -\frac{u_0}{(1+h)} \\ \frac{dq_0}{dh} &= -\frac{q_0}{(1+h)}\left(1 - \frac{q_0^2}{u_0}\right) \\ \frac{d\alpha_0}{dh} &= \frac{1}{(1+h)\tan\gamma_0} \\ \frac{d\Omega_0}{dh} &= 0 \\ \frac{dI_0}{dh} &= 0 \end{aligned} \tag{14-20}$$

The solution of this system is

$$\begin{aligned} u_0(1+h) &= C_1 \\ \frac{1}{q_0^2} &= \frac{2(1+h)}{C_1} - C_2(1+h)^2 \end{aligned} \tag{14-21}$$

$$u_0 = 1 + \sqrt{1 - C_1^2 C_2^2}\cos(\alpha_0 - C_3)$$

$$\Omega_0 = C_4$$

$$I_0 = C_5 \qquad (14\text{-}21)$$

(con't)

where the $C_n$ are constants of integration. The first-order and higher-order solutions are all equal to zero because at high altitude, in the limit the atmospheric density is zero and the motion is Keplerian.

## 14-3.2. Inner Expansions (Aerodynamic-Predominated Region)

The inner expansions are introduced to study the limiting condition of the solution near the planetary surface where the aerodynamic force is predominant. They are obtained by repeated application of the inner limit, which is defined as the limit when $\epsilon \to 0$ with the new stretched altitude

$$\tilde{h} = \frac{h}{\epsilon} \qquad (14\text{-}22)$$

and the other dimensionless quantities held fixed.

We assume the following expansions

$$u = \tilde{u}_0(\tilde{h}) + \epsilon\,\tilde{u}_1(\tilde{h}) + \ldots$$

$$q = \tilde{q}_0(\tilde{h}) + \epsilon\,\tilde{q}_1(\tilde{h}) + \ldots$$

$$\alpha = \tilde{\alpha}_0(\tilde{h}) + \epsilon\,\tilde{\alpha}_1(\tilde{h}) + \ldots$$

$$\Omega = \tilde{\Omega}_0(\tilde{h}) + \epsilon\,\tilde{\Omega}_1(\tilde{h}) + \ldots$$

$$I = \tilde{I}_0(\tilde{h}) + \epsilon\,\tilde{I}_1(\tilde{h}) + \ldots \qquad (14\text{-}23)$$

From Eqs. (14-17), the differential equations with zero order of $\epsilon$ are

$$\frac{d\tilde{u}_0}{d\tilde{h}} = -\frac{2B\tilde{u}_0(1 + \lambda\tan\tilde{\gamma}_0)}{\sin\tilde{\gamma}_0}\,e^{-\tilde{h}}$$

$$\frac{d\tilde{q}_0}{d\tilde{h}} = -\lambda B e^{-\tilde{h}}$$

$$\frac{d\tilde{\alpha}_0}{d\tilde{h}} = -\frac{B\delta\sin\tilde{\alpha}_0}{\tan\tilde{I}_0\sin\tilde{\gamma}_0\cos\tilde{\gamma}_0}\,e^{-\tilde{h}} \qquad (14\text{-}24)$$

$$\frac{d\tilde{\Omega}_0}{d\tilde{h}} = \frac{B\delta \sin \tilde{\alpha}_0}{\sin \tilde{I}_0 \sin \tilde{\gamma}_0 \cos \tilde{\gamma}_0} e^{-\tilde{h}}$$

$$\frac{d\tilde{I}_0}{d\tilde{h}} = \frac{B\delta \cos \tilde{\alpha}_0}{\sin \tilde{\gamma}_0 \cos \tilde{\gamma}_0} e^{-\tilde{h}} \qquad (14\text{-}24)$$

(con't)

The solution of this system is

$$\tilde{u}_0 = \tilde{C}_1 \tilde{q}_0^2 \exp\left[-\frac{2\tilde{\gamma}_0}{\lambda}\right]$$

$$\tilde{q}_0 = \lambda B e^{-\tilde{h}} + \tilde{C}_2$$

$$\sin \tilde{\alpha}_0 \sin \tilde{I}_0 = \sin \tilde{C}_3$$

$$\cos \tilde{\alpha}_0 = \cos \tilde{C}_3 \cos(\tilde{C}_4 - \tilde{\Omega}_0)$$

$$\cos \tilde{I}_0 = \cos \tilde{C}_3 \cos\left\{\frac{\delta}{\lambda} \log\left[\tan\left(\frac{\pi}{4} + \frac{\tilde{\gamma}_0}{2}\right)\right] + \tilde{C}_5\right\} \qquad (14\text{-}25)$$

where the $\tilde{C}_n$ are constants of integration.

## 14-3.3. Asymptotic Matching and Composite Expansions

The constants of integration $\tilde{C}_n$ in the inner expansions will be determined by matching with the outer expansions. In this problem, matching is accomplished by expanding the inner solutions for large $\tilde{h}$, expressing the results in terms of the outer variables and matching with the outer solutions for small $h$.

The outer solutions, Eqs. (14-21), become for small $h$

$$u_0 = C_1$$

$$q_0 = \sqrt{\frac{C_1}{2 - C_1 C_2}}$$

$$\alpha_0 = \cos^{-1}\left[\frac{C_1 - 1}{\sqrt{1 - C_1^2 C_2}}\right] + C_3$$

$$\Omega_0 = C_4$$

$$I_0 = C_5 \qquad (14\text{-}26)$$

On the other hand, the inner solutions, Eqs. (14-25), become for large $\tilde{h}$

$$\tilde{u}_0 = \tilde{C}_1 \tilde{C}_2^2 \exp\left[-\frac{2}{\lambda}\cos^{-1}\tilde{C}_2\right]$$

$$\tilde{q}_0 = \tilde{C}_2$$

$$\sin\tilde{\alpha}_0 \sin\tilde{I}_0 = \sin\tilde{C}_3$$

$$\cos\tilde{\alpha}_0 = \cos\tilde{C}_3 \cos(\tilde{C}_4 - \tilde{\Omega}_0)$$

$$\cos\tilde{I}_0 = \cos\tilde{C}_3 \cos\left\{\frac{\delta}{\lambda}\log\left[\tan\left(\frac{\pi}{4}+\frac{1}{2}\cos^{-1}\tilde{C}_2\right)\right] + \tilde{C}_5\right\} \tag{14-27}$$

Matching Eqs. (14-27) with Eqs. (14-26) provides the constants $\tilde{C}_n$ in terms of the constants $C_n$. We have

$$\tilde{C}_1 = (2 - C_1 C_2)\exp\left[\frac{2}{\lambda}\cos^{-1}\sqrt{\frac{C_1}{2 - C_1 C_2}}\right]$$

$$\tilde{C}_2 = \sqrt{\frac{C_1}{2 - C_1 C_2}}$$

$$\sin\tilde{C}_3 = \sin C_5 \sin\left[\cos^{-1}\left(\frac{C_1 - 1}{\sqrt{1 - C_1^2 C_2}}\right) + C_3\right]$$

$$\tilde{C}_4 = \cos^{-1}\left\{\cos\left[\cos^{-1}\frac{C_1 - 1}{\sqrt{1 - C_1^2 C_2}} + C_3\right] \Big/ \cos\tilde{C}_3\right\} + C_4$$

$$\tilde{C}_5 = \cos^{-1}\left[\cos C_5 / \cos\tilde{C}_3\right] - \frac{\delta}{\lambda}\log\left[\tan\left[\frac{\pi}{4}+\frac{1}{2}\cos^{-1}\sqrt{\frac{C_1}{2-C_1C_2}}\right]\right] \tag{14-28}$$

Hence, the constants $\tilde{C}_n$ are expressed explicitly in terms of the constants $C_n$. Substitution into Eqs. (14-25) gives the inner solutions. It is convenient to use the following notation to write these solutions in a symmetric form. Let

$$u_* = C_1$$

$$\cos \gamma_* = \sqrt{\frac{C_1}{2 - C_1 C_2}}$$

$$\sin \phi_* = \sin C_5 \sin \left[ \cos^{-1} \left( \frac{C_1 - 1}{\sqrt{1 - C_1^2 C_2}} \right) + C_3 \right]$$

$$\theta_* = \cos^{-1} \left\{ \cos \left[ \cos^{-1} \left( \frac{C_1 - 1}{\sqrt{1 - C_1^2 C_2}} \right) + C_3 \right] \Big/ \cos \phi_* \right\} + C_4$$

$$I_* = C_5 \qquad (14\text{-}29)$$

The constants with subscript $*$ are explicit functions of the constants $C_n$. Then the inner solutions are

$$\frac{\tilde{u}_0}{u_*} = \frac{\cos^2 \tilde{\gamma}_0}{\cos^2 \gamma_*} \exp \left[ \frac{2}{\lambda} (\lambda_* - \tilde{\gamma}_0) \right]$$

$$\cos \tilde{\gamma}_0 = \cos \gamma_* + \lambda B e^{-\tilde{h}}$$

$$\sin \tilde{\alpha}_0 \sin \tilde{I}_0 = \sin \phi_*$$

$$\cos \tilde{\alpha}_0 = \cos \phi_* \cos (\theta_* - \tilde{\Omega}_0)$$

$$\cos^{-1} \left( \frac{\cos \tilde{I}_0}{\cos \phi_*} \right) - \cos^{-1} \left( \frac{\cos I_*}{\cos \phi_*} \right)$$

$$= \frac{\delta}{\lambda} \log \left[ \tan \left( \frac{\pi}{4} + \frac{\tilde{\gamma}_0}{2} \right) \Big/ \tan \left( \frac{\pi}{4} + \frac{\gamma_*}{2} \right) \right] \qquad (14\text{-}30)$$

From the Eqs. (14-15) and (14-16) the meaning of the starred constants can be seen. The Eqs. (14-30) show that during the phase of aerodynamic turning, the latitude $\phi$ and the longitude $\theta$ remain constant. The last equation gives the change in the heading $\psi$ during that phase.

The composite expansions, uniformly valid everywhere, can be constructed by the method of additive composition. The additive composition is obtained by taking the sum of the inner and the outer expansions, Eqs. (14-30) and (14-21), and subtracting the part they have in common (the inner limit of the outer expansions or the outer limit of the inner expansions), Eqs. (14-26) and (14-27). Thus, for the variables $u$ and $\gamma$, using subscript $c$ for the composite solution,

$$\frac{u_c}{u_*} = -\frac{h}{(1+h)} + \frac{\cos^2 \tilde{\gamma}_0}{\cos^2 \gamma_*} \exp\left[\frac{2}{\lambda}(\gamma_* - \tilde{\gamma}_0)\right] \quad (14\text{-}31)$$

and

$$\cos \gamma_c = \cos \gamma_* \sqrt{\frac{u_*}{2\cos^2\gamma_*(1+h) + (u_* - 2\cos^2\gamma_*)(1+h)^2}} + \lambda\, Be^{-h/\epsilon} \quad (14\text{-}32)$$

For the angular variables $\alpha$ , $\Omega$ and $I$ , the composite solutions are

$$\alpha_c = \alpha_0 + \tilde{\alpha}_0 - C_3 - \cos^{-1}\left(\frac{C_1 - 1}{\sqrt{1 - C_1^2 C_2}}\right)$$

$$\Omega_c = \Omega_0 + \tilde{\Omega}_0 - C_4$$

$$I_c = I_0 + \tilde{I}_0 - C_5 \quad (14\text{-}33)$$

Hence, from Eq. (14-21), $\Omega_c = \tilde{\Omega}_0$ and $I_c = \tilde{I}_0$ . From the last of the Eqs. (14-30)

$$\cos I_c = \cos \phi_* \cos\left\{\cos^{-1}\left(\frac{\cos I_*}{\cos \phi_*}\right) + \frac{\delta}{\lambda} \log\left[\tan\left(\frac{\pi}{4} + \frac{\tilde{\gamma}_0}{2}\right) \Big/ \tan\left(\frac{\pi}{4} + \frac{\gamma_*}{2}\right)\right]\right\} \quad (14\text{-}34)$$

For the angle $\Omega_c = \tilde{\Omega}_0$ , the second Eq. (14-15) yields

$$\Omega_c = \theta_* - \sin^{-1}\left(\frac{\tan \phi_*}{\tan I_c}\right) \quad (14\text{-}35)$$

where $I_c$ is given by Eq. (14-34) .

Finally, the angle $\alpha_c$ is given by

$$\alpha_c = \sin^{-1}\left(\frac{\sin \phi_*}{\sin I_c}\right) + \cos^{-1}\left[\frac{\cos \gamma_*}{\sqrt{u_*^2 + (1 - 2u_*)\cos^2 \gamma_*}}\left(\frac{u_*}{1+h} - 1\right)\right] - \cos^{-1}\left[\frac{\cos \gamma_*(u_* - 1)}{\sqrt{u_*^2 + (1 - 2u_*)\cos^2 \gamma_*}}\right] \quad (14\text{-}36)$$

The composite solutions are expressed explicitly in terms of the five constants of integration $u_*, \gamma_*, \phi_*, \theta_*$ and $I_*$. For computation in terms of the independent variable $h$, the angle $\tilde{\gamma}_0$ is first calculated from the second Eq. (14-30). Subsequently, we obtain $u_c$, $\gamma_c$ and $I_c$, and finally $\Omega_c$ and $\alpha_c$.

## 14-3.4. Solution for the Planar Case

When $\delta = 0$, the motion is planar. The trajectory remains in the equatorial plane and the variable $\alpha$ is the same as the longitude $\theta$.

The composite solutions for $u$ and $\gamma$, Eqs. (14-31) and (14-32), remain valid. The composite solutions for $\theta$ can be seen from Eq. (14-36) to be

$$\cos(\theta - w_*) = \frac{\cos \gamma_*}{\sqrt{u_*^2 + (1 - 2u_*) \cos^2 \gamma_*}} \left( \frac{u_*}{1 + h} - 1 \right) \tag{14-37}$$

where $w_*$ is a constant of integration. The three constants of integration $u_*$, $\gamma_*$ and $w_*$ in Eqs. (14-31), (14-32) and (14-37) for the planar case are evaluated using the initial conditions $u_i$, $\gamma_i$ and $\theta_i$ at $h_i$.

It is obvious that when $C_L = 0$, $(\lambda = 0)$, then $\delta = 0$ and the ballistic entry is planar. To show that solution is valid for all ranges of $\lambda$ we shall obtain the solution for ballistic entry using a limiting process. The second of the Eqs. (14-30) shows that, when $\lambda \to 0$, $\tilde{\gamma}_0 \to \gamma_*$. Hence we write that equation in the limit

$$Be^{-\tilde{h}} = \frac{\cos \tilde{\gamma}_0 - \cos \gamma_*}{\lambda} = 2 \frac{\sin \left( \frac{\gamma_* - \tilde{\gamma}_0}{2} \right) \sin \left( \frac{\gamma_* + \tilde{\gamma}_0}{2} \right)}{\lambda}$$

$$= \sin \gamma_* \left( \frac{\gamma_* - \tilde{\gamma}_0}{\lambda} \right)$$

By substituting in Eq. (14-31), we have the solution for ballistic entry, $\lambda \to 0$

$$\frac{u_c}{u_*} = - \frac{h}{(1 + h)} + \exp \left[ \frac{2Be^{-h/\epsilon}}{\sin \gamma_*} \right] \tag{14-38}$$

This solution can also be obtained by reintegrating the inner equations with $\lambda = 0$ and then matching with the outer solutions.

## 14-4. APPLICATIONS

For the initial conditions to be satisfied identically, the five constants of integration $C_n$, or equivalently the five constants with subscript $*$, as defined by Eqs. (14-29), are to be evaluated by using the composite solutions. Let the conditions at $h_i$ be

$$u = u_i \ , \ \gamma = \gamma_i \ , \ \alpha = \alpha_i \ , \ \Omega = \Omega_i \ , \ I = I_i \tag{14-39}$$

With these conditions in the composite solutions, the constants $u_*$, $\gamma_*$, $\phi_*$, $\theta_*$ and $I_*$ are obtained by solving a set of transcendental equations which can only be done numerically. Another obstacle arises when, as is a common practice, in order to reduce the number of prescribed initial values, one takes the initial $(\vec{r}_i, \vec{V}_i)$ plane as the reference $OXY$ plane with the axis $OX$ along $\vec{r}_i$. In doing so $\alpha_i = 0$ and $I_i = 0$. But when $I = 0$, the longitude of the ascending node $\Omega$ is not defined, as evidenced by Eq. (14-35). This singularity can always be avoided by rotating the $OXY$ plane through a fixed and arbitrary angle, say $45^\circ$, about the $\vec{r}_i$ axis. Then the initial conditions at $h_i$ are

$$u = u_i \ , \ \gamma = \gamma_i \ , \ \alpha_i = 0 \ , \ \Omega_i = 0 \ , \ I_i = 45^\circ \tag{14-40}$$

The equivalent conditions for the variables $\theta$, $\phi$, and $\psi$ are

$$\theta_i = 0 \ , \ \phi_i = 0 \quad \psi_i = 45^\circ \tag{14-41}$$

This method of directly matched asymptotic expansions has provided highly accurate and useful solutions to less general atmospheric trajectory equations, Ref. 1. In that work, extensive numerical calculations demonstrated the accuracy compared with exact numerical solutions. The method was also proven valid for some restricted problems in Refs. 2-4. The present development which is based on Ref. 5 has accomplished the wedding of the exact atmospheric trajectory equations, using the powerful modified Chapman variables, with the method of directly matched asymptotic expansions. Numerical experiments using the composite solutions obtained show that the resulting solution is accurate and reliable. Thus, this analytical solution for atmospheric entry trajectories, in many ways completes the search for explicit, analytic, and yet accurate, solutions to this broad class of problems.

Before we close this chapter, one pertinent remark is in order:

In using the method of directly matched asymptotic expansions, the logical choice for the independent variable is the dimensionless altitude $h$. From the composite solutions, it is seen that the ballistic coefficient $B$, defined by Eq. (14-11), has to be prescribed. Hence, it seems that the solutions apply to a particular vehicle and the generality of Chapman's $Z$ variable is lost. This is true for the previously developed solutions concerning restricted cases (Refs. 1-4).

In the present theory, the dimensionless ballistic coefficient $B$, and the dimensionless altitude $h$ are related to the Z function through the explicit relation (14-12). Evaluating that equation at $h_i$, yields

$$Z_i = B \sqrt{\frac{(1 + h_i)}{\epsilon}}\, e^{-h_i/\epsilon} \qquad (14\text{-}42)$$

Equation (14-12) and its initial condition (14-42) provide the link between the two theories, the numerical theory in Chapter 13 and the present analytical theory.

It has been explained in Chapter 13 that the selection of the initial value $Z_i$ depends implicitly on the ballistic coefficient of the vehicle, since the way that the dimensionless deceleration due to atmospheric force builds up to a sensible value, $f = 0.05$, or the altitude where the variable $u$ starts to decrease, are functions of the ballistic coefficient. In the unified theory, both the altitude and the ballistic coefficient are hidden in the universal variable $Z$.

Now, assume a $Z$ function has been numerically generated for a certain universal entry trajectory, with $u_i$, $\gamma_i$, $\lambda$ prescribed. Then we also have the initial value $Z_i$. To compare this solution with the solution developed in this chapter we can choose a standard value for $h_i$. Then, the coefficient $B$ can be evaluated by Eq. (14-42) for use in the analytic solution. At each instant, the universal $Z$ function is given by Eq. (14-12).

In conclusion, we consider the case of ballistic entry. Figure 14-3 plots the deceleration $30\,\bar{Z}\,\bar{u}$ for ballistic entry from circular speed $\bar{u}_i = 1$, into the Earth's atmosphere, at different small flight path angles. The figure is taken from Chapman's report (Ref. 6), and as has been shown in Chapter 13, in this case Chapman's analysis is very accurate.

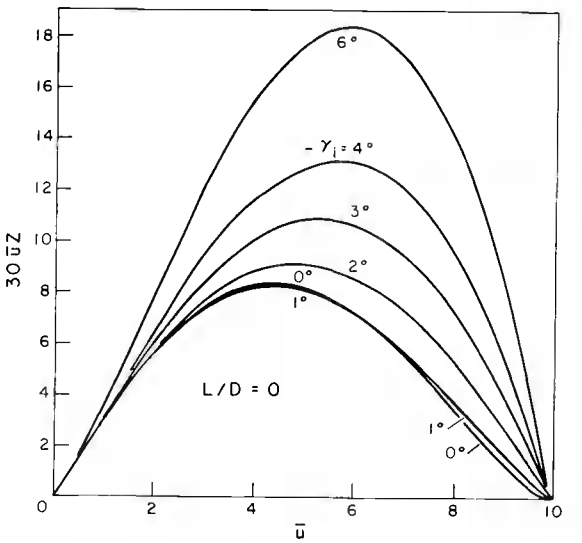


Fig. 14-3. Ballistic entries into the Earth's atmosphere from circular speed.

Omitting the subscript c for convenience, we write the composite solutions

$$Z = B\sqrt{\frac{1+h}{\epsilon}}\; e^{-h/\epsilon}$$

$$\frac{u}{u_*} = -\frac{h}{1+h} + \exp\left[\frac{2\,B\,e^{-h/\epsilon}}{\sin\gamma_*}\right]$$

$$\cos\gamma = \cos\gamma_* \sqrt{\frac{u_*}{2\cos^2\gamma_*(1+h) + (u_* - 2\cos^2\gamma_*)(1+h)^2}} \tag{14-43}$$

We are interested in the maximum of the deceleration $a/g = \sqrt{\beta r}\,\bar{Z}\,\bar{u}$. Since $\bar{Z}\,\bar{u} = Zu$, the equation for maximum deceleration, $d(Zu)/dh = 0$, is written explicitly as

$$\frac{1}{(1+h)}\left[\frac{1}{(1+h)} + \frac{h}{2(1+h)} - \frac{h}{\epsilon}\right] = \left[\frac{1}{2(1+h)} - \frac{1}{\epsilon} - \frac{2\,B\,e^{-h/\epsilon}}{\epsilon\,\sin\gamma_*}\right] \times \exp\left[\frac{2\,B\,e^{-h/\epsilon}}{\sin\gamma_*}\right] \tag{14-44}$$

Since $\epsilon$ is small we have approximately

$$-\frac{h}{1+h} + \exp\left[\frac{2\,B\,e^{-h/\epsilon}}{\sin\gamma_*}\right] = -\frac{2\,B\,e^{-h/\epsilon}}{\sin\gamma_*}\exp\left[\frac{2\,B\,e^{-h/\epsilon}}{\sin\gamma_*}\right] \tag{14-45}$$

Using the equation for $u$, we have the simple relation, valid at the stationary point of the deceleration

$$\frac{u}{u_*} = x\exp(-x) \tag{14-46}$$

where

$$x = -\frac{2\,B\,e^{-h/\epsilon}}{\sin\gamma_*} \tag{14-47}$$

For steep entry, the gravity effect can be neglected, and from the solution for $u$, with $x_i \approx 0$

$$\frac{u}{u_*} = \frac{u}{u_i} = \exp(-x) \tag{14-48}$$

Substitution into Eq. (14-46), provides the simple solution $x = 1$ and

$$\frac{u}{u_i} = \frac{1}{e} = 0.367879 \tag{14-49}$$

In Fig. 14-3, it is seen that, as $-\gamma_i$ becomes larger, the value $\bar{u} = u^{1/2}$ for peak deceleration becomes larger reaching the limit

$$\bar{u} = e^{-1/2}\,\bar{u}_i = 0.606531\,\bar{u}_i \quad .$$

The fact that this is the limit can be seen by considering the function $u/u_*$ as defined by Eq. (14-46). Its derivative is

$$\frac{d}{dx}\left(\frac{u}{u_*}\right) = (1 - x)\,\exp(-x) \tag{14-50}$$

Hence the function reaches its maximum at $x = 1$ as seen in Fig. 14-4.

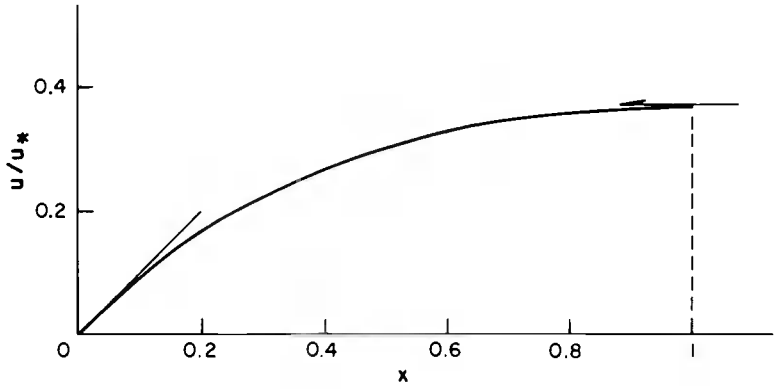


Fig. 14-4. $u/u_*$ as a function of $x$ for maximum deceleration during ballistic entry.

For shallow ballistic entry, we rewrite the Eq. (14-45)

$$(1 - x)\,\exp(-x) = \frac{h}{1 + h} \tag{14-51}$$

valid at the point of maximum deceleration.

From this equation we see that $x < 1$, and since $h$ is small, $x$ remains near unity. Using the definition of $Z$ in Eq. (14-47) we can write

$$x = -\frac{2\,Z}{\sqrt{\beta r}\,\sin\gamma_*} \tag{14-52}$$

Now, from Eq. (14-1), with $\lambda = 0$, we have the condition at the point where maximum deceleration occurs, $d(Zu)/ds = 0$

$$1 = -\frac{2Z}{\sqrt{\beta r}\sin\gamma} \tag{14-53}$$

From this equation, for maximum deceleration,

$$x = \frac{\sin\gamma}{\sin\gamma_*} \tag{14-54}$$

which should be compared with Eq. (14-52). This relation sheds light on the meaning of the constant $\gamma_*$. It is not the initial flight path angle, but it is the angle near which the maximum deceleration occurs, and is in general larger than $\gamma_i$.

The constants of integration $u_*$ and $\gamma_*$ are calculated by applying the initial conditions to the solution (14-43) at $h = h_i$. Since the selection of $h_i$ is rather arbitrary the initial conditions may not provide a solution for $u_*$ and $\gamma_*$. For example, we consider the case where $\gamma_i = 0$. Then

$$\cos^2\gamma_* = \frac{u_*(1+h_i)^2}{u_* + 2h_i(1+h_i)} \tag{14-55}$$

For $\gamma_*$ to be real

$$u_* < \frac{2(1+h_i)}{2+h_i} \approx 1 + \frac{h_i}{2} \tag{14-56}$$

for small $h_i$. Since by Eq. (14-43)

$$\frac{u_i}{u_*} \approx 1 - \frac{h_i}{1+h_i} = \frac{1}{1+h_i}$$

we have the condition

$$u_i < 1 - \frac{h_i}{2} \tag{14-57}$$

For grazing entry with deceleration building up, that is, one-pass ballistic entry, the entry speed must be subcircular.

Strictly speaking, for $\gamma_i = 0$, $u_i = 1$, $Z_i \approx 0$ the entry process is by orbital decay. This topic will be discussed in detail in Chapter 15. For the last phase of entry we can integrate directly the Eqs. (14-1), with $\gamma \approx 0$, $\lambda = 0$

$$\frac{dZ}{ds} = -\beta r\, Z\, \gamma$$

$$\frac{du}{ds} = -2\sqrt{\beta r}\, Zu$$

$$\frac{d\gamma}{ds} = \frac{u-1}{u} \tag{14-58}$$

Changing the independent variable to $u$

$$\frac{dZ}{du} = \frac{\sqrt{\beta r}\,\gamma}{2u}$$

$$\frac{d\gamma}{du} = \frac{1-u}{2\sqrt{\beta r}\, Z\, u^2} \tag{14-59}$$

Using a monotonically increasing variable $\mu$ by the transformation

$$u = e^{-2\mu} \tag{14-60}$$

we obtain

$$\frac{dZ}{d\mu} = -\sqrt{\beta r}\,\gamma$$

$$\frac{d\gamma}{d\mu} = \frac{1-e^{2\mu}}{\sqrt{\beta r}\, Z} \tag{14-61}$$

By eliminating $\gamma$

$$\frac{d^2Z}{d\mu^2} = \frac{e^{2\mu}-1}{Z} \tag{14-62}$$

with the initial conditions

$$Z(0) = 0 \quad , \quad Z'(0) = 0 \tag{14-63}$$

This is precisely Yaroshevskii's formulation as discussed in Chapter 10. It has been found that, in this case, the peak deceleration occurs at

$$\mu = 0.835 \quad , \quad u^{1/2} = \bar{u} = 0.434 \tag{14-64}$$

which is consistent with Chapman's numerical calculation in Fig. 14-3.

## References

1. Yang, Ching-Yew, "On the Use of Aerodynamic Forces to Effect Maneuvers of Orbiting Vehicles," Ph. D. Thesis, University of Colorado, August 1972.

2. Shi, Y. Y., and Pottsepp, L., "On the Asymptotic Expansions of a Hypervelocity Atmospheric Entry Problem," AIAA Journal, Vol. 7, No. 2, pp. 353-355, 1969.

3. Shi, Y. Y., Pottsepp, L., and Eckstein, M. C., "A Matched Asymptotic Solution for Skipping Entry into Planetary Atmosphere," AIAA Journal, Vol. 9, No. 4, pp. 736-738, 1971.

4. Shi, Yun-Yuan, "Matched Asymptotic Solutions for Optimum Lift Controlled Atmospheric Entry," AIAA Journal, Vol. 9, No. 11, pp. 2229-2238, 1971.

5. Busemann, A., Vinh, N. X., and Culp, R. D., "Solution of the Exact Equations for Three-Dimensional Atmospheric Entry Using Directly Matched Asymptotic Expansions," NASA Report CR-2643, 1976.

6. Chapman, D. R., "An Approximate Analytical Method For Studying Entry Into Planetary Atmospheres," NASA Report R-11, 1959.

# Chapter 15

# Orbit Contraction Due to Atmospheric Drag

## 15-1. INTRODUCTION

In Chapters 10-13, we have considered, among different types of trajectories, the special case of the trajectory of a vehicle subject to pure aerodynamic drag. If the periapsis altitude of the initial orbit is high anough, the vehicle will make several passes through the atmosphere before completing its entry.

On the other hand, for very high periapsis altitude the vehicle will stay aloft for several days, weeks or even years before the effect of aerodynamic drag has reduced the lowest altitude far enough into the sensible atmosphere to effectively initiate the entry trajectory. During this time the trajectory of the vehicle is essentially a Keplerian orbit subject to a small perturbing effect due to the resistance of a tenuous atmosphere. The analysis of such a trajectory is the subject of the present chapter.

In the early days, development of the theory of flight near orbital speed inside an atmosphere was conducted in two separated aspects. On the one hand, researchers analyzed the small perturbations of satellite orbits at very high altitude. The mathematical tools are perturbation theories in celestial mechanics based on Lagrange's equations for the variations of orbital elements. The space vehicle, usually referred to as a satellite, is not intended for recovery. The main subjects of concern are first, its life expectancy, and second, the slow variations of its orbital elements. The variables of interest are primarily the major axis and the eccentricity of the osculating orbit. On the other hand, engineers and scientists who were concerned with the safe recovery of an entry vehicle concentrated their effort on the study of the deceleration and heating during entry. The elements of prime consideration are the position and the velocity of the vehicle, both varying rapidly. The nice behavior of the near-Keplerian orbit is no longer available, and strong physical assumptions were made to such an extent that, although describing the same phenomenon, namely, flight of an object inside a planetary atmosphere, the equations became totally different. The gap got wider as the two theories became more and more sophisticated. Now the two groups, one consisting mostly of mathematicians, and one consisting mostly of physicists, seldom reference the other group's work.

With the objective of providing a unified theory for flight inside a planetary atmosphere, we have formulated a set of universal, exact equations in Chapter 13. These equations have been successfully applied to the study of planetary entry of a space vehicle (Refs. 1-2), and to optimization of such an entry (Refs. 3-4). In this chapter we shall present the necessary transformation such that the equations can be used for analyzing the slow variations of the orbital elements while the vehicle is still in the near vacuum. This successful wedding is necessary since future space vehicles are designed to stay for an extended period in orbit as satellites, and also to be recovered safely after a fiery entry which is followed by a glide, an approach, and a landing on an airfield.

## 15-2. FORCES ON A SATELLITE IN ORBIT

The satellite and the planet are assumed in two-body relative motion. For a spherical planet, the gravitational force is an inverse square force of attraction with acceleration

$$g(r) = \frac{\mu}{r^2} \tag{15-1}$$

where $r$ is the distance from the satellite to the center of the planet and $\mu$ the planet gravitational constant.

The atmospheric force is in the form of drag acting in a direction opposite to the velocity $\vec{V}_A$ of the satellite relative to the ambient atmosphere

$$D_A = \frac{1}{2} \rho S C_D V_A^2 \tag{15-2}$$

We shall use a strictly exponential law for the density of the atmosphere

$$\rho = \rho_{p_o} e^{\beta (r_{p_o} - r)} \tag{15-3}$$

where $\beta$ is now considered as a constant

$$\beta = \frac{1}{H} \tag{15-4}$$

The quantity $H$ which has the dimension of a length, is the scale height, and subscript $p_o$ denotes the initial periapsis condition.

The equations of motion are written with respect to an inertial frame with origin at the center of the planet. Let $\vec{V}$ be the absolute velocity of the satellite

$$\vec{V} = \vec{V}_A + \vec{V}_e \tag{15-5}$$

where $\vec{V}_e$ is the velocity of the ambient air relative to the inertial frame (Fig. 15-1). We shall assume that the atmosphere has a uniform rotation of angular velocity $\vec{w}$ about the South-North axis taken as the Z inertial axis. Then

$$V_e = rw \cos \phi \tag{15-6}$$

where $\phi$ is the latitude of the point M representing the satellite.

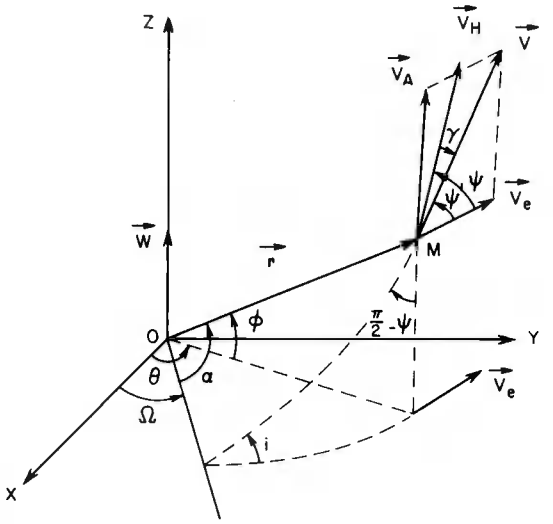


Fig. 15-1. Notation.

Let $\psi'$ be the angle between $\vec{V}_e$ and $\vec{V}$. Then by squaring Eq. (15-5)

$$V_A^2 = V^2 + V_e^2 - 2VV_e \cos \psi' \tag{15-7}$$

The vector $\vec{V}_e$ is in the local horizontal plane. Also, near the periapsis where the aerodynamic drag is most effective, the satellite travels nearly horizontally, that is the angle $\gamma$ between the velocity $\vec{V}$ and the horizontal plane is small. Hence, following King-Hele (Ref. 5), we can evaluate approximately the relative speed $V_A$ in terms of the absolute speed $V$ as follows.

First, the angle $\psi'$ between $\vec{V}_e$ and $\vec{V}$ is seen as nearly equal to the angle $\psi$ between $\vec{V}_e$ and the projection $\vec{V}_H$ of $\vec{V}$ on the local horizontal plane. This angle $\psi$, called the heading, is related to the latitude $\phi$ and the inclination $i$ of the osculating orbital plane by the well-known relation

$$\cos \psi \cos \phi = \cos i \tag{15-8}$$

Therefore, we have approximately

$$V_e \cos \psi' \approx V_e \cos \psi = rw \cos \phi \cos \psi = rw \cos i \tag{15-9}$$

Upon substituting Eqs. (15-6) and (15-9) into Eq. (15-7), we have

$$V_A^2 = V^2 \left(1 - \frac{rw}{V} \cos i\right)^2 + r^2 w^2 (\cos^2 \phi - \cos^2 i) \tag{15-10}$$

The rotation of the atmosphere is generally slow so that the term $w^2$ can be neglected. In the small term $rw/V$, it is appropriate to use an average value. King-Hele suggested using the value $r_{p_o} / V_{p_o}$ at the periapsis to replace $r/V$. Finally, the inclination $i$, which usually varies by less than $0.3^o$ during a satellite's life, may be taken equal to its initial value $i_o$. Then, we have King-Hele's expression

$$V_A^2 = f V^2 \tag{15-11}$$

where the average constant value $f$ is

$$f = \left(1 - \frac{r_{p_o} w}{V_{p_o}} \cos i_o\right)^2 \tag{15-12}$$

Thus, in terms of the absolute speed, the drag force is

$$D_A = \frac{1}{2} \rho S f C_D V^2 \tag{15-13}$$

acting opposite to the direction of the velocity $\vec{V}_A$ of the satellite relative to the ambient atmosphere.

## 15-3. THE EQUATIONS OF MOTION

The set of dimensionless universal equations for the motion of a vehicle inside a planetary atmosphere has been derived in Chapter 13. For a locally exponential atmosphere, we have the equations with the notation in Fig. 15-1

$$\frac{dZ}{ds} = -\beta r \left(1 - \frac{1}{2\beta r} + \frac{1}{2\beta^2} \frac{d\beta}{dr}\right) Z \tan \gamma$$

$$\frac{du}{ds} = -\frac{2\sqrt{\beta r}\, Zu}{\cos \gamma} \left[1 + \frac{C_L}{C_D} \cos \sigma \tan \gamma + \frac{\sin \gamma}{2\sqrt{\beta r}\, Z}\right] \tag{15-14}$$

$$\frac{d\gamma}{ds} = \frac{\sqrt{\beta r}\, Z}{\cos\gamma}\left[\frac{C_L}{C_D}\cos\sigma + \frac{\cos\gamma}{\sqrt{\beta r}\, Z}\left(1 - \frac{\cos^2\gamma}{u}\right)\right]$$

$$\frac{d\theta}{ds} = \frac{\cos\psi}{\cos\phi}$$

$$\frac{d\phi}{ds} = \sin\psi$$

$$\frac{d\psi}{ds} = \frac{\sqrt{\beta r}\, Z}{\cos^2\gamma}\left[\frac{C_L}{C_D}\sin\sigma - \frac{\cos^2\gamma\cos\psi\tan\phi}{\sqrt{\beta r}\, Z}\right] \qquad (15\text{-}14)\ (\text{con't})$$

The variables $u$ and $Z$ are the modified Chapman's variables

$$u \equiv \frac{V^2\cos^2\gamma}{gr}\ , \qquad Z \equiv \frac{\rho S C_D}{2m}\sqrt{\frac{r}{\beta}} \qquad (15\text{-}15)$$

The independent variable $s$ is the dimensionless arc length from the initial time

$$s \equiv \int_0^t \frac{V}{r}\cos\gamma\, dt \qquad (15\text{-}16)$$

The variable $\theta$ is the longitude, and the angle $\sigma$, the "bank angle," is the angle between the vertical plane passing through the velocity, the $(\vec{r}, \vec{V})$ plane, and the plane containing the aerodynamic force and the velocity, the $(\vec{V}_A, \vec{V})$ plane. As has been mentioned above, the aerodynamic force is in the direction opposite to the velocity $\vec{V}_A$, the relative velocity of the satellite with respect to the ambient air. Finally, $C_L$ and $C_D$ denote the coefficients of the aerodynamic forces resolved in the direction perpendicular and parallel to the absolute velocity $\vec{V}$.

The equations (15-14) are convenient for analyzing the entry portion of the trajectory. For satellite orbits, it is more advantageous to use the orbital elements. First, we use the relations from spherical trigonometry

$$\cos\phi\cos\psi = \cos i$$

$$\cos\phi\sin\psi = \sin i\cos\alpha$$

$$\cos\alpha = \cos\phi\cos(\theta - \Omega) \qquad (15\text{-}17)$$

to transform the last three equations (15-14) into

$$\frac{d\alpha}{ds} = 1 - \frac{\sqrt{\beta r}\ Z \sin\alpha}{\tan i \cos^2\gamma}\left(\frac{C_L}{C_D}\right)\sin\sigma$$

$$\frac{d\Omega}{ds} = \frac{\sqrt{\beta r}\ Z \sin\alpha}{\sin i \cos^2\gamma}\left(\frac{C_L}{C_D}\right)\sin\sigma$$

$$\frac{di}{ds} = \frac{\sqrt{\beta r}\ Z \cos\alpha}{\cos^2\gamma}\left(\frac{C_L}{C_D}\right)\sin\sigma \qquad (15\text{-}18)$$

From Fig. 15-1, we notice that $i$ is the inclination and $\Omega$ the longitude of the ascending node of the osculating plane. The angle $\alpha$ is the angle between the ascending node and the position vector.

For satellite motion, we have a simplification and at the same time, a complication. The simplification is that there is no lift force. The complication is that the drag force is modified by the factor $f$ as explained in Section 15-2, and it is directed opposite to the velocity $\vec{V}_A$ and not to the absolute velocity $\vec{V}$.

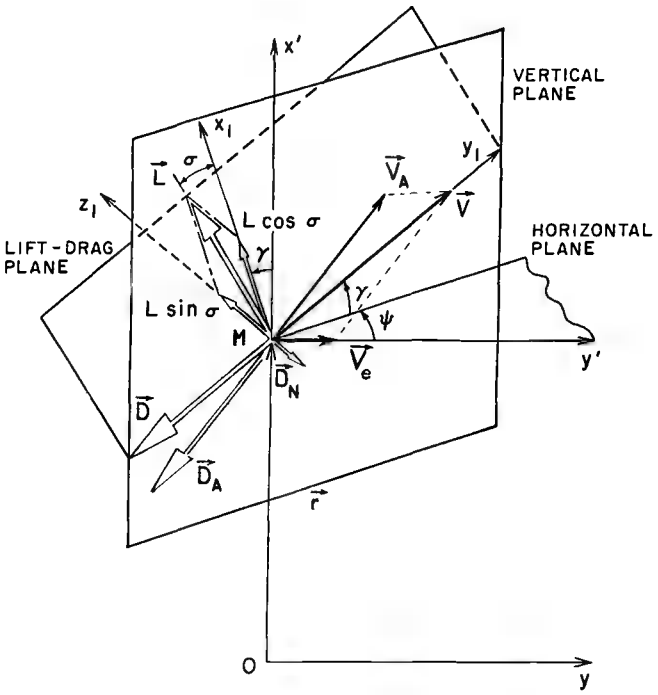


Fig. 15-2. Aerodynamic forces.

Figure 15-2 is the aerodynamic force diagram used in Chapter 2 in deriving the general equations of motion, to which we have added the velocity $\vec{V}_A$ with respect to the ambient air and the drag force $\vec{D}_A$

opposite in direction to $\vec{V}_A$ . In the present situation, we remove the lift force $\vec{L}$ and replace the vector drag $\vec{D}$ by the force $\vec{D}_A$ . This force $\vec{D}_A$ can be decomposed into one component in the orbital plane and one component normal to the orbital plane. Since $\vec{V}_e$ is small, $\vec{V}_A$ is nearly aligned to $\vec{V}$ and the component of $\vec{D}_A$ in the orbital plane can be considered as directly opposite to $\vec{V}$ , with magnitude $D_A$ as given by Eq. (15-13). Rigorously, the component of $\vec{D}_A$ in orbital plane has a component along the $y_1$ axis and a component along the $x_1$ axis (Fig. 15-2) with the component along the $y_1$ axis nearly equal to $D_A$ and the lift component along the $x_1$ axis negligible for all practical purposes. To obtain the component $\vec{D}_N$ of $\vec{D}_A$ orthogonal to the orbital plane we find the projection of

$$\vec{D}_A = -\frac{1}{2}\rho S f C_D V^2 \frac{\vec{V}_A}{V_A} \tag{15-19}$$

By the vector relation (15-5), since $\vec{V}$ is in the orbital plane and since $\vec{V}_A$ makes an angle $\psi$ with the orbital plane, the projection of $\vec{V}_A$ on the normal to the orbital plane is the same as the projection of $\vec{V}_e$ which has magnitude

$$V_e \sin\psi = rw \cos\phi \sin\psi = rw \sin i \cos\alpha \tag{15-20}$$

Hence, the vector $\vec{D}_N$ has magnitude

$$D_N = \frac{1}{2}\rho S f C_D rw \sin i \cos\alpha \frac{V^2}{V_A} \tag{15-21}$$

or, using (15-11),

$$D_N = \frac{1}{2}\rho S f^{1/2} C_D V rw \sin i \cos\alpha \tag{15-22}$$

and its direction is opposite to the vector $\overrightarrow{L \sin\sigma}$ in Fig. 15-2. The end result of the analysis is that, in the Eqs. (15-14) and (15-18) we replace $C_D$ by the modified drag coefficient $fC_D$ , we delete the component $C_L \cos\sigma$ and replace the component $C_L \sin\sigma$ by

$$C_L \sin\sigma = -f^{1/2} C_D \left(\frac{rw}{V}\right) \sin i \cos\alpha \tag{15-23}$$

Finally, the variable $Z$ , called the modified Chapman $Z$ function, is most effective in analyzing the entry phase of the vehicle. While the vehicle is still a satellite in orbit we use it in the form

$$\sqrt{\beta r}\, Z = Z_o \left(\frac{r}{r_{p_o}}\right) e^{\beta(r_{p_o} - r)} \tag{15-24}$$

where the dimensionless constant $Z_o$ is

$$Z_o = \frac{\rho_{p_o} S f C_D r_{p_o}}{2m} \tag{15-25}$$

We can now rewrite the Eqs. (15-14) and (15-18), introducing the equation for $r/r_{p_o}$ to replace the equation for $Z$

$$\begin{aligned}
\frac{d}{ds}\left(\frac{r}{r_{p_o}}\right) &= \left(\frac{r}{r_{p_o}}\right) \tan\gamma \\
\frac{du}{ds} &= -u\tan\gamma - \frac{2Z_o u}{\cos\gamma}\left(\frac{r}{r_{p_o}}\right) e^{\beta(r_{p_o}-r)} \\
\frac{d\gamma}{ds} &= 1 - \frac{\cos^2\gamma}{u} \\
\frac{d\alpha}{ds} &= 1 + \frac{r_{p_o} w Z_o}{\sqrt{\mu f/r_{p_o}}}\left(\frac{r}{r_{p_o}}\right)^{5/2} \frac{\cos i \sin\alpha\cos\alpha}{u^{1/2}\cos\gamma} e^{\beta(r_{p_o}-r)} \\
\frac{d\Omega}{ds} &= -\frac{r_{p_o} w Z_o}{\sqrt{\mu f/r_{p_o}}}\left(\frac{r}{r_{p_o}}\right)^{5/2} \frac{\sin\alpha\cos\alpha}{u^{1/2}\cos\gamma} e^{\beta(r_{p_o}-r)} \\
\frac{di}{ds} &= -\frac{r_{p_o} w Z_o}{\sqrt{\mu f/r_{p_o}}}\left(\frac{r}{r_{p_o}}\right)^{5/2} \frac{\sin i\cos^2\alpha}{u^{1/2}\cos\gamma} e^{\beta(r_{p_o}-r)}
\end{aligned} \tag{15-26}$$

## 15-4. THE PERTURBATION EQUATIONS

The Eqs. (15-26) are the bridge between satellite theory and entry theory. As a matter of fact, they can be used to follow the motion of a vehicle subject to gravitational force and drag force of a uniformly rotating atmosphere and planet for its entire life in orbit until its entry and contact with the planetary surface. The accuracy depends on the readjustment, for each layer of the atmosphere, of the constant value $\beta$.

The variables $\alpha$, $\Omega$ and $i$ which are orbital elements are related to the entry elements $\theta$, $\phi$ and $\psi$ through the relations (15-17). On the other hand, the variables $r$, $u$ and $\gamma$, which are the entry variables, can be transformed into the orbital elements through explicit relations.

Consider the osculating orbit, which is the orbit the vehicle would follow if at any time the drag force suddenly vanished. Putting

$Z_o = 0$ in Eqs. (15-26), we have

$$\frac{d}{ds}\left(\frac{r}{r_{p_o}}\right) = \left(\frac{r}{r_{p_o}}\right)\tan\gamma$$

$$\frac{du}{ds} = -u\tan\gamma$$

$$\frac{d\gamma}{ds} = 1 - \frac{\cos^2\gamma}{u}$$

$$\frac{d\alpha}{ds} = 1$$

$$\frac{d\Omega}{ds} = 0$$

$$\frac{di}{ds} = 0 \qquad (15\text{-}27)$$

The integration is simple and we have the general solution

$$\cos^2\gamma = \frac{u^2}{2u - c_1}$$

$$r = \frac{c_2}{u}$$

$$u = 1 + \sqrt{1 - c_1}\,\cos(s - c_3)$$

$$s = \alpha + c_4$$

$$\Omega = c_5$$

$$i = c_6 \qquad (15\text{-}28)$$

where the $c_i$ are constants of integration. We see that $s$ is equivalent to $\alpha$ and actually we only have 5 constants of integration. The last constant of integration is obtained by integrating the time equation, Eq. (15-16).

In the first three equations (15-28), we evaluate the constants of integration by taking the origin of time at the time of passage through the periapsis.

$$\cos^2\gamma = \frac{u^2}{2u - (1 - e^2)}$$

$$u = 1 + e\cos(\alpha - \omega)$$

$$r = \frac{a(1 - e^2)}{1 + e\cos(\alpha - \omega)} \qquad (15\text{-}29)$$

These three equations provide the link between the entry variables $r$, $u$ and $\gamma$ and the semi-major axis $a$, the eccentricity $e$ and the argument of periapsis, $\omega$, which are the orbital elements used in the theory of orbits.

During the phase in orbit, $Z_o$ is small and the orbital elements vary slowly. By taking the derivatives of Eqs. (15-29), considering $a$, $e$ and $\omega$ as varying quantities and using the Eqs. (15-26) for the derivatives of $r$, $u$ and $\gamma$, we have the perturbation equations for $a$, $e$ and $\omega$.

First, for the eccentricity $e$ we have

$$\frac{de}{ds} = \frac{2Z_o u^2}{e \cos^3 \gamma} \left( \frac{\cos^2 \gamma}{u} - 1 \right) \left( \frac{r}{r_{p_o}} \right) e^{\beta(r_{p_o} - r)} \tag{15-30}$$

We present the equation in this form to show an interesting behavior of the eccentricity of the osculating orbit. It is a general belief that the eccentricity decreases continuously under the action of atmospheric drag. But this is the secular effect. During each revolution, the flight path angle passes through a maximum and a minimum as seen by the third of the Eqs. (15-26), and by Eq. (15-30) it is seen that, at the same time, the eccentricity passes through a minimum and a maximum respectively.

Next, we shall use the more familiar eccentric anomaly $E$ to replace $s$ as the independent variable in the perturbation equations. The following relations are obtained.

$$\frac{r}{a} = \frac{(1 - e^2)}{1 + e \cos(\alpha - \omega)} = 1 - e \cos E$$

$$u = \frac{(1 - e^2)}{1 - e \cos E}$$

$$\cos^2 \gamma = \frac{(1 - e^2)}{(1 - e \cos E)(1 + e \cos E)} \tag{15-31}$$

Also, it is seen that between $s$ and $E$ we have the differential relation

$$\frac{ds}{dE} = \frac{\sqrt{1 - e^2}}{1 - e \cos E} \tag{15-32}$$

Hence, the equation for $e$ has the form

$$\frac{de}{dE} = -2Z_o(1 - e^2) \left( \frac{a}{r_{p_o}} \right) \cos E \left( \frac{1 + e \cos E}{1 - e \cos E} \right)^{1/2} e^{\beta(r_{p_o} - r)} \tag{15-33}$$

Similarly, the variation of the semi-major axis is governed by

$$\frac{da}{dE} = -2Z_o \frac{a^2}{r_{p_o}} \frac{(1+e\cos E)^{3/2}}{(1-e\cos E)^{1/2}} e^{\beta(r_{p_o}-r)} \tag{15-34}$$

Under the same transformation, the last three equations of the Eqs. (15-26) become

$$\frac{d\alpha}{dE} - \frac{d\omega}{dE} = \frac{\sqrt{1-e^2}}{1-e\cos E}\left[1+\frac{2Z_o}{e}\left(\frac{a}{r_{p_o}}\right)\sin E(1-e\cos E)^{\frac{1}{2}}(1+e\cos E)^{\frac{1}{2}} e^{\frac{1}{2}\beta(r_{p_o}-r)}\right]$$

$$\frac{d\Omega}{dE} = -\frac{r_{p_o} wZ_o}{\sqrt{\mu f/r_{p_o}}\sqrt{1-e^2}}\left(\frac{a}{r_{p_o}}\right)^{\frac{5}{2}} (1-e\cos E)^{\frac{5}{2}} (1+e\cos E)^{\frac{1}{2}} \sin\alpha\cos\alpha\, e^{\beta(r_{p_o}-r)}$$

$$\frac{di}{dE} = -\frac{r_{p_o} wZ_o}{\sqrt{\mu f/r_{p_o}}\sqrt{1-e^2}}\left(\frac{a}{r_{p_o}}\right)^{\frac{5}{2}} (1-e\cos E)^{\frac{5}{2}} (1+e\cos E)^{\frac{1}{2}} \sin i\cos^2\alpha\, e^{\beta(r_{p_o}-r)} \tag{15-35}$$

## 15-5. ORBIT DECAY

The equations (15-33) - (15-35) give the slow variation of the five orbital elements $a$, $e$, $\omega$, $\Omega$ and $i$. In the present chapter we are concerned with the variation of the semi-major axis $a$ and the eccentricity $e$ of the osculating orbit. As seen from Eqs. (15-33) and (15-34), under the dissipative effect of the drag, the major axis decreases continuously while the eccentricity, although having an oscillatory behavior, also decreases secularly with the time. We say that the orbit undergoes a contraction and as $e$ decreases, tends to circularize itself. We shall use the method of averaging for the integration of the equations.

### 15-5.1. The Averaged Equation

First, we have for the radial distance

$$r = a(1 - e\cos E)$$

$$r_{p_o} = a_o(1 - e_o) \tag{15-36}$$

With this we write the exponential function in the equations

$$\exp\left[\beta(r_{p_o} - r)\right] = \exp\left[\beta\,(a_o - a - a_o e_o) + \beta ae\cos E\right] \tag{15-37}$$

Along each revolution, $a$ is nearly constant while the varying quantity $\beta ae\cos E$ provides the fluctuation in the air density. This leads to a natural choice of the variable

$$x \equiv \beta ae \tag{15-38}$$

to replace the eccentricity $e$, (Ref. 5).

By taking the derivative of Eq. (15-38) using the Eqs. (15-33) and (15-34) we have the equation for $x$

$$\frac{dx}{dE} = -\frac{2Z_o\beta a^2}{r_{p_o}}(e+\cos E)\left(\frac{1+e\cos E}{1-e\cos E}\right)^{\frac{1}{2}} e^{\beta(r_{p_o} - r)} \tag{15-39}$$

The new dimensionless variable $x$ behaves like the eccentricity $e$; that is, during each revolution $x$ passes through stationary values when $\cos E = -e$, but, on the average, $x$ decreases with the time. Since the decaying process is slow we can use an averaging technique (Ref. 6) applied to the right-hand sides of Eqs. (15-34) and (15-39) for $a$ and $x$.

For the equation for $a$, we have the averaged equation

$$\frac{da}{dE} = -2Z_o\frac{a^2}{r_{p_o}}\exp\left[\beta(a_o - a - a_o e_o)\right]\frac{1}{2\pi}\int_0^{2\pi}\frac{(1+e\cos E)^{3/2}}{(1-e\cos E)^{1/2}}\exp(x\cos E)\,dE \tag{15-40}$$

For small eccentricity, the integrand can be expanded in power series in $e$. Upon integrating, we have

$$\frac{da}{dE} = -2Z_o\frac{a^2}{r_{p_o}}\exp\left[\beta(a_o - a - a_o e_o)\right]\left[I_0 + 2eI_1 + \frac{3}{4}e^2(I_0 + I_2) + \frac{1}{4}e^3(3I_1 + I_3) + 0(e^4)\right] \tag{15-41}$$

where $I_n(x)$ is the Bessel function of the first kind and of imaginary argument, of order $n$

$$I_n(x) = \frac{1}{2\pi}\int_0^{2\pi}\cos nE\exp(x\cos E)\,dE \tag{15-42}$$

Similarly, the averaged equation for $x$ is

$$\frac{dx}{dE} = -2Z_o \frac{\beta a^2}{r_{p_o}} \exp\left[\beta(a_o - a - a_o e_o)\right]\left[I_1 + \frac{1}{2}e(3I_0 + I_2)\right.$$

$$\left. + \frac{1}{8}e^2(11I_1 + I_3) + \frac{1}{16}e^3(7I_0 + 8I_2 + I_4) + 0(e^4)\right] \tag{15-43}$$

The Eqs. (15-41) and (15-43) were given by Cook, King-Hele and Walker. As shown in Ref. 5, they truncated the equations to the order $e^4$, formed the equation $da/dx$ and integrated it separately for the cases where $x$ is very large and $x$ very small. We shall integrate the equation without making that asymptotic simplification, thus obtaining the solution uniformly valid for any $x$.

First, by dividing Eq. (15-41) by Eq. (15-43) and expanding the ratio in power series in $e$, we have

$$\beta \frac{da}{dx} = y_0 + \frac{1}{2}e(4 - 3y_0^2 - y_0 y_2) + \frac{1}{8}e^2\left[2y_0(3y_0 + y_2)^2 - 29y_0\right.$$

$$\left. - 2y_2 - y_0 y_3\right] + \frac{1}{16}e^3\left[-32 + 113y_0^2 + 38y_0 y_2 - y_0 y_4\right.$$

$$\left. + 2y_2^2 + 6y_0^2 y_3 + 2y_0 y_2 y_3 - 2y_0(3y_0 + y_2)^3\right] + 0(e^4) \tag{15-44}$$

where we have defined the ratios of the Bessel functions

$$y_n \equiv \frac{I_n}{I_1}, \quad n \neq 1 \tag{15-45}$$

For $x > 3$, Cook, King-Hele and Walker integrated this equation by using the asymptotic expansions of the function $y_n(x)$. In this case, the right-hand side of Eq. (15-44) has a very simple form and the major axis $a$ is obtained by quadrature. Mathematically, the method of integration they used is not rigorous since on the right-hand side, the eccentricity $e$ is a function of $x$ and $a$ by definition (15-38), so that the equation is actually a nonlinear equation in $a$. We shall arrange the equation in a form where the Poincaré method of perturbations can be applied (Ref. 7).

The Bessel functions satisfy the recurrence formula

$$I_{n-1}(x) - I_{n+1}(x) = \frac{2n}{x} I_n(x) \tag{15-46}$$

Hence, any function $y_n(x)$ can be expressed in terms of $y_0(x)$ and $x$. For example,

$$y_2(x) = y_0 - \frac{2}{x}$$

$$y_3(x) = 1 + \frac{8}{x^2} - \frac{4}{x} y_0$$

$$y_4(x) = -\frac{8}{x} - \frac{48}{x^3} + y_0 + \frac{24}{x^2} y_0$$

$$\ldots \qquad (15\text{-}47)$$

Let

$$z \equiv \frac{a}{a_o} \qquad (15\text{-}48)$$

be the dimensionless semi-major axis. Then, from Eq. (15-38) we have for the eccentricity

$$e = \epsilon \frac{x}{z} \qquad (15\text{-}49)$$

where

$$\epsilon \equiv \frac{1}{\beta a_o} \qquad (15\text{-}50)$$

is a small quantity of the order of $10^{-3}$. Then, we can write Eq. (15-44) as an equation in $z = a/a_o$

$$\frac{dz}{dx} = \epsilon y_0 + \epsilon^2 \frac{x}{z}\left(2 + \frac{y_0}{x} - 2y_0^2\right) + \epsilon^3 \frac{x^2}{2z^2}\left(\frac{1}{x} - 8y_0 - \frac{7y_0^2}{x} + 8y_0^3\right)$$

$$+ \epsilon^4 \frac{x^3}{2z^3}\left(-4 + \frac{1}{x^2} + 20y_0^2 - 10\frac{y_0}{x} + 4\frac{y_0}{x^3} - 5\frac{y_0^2}{x^2} + 20\frac{y_0^3}{x} - 16y_0^4\right)$$

$$+ 0(\epsilon^5) \qquad (15\text{-}51)$$

We see that the true nature of the equation is a nonlinear equation. Since $\epsilon$ is a very small quantity we need not go further with the expansion, and to the order of $\epsilon^4$ included, the solution of this equation can be considered as the exact solution of Eq. (15-44), truncated to the order $e^4$.

## 15-5.2. Integration by Poincaré's Method of Small Parameters

Poincaré's method for integration of a nonlinear differential equation containing a small parameter is a rigorous mathematical

technique, proven to be convergent for small values of the parameter $\epsilon$ . We assume a solution for $z$ of the form

$$z = \sum_{k=0}^{\infty} \epsilon^k z_k \tag{15-52}$$

Upon substituting into Eq. (15-51) and equating coefficients of like powers in $\epsilon$ , we have the equations for $z_k(x)$

$$\frac{dz_0}{dx} = 0$$

$$\frac{dz_1}{dx} = y_0$$

$$\frac{dz_2}{dx} = \frac{x}{z_0}\left(2 + \frac{y_0}{x} - 2y_0^2\right)$$

$$\frac{dz_3}{dx} = -\frac{xz_1}{z_0^2}\left(2 + \frac{y_0}{x} - 2y_0^2\right) + \frac{x^2}{2z_0^2}\left(\frac{1}{x} - 8y_0 - \frac{7y_0^2}{x} + 8y_0^3\right)$$

$$\frac{dz_4}{dx} = -\frac{x^2 z_1}{z_0^3}\left(\frac{1}{x} - 8y_0 - \frac{7y_0^2}{x} + 8y_0^3\right) + \frac{x}{z_0}\left(2 + \frac{y_0}{x} - 2y_0^2\right)\left(\frac{z_1^2}{z_0^2} - \frac{z_2}{z_0}\right)$$

$$+ \frac{x^3}{2z_0^3}\left(-4 + \frac{1}{x^2} + 20y_0^2 - \frac{10y_0}{x} + \frac{4y_0}{x^3} - \frac{5y_0^2}{x^2} + \frac{20y_0^3}{x} - 16y_0^4\right) \tag{15-53}$$

We also have the initial conditions.

$$z_0(x_o) = 1 \quad , \quad z_1(x_o) = z_2(x_o) = \ldots = 0 \tag{15-54}$$

The integration of Eqs. (15-53) is accomplished by successive quadratures. Its success depends on whether or not the integrals can be expressed in terms of known functions. It has been found that the following recurrence formula is useful.

$$\int p(x)\, y_0^{n+1} dx = -\frac{p(x)}{n} y_0^n + \int p(x)\, y_0^{n-1} dx + \int \left[\frac{p(x)}{x} + \frac{p'(x)}{n}\right] y_0^n \, dx \tag{15-55}$$

where $n \neq 0$ and $p(x)$ is any arbitrary function. To derive this formula, we use the well-known relation

$$xI_n'(x) + nI_n(x) = xI_{n-1}(x) \tag{15-56}$$

For $n = 1$

$$y_0 = \frac{I_1'}{I_1} + \frac{1}{x} \tag{15-57}$$

and for $n = 0$

$$I_0' = I_1(x) \tag{15-58}$$

Therefore, if $y_0 = I_0 / I_1$

$$y_0' = \frac{I_0'}{I_1} - \frac{I_0 I_1'}{I_1^2} = 1 + \frac{y_0}{x} - y_0^2 \tag{15-59}$$

Now, consider

$$\int p(x)\, d\left(\frac{y_0^n}{n}\right) = \frac{p(x)}{n} y_0^n - \int \frac{p(x)}{n} y_0^n\, dx$$

or

$$\int p(x)\, y_0^{n-1} y_0'\, dx = \int p(x)\, y_0^{n-1}\left(1 + \frac{y_0}{x} - y_0^2\right) dx = \frac{p(x)}{n} y_0^n - \int \frac{p'(x)}{n} y_0^n\, dx$$

Rearranging this equation, we have the recurrence formula (15-55). Using these relations we proceed with the integrations of the Eqs. (15-53), using the initial conditions (15-54).

First, we have

$$z_0(x) = 1 \tag{15-60}$$

and by Eq. (15-57)

$$z_1 = \log \frac{xI_1(x)}{x_o I_1(x_o)} \tag{15-61}$$

where $x_o = \beta a_o e_o$ is the initial value of $x$.

With $z_0 = 1$, the equation for $z_2$ is

$$\frac{dz_2}{dx} = 2x + y_0 - 2xy_0^2$$

Integrating

$$z_2 = x^2 + \log x\, I_1(x) - 2\int xy_0^2\, dx \tag{15-62}$$

But, by the recurrence formula (15-55) with $p(x) = x$ , $n = 1$

$$\int xy_0^2\, dx = \frac{x^2}{2} - xy_0 + 2 \log x\, I_1(x) \tag{15-63}$$

so that using in Eq. (15-62) with its initial condition, we have

$$z_2 = 2xy_0(x) - 2x_o y_0(x_o) - 3 \log \frac{xI_1(x)}{x_o I_1(x_o)} \tag{15-64}$$

The integrations for obtaining $z_3$ and $z_4$ are performed the same way but they are much more laborious. It is found that the $z_k(x)$ can be expressed in terms of two functions

$$A(x) \equiv x \frac{I_0(x)}{I_1(x)} = xy_0(x)$$

$$B(x) \equiv \log [\, xI_1(x)\,] \tag{15-65}$$

We have the final solution

$$\begin{aligned}
z_0(x) &= 1 \\
z_1(x) &= B - B_o \\
z_2(x) &= 2(A - A_o) - 3(B - B_o) \\
z_3(x) &= \frac{7}{2}(x^2 - x_o^2) - \frac{13}{2}(A - A_o) - 2(A^2 - A_o^2) \\
&\quad + 13(B - B_o) - 2A(B - B_o) + \frac{3}{2}(B - B_o)^2 \\
z_4(x) &= -\frac{35}{2}(x^2 - x_o^2) + \frac{71}{2}(A - A_o) + 3(A^2 - A_o^2) + \frac{8}{3}(A^3 - A_o^3) \\
&\quad + 4A_o(A - A_o) - 2(x^2 A - x_o^2 A_o) \\
&\quad - (69 + 6A_o + 7x^2 - 19A - 4A^2)(B - B_o) \\
&\quad - \frac{35}{2}(B - B_o)^2 - (B - B_o)^3 + 2A(B - B_o)^2
\end{aligned} \tag{15-66}$$

where $A_o$ and $B_o$ are the values of A and B evaluated at $x = x_o$ .

The semi-major axis of the orbit under contraction is

$$\frac{a}{a_o} = 1 + \epsilon z_1 + \epsilon^2 z_2 + \epsilon^3 z_3 + \epsilon^4 z_4 \tag{15-67}$$

Using $x$ as a parameter, we easily express the other quantities of interest. The eccentricity $e$ is given by Eq. (15-49), while the

drop in the periapsis is obtained from

$$\frac{r_{p_o} - r_p}{H} = \beta[\, r_{p_o} - a(1-e)] = \beta a_o - \beta a_o e_o + \beta a e - \beta a_o (1 + \epsilon z_1 + \ldots)$$

or

$$\frac{r_{p_o} - r_p}{H} = (x - x_o) - (z_1 + \epsilon z_2 + \epsilon^2 z_3 + \epsilon^3 z_4) \tag{15-68}$$

The ratio of the eccentricity is given by

$$\frac{e}{e_o} = \frac{x}{x_o z} \tag{15-69}$$

During the process of orbit contraction, the drag force is most significant along the lower part of the trajectory, near the periapsis. This results in a strong braking force at the periapsis which has the effect of reducing drastically the apoapsis distance while the periapsis distance remains nearly constant. To show this effect we can calculate the ratios of the apsidal distances as function of the variable $x$. We have

$$\frac{r_p}{r_{p_o}} = \frac{a(1-e)}{a_o(1-e_o)} = \frac{z - \epsilon x}{(1-e_o)} \tag{15-70}$$

Similarly, for the ratio of the apoapsis distances, we have

$$\frac{r_a}{r_{a_o}} = \frac{a(1+e)}{a_o(1+e_o)} = \frac{z + \epsilon x}{(1+e_o)} \tag{15-71}$$

If we want to calculate the drop in the apoapsis, we can use the formula

$$\frac{r_{a_o} - r_a}{H} = \beta[\, a_o(1+e_o) - a(1+e)] = \beta a_o - \beta a + x_o - x$$

or

$$\frac{r_{a_o} - r_a}{H} = (x_o - x) - (z_1 + \epsilon z_2 + \epsilon^2 z_3 + \epsilon^3 z_4) \tag{15-72}$$

Finally, the orbital period is simply

$$\frac{T}{T_o} = \left(\frac{a}{a_o}\right)^{3/2} = z^{3/2}(x) \tag{15-73}$$

For each initial value $\epsilon = H/a_o$, and initial eccentricity $e_o$, we can calculate the initial value $x_o = \beta a_o e_o = e_o/\epsilon$. Then, we can compute the expressions $a/a_o$, $e/e_o$, $T/T_o$, etc., as functions of $x$. Subsequently, they can be cross-plotted in any combination.

Since the quantities $a$, $e$, $T$ are all easily observable, and the integration has been performed to the order of $e^4$, for small eccentricity (which is the case for most scientific Earth satellites) the equations can be used to verify the assumption made on the atmosphere. In general, it can be, as a first approximation, assumed to be locally exponential. That is to say, the parameter $\beta$, or $H = 1/\beta$, can be assumed constant for each layer of the atmosphere. Since the value of $\beta$ enters analytically in the solution, by adjusting for concordance between the theory and the observation, determination of $\beta$ can be made.

The theory can be modified to take into account the oblateness of the planet and the atmosphere, as has been done by King-Hele (Ref. 5).

### 15-5.3. Explicit Formulas For the Orbital Elements

For small eccentricity, $e < 0.2$, the solutions obtained, Eqs. (15-66) - (15-73), are very accurate. They are in parametric form, and for each pair of values $\epsilon$ and $x_o$ they can be used to cross plot the relationship between any pair of orbital elements.

It would be useful to derive explicit formulas between any pair of orbital elements. This amounts to eliminating $x$ between any two of the equations (15-67) - (15-73). Because of the transcendental nature of the solutions, the task is cumbersome. In this respect, King-Hele, (Ref. 5), used an asymptotic expansion for the Bessel function $I_n(x)$. Since the asymptotic expansion is only valid for $x > 3$ which approximately corresponds to $e > 0.02$, it was necessary to divide the process of orbit contraction into two phases. In the first phase, $0.02 < e < 0.2$, asymptotic expansions can be used. Somewhat heuristically, an accurate and explicit expression for the major axis was obtained in terms of the eccentricity. In the second phase, $e < 0.02$, by neglecting higher order terms in $e$, the solution $z(x)$, identical to the present theory, but only to the order of $\epsilon^2$, was obtained. Explicit formulas for the second phase are not available. Since the partition of the process of orbit contraction into two phases is rather artificial, we shall offer an accurate theory uniformly valid for all values of the eccentricity in the range $0 < e < 0.2$. For very small values of $e$ the theory is no longer valid, but by then the satellite is only a few revolutions before effective entry into the planetary atmosphere.

To derive the explicit expression for the major axis in terms of the eccentricity, we write the equation (15-67) as

$$z = p + \epsilon\phi(z) \tag{15-74}$$

where, by observing that

$$x \equiv \beta a e = \beta a_o e_o \left(\frac{a}{a_o}\right)\left(\frac{e}{e_o}\right)$$

we can write

$$x = \alpha z \tag{15-75}$$

with

$$\alpha \equiv x_o k \quad , \quad k \equiv \frac{e}{e_o} \tag{15-76}$$

Then, explicitly

$$\phi(z) = z_1(\alpha z) + \epsilon z_2(\alpha z) + \epsilon^2 z_3(\alpha z) + \ldots \tag{15-77}$$

Equation (15-74) is in the form to which a Lagrange expansion can be successfully applied. We have, (Ref. 8),

$$z = p + \sum_{n=1}^{\infty} \frac{\epsilon^n}{n!}\left(\frac{d}{dp}\right)^{n-1}[\phi(p)]^n \tag{15-78}$$

If we carry out the expansion and then put $p = 1$, we shall have to the order of $\epsilon^4$

$$z = 1 + \epsilon h_1(\alpha) + \epsilon^2 h_2(\alpha) + \epsilon^3 h_3(\alpha) + \epsilon^4 h_4(\alpha) \tag{15-79}$$

where

$$\begin{aligned}
h_1 &= B - B_o \\
h_2 &= 2(A - A_o) + (A - 3)(B - B_o) \\
h_3 &= \frac{7}{2}(\alpha^2 - x_o^2) - (2A_o + \frac{13}{2})(A - A_o) + (13 + 2\alpha^2 - 4A - A^2)(B - B_o) \\
&\quad + \frac{1}{2}(3 + \alpha^2 + A - A^2)(B - B_o)^2 \\
h_4 &= -\frac{1}{2}(\alpha^2 - x_o^2)(35 + 4A_o - 7A) \\
&\quad + \frac{1}{6}(A - A_o)(213 + 42A_o + 16A_o^2 + 12\alpha^2 - 9A + 4A_o A - 8A^2) \\
&\quad - \frac{1}{2}(B - B_o)(138 + 25\alpha^2 - 46A - 7A^2 - 2A^3) \\
&\quad - \frac{1}{2}(B - B_o)^2(35 + 7\alpha^2 - 6A^2 + \alpha^2 A - A^3) \\
&\quad + 2(A - A_o)(B - B_o)(3 + \alpha^2 + A - A^2) \\
&\quad - \frac{1}{6}(B - B_o)^3(6 - \alpha^2 + 2\alpha^2 A + 3A^2 - 2A^3)
\end{aligned} \tag{15-80}$$

with the definition

$$A \equiv \alpha \frac{I_0(\alpha)}{I_1(\alpha)}$$

$$B \equiv \log [\alpha I_1(\alpha)] \tag{15-81}$$

Since $\alpha = \beta a_o e$, the solution, as given by Eqs. (15-79) - (15-81) provides an explicit expression of the variation of the dimensionless major axis $a/a_o$ in terms of the eccentricity.

The other orbital elements can also be expressed in terms of $e$. The drop in the periapsis is seen to be

$$\frac{r_{p_o} - r_p}{H} = (\alpha - x_o) - (1 - e)(h_1 + \epsilon h_2 + \epsilon^2 h_3 + \epsilon^3 h_4) \tag{15-82}$$

For the apoapsis, we have

$$\frac{r_{a_o} - r_a}{H} = (x_o - \alpha) - (1 + e)(h_1 + \epsilon h_2 + \epsilon^2 h_3 + \epsilon^3 h_4) \tag{15-83}$$

By replacing $x$ by $\alpha z$ in Eq. (15-70), we have the ratio of the periapsis distances

$$\frac{r_p}{r_{p_o}} = \frac{(1 - \epsilon\alpha)}{(1 - e_o)} z \tag{15-84}$$

where $z$ is given by the Eqs. (15-79) and (15-80).

For the ratio of the apoapsis distances, we have

$$\frac{r_a}{r_{a_o}} = \frac{(1 + \epsilon\alpha)}{(1 + e_o)} z \tag{15-85}$$

The orbital period is now

$$\frac{T}{T_o} = z^{3/2}(\alpha) \tag{15-86}$$

which is a function of the eccentricity. As pointed out by King-Hele, this equation provides a powerful method of verifying the assumption made on the atmosphere from two of the most accurate and easily measured orbital parameters, namely the period of revolution and the eccentricity.

### 15-5.4. The Contraction of Orbits

The solution (15-66) can be considered as the exact analytical solution of the nonlinear differential equation (15-51). Both this solution and the explicit solution in terms of the eccentricity, Eq. (15-80), have been computed for a number of orbits and they provide about nearly identical results. As illustrative examples, we consider the following initial orbits

$$\text{Orbit 1 : } \epsilon = 0.008 \quad , \quad e_o = 0.2 \rightarrow x_o = 25$$

$$\text{Orbit 2 : } \epsilon = 0.009 \quad , \quad e_o = 0.225 \rightarrow x_o = 25$$

Figure 15-3 plots the variation of the major axis versus the eccentricity using the explicit solution, uniformly valid for all eccentricities. In this figure and in the following figures the circles represent the exact solution.

Figure 15-4 plots the variation of the orbital period while Fig. 15-5 presents the drop in the periapsis. It is seen that the decrease in the periapsis is very slow. This can be seen clearly in Fig. 15-6 where the ratios $r_p / r_{p_o}$ and $r_a / r_{a_o}$ are plotted versus the eccentricity. When $e / e_o = 0.1$ the calculated values for orbit 1 are $r_p / r_{p_o} = 0.987160$ and $r_a / r_{a_o} = 0.684968$ and the corresponding values for orbit 2 are found to be $r_p / r_{p_o} = 0.985136$ and $r_a / r_{a_o} = 0.651941$.

### 15-5.5. Contraction of Highly Eccentric Orbits

For the case of orbits with large eccentricities, since $x = \beta a e$, when $e \rightarrow 1$, $a \rightarrow \infty$, x becomes very large and the asymptotic expression for Bessel's ratio $y_0(x)$ is

$$y_0 = 1 + \frac{1}{2x} + \ldots$$

$$y_0^2 = 1 + \frac{1}{x} + \ldots \tag{15-87}$$

Using this form in Eq. (15-51) we have

$$\frac{dz}{dx} = \epsilon \left(1 + \frac{1}{2x}\right) - \frac{\epsilon^2}{z} + \frac{\epsilon^3 x}{z^2} - \frac{\epsilon^4 x^2}{z^3} + \ldots \tag{15-88}$$

an equation which can be seen as the development of

$$\frac{dz}{dx} = \epsilon \left(1 + \frac{1}{2x}\right) - \frac{\epsilon^2}{z + \epsilon x} \tag{15-89}$$

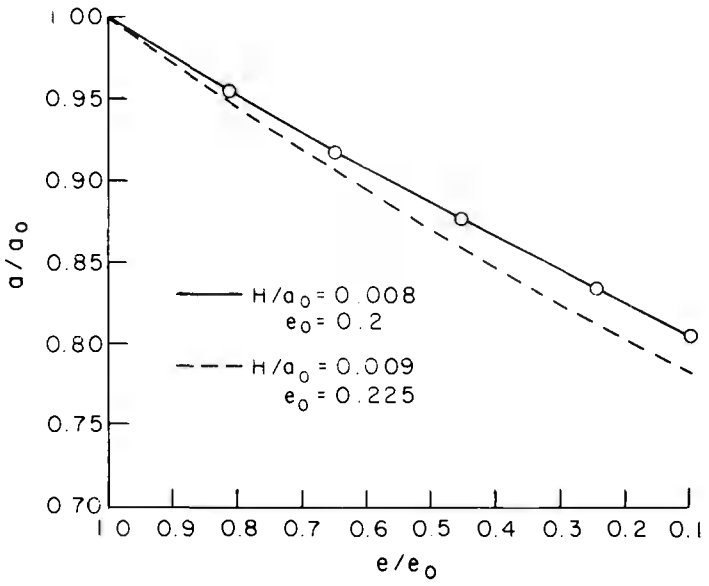


Fig. 15-3. Variation of semi-major axis with eccentricity.

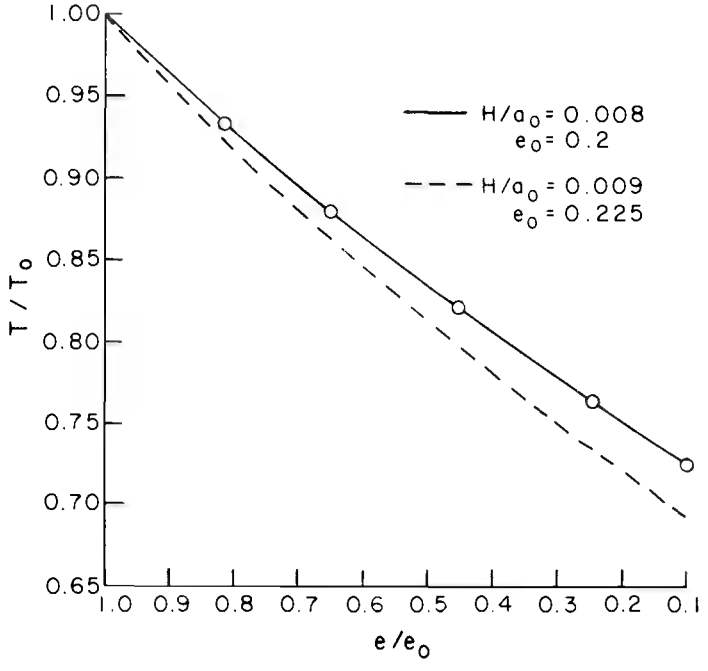


Fig. 15-4. Variation of orbital period with eccentricity.

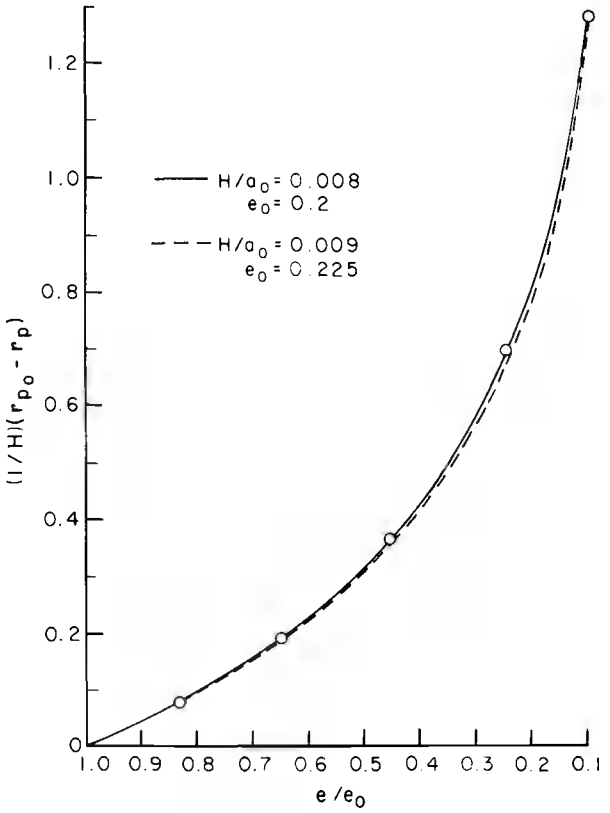


Fig. 15-5. Variation of periapsis with eccentricity.

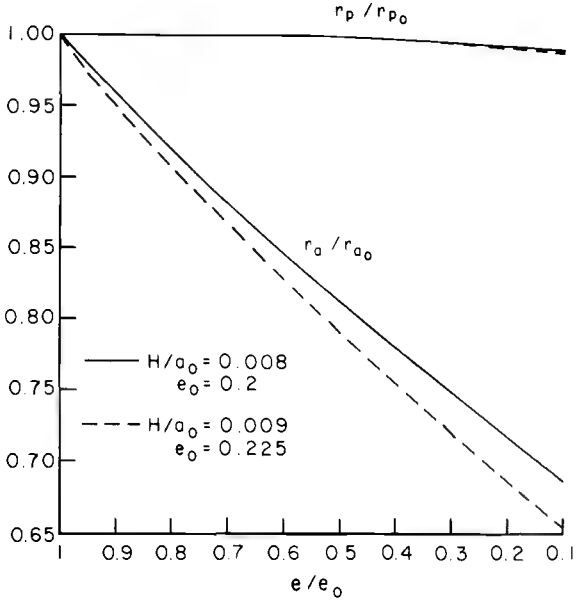


Fig. 15-6. Comparison between periapsis drop and apoapsis drop.

Using the transformation

$$z = \epsilon (x + q) \tag{15-90}$$

and changing the independent variable from $x$ to $q$ we have the Bernouilli equation

$$\frac{dx}{dq} = 2x + \frac{4x^2}{q} \tag{15-91}$$

By the change of variable

$$x = \frac{e^{2q}}{K(q)} \tag{15-92}$$

the equation becomes

$$\frac{dK}{dq} = -\frac{4e^{2q}}{q}$$

Integrating, we find that K can be expressed in terms of the exponential integral

$$K = -4 \int \frac{e^{2q}}{2q} \, d(2q) + C$$

$$= -4 \, E_i(2q) + C \tag{15-93}$$

Thus, in the case of highly eccentric orbit we have the exact solution in parametric form

$$x = \frac{e^{2(q - q_o)}}{\frac{1}{x_o} + 4e^{-2q_o} \left[ E_i(2q_o) - E_i(2q) \right]} \tag{15-94}$$

along with Eq. (15-90) and the initial conditions

$$z(x_o) = 1 \quad , \quad q_o = \frac{(1 - e_o)}{\epsilon} \tag{15-95}$$

To evaluate the exponential integral, we first observe that the argument $2q$ is large, hence its asymptotic form is adequate. In general, we consider the integral

$$E_n(x) = \int e^x x^{n-1} \, dx \tag{15-96}$$

By integration by parts

$$E_n(x) = x^{n-1} e^x - (n - 1) E_{n-1}$$

By repeated application of this formula, we deduce the asymptotic expansion for large $x$

$$E_n(x) = x^{n-1} e^x \left[ 1 - \frac{(n-1)}{x} + \frac{(n-1)(n-2)}{x^2} - \frac{(n-1)(n-2)(n-3)}{x^3} + \dots \right] \tag{15-97}$$

When $n = 0$, we have the exponential integral and by taking 6 terms of the series, for $x > 50$, the solution is identical to the numerical values tabulated in Ref. 9.

## 15-6. LIFETIME OF THE SATELLITE

We now examine the problem of the duration of the satellite in its orbit. First we consider the Kepler's equation

$$\sqrt{\frac{\mu}{a^3}}\, t = E - e \sin E$$

or in its differential form

$$\frac{dt}{dE} = \frac{a^{3/2}}{\sqrt{\mu}} (1 - e \cos E) \tag{15-98}$$

The average equation is obviously

$$\frac{dt}{dE} = \frac{a^{3/2}}{\sqrt{\mu}} = \frac{T_o}{2\pi} \left( \frac{a}{a_o} \right)^{3/2} \tag{15-99}$$

where $T_o$ is the initial orbital period. By dividing this equation by Eq. (15-43), we have the average equation for the time

$$\frac{dt}{dx} = - \frac{T_o r_{p_o} \exp(x_o)}{4\pi \beta a_o^2 z_o} \frac{\exp[\beta a_o (z-1)]}{z^{1/2} [I_1 + \frac{1}{2} e (3I_0 + I_2) + \dots]} \tag{15-100}$$

Using the solution (15-67) for $z = a/a_o$ we have for the exponential

$$\begin{aligned} \exp[\beta a_o (z-1)] &= \exp[z_1 + \epsilon z_2 + \epsilon^2 z_3 + \dots] \\ &= \exp(z_1) [1 + \epsilon z_2 + \frac{\epsilon^2}{2} (z_2^2 + 2z_3) + \dots] \\ &= \frac{x I_1(x)}{x_o I_1(x_o)} [1 + \epsilon z_2 + \frac{\epsilon^2}{2} (z_2^2 + 2z_3) + \dots] \end{aligned}$$

Next, we define the dimensionless time $\tau$ as

$$\tau \equiv \frac{2\pi\beta a_o^2 \rho_{p_o} SfC_D}{m T_o} x_o I_1(x_o)\left[\exp(-x_o)\right]t \tag{15-101}$$

Then, the dimensionless time equation has the form

$$\frac{d\tau}{dx} = -\frac{x\left[1+\epsilon z_2+\frac{\epsilon^2}{2}(z_2^2+2z_3)+\ldots\right]}{z^{1/2}\left[1+\frac{\epsilon x}{2z}(3y_0+y_2)+\frac{\epsilon^2 x^2}{8z^2}(11+y_3)+\ldots\right]} \tag{15-102}$$

If $z$ is replaced by its expression and then the binomial expansion is applied, we have to the order of $\epsilon^2$, inclusively,

$$\begin{aligned}\frac{d\tau}{dx} = -x\Big[1-\frac{\epsilon}{2}(z_1-2z_2+3xy_0+xy_2)+\frac{\epsilon^2}{8}(-11x^2-x^2y_3+18xy_0z_1 \\ +6xy_2z_1+18x^2y_0^2+2x^2y_2^2+12x^2y_0y_2-12xy_0z_2-4xy_2z_2 \\ +3z_1^2-4z_2-4z_1z_2+4z_2^2+8z_3)\Big]\end{aligned} \tag{15-103}$$

Finally, if the functions $z_i(x)$ as given by the solution (15-66) are substituted into this equation, the time $\tau$ is obtained by quadrature. Explicitly, by letting

$$\tau = \tau_0+\epsilon\tau_1+\epsilon^2\tau_2 \tag{15-104}$$

we have the following equations

$$\begin{aligned}\tau_0' &= -x \\ \tau_1' &= (2A_o-1)x+\frac{7}{2}x(B-B_o) \\ \tau_2' &= -2x^3+\frac{1}{2}(7x_o^2-8A_o^2-11A_o)x+9x^2y_0 \\ &\quad -(10+7A_o)(B-B_o)x-\frac{63}{8}x(B-B_o)^2\end{aligned} \tag{15-105}$$

with $(\,)' = d(\,)/dx$. Integrating the first equation from $x_o$, we have

$$\tau_0 = \frac{1}{2}(x_o^2-x^2) \tag{15-106}$$

For the other two equations some of the quadratures cannot be expressed in terms of elementary functions. For an accurate treatment, we can tabulate these integrals. But, to obtain an explicit expression for the time, an approximation has to be used.

For elliptic orbits, when $e > 0.02$ (which corresponds approximately to $x > 3$), we have the following asymptotic expansion for the Bessel function $I_n(x)$

$$I_n(x) = \frac{\exp x}{\sqrt{2\pi x}} \left[ \sum_{m=0}^{\infty} \frac{(-1)^m (4n^2 - 1^2)(4n^2 - 3^2) \cdots [4n^2 - (2m-1)^2]}{m!\,(8x)^m} \right] \tag{15-107}$$

In particular, we have for $x > 3$

$$I_0(x) = \frac{\exp x}{\sqrt{2\pi x}} \left[ 1 + \frac{1}{8x} + \frac{9}{128x^2} + \cdots \right]$$

$$I_1(x) = \frac{\exp x}{\sqrt{2\pi x}} \left[ 1 - \frac{3}{8x} - \frac{15}{128x^2} - \cdots \right] \tag{15-108}$$

Using these expansions, we have to the order of $1/x$

$$A = x \frac{I_0(x)}{I_1(x)} = x + \frac{1}{2} + \frac{3}{8x} + \cdots$$

$$B - B_o = \log \frac{x I_1(x)}{x_o I_1(x_o)} = (x - x_o) + \frac{1}{2} \log \frac{x}{x_o} + \frac{3(x - x_o)}{8 x x_o} + \cdots \tag{15-109}$$

With the expansions substituted into the equation for $\tau_1$, we have after integration

$$\tau_1 = \frac{21}{16}(x_o - x) + \frac{1}{4}\left(3x_o + \frac{7}{4} - \frac{33}{8x_o}\right)(x_o^2 - x^2) - \frac{7}{6}(x_o^3 - x^3) + \frac{7}{8} x^2 \log \frac{x}{x_o} \tag{15-110}$$

For the equation in $\tau_2$, we take approximately

$$x^2 y_0 = x^2$$

$$A_o = x_o$$

$$A_o^2 = x_o^2 + x_o$$

$$B - B_o = (x - x_o)$$

to have

$$\tau_2' = \frac{1}{8}(4x_o - 11x_o^2)\,x + \frac{1}{4}(35x_o - 4)\,x^2 - \frac{79}{8}\,x^3 \qquad (15\text{-}111)$$

Integrating, we obtain

$$\tau_2 = -\frac{1}{16}(4x_o - 11x_o^2)(x_o^2 - x^2) - \frac{1}{12}(35x_o - 4)(x_o^3 - x^3) + \frac{79}{32}(x_o^4 - x^4) \qquad (15\text{-}112)$$

The solution(15-104) with $\tau_i(x)$ as given by the Eqs. (15-106), (15-110) and (15-112) , gives the dimensionless time $\tau$ as a function of $x$ for large $x$ . Although it is valid for $x > 3$ , we can have a good estimate of the time the satellite remains in orbit by evaluating the lifetime $\tau_L$ obtained by putting $e = 0$ , or equivalently $x = 0$ . Then, we have the lifetime given as:

$$\epsilon^2 \tau_L = \frac{1}{2} e_o^2 \left(1 - \frac{5}{6} e_o + \frac{23}{48} e_o^2 + \frac{7}{8}\epsilon + \frac{\epsilon e_o}{6} + \frac{9\epsilon^2}{16 e_o}\right) \qquad (15\text{-}113)$$

As with the orbital elements, it is possible to express the time in terms of the eccentricity. For this purpose, we use the relation $x = x_o zk$ to write the expression for the time,

$$\begin{aligned}\epsilon^2 \tau = {} & \frac{e_o^2}{2}(1 - z^2k^2)\left[1 + \frac{1}{2}(3 - \epsilon)e_o + \frac{11}{8}e_o^2 + \frac{7}{8}\epsilon - \frac{33\epsilon^2}{16 e_o}\right] \\ & - \frac{e_o^3}{12}(1 - z^3k^3)(14 + 35e_o - 4\epsilon) + \frac{79}{32}e_o^4(1 - z^4k^4) \\ & + \frac{21}{16}\epsilon^2 e_o(1 - zk) + \frac{7}{8}\epsilon e_o^2 z^2k^2 \log(zk)\end{aligned} \qquad (15\text{-}114)$$

Since $z$ has been obtained explicitly in terms of $k = e/e_o$ through the Eqs. (15-79) and (15-80), this expression gives the dimensionless time in terms of the eccentricity. To be consistent with the approximation used in deriving Eq. (15-114), we shall use the expression for $z$ in its asymptotic expansion form. Then, to the order of $\epsilon$ ,

$$\begin{aligned} z &= 1 + \epsilon\,[\,B(\alpha) - B_o\,] \\ &= 1 + \epsilon(\alpha - x_o) + \frac{\epsilon}{2}\log\frac{\alpha}{x_o} \end{aligned}$$

or

$$z = 1 - e_o(1 - k) + \frac{\epsilon}{2}\log k \qquad (15\text{-}115)$$

By substituting into Eq. (15-114), we have, to the order of $\epsilon$,

$$\epsilon^2\tau = \epsilon^2\tau_L - \frac{e_o^2}{2} z^2 k^2 \left[1 + \frac{3e_o}{2} + \frac{11}{8} e_o^2 + \frac{7}{8}\epsilon - \frac{\epsilon e_o}{2} - \frac{e_o}{6} zk(14 + 35e_o - 4\epsilon) + \frac{79}{16} e_o^2 z^2 k^2 - \frac{7}{4}\epsilon \log k\right] \tag{15-116}$$

Dividing this equation by Eq. (15-113), we have

$$\frac{\tau}{\tau_L} = 1 - z^2 k^2 \left[1 + \frac{3e_o}{2} + \frac{11}{8} e_o^2 + \frac{7}{8}\epsilon - \frac{\epsilon e_o}{6} zk(14 + 35e_o - 4\epsilon) + \frac{79}{16} e_o^2 z^2 k^2 - \frac{7}{4}\epsilon \log k\right] / \left[1 - \frac{5}{6} e_o + \frac{23}{48} e_o^2 + \frac{7}{8}\epsilon + \frac{\epsilon e_o}{6}\right] \tag{15-117}$$

where $z$ is given by its simple expression (15-115).

Figure 15-7 plots the ratio $\tau/\tau_L$ for the two orbits considered in the previous section using the Eqs. (15-115) and (15-117). The two curves plotted in solid lines are nearly identical. It is found that they are very close to the curve using the simple parabolic law suggested by King-Hele (Ref. 5).

$$\frac{\tau}{\tau_L} = 1 - k^2 \tag{15-118}$$

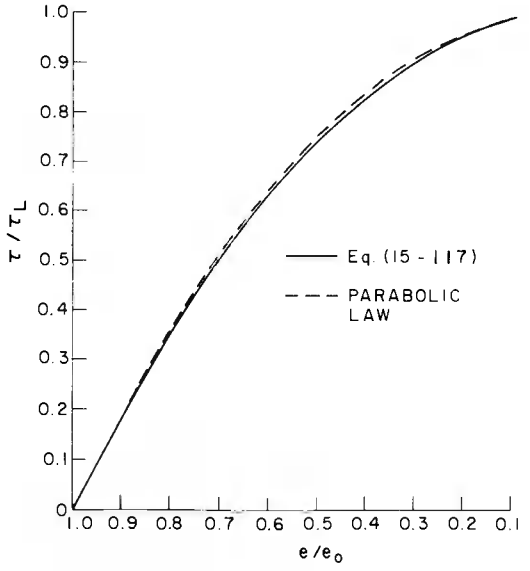


Fig. 15-7. Variation of $\tau/\tau_L$ with eccentricity.

In practice, the solution (15-117) is valid down to an eccentricity of about $e \approx 0.02$. When this eccentricity is reached, solution by asymptotic expansions is no longer valid. The equation (15-103) has to be integrated again using a different approximation. This is also the case where the initial orbit is nearly circular. Since $e$ is very small, the value of $x$ is also small, with $x < 3$, and we only need to consider the solution for $\tau_0$ and $\tau_1$. The solution for $\tau_0$ is exact, as given by Eq. (15-106). For the equation in $\tau_1$, the second of the Eqs. (15-105), we have the series expansion of the Bessel function $I_n(x)$ for small $x$

$$I_n(x) = \sum_{m=0}^{\infty} \frac{(\frac{1}{2}x)^{n+2m}}{m!(n+m)!} \tag{15-119}$$

In particular, we have

$$I_0 = 1 + \frac{x^2}{4} + \frac{x^4}{64} + \frac{x^6}{2304} + \cdots$$

$$I_1 = \frac{x}{2}\left(1 + \frac{x^2}{8} + \frac{x^4}{192} + \frac{x^6}{9216} + \cdots\right) \tag{15-120}$$

Therefore,

$$A = xy_0 = 2 + \frac{x^2}{4} - \frac{x^4}{96} + \cdots \tag{15-121}$$

This series is obtained by the binomial expansion and its convergence requires that $x > I_1(x)$, that is, $x < 2.4$. To extend its validity, King-Hele suggested the empirical formula

$$A = xy_0 = 2 + \frac{x^2}{5} \tag{15-122}$$

which, although less accurate than the exact expansion, (15-121), for small $x$, never has an error more than $0.07$ for larger values of $x$.

We now write the equation for $\tau_1$

$$\frac{d\tau_1}{dx} = \left(\frac{A_o}{4} - 1 - \frac{7}{2}B_o\right)x - \frac{7}{4}x(A - A_o) + \frac{7}{2}\frac{d}{dx}\left(\frac{1}{2}x^2 B\right) \tag{15-123}$$

Using the approximation (15-122) for $A$ and $A_o$, we have, upon integrating the equation from $x_o$,

$$\tau_1 = -\frac{1}{20}(4x_o^2 - 5)(x_o^2 - x^2) + \frac{7}{80}(x_o^4 - x^4) - \frac{7}{4}x^2(B_o - B) \tag{15-124}$$

Hence, for small eccentricity, the expression for the dimensionless time is

$$\epsilon^2\tau = \frac{e_o^2}{2}\left\{(1-\frac{x^2}{x_o^2})[\,1+\frac{\epsilon}{2}(1+\frac{7}{20}x^2-\frac{9}{20}x_o^2)] - \frac{7}{2}\epsilon\frac{x^2}{x_o^2}(B_o-B)\right\} \tag{15-125}$$

This expression is identical to the one given in Ref. 5, since that analysis corresponds to the present theory up through the order of $\epsilon^2$. Beyond this order, the integration in Ref. 5 involves some heuristic steps which have been avoided in the present development. By putting $x = 0$ in the equation above, we obtain the lifetime of the satellite from the initial eccentricity, $e_o$, assumed small.

$$\epsilon^2\tau_L = \frac{e_o^2}{2}\left[\,1-\frac{\epsilon}{2}(\frac{9}{20}x_o^2-1)\right] \tag{15-126}$$

By dividing Eq. (15-125) by Eq. (15-126), retaining only the order $\epsilon$, we have

$$\frac{\tau}{\tau_L} = 1-\frac{x^2}{x_o^2}+\frac{7}{2}\epsilon\frac{x^2}{x_o^2}\left[\frac{(x_o^2-x^2)}{20}-(B_o-B)\right] \tag{15-127}$$

Now, if we write $x = x_o kz = x_o k - \epsilon x_o k(B_o - B)$, we can put the equation in the form

$$\frac{\tau}{\tau_L} = 1-k^2+\frac{7}{2}\epsilon k^2\left[\frac{x_o^2}{20}(1-k^2)-\frac{3}{7}(B_o-B)\right] \tag{15-128}$$

where the argument of $B$ is $x = x_o kz = \alpha z$. But, to the order $\epsilon$, the solution

$$z = 1-\epsilon(B_o-B) \tag{15-129}$$

is the same for both arguments $x$ and $\alpha = x_o k$. Hence, to the order of $\epsilon$, Eqs. (15-128) gives the explicit expression for the ratio $\tau/\tau_L$ in terms of $k$ where

$$B = \log\,[\alpha\, I_1(\alpha)]\,,\quad \alpha = x_o k \tag{15-130}$$

Considering the fact that both $x_o$ and $B_o$ are about 3, the contribution of the $\epsilon$ term in Eq. (15-128) is small and for small eccentricity, the parabolic law as given by Eq. (15-118) is still valid.

Equation (15-128) is of the form (15-74) where $p = 1 - \tau/\tau_L$ and the function to be found is $k^2$. Hence, applying the Lagrange expansion to find $k^2$ and then taking the square root, we can express the eccentricity as a function of the time:

$$\frac{e}{e_o} = \sqrt{1-\frac{\tau}{\tau_L}}\left[1+\frac{7}{80}\epsilon x_o^2(\frac{\tau}{\tau_L})-\frac{3\epsilon}{4}(B_o-B)\right] \tag{15-131}$$

where

$$B_o = \log x_o I_1(x_o)$$

$$B = \log \left[ x_o \sqrt{1 - \frac{\tau}{\tau_L}} \; I_1\left(x_o \sqrt{1 - \frac{\tau}{\tau_L}}\right) \right] \qquad (15\text{-}132)$$

Numerical computation has been done for several orbits and it is found that the parabolic law is adequate. Hence, Fig. 15-7 can be used for any elliptic orbit up to $e_o \approx 0.2$.

A higher order analysis of the theory has been presented in Ref. 10. Using the same approach, the theory has been extended to the case of an oblate planet and oblate atmosphere in Ref. 12.

## References


1. Vinh, N. X., and Brace, F. C., "Qualitative and Quantitative Analysis of the Exact Atmospheric Entry Equations Using Chapman's Variables," IAF paper No. 74-010, XXVth Congress of the International Astronautical Federation, Amsterdam, October 1974.

2. Busemann, A., Vinh, N. X., and Culp, R. D., "Solution of the Exact Equations for Three-Dimensional Atmospheric Entry Using Directly Matched Asymptotic Expansions," NASA Report CR-2643, 1976.

3. Vinh, N. X., Busemann, A., and Culp, R. D., "Optimum Three-Dimensional Atmospheric Entry," Acta Astronautica, Vol. 2, pp. 593-611, 1975.

4. Frostic, F., and Vinh, N. X., "Optimal Aerodynamic Control By Matched Asymptotic Expansions," Acta Astronautica, Vol. 3, pp. 319-332, 1976.

5. King-Hele, D., Theory of Satellite Orbits in An Atmosphere, Butterworths, London, 1964.

6. Bogoliubov, N. N., and Mitropolsky, Y. A., Asymptotic Methods in the Theory of Non-Linear Oscillations, Gordon and Breach Sc. Publishers, Inc., New York, 1961.

7. Poincaré, H., Les Méthodes Nouvelles de la Mécanique Céleste, Vol. 2, Dover reprint, 1957.

8. Bellman, R., Perturbation Techniques in Mathematics, Physics and Engineering, Holt, Rinehart and Winston, Inc., New York, 1964.

9. Abramowitz, M., and Stegun, I. A., Handbook of Mathematical Functions, Dover Publications, Inc., New York, 1972.

10. Longuski, J.M., "Analytic Theory of Orbit Contraction and Ballistic Entry into Planetary Atmopsheres," Ph. D. thesis, The University of Michigan, 1979.

11. Vinh, N.X., Longuski, J.M., Busemann, A. and Culp, R.D., "Analytic Theory of Orbit Contraction Due to Atmospheric Drag," Acta Astronautica, Vol. 6, pp. 697-723, 1979.

12. Chen, W.T., "Satellite Orbits under the Influence of Air Drag, Rotating Oblate Atmosphere and Planet's Oblateness," Ph. D. thesis, University of Colorado, 1977.

# Chapter 16

# Flight with Lift Modulation

## 16-1. INTRODUCTION

Until now we have considered entry trajectories with constant angle of attack and constant bank angle. A space vehicle entering a planetary atmosphere and having control devices allowing modulation of the lift coefficient and the bank angle will have more flexibility in the selection of the appropriate trajectory. For a highly maneuverable vehicle, lift and bank controls can guide the vehicle along a prescribed trajectory to a correct presentation for making the final approach and landing. Also, as has been shown in Chapter 9 and Chapter 12, lift control can be performed to reduce the overall heating or the peak deceleration. It can be used to widen the entry corridor. Lift and bank controls, used in an optimally coordinated manner, may reduce to a strict minimum the fuel consumption for an orbital maneuver of a lifting vehicle (Ref. 1).

For these reasons, starting with this chapter, we shall analyze the motion of an entry vehicle having the capability of controlling the lift program along its trajectory.

We shall first modify the universal equations, developed in Chapter 13 for constant angle of attack and bank angle, put them in the form where the lift coefficient and the bank angle are variable, and then use these equations to study successively the following entry trajectories:

1. Entry at constant flight path angle.
2. Entry at constant rate of descent.
3. Entry at constant speed.
4. Entry at constant dynamic pressure.
5. Entry at constant heating rate.

The equations with lift and bank modulation are derived in this chapter. Different constraints imposed upon the state of the vehicle will be discussed and a theory of flight path control for satisfying these constraints will be presented. Examples of flight subject to constraints as mentioned above will be analyzed later.

The examples considered above are selected solely to present some fascinating aspects of entry with aerodynamic maneuvering capabilities, but the equations derived can be used to analyze entry

satisfying any other prescribed constraint. In particular, they can be used in connection with optimization problems.

## 16-2. THE DRAG POLAR

It has been noted earlier that the drag coefficient $C_D$ and the lift coefficient $C_L$ are functions of the angle of attack, the Mach number, and the Reynolds number

$$C_D = C_D(\alpha, M, R_e)$$

$$C_L = C_L(\alpha, M, R_e) \tag{16-1}$$

For each aerodynamic configuration, elimination of the angle of attack from the parametric equation (16-1) leads to the drag-lift relationship

$$C_D = C_D(C_L, M, R_e) \tag{16-2}$$

For constant Mach number and Reynolds number the plot of the drag coefficient $C_D$ versus the lift coefficient $C_L$ is called the drag polar (Fig. 16-1).

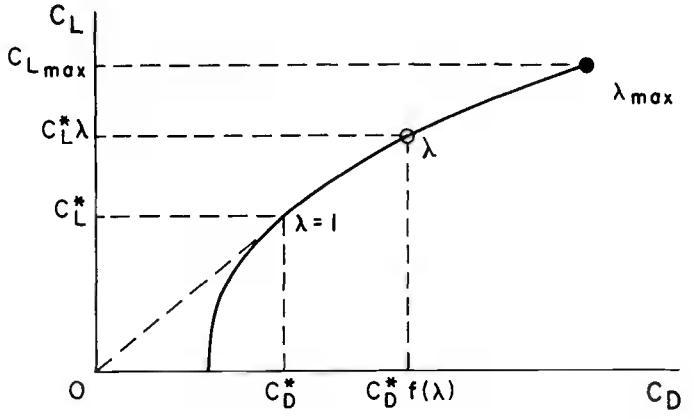


Fig. 16-1. The drag polar.

In general, the relationship holds for the range of the angle of attack less than a critical angle of attack called the stalling angle of attack. When this angle is exceeded, the effect of flow separation becomes important; the value of $C_L$ drops suddenly, while $C_D$ continues to increase to a maximum value. While the maximum value of $C_D$ can be used for pure ballistic entry, flight with lift modulation is always effected at an angle of attack less than the critical value. For safety reasons, the angle of attack is limited at a maximum value, $\alpha_M$,

near the stalling angle of attack, $\alpha_S$ . To this value, corresponds a maximum value of the lift coefficient, $C_{L_{max}}$ .

An important parameter in the design of lifting vehicles is the lift-to-drag ratio, or aerodynamic efficiency

$$E = \frac{C_L}{C_D} \tag{16-3}$$

As are the lift and the drag coefficients, the aerodynamic efficiency is a function of the angle of attack, the Mach number and the Reynolds number. For constant Mach number and Reynolds number, $E$ varies with the angle of attack; as $\alpha$ increases, $E$ increases, reaches a maximum value $E^*$ , and then decreases.

The drag coefficient $C_D$ can be decomposed into two parts, the zero-lift drag coefficient $C_{D_o}$ and the induced drag coefficient $C_{D_i}$ (Ref. 2).

$$C_D = C_{D_o} + C_{D_i} \tag{16-4}$$

For most vehicle aerodynamic configurations, the induced drag coefficient can be represented in the form

$$C_{D_i} = K C_L^{\,n} \tag{16-5}$$

Hence, we write the lift-drag relationship

$$C_D = C_{D_o} + K C_L^{\,n} \tag{16-6}$$

This is a modeling form of the general relationship (16-2). Hence, the zero-lift drag coefficient $C_{D_o}$ , the induced drag factor $K$ , and also the exponent $n$ are functions of the Mach number and the Reynolds number. For constant Mach and Reynolds number these coefficients are constants and can be selected to best represent the drag polar obtained through wind tunnel measurements. For subsonic flight, the approximation $n = 2$ can be used and the drag polar is called the parabolic polar. For thin-winged vehicles operating in the hypervelocity regime, $n$ is about 3/2.

With the assumed form, (16-6), the lift-to-drag ratio is

$$E = \frac{C_L}{C_{D_o} + K C_L^{\,n}} \tag{16-7}$$

$E$ reaches its maximum when $dE/dC_L = 0$ , that is when

$$C_L = \left[\frac{C_{D_o}}{(n-1)\,K}\right]^{1/n} = C_L^* \tag{16-8}$$

To this value, corresponds a $C_D^*$

$$C_D^* = \frac{n}{n-1}\, C_{D_o} \tag{16-9}$$

with the maximum lift-to-drag ratio being

$$E^* = \left(\frac{1}{n}\right)\left(\frac{1}{K}\right)^{1/n}\left(\frac{n-1}{C_{D_o}}\right)^{(n-1)/n} \tag{16-10}$$

To simplify the analysis we shall assume that the lift-drag relationship is independent of the Mach number and the Reynolds number. This assumption is essentially correct for flight in the hypervelocity regime. On the other hand, it is possible to write the equations of motion with a general drag polar. In this respect, we define a rescaled lift coefficient $\lambda$ such that

$$C_L = C_L^*\, \lambda \tag{16-11}$$

where $C_L^*$ is the lift coefficient corresponding to maximum lift-to-drag ratio. When $C_L$ reaches its maximum, $\lambda$ has its maximum value, $\lambda_{max} = C_{L_{max}} / C_L^*$ . Then, for constant Mach number and Reynolds number, we write the general lift-drag relationship (16-2) as

$$C_D = C_D^*\, f(\lambda) \tag{16-12}$$

where $f(\lambda)$ is some appropriate function defining the drag polar, and $C_D^*$ is the value of $C_D$ at maximum lift-to-drag ratio. When $\lambda = 1$ , the flight is effected at maximum lift-to-drag ratio, and as a consequence $f(1) = 1$ . For a generalized drag polar representing the relation (16-6), using the relations (16-8), (16-9) and (16-11) we have

$$C_D = \frac{n-1}{n}\, C_D^* + \frac{\lambda^n}{n}\, C_D^* \tag{16-13}$$

Comparing with Eq. (16-12) we see that, for a generalized drag polar

$$f(\lambda) = \frac{(n-1) + \lambda^n}{n} \tag{16-14}$$

When $n = 2$ , we have a parabolic drag polar.

## 16-3. UNIFIED EQUATIONS WITH VARYING LIFT COEFFICIENT AND BANK ANGLE

The dimensionless equations, using modified Chapman's variables, have been derived in Chapter 13. The equations can be used to analyze motion with modulation of the lift coefficient and the bank angle if we assume that the drag coefficient remains unchanged. This simplification has been used by various authors, but, as has been pointed out in Chapter 12 on the entry corridor, strong coupling between the drag and the lift coefficients has important effects on entry physical quantities. Thus, the lift-drag relationship must be considered for accurate analysis.

We recall the equations for constant lift coefficient and bank angle derived in Chapter 13. We have

$$
\begin{aligned}
\frac{dZ}{ds} &= -\beta r\, Z \tan\gamma \\
\frac{du}{ds} &= -\frac{2\sqrt{\beta r}\, Z\, u}{\cos\gamma}\left[1+\frac{C_L}{C_D}\cos\sigma\tan\gamma+\frac{\sin\gamma}{2\sqrt{\beta r}\, Z}\right] \\
\frac{d\gamma}{ds} &= \frac{\sqrt{\beta r}\, Z}{\cos\gamma}\left[\frac{C_L}{C_D}\cos\sigma+\frac{\cos\gamma}{\sqrt{\beta r}\, Z}\left(1-\frac{\cos^2\gamma}{u}\right)\right] \\
\frac{d\theta}{ds} &= \frac{\cos\psi}{\cos\phi} \\
\frac{d\phi}{ds} &= \sin\psi \\
\frac{d\psi}{ds} &= \frac{\sqrt{\beta r}\, Z}{\cos^2\gamma}\left[\frac{C_L}{C_D}\sin\sigma-\frac{\cos^2\gamma\cos\psi\tan\phi}{\sqrt{\beta r}\, Z}\right]
\end{aligned}
\qquad (16\text{-}15)
$$

where in spherical coordinates, the position of the vehicle is defined by its altitude, through the variable $Z$, longitude $\theta$ and latitude $\phi$. The velocity vector is specified by the variable $u$, the flight path angle $\gamma$ and the heading angle $\psi$. The angle $\sigma$ is the bank angle.

The variable $Z$ and $u$, called Chapman's modified variables are defined as

$$
\begin{aligned}
Z &\equiv \frac{\rho S C_D}{2m}\sqrt{\frac{r}{\beta}} \\
u &\equiv \frac{V^2\cos^2\gamma}{gr}
\end{aligned}
\qquad (16\text{-}16)
$$

while the independent variable $s$ is the dimensionless arc length

$$
s = \int_0^t \frac{V}{r}\cos\gamma\, dt \qquad (16\text{-}17)
$$

For flight with lift modulation, since the drag coefficient $C_D$ is varying, in the definition of the variable $Z$, we replace $C_D$ by the constant $C_L^*$, that is

$$Z \equiv \frac{\rho S C_L^*}{2m} \sqrt{\frac{r}{\beta}} \tag{16-18}$$

Also, it has been found convenient to replace $u$ by the variable $v$ defined as

$$v \equiv \frac{V^2}{gr} = \frac{u}{\cos^2 \gamma} \tag{16-19}$$

Hence the variable $v$ is the square of the dimensionless speed. With these modifications, and using Eqs. (16-11) and (16-12), it is seen that the new equations are

$$\begin{aligned}
\frac{dZ}{ds} &= -\beta r \, Z \tan \gamma \\
\frac{dv}{ds} &= -\frac{2\sqrt{\beta r}\, Z\, v\, f(\lambda)}{E^* \cos \gamma} - (2 - v) \tan \gamma \\
\frac{d\gamma}{ds} &= \frac{\sqrt{\beta r}\, Z}{\cos \gamma} \left[ \lambda \cos \sigma + \frac{\cos \gamma}{\sqrt{\beta r}\, Z} \left(1 - \frac{1}{v}\right) \right] \\
\frac{d\theta}{ds} &= \frac{\cos \psi}{\cos \phi} \\
\frac{d\phi}{ds} &= \sin \psi \\
\frac{d\psi}{ds} &= \frac{\sqrt{\beta r}\, Z\, \lambda \sin \sigma}{\cos^2 \gamma} - \cos \psi \tan \phi
\end{aligned} \tag{16-20}$$

where $E^* = C_L^*/C_D^*$ is the maximum lift-to-drag ratio.

Equations (16-20) are in the form suitable for the analysis of entry with lift and bank modulation (Refs. 3-4) and even for the optimization of such entry trajectories (Refs. 5-7).

With lift and bank modulation, the entry trajectory can be controlled in such a way that a certain requirement can be satisfied. For example, one may control the glide angle to be constant or the rate of descent, also called the sinking speed, to have a predetermined value. The required lift modulation to keep the vehicle along such a trajectory will be analyzed in the next chapter. In the following section we shall discuss the characteristics of each family of trajectories satisfying a specified condition.

## 16-4. TRAJECTORY IN THE PHASE SPACE

We shall consider lift-modulated entry trajectories in the plane of a great circle. Hence, taking $\sigma = 0$ , the equations of interest are

$$\frac{dZ}{d\theta} = -\beta r \; Z \tan\gamma$$

$$\frac{dv}{d\theta} = -\frac{2\sqrt{\beta r}\; Z\, v\, f(\lambda)}{E^* \cos\gamma} - (2 - v)\tan\gamma$$

$$\frac{d\gamma}{d\theta} = \frac{\sqrt{\beta r}\; Z\, \lambda}{\cos\gamma} + 1 - \frac{1}{v} \qquad (16\text{-}21)$$

where, as in Chapter 13, the quantity $\beta r$ will be considered as constant with $\beta r = 900$ for the Earth's atmosphere. In planar entry the independent variable $s$ becomes the range angle $\theta$ . Here the variable $Z$ and $v$ are defined by the Eqs. (16-18) and (16-19) respectively.

It is convenient for the representation and visualization of the trajectory to use a cylindrical coordinate system $(v, \gamma, w)$ where

$$w = \frac{1}{\sqrt{\beta r}\; Z} \qquad (16\text{-}22)$$

In this way, $w$ varies in the same direction as the altitude (Fig. 16-2).

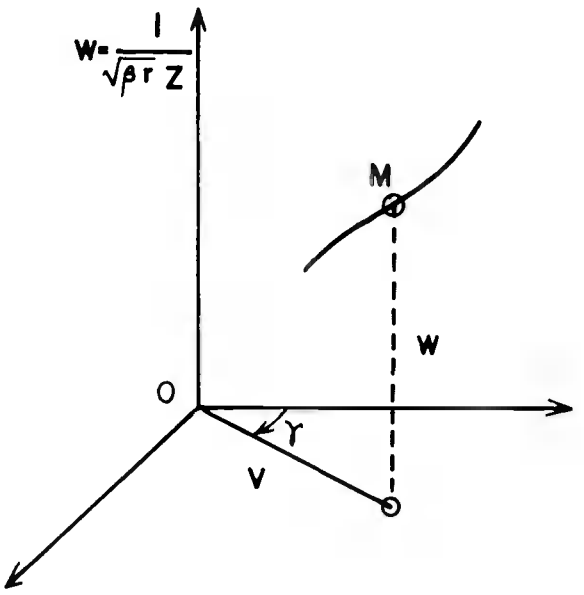


Fig. 16-2. Trajectory in the phase space.

Let us assume that the **entry** trajectory is such that a certain relationship exists among the three variables, speed, flight path angle, and altitude

$$F(v, \gamma, w) = 0 \tag{16-23}$$

Then, in the phase space the totality of entry trajectories satisfying Eq. (16-23) forms a two-dimensional surface. Hence, if two different constraints must be satisfied simultaneously, the trajectory, if physically possible, is in general unique, being the intersection of two constraining surfaces. We shall consider these constraining surfaces in the following cases:

16-4.1. Flight at Constant Flight Path Angle

In this flight program, we have constantly

$$\gamma = \gamma_i \tag{16-24}$$

where $\gamma_i$ is the initial flight path angle. In the phase space, the trajectory must lie on the vertical plane defined by Eq. (16-24). In the $(v, \gamma)$ plane the trajectory is a straight line while in the physical plane of the great circle it is a logarithmic spiral.

16-4.2. Flight at Constant Rate of Descent

The rate of descent, or sinking speed $V_s$, is the vertical component of the velocity

$$V_s = V \sin \gamma \tag{16-25}$$

In dimensionless form, by expressing that the sinking speed is constant, we have the relation

$$v \sin^2 \gamma = C \tag{16-26}$$

where $C$ is a constant. In the phase space, the trajectory must lie on a cylinder whose projection in the $(v, \gamma)$ plane is the curve defined by Eq. (16-26).

A geometric construction of this curve is as follows. In the $(v, \gamma)$ plane, we draw a circle with center at the origin and radius $C$. Since $C$ is the square of the dimensionless sinking speed, this circle is small if the sinking speed is small. At the point $P$ on the circle, defined by the polar angle $\gamma$, we draw the perpendicular $PQ$ to the radius $OP$ and then the perpendicular $QR$ to $OQ$ as shown in Fig. 16-3. The intersection $R$ of this perpendicular and the radius $OP$ is on the curve. The point $R$ describes the curve as given by Eq. (16-26) in dashed line as the point $P$ moves on the circle.

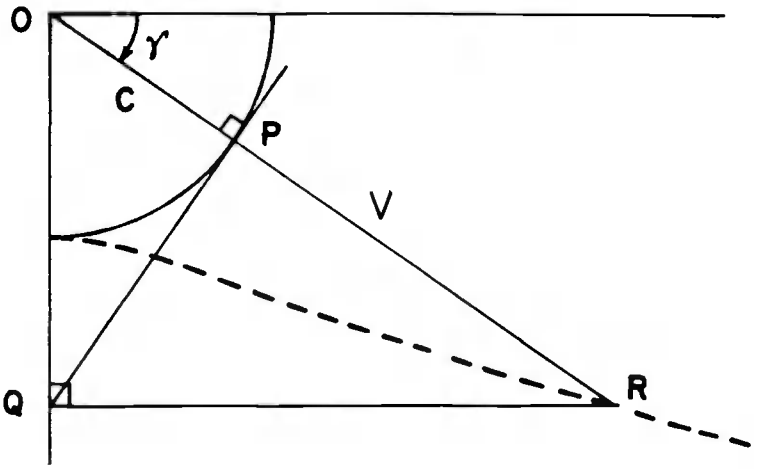


Fig. 16-3. Trajectory at constant sinking speed in the $(v, \gamma)$ plane.

16-4.3. Flight at Constant Speed

In this flight program, the constraining surface is defined by the equation

$$v = C \tag{16-27}$$

where $C$ is a positive constant equal to the square of the prescribed dimensionless speed. In the phase space, the trajectory must lie on the right circular cylinder with axis $Ow$.

16-4.4. Flight at Constant Dynamic Pressure

The dimensionless dynamic pressure is expressed as

$$\frac{1}{2}\rho V^2/(mg/SC_L^*) = \sqrt{\beta r}\ Z\ v \tag{16-28}$$

If $C$ is the prescribed constant dynamic pressure, in the phase space the trajectory must lie on the constraining surface defined by the equation

$$\frac{v}{w} = C \tag{16-29}$$

This is the equation of a circular cone with axis $Ow$.

16-4.5. Flight at Constant Heating Rate

The laminar heating rate at any point on the surface of the vehicle entering a planetary atmosphere is equal to a fraction of the heating

rate $q_s$ at a stagnation point. Since $q_s$ is proportional to $\rho^{1/2} V^3$, by expressing that this quantity is constant during entry, we are led to the equation of the constraining surface

$$\frac{v^3}{w} = C \tag{16-30}$$

In the phase space, this is the equation of a surface of revolution about the Ow axis, generated by a cubical parabola.

The different constraining surfaces discussed in this section are drawn in Fig. 16-4.

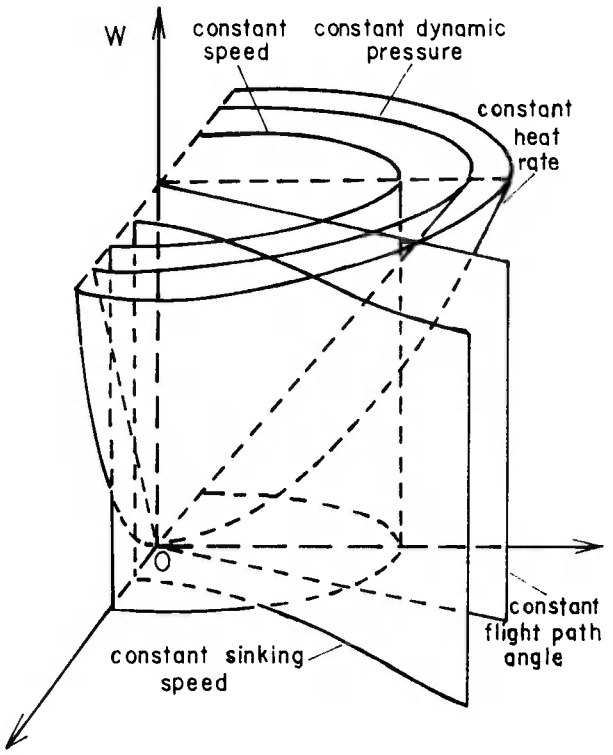


Fig. 16-4. Constraining surfaces in the phase space.

## 16-5. FLIGHT SUBJECT TO CONSTRAINTS ON STATE VARIABLES

The equations (16-20) are the equations of motion describing a dynamical system subject to arbitrary control. The variables $Z$, $v$, $\gamma$, $\theta$, $\phi$ and $\psi$ are the state variables, while the variables $\lambda$ and $\sigma$ are called the control variables. The variable $s$ is the independent variable and, in the case where $s$ is monotonically increasing, can be called the time variable. For each prescribed initial condition on the state variables, at the initial time $s = 0$, if the control histories in $\lambda$ and $\sigma$ are given as functions of the independent variable $s$, a forward integration of the system of equations, called the state equations, yields the state variables as functions of $s$. The

plot of the state variables in the phase space will be called the trajectory.

In general, we consider an n-dimensional dynamical system governed by the system of differential equations

$$\frac{dx_j}{dt} = f_j(\vec{x}, \vec{u}, t) \qquad (16\text{-}31)$$

$$j = 1, 2, \ldots, n \ .$$

where $\vec{x}$ is the n-dimensional state vector

$$\vec{x} = (x_1, x_2, \ldots, x_n) \qquad (16\text{-}32)$$

and $\vec{u}$ is the m-dimensional control vector

$$\vec{u} = (u_1, u_2, \ldots, u_m) \qquad (16\text{-}33)$$

In general $\vec{u}$ is an element of $U$, where $U$ is the bounded, m-dimensional control space. For example, in the Eqs. (16-20), we can take $u_1 = \lambda$ and $u_2 = \sigma$. If the lift coefficient $\lambda$ and the bank angle $\sigma$ are bounded, $U$ is defined by

$$|\lambda| \leq \lambda_{max}$$

$$|\sigma| \leq \sigma_{max} \qquad (16\text{-}34)$$

where $\lambda_{max}$ is the maximum rescaled lift coefficient and $\sigma_{max}$ is the maximum allowable bank angle.

In the previous section, we gave examples where some of the state variables are related by certain equation which must be satisfied along the trajectory. These equations impose constraints on the trajectory. In general, if the relations are independent of the controls, they are of the form

$$F_k(\vec{x}, t) = 0 \qquad (16\text{-}35)$$

$$k = 1, 2, \ldots, p \ .$$

Each of the $p$ relations (16-35), if it is time independent, defined a (n-1)-dimensional surface in the n-dimensional phase space. The trajectory satisfying the relation must lie on this constraining surface. In particular, the initial point must be taken on the surface itself. When the relation depends on the time, we can still consider it as defining a varying constraining surface. However, in this present analysis we shall invariably consider time independent state equations

$$\frac{dx_j}{dt} = f_j(\vec{x}, \vec{u}) \qquad (16\text{-}36)$$

$$j = 1, 2, \ldots, n.$$

and time independent constraining relations

$$F_k(\vec{x}) = 0 \qquad (16\text{-}37)$$

$$k = 1, 2, \ldots, p.$$

Consider the case $p = 1$, and the constraining surface $F_1 = 0$, in the n-dimensional space $E^n$ (Fig. 16-5). Let I be the initial point taken on the constraining surface. The trajectory starting from the point I must lie on the surface. Using the constraining relation $F_1(\vec{x}) = 0$, we can express one of the state variables, say $x_n$, in terms of the remaining (n-1) variables. Hence, we can delete the equation for $x_n$ from the system (16-36). Furthermore, the condition for the trajectory to lie on the constraining surface requires that, at each instant, the tangent to the trajectory is also a tangent of the surface. That is, it is orthogonal to the normal $\vec{N}$ of the surface at the point. Mathematically, this is expressed by taking the differential of the Eq. (16-37)

$$\frac{\partial F_k}{\partial x_1} dx_1 + \frac{\partial F_k}{\partial x_2} dx_2 + \ldots + \frac{\partial F_k}{\partial x_n} dx_n = 0 \qquad (16\text{-}38)$$

This equation expresses the orthogonality of the vector velocity $\vec{V} = (dx_j/dt)$ and the normal $\vec{N} = (\partial F_k / \partial x_j)$.

Using the state equations (16-36), we can write this equation as

$$\sum_{j=1}^{n} \frac{\partial F_k}{\partial x_j} f_j(\vec{x}, \vec{u}) = 0 \qquad (16\text{-}39)$$

At each instant, Eq. (16-39) can be satisfied by a proper selection of the vector control $\vec{u}$ in its bounded space. The trajectory cannot be generated if $\vec{u}$ cannot be found within its bound. If $p = 1$, and if $\vec{u}$ has only one component $u_1$, then from Eq. (16-39), $u_1$ can be obtained in terms of the remaining (n-1) state variables. Substituting into the remaining (n-1) state equations and integrating from the initial conditions, we generate a unique trajectory. (In some instances, Eq. (16-39) provides more than one solution for $u_1$ and the proper selection of the control is dictated by physical considerations.)

In general, the number of constraints cannot exceed the number of controls, that is $p \leq m$. If $p < m$, then, from the p equations (16-39), (m - p) components of the control vector $\vec{u}$ can be selected arbitrarily in some manner in the bounded space U.

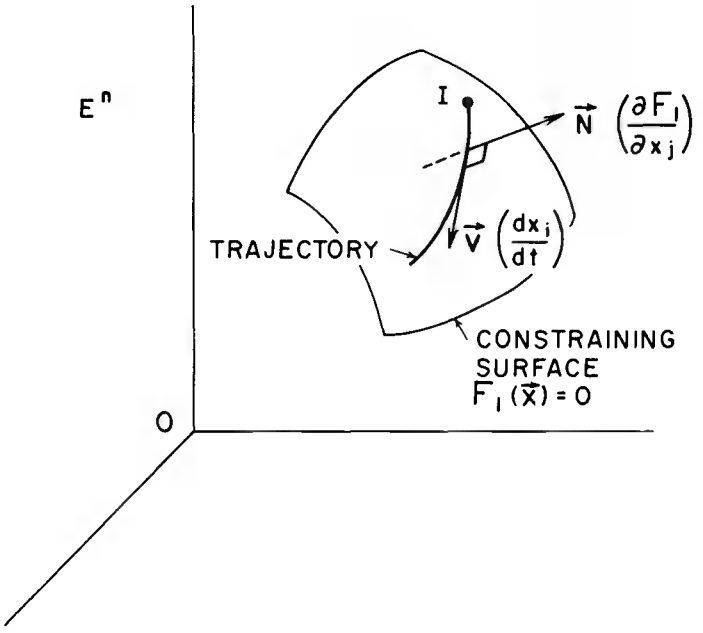


Fig. 16-5. Trajectory on constraining surface.

On the other hand, if $p = n$, the solution of the n equations (16-37) gives a finite number of points in $E^n$, and hence one of the solutions must be taken as the initial point. The trajectory cannot be generated as a continuous function. Hence, we must have $p < n$.

In optimization problems, there is at least one free component of the control vector to be selected in the bounded control space. The problem then is to find the best control history to achieve the maximization of a certain function of the state variables at the final time.

In this presentation we shall invariably study flight trajectories such that the number of constraints is equal to the number of controls. More specifically, all the cases considered are such that $m = p = 1$. The unique control used is the lift control $\lambda$. The state variables involved are the variables $w$, $v$, $\gamma$ and hence, the constraining relation is of the form

$$F(w, v, \gamma) = 0 \tag{16-40}$$

Relations involving only the altitude variable $w$ and the flight path angle $\gamma$ are called kinematic constraints. They are of the form

$$F(w, \gamma) = 0 \tag{16-41}$$

In this case, the trajectory in the physical plane is obtained by quadrature. To prove this, we rewrite the first of the Eqs. (16-20) using $w$ to replace $Z$

$$\frac{dw}{d\theta} = \beta r \, w \tan \gamma \qquad (16\text{-}42)$$

From Eq. (16-41) we obtain $\gamma$ as function of $w$, to be used in Eq. (16-42). Thus, $w$ is obtained by quadrature.

This provides the equations for the trajectory in the physical plane.

$$w = f_1(\theta)$$
$$\gamma = f_2(\theta) \qquad (16\text{-}43)$$

On the other hand, constraining relations involving only the speed $v$ and the flight path angle $\gamma$ give directly the trajectory in the $(v, \gamma)$ plane. Such trajectory constraints will be analyzed in Chapter 17. General relations such as Eq. (16-40) are dynamic constraints.

## References


1. Busemann, A., Vinh, N. X., and Culp, R. D., "Optimum Maneuvers of Hypervelocity Vehicles Using Thrust and/or Aerodynamic Force," ARL Report No. TR-74-0104, Vol. IV, USAF, 1974.

2. Miele, A., Flight Mechanics, Vol. 1, Theory of Flight Paths, Addison-Wesley Publishing Company, Inc., Reading, Massachusetts, 1962.

3. Bletsos, N. A., "Performance and Control with Lift Modulation of Hypervelocity Entry Vehicles," Ph. D. thesis, The University of Michigan, 1976.

4. Vinh, N. X., Bletsos, N. A., Busemann, A., and Culp, R. D., "Flight with Lift Modulation Inside a Planetary Atmosphere," AIAA Journal, Vol. 15, No. 11, pp. 1617-1623, 1977.

5. Vinh, N. X., Busemann, A., and Culp, R. D., "Optimum Three-Dimensional Atmospheric Entry," Acta Astronautica, Vol. 2, pp. 593-611, 1975.

6. Frostic, F., and Vinh, N. X., "Optimal Aerodynamic Control by Matched Asymptotic Expansions," Acta Astronautica, Vol. 3, pp. 319-332, 1976.

7. Vinh, N. X., and Chern, J. S., "Three-Dimensional Optimum Maneuvers of a Hypervelocity Vehicle," IAF paper No. 79-F-184, presented at the XXXth Congress of the International Astronautical Federation, Munich, September 1979.

# Chapter 17

# Lift Modulation with Constraints on Speed and Flight Path Angle

## 17-1. STATE AND CONSTRAINT EQUATIONS

The equations for flight with variable lift and bank control were derived in Chapter 16. For flight along a great circle, with the variables

$$v \equiv \frac{V^2}{gr} \quad , \quad Z = \frac{\rho S C_L^*}{2m} \sqrt{\frac{r}{\beta}} \tag{17-1}$$

the state equations are

$$\begin{aligned} \frac{dZ}{d\theta} &= -\beta r Z \tan\gamma \\ \frac{dv}{d\theta} &= -\frac{2\sqrt{\beta r}\ Z\, v\, f(\lambda)}{E^* \cos\gamma} - (2 - v)\tan\gamma \\ \frac{d\gamma}{d\theta} &= \frac{\sqrt{\beta r}\ Z \lambda}{\cos\gamma} + 1 - \frac{1}{v} \end{aligned} \tag{17-2}$$

The rescaled lift coefficient $\lambda$ is used as a control and has been defined as

$$\lambda = \frac{C_L}{C_L^*} \tag{17-3}$$

where $C_L^*$ is the lift coefficient corresponding to maximum lift-to-drag ratio, $E^* = (L/D)_{max}$. Hence, when $\lambda = 1$ the flight is at maximum lift-to-drag ratio. The lift coefficient is bounded by an upper limit and proportionally we have the constraint on the lift control

$$|\lambda| \leq \lambda_{max} \tag{17-4}$$

The function $f(\lambda) = C_D / C_D^*$ is the rescaled drag coefficient. Its form is dictated by the drag polar. In particular, for a parabolic drag polar

$$f(\lambda) = \frac{1 + \lambda^2}{2} \tag{17-5}$$

For planar entry, to visualize the trajectory in the phase space, in Chapter 16, it has been found convenient to change the variable $Z$ into the variable $w$ such that

$$w = \frac{1}{\sqrt{\beta r}\ Z} \tag{17-6}$$

In this way, since $w$ is the inverse of the density of the atmosphere, it varies in the same direction as the altitude. Then, we have the equations of motion in the variables $w$, $v$ and $\gamma$, using a parabolic drag polar

$$\begin{aligned}
\frac{dw}{d\theta} &= \beta r\ w \tan\gamma \\
\frac{dv}{d\theta} &= -\frac{v(1+\lambda^2)}{E^* w \cos\gamma} - (2 - v)\tan\gamma \\
\frac{d\gamma}{d\theta} &= \frac{\lambda}{w \cos\gamma} + 1 - \frac{1}{v}
\end{aligned} \tag{17-7}$$

In Chapter 16, we have seen that if a constraint of the form

$$F(v, \gamma, w) = 0 \tag{17-8}$$

is imposed upon the entry variables, then it is possible to deduce the lift control law to flight the vehicle along this constraint. Once a certain constraint is prescribed, it is of interest to study the behavior of the lift control along the flight. The analysis would be valuable to mission planning and design of guidance system. Several trajectories of practical interest have been analyzed in Ref. 1. In this chapter the following flight trajectories will be considered:

a/ Flight at constant flight path angle.
The constraining relation is simply

$$\gamma = \gamma_i \tag{17-9}$$

where $\gamma_i$ is the initial flight path angle.

b/ Flight at constant sinking speed.
The constraining relation in this case is

$$v \sin^2\gamma = C \tag{17-10}$$

where the constant C is the square of the dimensionless sinking speed.

For each flight program, the lift control required to satisfy the constraining relation will be derived. The variation of the state variables and the behavior of the trajectory in the phase space will be analyzed. Pertinent properties of the flight path will be displayed explicitly.

## 17-2. FLIGHT AT CONSTANT FLIGHT PATH ANGLE

In this flight program, it is required to keep the entry angle constant throughout the portion of trajectory under consideration. This scheme is most attractive during the initial phase of descent, and also at a later phase during an approach before landing.

### 17-2.1. The Lift Control Law

The constraining relation is Eq. (17-9). Hence, $d\gamma/d\theta = 0$, and from Eq. (17-7), in terms of the variables $v$ and $w$, the lift control is given by

$$\lambda = \frac{w \cos \gamma_i (1 - v)}{v} \tag{17-11}$$

The lift is positive for subcircular speed flight, $v < 1$. At higher speed, when $v > 1$, negative lift should be used to hold constant glide angle. Since $\gamma$ is constant, the first of the Eqs. (17-7) can be integrated.

$$w = w_i \exp [ (\beta r \tan \gamma_i) \theta ] \tag{17-12}$$

In the plane of motion, the trajectory is a logarithmic spiral and, for an entry trajectory, $\gamma_i < 0$, the "altitude" $w$ decreases according to the law (17-12).

### 17-2.2. The Characteristic Curves

In the $(v, \gamma)$ plane, the trajectory is the ray $\gamma = \gamma_i$. In the phase space, the trajectory lies in the vertical plane $(v, w)$. A simplification can be made by using the modified variable

$$Y \equiv w \cos \gamma_i \tag{17-13}$$

and the modified parameter

$$E_i \equiv - E^* \tan \gamma_i > 0 \tag{17-14}$$

to replace $w$ and $E^*$ respectively. The lift control is simply

$$\lambda = \frac{Y(1 - v)}{v} \tag{17-15}$$

In the ( v, Y) plane, the lines of equal lift coefficient, $\lambda =$ constant, are the hyperbolas defined by Eq. (17-15) with the line, $v = 1$, a common asymptote. Because of the constraint (17-4), the ( v, Y) space is bounded by the hyperbolas (Fig. 17-1)

$$Y = \frac{\lambda_{max} v}{1 - v}$$

$$Y = \frac{\lambda_{max} v}{v - 1} \tag{17-16}$$

The initial point must be within the boundary of lift capability and, for flight initiated at high altitude, $Y \to \infty$, the initial speed is restricted to near circular speed, $v_i \to 1$. At any altitude, the speed is bounded by

$$\frac{Y}{Y + \lambda_{max}} \leq v \leq \frac{Y}{Y - \lambda_{max}} \tag{17-17}$$

with the upper bound being infinite for $Y < \lambda_{max}$.

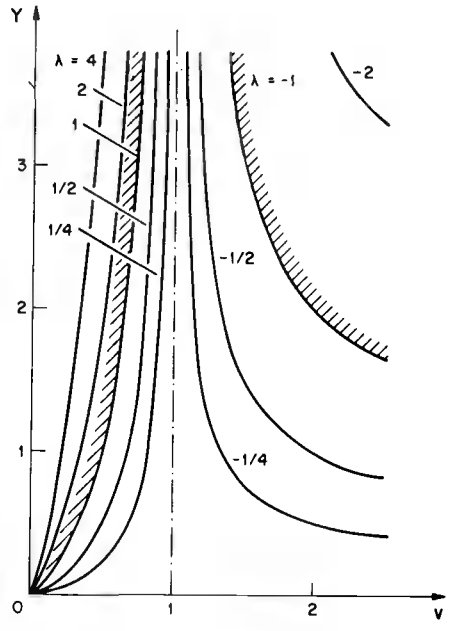


Fig. 17-1. Iso-lift coefficient curves in the (v , Y) plane. Bounded space for $\lambda_{max} = 1$.

From Eq. (17-7), it is seen that for a general drag polar the speed decreases if and only if

$$f(\lambda) + E_i Y \left(\frac{1}{2} - \frac{1}{v}\right) > 0 \tag{17-18}$$

With a parabolic polar, as defined by Eq. (17-5), and the lift control law (17-15), the condition for decreasing $v$ is

$$A \equiv (1 - v)^2 Y^2 - E_i(2 - v)\, vY + v^2 > 0 \tag{17-19}$$

In the constraining plane $(v, Y)$ of the trajectory, we consider the quartic curve $A = 0$ .

$$(1 - v)^2 Y^2 - E_i(2 - v)\, vY + v^2 = 0 \tag{17-20}$$

The origin is a double point having the tangents defined by the lowest order of the equation of the curve.

$$Y^2 - 2E_i vY + v^2 = 0 \tag{17-21}$$

The tangents to the curve at the origin are real, provided that

$$E_i > 1 \tag{17-22}$$

The condition is satisfied for a steep glide of a vehicle having relatively high maximum lift-to-drag ratio.

If the condition is not satisfied, the tangents at the origin to the curve are imaginary and the origin is an isolated point. In the positive $(v, Y)$ space, the curve delimits the regions where $v$ is increasing and where $v$ is decreasing as shown in Fig. 17-2, for the case where the origin is an isolated point. The asymptote is the line

$$v = 1 \tag{17-23}$$

The point where the tangent to the curve is parallel to the Y-axis is obtained by setting the discriminant of the quadratic equation in $Y$ , Eq. (17-20), equal to zero.

$$E_i^2 (2 - v)^2 - 4(1 - v)^2 = 0 \tag{17-24}$$

Solving for $v$ , we obtain two roots

$$v_1 = \frac{2(1 + E_i)}{2 + E_i}$$

$$v_2 = \frac{2(1 - E_i)}{2 - E_i} \tag{17-25}$$

The first root is always positive and larger than 1 . It gives the point to the right of the asymptote with the value for Y

$$Y_1 = \frac{2(1 + E_i)}{E_i} \tag{17-26}$$

This point is above the point

$$v_3 = 1 \ , \quad Y_3 = \frac{1}{E_i} \tag{17-27}$$

where the curve intersects the asymptote. As expected, if the origin is an isolated point, $1 - E_i > 0$ , the second root is also positive. The corresponding value of Y is

$$Y_2 = \frac{2(1 - E_i)}{E_i} \tag{17-28}$$

This point $(v_2 , Y_2)$ is below the point $(v_1 , Y_1)$ . It is above the point $(v_3 , Y_3)$ if and only if $1 - 2E_i > 0$ . We can verify that the point $(v_1 , Y_1)$ is on the iso-lift coefficient hyperbola with $\lambda = -1$, and the point $(v_2 , Y_2)$ is on the hyperbola with $\lambda = 1$ .

The point where the tangent to the curve is parallel to the v-axis is given by the value of Y

$$Y_4 = \frac{1 - E_i^2}{E_i} \tag{17-29}$$

It is positive if the origin is an isolated point. The corresponding value of v is

$$v_4 = 1 - E_i^2 \tag{17-30}$$

The point $(v_4 , Y_4)$ is on the iso-lift coefficient hyperbola with the value for $\lambda$

$$\lambda = E_i \tag{17-31}$$

In the (v , Y) plane, the curves $\lambda = \pm \lambda_{max}$ intersect the curve $A = 0$ between the points $v_1$ and $v_2$ if $\lambda_{max} \leq 1$ . The intersections are outside when $\lambda_{max} > 1$.

The sense of variation of the lift coefficient along the trajectory is given by the sign of the derivative $d\lambda/d\theta$ . From Eq. (17-15) for $\lambda$ and using the state equations, Eqs. ( 17-7), we have

$$\frac{d\lambda}{d\theta} = \beta r \ \lambda \ \tan \gamma_i + \frac{A}{E^* v^3} \tag{17-32}$$

where A is defined by Eq. (17-19), with $A > 0$ for decreasing v. In the following we shall consider the case of shallow glide with low maximum lift-to-drag ratio, $E_i < 1$, which is likely to occur in practice.

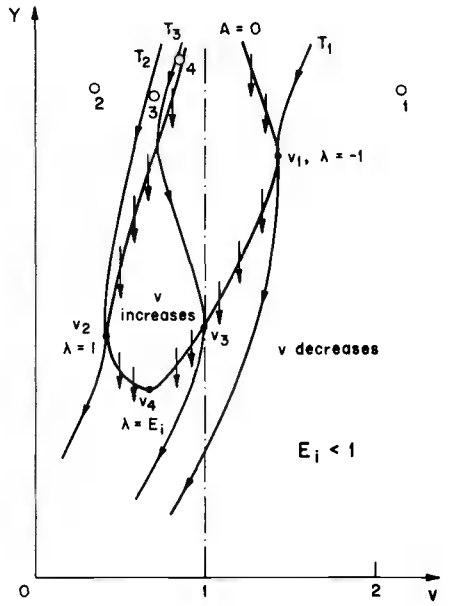


Fig. 17-2. Curve of stationary v (A = 0) and flow of trajectories in the (v, Y) plane.

17-2.3. The Behavior of the Trajectory

We can now discuss the behavior of the trajectory in the (v, Y) plane as shown in Fig. 17-2 for the case where $E_i < 1$. Using Y as the independent variable, with Y always decreasing, the equation of the trajectory is

$$\frac{dv}{dY} = \frac{A}{\beta r \, E_i Y^2 v} \tag{17-33}$$

First, we consider the intersection of the trajectory with the curve $A = 0$. In this respect, we evaluate the slope $dY/dv$ of the curve $A = 0$, and compare it with the slope of the trajectory. By taking the derivative of Eq. (17-20), and evaluating it at $A = 0$, we obtain

$$\left(\frac{dY}{dv}\right)_A = \frac{2Y^2 [\,(1 - v)\, Y - E_i v\,]}{v[\,(1 - v)^2 Y^2 - v^2\,]} \tag{17-34}$$

where subscript A means that $(dY/dv)_A$ is the slope of the curve A. Likewise the slope of the trajectory T is

$$\left(\frac{dY}{dv}\right)_T = \frac{\beta r E_i Y^2 v}{A} \tag{17-35}$$

Note that it is infinite at $A = 0$; that is, at the intersection of the trajectory and the curve A. Using Eq. (17-15) we can rewrite Eq. (17- 34) as

$$\left(\frac{dY}{dv}\right)_A = \frac{2\lambda^2(\lambda - E_i)}{(\lambda^2 - 1)(1 - v)^2} \tag{17-36}$$

Moving clockwise around the curve A from infinity, we see that between the points $v = 1 + \epsilon$ and $v_1$, $\lambda < 0$, $\lambda^2 - 1 > 0$, and the slope of the curve A=0 is negative. Between the points $v_1$ and $v_4$, $\lambda^2 - 1 < 0$, $\lambda - E_i < 0$ and the slope is positive. Similarly, we see that the slope is negative between $v_4$ and $v_2$ and becomes positive between $v_2$ and $v = 1 - \epsilon$. The trajectory, in the case $E_i < 1$ of Fig. 17-2, can only intersect vertically the curve $A = 0$, always in the decreasing direction of Y, as shown by the arrows. We immediately have the following properties:

a/ The speed can only have one relative minimum and one relative maximum with the relative minimum occurring first.

b/ Once through a relative maximum, the speed continues to decrease.

To discuss the behavior of the trajectory in terms of the initial point $(v_i, Y_i)$, we introduce the limiting trajectories $T_1$, $T_2$ and $T_3$ as shown in Fig. 17-2. The trajectory $T_1$ is obtained by integrating Eq. (17-33) forward and backward from the point $(v_1, Y_1)$. Likewise, the trajectories $T_2$ and $T_3$ are obtained by integrating forward and backward from the points $(v_2, Y_2)$ and $(v_3, Y_3)$, respectively. By the existence and uniqueness of the solution of Eq. (17-33), the limiting trajectories partition the flow of the trajectories in the (v, Y) space.

From the figure, the type of the trajectory can be classified in terms of the initial point. For example, the trajectories initiated from points 1 and 2 will have the speed continuously decreasing. The trajectories initiated from points 3 and 4 will have the speed decreasing first and then increasing after passing through a minimum. After the minimum, the speed will increase, pass through a maximum, and then decrease again until the end. Speed along the trajectory initiated from point 3 will remain subcircular, while the speed along the trajectory initiated from point 4 will go from subcircular to supercircular before decreasing to subcircular again.

It should be noted that the trajectory must remain within the iso-lift coefficient hyperbolas $\lambda = \pm \lambda_{max}$ and above the level $Y = Y_s = w_s \cos\gamma_i$, where $w_s$ is the value of w evaluated at sea level.

Hence, the trajectory must be such that $|\lambda_i| \leq \lambda_{max}$. It terminates either at the point where $|\lambda| = \lambda_{max}$ where the maximum lift capability is reached, or at $Y = Y_s$ where the vehicle has reached sea level.

### 17-2.4. The Variation of the Angle of Attack

It is interesting to follow the variation of the angle-of-attack along the trajectory. In this respect the lift control $\lambda$ is useful. It varies in the same direction as the angle of attack, and furthermore, for $\lambda = 1$, the corresponding angle of attack is the one giving maximum lift-to-drag ratio for the case where $\lambda_{max} \geq 1$. In the case where $\lambda_{max} < 1$, the maximum lift-to-drag ratio is reached at $\lambda = \lambda_{max}$. From Eq. (17-32), the lift coefficient is increasing if and only if

$$B \equiv -\beta r E_i \lambda v^3 + A > 0 \qquad (17\text{-}37)$$

In the (v, Y) plane, the curve $B = 0$ delimits the region where $\lambda$ is increasing (outside the curve) and where $\lambda$ is decreasing (inside the curve). The curve $B = 0$ is plotted in Fig. 17-3 for the case where $E_i < 1$. Since $B = 0$ when $\lambda = 0$ and $A = 0$ simultaneously, the curve $A = 0$ and $B = 0$ have their intersection at the point $(v_3, Y_3)$. Furthermore since $B < 0$ when $\lambda > 0$ and $A \leq 0$, the portion of the curve $A = 0$ on the left of the asymptote $v = 1$ is entirely in the region $B < 0$. Similarly, since $B > 0$ when $\lambda < 0$ and $A \geq 0$, the portion of the curve $A = 0$ on the right of the asymptote is entirely in the region $B > 0$. As a consequence, we have the following properties:

a/ In the subcircular speed regime, the angle-of-attack passes through its stationary value with decreasing speed.

b/ In the supercircular speed regime, the angle-of-attack passes through its stationary value with increasing speed.

This theorem can be made stronger by specifying that, in both cases, the stationary value is a minimum, as we shall prove. Explicitly, we write the equation of the curve $B = 0$

$$B = (1-v)^2 Y^2 - E_i \left[ 2 + (\beta r - 1) v - \beta r v^2 \right] vY + v^2 = 0 \qquad (17\text{-}38)$$

Like the curve $A = 0$, this quartic curve has the line $v = 1$ as the vertical asymptote. The origin is a double point, and it is an isolated point if $E_i < 1$. The tangent to the curve is parallel to the Y-axis when

$$E_i^2 \left[ 2 + ( \beta r - 1) v - \beta r v^2 \right]^2 - 4(1-v)^2 = 0 \qquad (17\text{-}39)$$

The equation can be factored into two quadratic equations

$$\beta r\, E_i v^2 - [(\beta r - 1)\, E_i - 2]\, v - 2(1 + E_i) = 0$$

$$\beta r\, E_i v^2 - [(\beta r - 1)\, E_i + 2]\, v + 2(1 - E_i) = 0 \qquad (17\text{-}40)$$

The first equation provides one positive and one negative root. In the case where $1 - E_i > 0$, that is when the origin is an isolated point, the second equation provides two positive roots, one root is less than 1 and the other root is larger than 1. If we write this second equation as

$$- E_i [\, 2 + (\beta r - 1)\, v - \beta r\, v^2] = 2(v - 1)$$

we see that taking the root $v > 1$ will make the coefficient of Y in Eq. (17-38) positive hence providing a negative value for Y. Hence, the two positive roots of interest in the Eqs. (17-40) are the positive root of the first equation and the smaller positive root of the second equation,

$$v_5 = \frac{[(\beta r - 1)\, E_i - 2] + \sqrt{[(\beta r + 1)\, E_i + 2]^2 + 4\beta r\, E_i^2}}{2\beta r\, E_i} \qquad (17\text{-}41)$$

and

$$v_6 = \frac{[(\beta r - 1)\, E_i + 2] - \sqrt{[(\beta r + 1)\, E_i - 2]^2 + 4\beta r\, E_i^2}}{2\beta r\, E_i} \qquad (17\text{-}42)$$

The root $v_5$ is larger than 1 and corresponds to the point inside the $A = 0$ curve. The corresponding value of Y is the double root of the Eq. (17-38). Hence

$$Y_5 = \frac{v_5}{v_5 - 1}, \quad \lambda = -1 \qquad (17\text{-}43)$$

and

$$Y_6 = \frac{v_6}{1 - v_6}, \quad \lambda = 1 \qquad (17\text{-}44)$$

If we rewrite the Eq. (17-38) as a cubic equation in v, the point where the tangent to the curve $B = 0$ is parallel to the v-axis is the point providing a double root in v. It can be shown that this is the point

$$2\lambda = E_i(2 + \beta r\, v^2) \qquad (17\text{-}45)$$

The point is in the range

$$E_i \leq \lambda \leq 1 \tag{17-46}$$

On the other hand, using $\lambda$ to replace $Y$, we rewrite the equation (17-38) as

$$\lambda^2 - \frac{E_i[2+(\beta r - 1)v - \beta r v^2]\lambda}{(1-v)} + 1 = 0 \tag{17-47}$$

By eliminating $\lambda$ between the two equations (17-45) and (17-47) we have a quintic equation to evaluate the value of $v = v_7$ where the tangent to the curve $B = 0$ is parallel to the v-axis.

$$(\beta r E_i)^2 v^5 - 3(\beta r E_i)^2 v^4 + 2\beta r(\beta r + 1) E_i^2 v^3 - 4\beta r E_i^2 v^2 + 4(1 + \beta r E_i^2) v - 4(1 - E_i^2) = 0 \tag{17-48}$$

Let us now consider the intersection of the trajectory with the curve of stationary value for $\lambda$, $B = 0$. Using the condition $B = 0$ in Eq. (17-33) we have the slope of the trajectory at the point of intersection

$$\left(\frac{dY}{dv}\right)_T = \frac{Y}{v(1-v)} = \frac{\lambda}{(1-v)^2} \tag{17-49}$$

On the other hand, if we evaluate the slope of the curve $B = 0$, using Eq. (17-38), we have, after simplification

$$\left(\frac{dY}{dv}\right)_B = \frac{\lambda^2[2\lambda - E_i(2+\beta r v^2)]}{(\lambda^2 - 1)(1-v)^2} \tag{17-50}$$

Referring to Fig. 17-3, we move along the curve $B = 0$ from the point $v = 1 + \epsilon$ to the point $v = 1 - \epsilon$ in the clockwise direction. Between the point $v = 1 + \epsilon$ and the point $v_5$, $\lambda \leq -1$, both the two slopes are negative, and

$$\left(\frac{dY}{dv}\right)_T > \left(\frac{dY}{dv}\right)_B$$

We find that this condition leads to

$$\lambda^2 - E_i\lambda(2+\beta r v^2) + 1 > 0$$

which is true for $\lambda < 0$. Hence we have the possible intersection indicated.

Between the point $v_5$ and the point $v_3$, $\lambda$ is negative and

$\lambda^2 < 1$ , the slope $(dY/dv)_T$ is negative while the slope $(dY/dv)_B$ is positive and again we have the trajectory going from inside the curve $B = 0$ to outside the curve as indicated by the arrows. Between the point $v_3$ and the point $v_7$ , $\lambda^2 < 1$ and

$$0 \leq 2\lambda \leq E_i(2+\beta r v^2)$$

Hence, the two slopes are positive. The condition

$$\left(\frac{dY}{dv}\right)_T > \left(\frac{dY}{dv}\right)_B$$

leads to

$$\lambda^2 - E_i(2+\beta r v^2)\lambda + 1 > 0$$

Since the point is on the curve $B = 0$ , Eq. (17-47) applies and we have the condition

$$\frac{v\left[\beta r(v-1)^2 + 1\right]}{(1-v)} > 0$$

This condition is satisfied since $(1 - v) > 0$ .

Similar arguments lead to the direction of intersection always from inside the curve $B = 0$ to outside the curve as shown in Fig. 17-3. Hence, the intersection is always from $d\lambda/d\theta < 0$ to $d\lambda/d\theta > 0$ . The angle of attack considered as an algebraic quantity never passes though a relative maximum and can only pass through a relative minimum once. More specifically, for positive $\alpha$ , the stationary value is a minimum while for negative $\alpha$ , the stationary value is a maximum in absolute value.

The discussion is more enlightening if we plot the trajectory and the curve $A = 0$ and $B = 0$ in the $(v , \lambda)$ plane. In this plane, the equation of the curve $A = 0$ is

$$\lambda^2 - \frac{E_i(2-v)\lambda}{(1-v)} + 1 = 0 \qquad (17\text{-}51)$$

The line $v = 1$ is the vertical asymptote. The curve passes through the point $\lambda = 0$ , $v = 1$ with a slope at that point equal to

$$\frac{d\lambda}{dv} = -\frac{1}{E_i} \qquad (17\text{-}52)$$

For any $v$ , the product of the roots of Eq. (17-51) is $\lambda_1\lambda_2 = 1$ . Hence, the points where the tangent is vertical are the points where $\lambda_1 = \lambda_2 = \pm 1$ . We have the values $v_1$ and $v_2$ for $v$ as found previously in Eq. (17-25). In the $(v , \lambda)$ plane, the equation of the

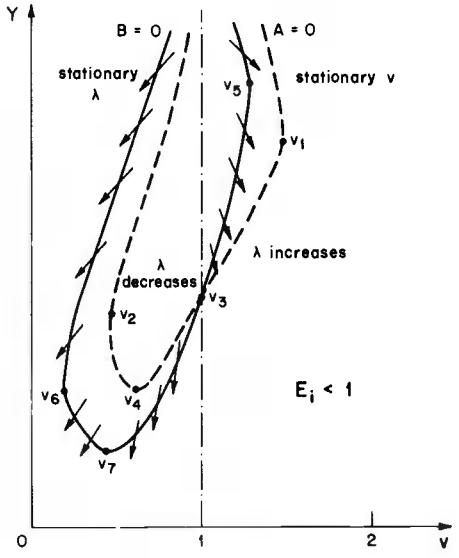


Fig. 17-3. Curve of stationary $\lambda$ ($B = 0$) and flow of trajectories in the ($v$, $Y$) plane.

curve $B = 0$ has been given in Eq. (17-47). The line $v = 1$ is the vertical asymptote. The curve also passes through the point $\lambda = 0$, $v = 1$ and has at that point the same tangent as the curve $A = 0$. The points with vertical tangent also occur at $\lambda = \pm 1$, with the values $v_5$ and $v_6$ as given in Eq. (17-41) and (17-42).

Figure 17-4 presents the plots of the curves in the ($v$, $\lambda$) plane. The limiting trajectories $T_1$, $T_2$ and $T_3$, as depicted in Fig. 17-2 are also replotted in this figure. Using these trajectories, we can describe the behavior of the trajectory and the variation of the angle of attack in terms of the initial condition.

For example, the trajectory starting from the point 1, at supercircular speed begins with negative lift with the speed always decreasing and the lift coefficient always increasing. The trajectory terminates whenever $\lambda = \lambda_{max}$ or $Y = Y_s$.

For the trajectory starting from the point 2, we first observe that by the uniqueness of the solution, it cannot cross the trajectory $T_2$. Since the point 2 is on the left of the curve $A = 0$, and on the right of the curve $B = 0$, the speed decreases continuously until the end while the angle of attack first decreases and then increases after the trajectory has intersected the curve $B = 0$.

The trajectory starting from the point 3 will be bounded by the trajectory $T_2$ and the trajectory $T_3$. Hence, the speed remains subcircular while the lift coefficient is always positive. The speed along the trajectory will first increase to a maximum, and then decrease. The lift coefficient will decrease to a minimum value and then increase to $\lambda_{max}$ at the end if the vehicle has not reached ground level. We also notice that the maximum speed is reached before the lift coefficient attains its minimum value.

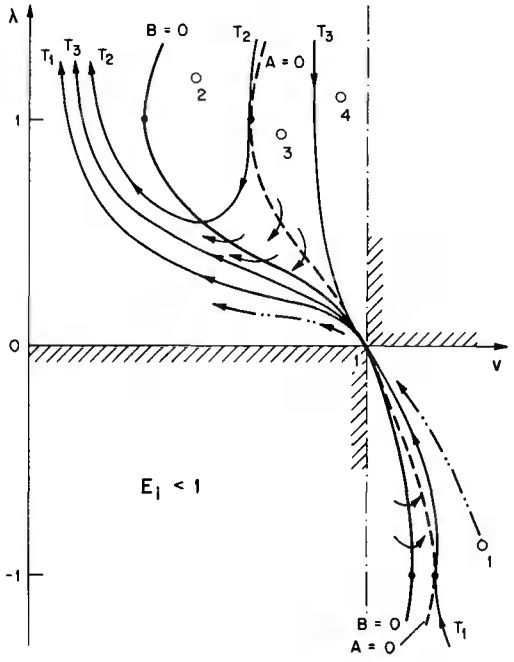


Fig. 17-4. Variations of the angle of attack and flow of trajectories in the $(v, \lambda)$ plane.

The trajectory starting from the point 4 will go supercircular. The lift coefficient decreases first, reaches a minimum with negative value, and then increases to $\lambda_{max}$. The speed increases first and passes through a maximum before decreasing to its final value. We also notice that the maximum speed is reached after the point of minimum lift coefficient.

It should be mentioned that the point $v = 1$, $\lambda = 0$ must be considered as an accumulation point for all trajectories passing through circular speed, and not the point of intersection of the trajectories. At that point each trajectory has a different value of $Y$. In particular, the trajectory $T_3$, which has a cusp at the accumulation point, has the value $Y_3 = 1/E_i^3$.

## 17-2.5. The Variation of the Dynamic Pressure

In general, along the entry trajectory at constant flight path angle, the dynamic pressure increases continuously and reaches its maximum value either at ground level or at some critical altitude. A thorough discussion of the variation of the dynamic pressure for this type of trajectory is given in Ref. 1. Here we mention briefly a few characteristics of the phenomenon.

The dimensionless dynamic pressure can be represented as

$$\frac{(1/2)\rho V^2}{mg\cos\gamma_i/SC_L^*} = \frac{v}{Y} \tag{17-53}$$

Hence, in the (v , Y) plane, the lines with constant dynamic pressure are the rays passing through the origin. As a consequence, when the vehicle passes through the point of maximum dynamic pressure, in the (v , Y) plane, the tangent to the trajectory passes through the origin. We obtain the equation of the curve of stationary dynamic pressure by writing

$$\frac{dv}{dY} - \frac{v}{Y} = 0 \tag{17-54}$$

Using Eq. (17-33) we get the condition for increasing dynamic pressure

$$C \equiv A - \beta r E_i Yv^2 < 0 \tag{17-55}$$

Hence, the dynamic pressure increases in the region where the speed increases ($A < 0$) . In the (v , Y) plane, if we plot the curve of stationary dynamic pressure, $C = 0$ , the curve is entirely outside the curve $A = 0$ . On the other hand, from Eq. (17-37) and (17-55), by writing

$$B = C + \beta r E_i Yv^3 \tag{17-56}$$

we see that for $B = 0$ , $C < 0$ . The curve $C = 0$ is entirely outside the curve of stationary $\lambda$ , $B = 0$ . As a consequence, minimum lift coefficient is reached while the dynamic pressure is increasing.

As a final remark for this case of entry at constant flight path angle, we should mention that, for a typical entry vehicle, the value of w (or equivalently Y ) is rather small, of the order of $2 \times 10^{-3}$ at 15 km , reaching $2 \times 10^{-2}$ at 30 km and 1.29 at 60 km. For practical applications, in the (v , Y) plane, the region of interest is the region at subcircular speed below the curve $A = 0$ where the speed decreases along the trajectory.

The case of vertical entry, $\gamma_i = -90^\circ$ is trivial. The case of constant altitude, coasting flight, $\gamma_i = 0$ has many interesting characteristics. This case has been discussed in detail by the authors in Ref. 2 .

## 17-3. FLAT EARTH TRANSFORMATION

In the second specific example, the rate of descent, or sinking speed, is kept at a constant value. This is a flight program of practical interest during the approach phase. The speed is relatively small; hence, an analysis using a flat planet model is adequate.

It must be emphasized here that the general equations (17-7), which are exact equations, can be used but to the scale of altitude and

range considered, it is better to change the variables, say the range angle $\theta$ in radians, into dimensionless linear range and disregard terms that are trivially small. In this purpose, instead of starting with the equations for flight over a flat planet and introducing the appropriate dimensionless transformation, it is enlightening to perform the transformation directly on the basic equations (17-7).

For a flat planet model, we define the dimensionless linear range

$$x \equiv \beta r \theta \tag{17-57}$$

and use the new altitude and speed variables

$$\begin{aligned} z &\equiv \beta r w \equiv \frac{2m\beta}{\rho S C_L^*} \\ \bar{v} &\equiv \beta r v \equiv \frac{V^2}{g/\beta} \end{aligned} \tag{17-58}$$

Using these definitions in Eqs. (17-7), we have

$$\begin{aligned} \frac{dz}{dx} &= z \tan\gamma \\ \frac{d\bar{v}}{dx} &= -\frac{\bar{v}(1+\lambda^2)}{E^* z \cos\gamma} - (2 - \frac{\bar{v}}{\beta r}) \tan\gamma \\ \frac{d\gamma}{dx} &= \frac{\lambda}{z \cos\gamma} - \frac{1}{\bar{v}} + \frac{1}{\beta r} \end{aligned} \tag{17-59}$$

Now, for nearly all planetary atmospheres, $\beta r$ is large and in the scale of speed considered $\bar{v}$ is now of the order of unity. Hence, it is trivial that the term $1/\beta r$ is negligibly small, and we have the dimensionless equation for flight over a flat planet.

$$\begin{aligned} \frac{dz}{dx} &= z \tan\gamma \\ \frac{d\bar{v}}{dx} &= -\frac{\bar{v}(1+\lambda^2)}{E^* z \cos\gamma} - 2 \tan\gamma \\ \frac{d\gamma}{dx} &= \frac{\lambda}{z \cos\gamma} - \frac{1}{\bar{v}} \end{aligned} \tag{17-60}$$

We obtain identical equations by starting from equations for flight over a flat planet. One interesting fact is that the new equations are free of the characteristic of the atmosphere although we continue to refer to the planet as the Earth.

## 17-4. FLIGHT AT CONSTANT SINKING SPEED

For this flight program, we write the constraining relation (17-10) as

$$\bar{v} \sin^2 \gamma = K^2 \tag{17-61}$$

where $K$ is a positive constant representing the absolute value of the dimensionless sinking speed.

### 17-4.1. The Lift Control Law

By taking the derivative of Eq. (17-61) using the state equations (17-60), we have the lift control law

$$\lambda^2 \sin\gamma - 2E^* \lambda \cos\gamma + \sin\gamma + (2E^* z \sin^2\gamma / K^2) = 0 \tag{17-62}$$

At each instant, the lift coefficient required to maintain constant sinking speed $K$ is obtained by solving this quadratic equation in $\lambda$. Since $\sin\gamma < 0$, then if

$$z > -K^2 / 2E^* \sin\gamma \tag{17-63}$$

we have a positive and a negative lift coefficient. Positive lift should be selected to reduce deceleration. When condition (17-63) is reversed, both roots are negative and low negative root must be selected.

Since the altitude is decreasing, the flight is terminated whenever the variable $z$ reaches the ground level value $z_s$ or when $|\lambda| = \lambda_{max}$ or when Eq. (17-62) no longer has real roots. From this equation, the condition for real roots is

$$z \geq -\frac{K^2(\sin^2\gamma - E^{*2}\cos^2\gamma)}{2E^* \sin^3\gamma} \tag{17-64}$$

### 17-4.2. Domain of Flight in the $(\gamma, \lambda)$ Space

The discussion of the variation of the angle of attack, or equivalently the lift coefficient, along the descending trajectory with constant sinking speed can be explicitly carried out in the $(\gamma, \lambda)$ space.

In this space, the constraint on maximum lift capability is represented by the lines $\lambda = \pm \lambda_{max}$. On the other hand, the boundary for real roots, as given by the equality sign in Eq. (17-64), with $z$ obtained from Eq. (17-62) is simply

$$\lambda = E^* \cot\gamma \tag{17-65}$$

Furthermore, the condition $z > 0$, in relation (17-62) for the lift control, implies that

$$\tan\gamma < \frac{2E^*\lambda}{1+\lambda^2} \tag{17-66}$$

If the equality sign is used, we have the equation for another boundary curve as depicted in Fig. 17-5. The two boundary curves and the lines $\lambda = \pm \lambda_{max}$ delimit the region in the $(\gamma, \lambda)$ space inside which the flight is physically possible.

More exactly, for a given vehicle, with a given atmosphere, we can evaluate $z_s$ and the boundary as prescribed by Eq. (17-66) is replaced by the curve given by the equation

$$\sin\gamma\,\lambda^2 - 2E^*\lambda\cos\gamma + \sin\gamma + (2E^* z_s \sin^2\gamma / K^2) = 0 \tag{17-67}$$

When the trajectory reaches this boundary, the vehicle is at sea level and the flight is terminated. The domain of flight in Fig. 17-5 is extended by plotting this boundary with $z_s = 0$.

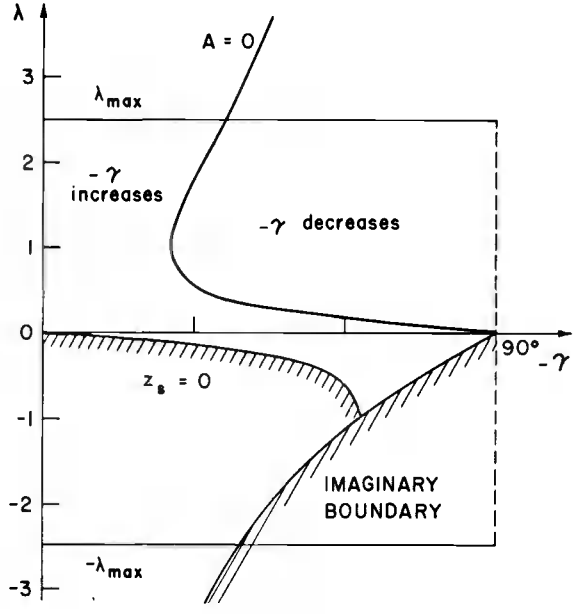


Fig. 17-5. Domain of flight in the $(\gamma, \lambda)$ space. Case of constant sinking speed.

In the figures we plot $-\gamma$ in abscissa to show the variation of the flight path angle in absolute value. In Fig. 17-5, we also plot the curve $A = 0$ for stationary value of $\gamma$. By the constraint (17-61), it is also the locus of points for stationary value of the speed $v$. From Eq. (17-60), with $d\gamma/dx = 0$, we have

$$\frac{z \sin^2 \gamma}{K^2} = \frac{\lambda}{\cos \gamma} \tag{17-68}$$

Hence, the curve $A = 0$ is in the positive $\lambda$ space. Combining this equation with Eq. (17-62) we have the equation for the curve $A = 0$

$$\lambda^2 + 2E^* \tan \gamma \lambda + 1 = 0 \tag{17-69}$$

In the $(\gamma, \lambda)$ space, this curve delimits the region inside which the absolute value $|\gamma|$, from here on referred to as the glide angle, is decreasing. The line $-\gamma = 90^\circ$ is the asymptote of the curve. The point where the tangent to the curve is vertical is the point

$$\lambda = 1 , \quad \tan \gamma = -1/E^* \tag{17-70}$$

From inspection of the figure, it can be deduced that the glide angle can never tend to $90^\circ$.

Another curve of interest is the $B = 0$ curve, that is the curve of stationary of the angle-of-attack. By taking the derivative of Eq. (17-62) with respect to $x$, using Eqs. (17-60) for the derivative of $\gamma$ and $z$, we have

$$\frac{d\lambda}{dx} = - \frac{E^* B}{z \sin \gamma \cos \gamma (E^* \cos \gamma - \lambda \sin \gamma)} \tag{17-71}$$

where

$$B = \frac{z^2 \sin^4 \gamma (\cos^2 \gamma - K^2)}{K^4} - \lambda^2 \tag{17-72}$$

Since $E^* \cos \gamma - \lambda \sin \gamma > 0$ in the domain of flight, the lift coefficient is increasing or decreasing according to $B$ positive or negative. In particular, if $K > 1$, the lift coefficient decreases monotonically along the flight path. When $K < 1$, $\lambda$ passes through a stationary value when $B = 0$, that is,

$$\frac{z \sin^2 \gamma}{K^2} = \pm \frac{\lambda}{\sqrt{\cos^2 \gamma - K^2}} \tag{17-73}$$

Using the (+) sign and substituting into Eq. (17-62), we have the equation of the $B = 0$ curve in the positive $\lambda$ region

$$\sin \gamma \lambda^2 + 2E^* \left[ \frac{1}{\sqrt{\cos^2 \gamma - K^2}} - \cos \gamma \right] \lambda + \sin \gamma = 0 \tag{17-74}$$

A detailed discussion of the B curve for both the flat planet and the spherical planet case is given in Ref. 1. This section follows the results for flat planet case analyzed in Ref. 3. For small values of K (low sinking speed), the allure of the B curve is shown in Fig. 17-6a. Figure 17-6c represents the case of large values of K (high sinking speed). Of course the B curve disappears when $K > 1$ (very high sinking speed). Figure 17-6b is the transition case for a critical value of K, $K = K_c$.

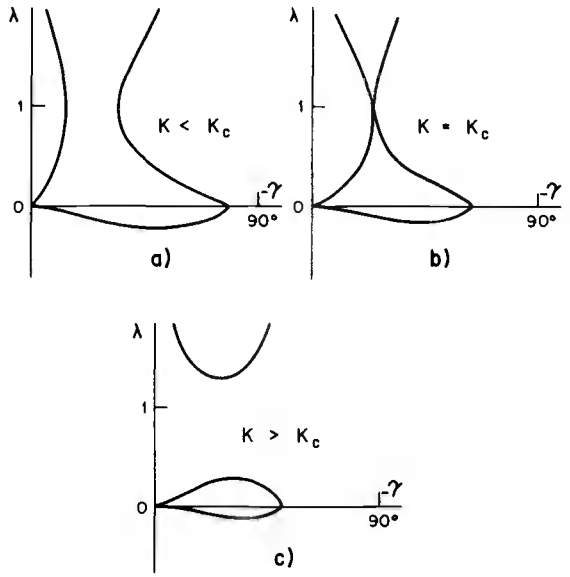


Fig. 17-6. Behavior of the $B = 0$ curve as function of K.

For a prescribed value of $E^*$, this critical value of K is obtained by first solving the quintic equation

$$E^{*3}\tau^5 + (1 - E^{*2})\tau^4 + E^*(3 + 2E^{*2})\tau^3 + E^{*2}\tau^2 + 2E^{*3}\tau - E^{*2} = 0 \tag{17-75}$$

to obtain

$$\tau = -\tan\gamma > 0 \tag{17-76}$$

Then $K_c$ is given by

$$K_c^2 = \frac{(1 - E^*\tau)(1 + E^*\tau^3)}{(1 + E^{*2})(1 + \tau^2)^2} \tag{17-77}$$

We can now discuss the characteristics of flight for glide at constant sinking speed.

17-4.3. Glide at Very High Sinking Speed

This is the case in which $K > 1$ . The B curve for stationary $\lambda$ is nonexistent and the lift coefficient decreases continuously along the flight path (Fig. 17-7). The limiting trajectory $T_1$ is obtained by integrating the equations of motion forward and backward from the point $\lambda = 1$ , $\tan\gamma = -1/E^*$ . In terms of the variation of the glide angle, there are three types of trajectories:

Type 1: Trajectories along which the glide angle increases continuously.

Type 2: Trajectories along which the glide angle first decreases, passes through a minimum, and then increases.

Type 3: When $\lambda_{max} > 1$ , we have a third type of trajectories along which the glide angle first increases, passes throug a relative maximum, then decreases, passes through a relative minimum, and finally increases until the end.

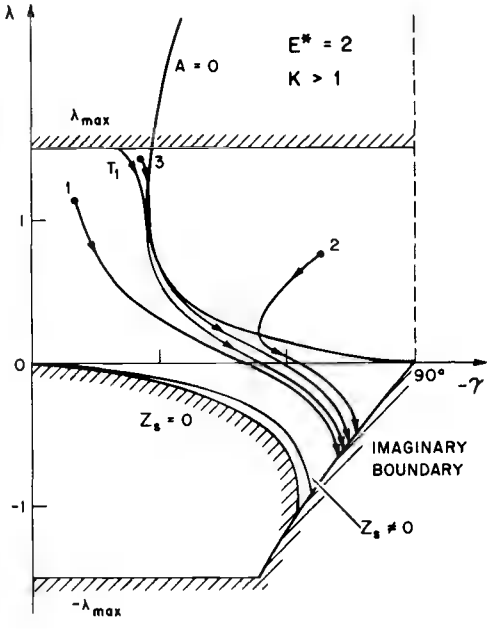


Fig. 17-7. Flow of trajectories for very high sinking speed, $K > 1$ .

17-4.4. Glide at High Sinking Speed

The case where

$$K_c < K < 1 \qquad (17\text{-}78)$$

is depicted in Fig. 17-8. The limiting trajectory $T_2$ is obtained by integrating the equations of motion forward and backward from the point of relative maximum of $\lambda$ on the B curve. Then, there are the following types of trajectories in terms of the variation of the lift coefficient:

Type 1 : If the initial point is in region I , the lift coefficient decreases continuously.

Type 2: If the initial point is in region II, the lift coefficient first increases, passes through a maximum, and then decreases.

Type 3: If the initial point is in region III, the lift coefficient first decreases, then increases, and finally decreases again.

In terms of the variation of the glide angle, the classification of the trajectories is the same as for the case of very high sinking speed.

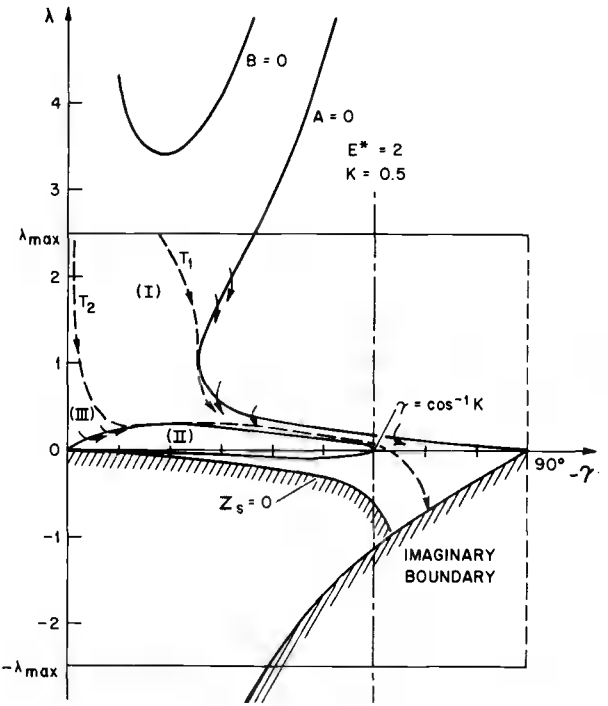


Fig. 17-8. Flow of trajectories for high sinking speed, $K_c < K < 1$.

17-4.5. Glide at Low Sinking Speed

This is the case widely used in practice. We have

$$0 < K < K_c \tag{17-79}$$

The flow of trajectories is depicted in Fig. 17-9. Among all the trajectories starting with a positive lift, there are three types:

Type 1: If the initial point is in region I (to the right of the B curve), then the lift coefficient decreases continuously.

Type 2: If the initial point is in region II (inside the B curve), then the lift coefficient first increases, passes through a maximum, and then decreases.

Type 3: If the initial point is in region III (to the left of the B curve), then the lift coefficient first decreases, passes through a relative minimum, increases until it reaches a relative maximum, and finally decreases until the end.

In terms of the variation of the glide angle, the classification of the trajectories is the same as for the case of very high sinking speed.

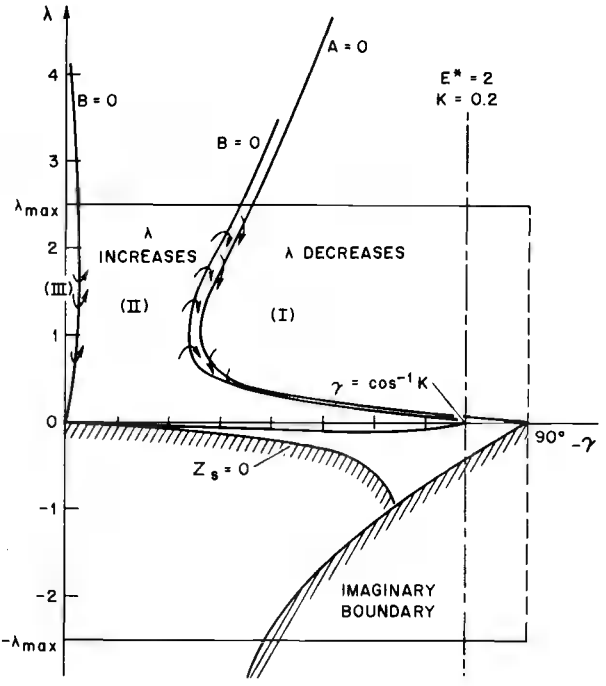


Fig. 17-9. Flow of trajectories for low sinking speed, $K < K_c$.

## 17-5. CONCLUSIONS

In this chapter we have examined two flight programs subject to constraint. The analysis shows that a complete analytical investigation can be carried out and properties of any specific flight program can be displayed explicitly. The discussion shows that the properties of the flight depend specifically on two parameters. The first parameter is the maximum lift-to-drag ratio $E^*$ which is the most important vehicle characteristic. The second parameter relates to the flight program adopted. It is the constant flight path angle $\gamma_i$ for

the first problem and the constant sinking speed $K$ for the second problem. The types of trajectories are classified according to either the variation of a state variable, speed or flight path angle, or the variation of the control variable, the lift coefficient. The variations of these variables along the trajectory depend on the initial condition.

Two accessory parameters are involved in the discussion, namely, the maximum rescaled lift coefficient $\lambda_{max}$ and the vehicle sea-level parameter $w_s$ or $z_s$. These parameters have no influence on the behavior of the trajectory. They only limit the domain of flight either in the physical plane or in the control plane.

## References

1. Bletsos, N. A., "Performance and Control with Lift Modulation of Hypervelocity Entry Vehicles," Ph. D. thesis, The University of Michigan, 1976.

2. Busemann, A., Vinh, N. X., and Culp, R. D., "Optimum Altitude for Coasting Flight of a Hypervelocity Vehicle," The Journal of the Astronautical Sciences, Vol. XXI, No. 1, pp. 32-48, 1973.

3. Vinh, N. X., Bletsos, N. A., Busemann, A., and Culp, R. D., "Flight with Lift Modulation Inside a Planetary Atmosphere," Paper No. 76-105, 27th International Astronautical Congress, Anaheim, California, U. S. A., 1976. Also, AIAA Journal, Vol. 15, No. 11, pp. 1617-1623, 1977.

# Chapter 18

# Lateral Maneuvers

## 18-1. INTRODUCTION

One interesting aspect of lifting entry is that the vehicle can rotate the lift force out of the vertical plane, thus creating a lateral component which can be used to change the heading. In this final chapter we shall consider such lateral maneuver. Of particular interest is the maximum lateral range which can be attained from a prescribed entry condition. Further consideration will be given to a maximum area on the surface of the planet which can be reached by the entry vehicle.

For convenience, we reproduce the dimensionless equations of motion for entry into a nonrotating spherical atmosphere derived in Chapter 16, using a parabolic drag polar. We have

$$\frac{dZ}{ds} = -\beta r\, Z \tan\gamma$$

$$\frac{dv}{ds} = -\frac{\sqrt{\beta r}\, Z v (1+\lambda^2)}{E^* \cos\gamma} - (2-v)\tan\gamma$$

$$\frac{d\gamma}{ds} = \frac{\sqrt{\beta r}\, Z}{\cos\gamma}\left[\lambda\cos\sigma + \frac{\cos\gamma}{\sqrt{\beta r}\, Z}\left(1-\frac{1}{v}\right)\right]$$

$$\frac{d\theta}{ds} = \frac{\cos\psi}{\cos\phi}$$

$$\frac{d\phi}{ds} = \sin\psi$$

$$\frac{d\psi}{ds} = \frac{\sqrt{\beta r}\, Z\, \lambda \sin\sigma}{\cos^2\gamma} - \cos\psi\tan\phi \qquad (18\text{-}1)$$

where by definition

$$Z \equiv \frac{\rho S C_L^*}{2m} \sqrt{\frac{r}{\beta}}$$

$$v \equiv \frac{V^2}{gr} \tag{18-2}$$

The product $\beta r$ characterizing the atmosphere will be considered as constant with the value $\beta r = 900$ for the Earth. The controls are the bank angle $\sigma$ and the rescaled lift coefficient

$$\lambda = \frac{C_L}{C_L^*} \tag{18-3}$$

where $C_L^*$ is the lift coefficient corresponding to maximum lift-to-drag ratio $E^*$. For a hypervelocity entry vehicle $E^*$ is in the range 1-3. The independent variable $s$ is the dimensionless arc length

$$s = \int_0^t \frac{V}{r} \cos\gamma \, dt \, . \tag{18-4}$$

## 18-2. EQUILIBRIUM GLIDE CONDITION

For entry from low altitude orbit, the initial speed is nearly circular. Furthermore, for moderate lift, the flight path angle can be kept small and nearly constant. This is the condition of equilibrium glide discussed previously. Hence, we shall take $\gamma \approx 0$ and have the reduced equations

$$\frac{dv}{ds} = -\frac{\sqrt{\beta r}\, Z\, v(1+\lambda^2)}{E^*}$$

$$\frac{d\theta}{ds} = \frac{\cos\psi}{\cos\phi}$$

$$\frac{d\phi}{ds} = \sin\psi$$

$$\frac{d\psi}{ds} = \sqrt{\beta r}\, Z\, \lambda \sin\sigma - \cos\psi \tan\phi \tag{18-5}$$

We recall that $\theta$ is the longitudinal range, $\phi$ is the lateral range, or latitude if the reference plane is taken as the equatorial plane. The angle $\psi$ is the heading angle measured from the reference plane. The equation for $\gamma$ becomes the equilibrium equation

$$\lambda \cos\sigma = \frac{(1-v)}{\sqrt{\beta r}\, Z\, v} \tag{18-6}$$

This equation shows that the vertical component of the lift force is used to balance the combined gravity and centrifugal force. The equation is used to evaluate the "altitude" $Z$ in terms of the kinetic energy $v$. Upon substituting into Eqs. (18-5), we have

$$\frac{dv}{ds} = -\frac{(1-v)(1+\lambda^2)}{E^*\lambda \cos\sigma}$$

$$\frac{d\theta}{ds} = \frac{\cos\psi}{\cos\phi}$$

$$\frac{d\phi}{ds} = \sin\psi$$

$$\frac{d\psi}{ds} = \frac{(1-v)}{v}\tan\sigma - \cos\psi\tan\phi \qquad (18\text{-}7)$$

## 18-3. MAXIMUM LATERAL RANGE

The equations (18-7) constitute the state equations for the four main variables $v$, $\theta$, $\phi$ and $\psi$. For equilibrium glide from circular speed we have at the initial time

$$v_o \approx 1, \quad \theta_o = 0, \quad \phi_o = 0, \quad \psi_o = 0 \qquad (18\text{-}8)$$

It is proposed to use lift and bank control, in the variables $\lambda$ and $\sigma$ to achieve a maximum lateral range when the speed has reduced to a final low speed $v_f \approx 0$. A full treatment will require the tool of modern optimum control theory and we refer to Ref. 1. A sub-optimum control law will be discussed in this chapter.

First, from the equation for $v$, it is seen that the speed decreases continuously. In atmospheric maneuvers at high speed, the kinetic energy is an important element since it can be used for an exchange with the potential energy, hence gaining the necessary altitude to extend both longitudinal and lateral ranges. Then, for a given bank angle, to minimize the decrease in the speed, we minimize the right-hand side of the equation for $v$, the first of Eqs. (18-7), with respect to the lift control $\lambda$. This gives

$$\lambda = 1 \qquad (18\text{-}9)$$

The optimal glide should be performed at maximum lift-to-drag ratio.

To achieve a maximum lateral range, the bank angle must be modulated in an optimum manner. In general, for maximum lateral range the optimum bank angle varies as a function of the time from a maximum permissible value, $\sigma = \sigma_{max}$, at the initial time, to the value zero at the final time (Refs. 1, 2). We shall assume that there exists a certain average constant value for the bank angle providing comparable performance. Furthermore, in order to obtain an analytic integration of the equations of motion, we shall assume that both the

changes in the heading $\psi$ , and latitude $\phi$ are small so that

$$\tan\phi \approx \phi \quad , \quad \cos\phi \approx 1 \quad , \quad \sin\psi \approx \psi \quad , \quad \cos\psi \approx 1 \tag{18-10}$$

With these simplifications and using $\lambda = 1$ in Eqs. (18-7) we have

$$\begin{aligned} \frac{dv}{ds} &= -\frac{2(1-v)}{E^* \cos\sigma} \\ \frac{d\phi}{ds} &= \psi \\ \frac{d\psi}{ds} &= \frac{(1-v)}{v}\tan\sigma - \phi \end{aligned} \tag{18-11}$$

We note that, for small $\psi$ and $\phi$ , $d\theta/ds \approx 1$ , and the variable s becomes the range angle $\theta$ .

For constant bank angle, the first of the Eqs. (18-11) can be integrated immediately. We have

$$v = 1 - (1 - v_o) \exp\left[\frac{2s}{E^* \cos\sigma}\right] \tag{18-12}$$

From this formula, it is seen that we must take $v_o \neq 1$ to avoid the indetermination. For all practical purpose, we can take $v_o = 0.995$ . For entry from circular speed, this is the point where the atmosphere has become sensible such that lifting force is effective. The expression (18-12) can be substituted into the equation for $\psi$ and this equation and the equation for $\phi$ can be integrated as has been done in Ref. 2. Here, we shall follow Ref. 3 and rewrite the two equations using the speed v as independent variable. Then, we have the equations

$$\begin{aligned} \frac{d\phi}{dv} &= -\frac{E^* \cos\sigma}{2(1-v)}\psi \\ \frac{d\psi}{dv} &= -\frac{E^* \sin\sigma}{2v} + \frac{E^* \cos\sigma}{2(1-v)}\phi \end{aligned} \tag{18-13}$$

By taking the derivative of the first equation, using the second equation of this system, we have a linear second-order differential equation for the lateral range

$$\frac{d^2\phi}{dv^2} - \frac{1}{(1-v)}\frac{d\phi}{dv} + \frac{E^{*2}\cos^2\sigma}{4(1-v)^2}\phi = \frac{E^{*2}\sin\sigma\cos\sigma}{4v(1-v)} \tag{18-14}$$

By the change of independent variable

$$1 - v = \tau \tag{18-15}$$

and dependent variable

$$\bar{\phi} = \frac{\phi}{E^{*2} \sin\sigma \cos\sigma} \tag{18-16}$$

we put the equation in the simpler form

$$\frac{d^2\bar{\phi}}{d\tau^2} + \frac{1}{\tau}\frac{d\bar{\phi}}{d\tau} + \frac{E^{*2}\cos^2\sigma}{4\tau^2}\bar{\phi} = \frac{1}{4\tau(1-\tau)} \tag{18-17}$$

The homogeneous equation

$$\frac{d^2\bar{\phi}}{d\tau^2} + \frac{1}{\tau}\frac{d\bar{\phi}}{d\tau} + \frac{E^{*2}\cos^2\sigma}{4\tau^2}\bar{\phi} = 0 \tag{18-18}$$

is an Euler equation and the change of variable

$$\tau = e^{\mu} \tag{18-19}$$

transforms it into a linear equation with constant coefficient

$$\frac{d^2\bar{\phi}}{d\mu^2} + \frac{E^{*2}\cos^2\sigma}{4}\bar{\phi} = 0 \tag{18-20}$$

Hence, we have the general solution of the homogeneous equation

$$\bar{\phi} = c_1 \cos\left[\frac{E^*\cos\sigma}{2}\log\tau\right] + c_2 \sin\left[\frac{E^*\cos\sigma}{2}\log\tau\right] \tag{18-21}$$

where $c_1$ and $c_2$ are two arbitrary constants of integration. To obtain a particular solution of Eq. (18-17), since by the definition (18-15), $\tau < 1$, we can use binomial expansion to write the equation as

$$4\tau^2\bar{\phi}'' + 4\tau\bar{\phi}' + E^{*2}\cos^2\sigma\,\bar{\phi} = \tau + \tau^2 + \tau^3 + \ldots \tag{18-22}$$

where the prime denotes derivative with respect to $\tau$. A particular solution to this equation can be constructed in the form of a power series

$$\bar{\phi} = \sum_{n=1}^{\infty} a_n \tau^n \tag{18-23}$$

By substituting this series into Eq. (18-22) and equating coefficients of like powers in $\tau$, it is found that

$$a_n = \frac{1}{E^{*2}\cos^2\sigma + 4n^2} \tag{18-24}$$

In summary, the solution for the latitude is

$$\frac{\phi}{E^{*2}\sin\sigma\cos\sigma} = c_1 \cos\left[\frac{E^*\cos\sigma}{2}\log\tau\right] + c_2 \sin\left[\frac{E^*\cos\sigma}{2}\log\tau\right] + \frac{1}{4}\sum_{n=1}^{\infty}\frac{\tau^n}{\left(\frac{E^*\cos\sigma}{2}\right)^2 + n^2} \tag{18-25}$$

By using the initial condition, $\tau = \tau_o$, $\phi_o = 0$, $\phi_o' = 0$ we can evaluate the constants of integration $c_1$ and $c_2$ and obtain the solution for $\phi$ as function of the kinetic energy $v$

$$\frac{\phi}{E^{*2}\sin\sigma\cos\sigma} = \frac{1}{4}\sum_{n=1}^{\infty}\frac{\tau^n}{\left(\frac{E^*\cos\sigma}{2}\right)^2 + n^2} - \frac{1}{4}\left[\sum_{n=1}^{\infty}\frac{\tau_o^n}{\left(\frac{E^*\cos\sigma}{2}\right)^2 + n^2}\right]\cos\left[\frac{E^*\cos\sigma}{2}\log\frac{\tau}{\tau_o}\right] - \frac{1}{2E^*\cos\sigma}\left[\sum_{n=1}^{\infty}\frac{n\tau_o^n}{\left(\frac{E^*\cos\sigma}{2}\right)^2 + n^2}\right]\sin\left[\frac{E^*\cos\sigma}{2}\log\frac{\tau}{\tau_o}\right] \tag{18-26}$$

This formula is to be used for entry at any arbitrary speed, $\tau_o = 1 - v_o$, provided that the equilibrium glide condition is realized. For entry from near circular speed $\tau_o \approx 0$, and we can neglect the contribution of the harmonic terms. Furthermore, for low final speed $v_f \approx 0$, $\tau_f = 1 - v_f \approx 1$, we have the expression for the final range as given in Ref. 2

$$\phi = \frac{E^{*2}}{4}\sin\sigma\cos\sigma\sum_{n=1}^{\infty}\frac{1}{n^2 + \frac{E^{*2}}{4}\cos^2\sigma} \tag{18-27}$$

We can write the summation as

$$\sum_{n=1}^{\infty} \frac{1}{n^2 + \frac{E^{*2}}{4}\cos^2\sigma} = \sum_{n=1}^{\infty} \frac{1}{n^2} - \sum_{n=1}^{\infty} \frac{1}{n^2}$$

$$+ \sum_{n=1}^{\infty} \frac{1}{n^2 + \frac{E^{*2}}{4}\cos^2\sigma} = \sum_{n=1}^{\infty} \frac{1}{n^2}$$

$$- \frac{E^{*2}\cos^2\sigma}{4} \sum_{n=1}^{\infty} \frac{1}{n^2\left[n^2 + \frac{E^{*2}}{4}\cos^2\sigma\right]} \qquad (18\text{-}28)$$

Noticing that the value of the first sum is $\pi^2/6$ , we have the final formula

$$\frac{48\phi}{E^{*2}\pi^2} = \sin 2\sigma \left[1 - \frac{3E^{*2}\cos^2\sigma}{2\pi^2} \sum_{n=1}^{\infty} \frac{1}{n^2\left[n^2 + \frac{E^{*2}}{4}\cos^2\sigma\right]}\right]$$

(18-29)

Neglecting the summation, an assumption which is valid for small values of $E^*$ , we have the formula as given by Eggers (Ref. 4)

$$\phi = \frac{E^{*2}\pi^2}{48} \sin 2\sigma \qquad (18\text{-}30)$$

From this, it is seen that the best value for the bank angle is

$$\sigma = 45^\circ \qquad (18\text{-}31)$$

Figure 18-1, presents the plot of Eq. (18-30), and Eq. (18-29) using two terms of the series with $\sigma = 45^\circ$ . Curve (a) is Eggers solution and curve (b) is the present solution with two terms. On the figure we also plot in curve (c) the numerical solution of system (18-7) using $\sigma = 45^\circ$ . In this integration, whenever the heading angle reaches $90^\circ$ we change the bank angle $\sigma$ into zero . Finally curve (d) is taken from Ref. 1. It shows the true maximum lateral range. It is obtained by modulating the bank angle according to the law

$$\tan\sigma = \frac{(1-v)}{v} \frac{\cos\phi \sin(\theta_f - \theta)}{\cos(\theta_f - \theta)\sin\psi - \cos\psi \sin\phi \sin(\theta_f - \theta)} \qquad (18\text{-}32)$$

where the constant $\theta_f$ is the final longitudinal range, selected such that we have perfect matching when $v = v_f = 0.001$.

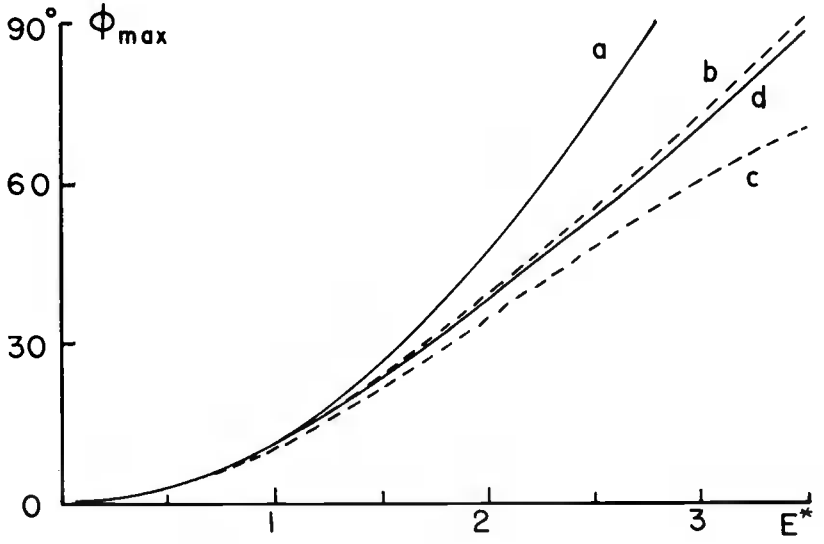


Fig. 18-1. Lateral range versus E* .

It is obvious that optimum modulated bank angle gives better lateral range than constant bank angle [ curve (d) as compared to curve (c)] . It must be emphasized here that solutions (a) and (b) are only approximate analytic solutions. Nevertheless, since the solution (b), as given by Eq. (18-29), gives a good estimate of the lateral range, it can be used to find an improved optimum constant bank angle to maximized the lateral range. A numerical study in Ref. 5 has shown that approximate solution agrees with numerical solution for values of maximum lift-to-drag ratio up to 1.5. We consider the function on the right-hand side of Eq. (18-29) using one term of the series

$$f(\sigma) = \sin 2\sigma \left[ 1 - \frac{\epsilon \cos^2\sigma}{1+\frac{E^{*2}}{4}\cos^2\sigma} \right] \tag{18-33}$$

where

$$\epsilon = \frac{3E^{*2}}{2\pi^2} \tag{18-34}$$

This function is maximized when $df/d\sigma = 0$ . Carrying out the derivation, we have

$$\cos 2\sigma = \frac{\epsilon \cos^2\sigma}{\left(1+\frac{E^{*2}}{4}\cos^2\sigma\right)^2} \left[ \cos 2\sigma \left(1+\frac{E^{*2}}{4}\cos^2\sigma\right) - 2\sin^2\sigma \right] \tag{18-35}$$

Let

$$\alpha = \cos^2 \sigma \tag{18-36}$$

We write the equation as

$$\alpha = \frac{1}{2} - \frac{\epsilon \alpha}{2(1 + \frac{E^{*2}}{4} \alpha)^2} \left[ 3 - (4 - \frac{E^{*2}}{4}) \alpha - \frac{E^{*2}}{2} \alpha^2 \right] \tag{18-37}$$

For low maximum lift-to-drag ratio, $\epsilon$ is small, and to the zero order, $\epsilon = 0$, we have the solution

$$\alpha = \frac{1}{2} = \cos^2 \sigma \quad , \quad \sigma = 45^\circ \quad .$$

For higher order, Eq. (18-37) is of the form

$$\alpha = p + \epsilon \, g(\alpha) \tag{18-38}$$

and by Lagrange's expansion, we have the solution

$$\alpha = p + \sum_{n=1}^{\infty} \frac{\epsilon^n}{n!} \left( \frac{d}{dp} \right)^{n-1} [ g(p) ]^n \tag{18-39}$$

To the order of $\epsilon^3$, we have the solution

$$\cos^2 \sigma = \frac{1}{2} - \frac{\epsilon}{4(1+\frac{1}{8} E^{*2})^2} - \frac{\epsilon^2}{16(1+\frac{1}{8} E^{*2})^5} (2+E^{*2}+\frac{1}{32} E^{*4})$$

$$- \frac{\epsilon^3}{64(1+\frac{1}{8} E^{*2})^8} (-4+2E^{*2} + \frac{19}{16} E^{*4} + \frac{1}{16} E^{*6} + \frac{1}{1024} E^{*8}) \tag{18-40}$$

This expression shows that the optimum constant bank angle is greater than $45^\circ$. This explicit solution is accurate for values of $E^*$ up to 3. For large values of $E^*$, we can solve the exact equation (18-37) which is a cubic equation in $\alpha$ written as

$$\frac{E^{*4}}{8} (1 - \frac{6}{\pi^2}) \alpha^3 + E^{*2} (1 - \frac{E^{*2}}{16}) (1 - \frac{6}{\pi^2}) \alpha^2$$

$$+ \left[ \frac{1}{4} (8 + E^{*2}) - \frac{3}{4} E^{*2} ( 1 - \frac{6}{\pi^2}) \right] \alpha - 1 = 0 \tag{18-41}$$

Another approximate solution to this equation can be obtained by putting

$$\sigma = \frac{\pi}{4} + \delta \quad , \quad \delta << 1 \tag{18-42}$$

Then, by series expansions and to the order of $\delta^2$ included

$$\cos\sigma = \frac{1}{\sqrt{2}}\left(1 - \delta - \frac{1}{2}\delta^2\right)$$

$$\alpha = \frac{1}{2}(1 - 2\delta)$$

$$\alpha^2 = \frac{1}{4}(1 - 4\delta + 4\delta^2)$$

$$\alpha^3 = \frac{1}{8}(1 - 6\delta + 12\delta^2) \tag{18-43}$$

Upon substituting into Eq. (18-41), we have a quadratic equation in $\delta$ .

$$\delta^2 - \frac{1}{4}\left(1 + \frac{a}{E^{*2}}\right)\delta + \frac{b}{(8 + E^{*2})} = 0 \tag{18-44}$$

where

$$a = \frac{8\pi^2}{\pi^2 - 6}$$

$$b = \frac{6}{\pi^2 - 6} \tag{18-45}$$

Upon solving, we have the solution

$$\delta = \frac{1}{8}\left(1 + \frac{a}{E^{*2}}\right)\left[1 - \sqrt{1 - \frac{64b}{(8+E^{*2})\left(1 + \frac{a}{E^{*2}}\right)^2}}\right] \tag{18-46}$$

This solution is identical to the approximate solution obtained by Shkadov in Ref. 2. He used the Eq. (18-42) to expand the function $f(\sigma)$ as given by Eq. (18-33) in series in $\delta$ before maximizing.

The exact solution for the optimum bank angle obtained by solving the cubic equation (18-41) is plotted in Fig. 18-2 versus the maximum lift-to-drag ratio. In the range of $E^*$ considered, $E^* \leq 3.5$, both the explicit solutions (18-40) and (18-46) are in excellent agreement with the exact solution.

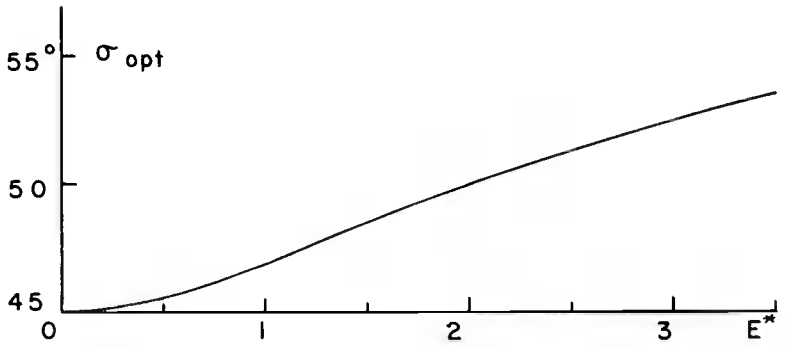


Fig. 18-2. Optimum bank angle as function of maximum lift-to-drag ratio.

## 18-4. FOOTPRINT OF REENTRY VEHICLE

The footprint of a reentry vehicle is the maximum area on the surface of the Earth the vehicle can reach in gliding flight. Using the equatorial plane as the initial plane of motion, if the point of departure is not specified, then the maximum area reachable is obviously a zone between the latitudes $-\phi_{max}$ and $\phi_{max}$ where $\phi_{max}$ is the maximum lateral range. The construction of the footprint from a specified point of departure is a difficult problem. Fig. 18-3 from Ref. 1 plots the footprint as function of the maximum lift-to-drag ratio.

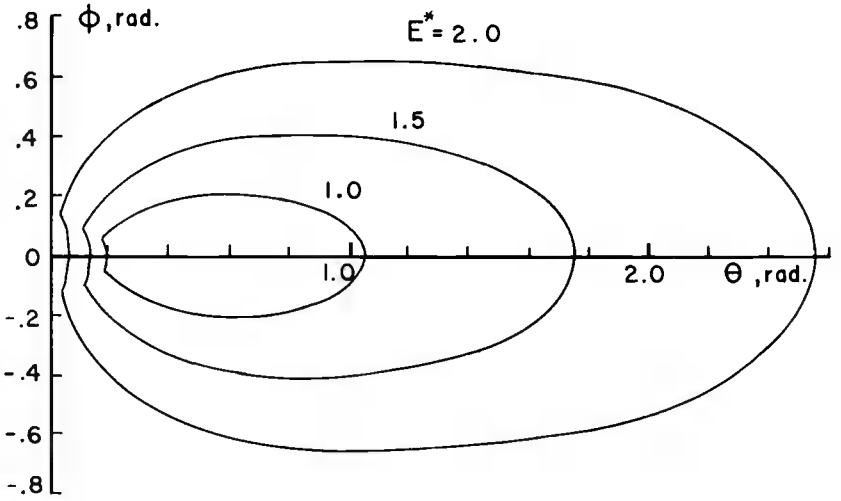


Fig. 18-3. Footprint for different values of E* when the point of departure is specified.

For a given value of $E^*$, consider a footprint in Fig. 18-3. The problem consists of maximizing the lateral range for each prescribed final value of the longitudinal range. Within the assumption of equilibrium glide, the optimum control law for the modulation of the bank angle is given by Eq. (18-32). If the lateral range is small, we can use the simplification $\sin\phi \approx 0$, $\cos\phi \approx 1$ to have the approximate law

$$\tan\sigma = \frac{(1-v)}{v} \quad \frac{\tan(\theta_f - \theta)}{\sin\psi} \tag{18-47}$$

This is the approximate law obtained by Fave (Ref. 6). Using Fave's simplification in Eqs. (18-7) with $v$ as independent variable, and $\lambda = 1$ for flight at maximum lift-to-drag ratio, we have

$$\frac{d\theta}{dv} = -\frac{E^* \cos\sigma \cos\psi}{2(1-v)}$$

$$\frac{d\phi}{dv} = -\frac{E^* \cos\sigma \sin\psi}{2(1-v)}$$

$$\frac{d\psi}{dv} = -\frac{E^* \sin\sigma}{2v} \tag{18-48}$$

Then, for each estimated value $\theta_f$, the control law (18-47) is used for the integration of the equations of motion (18-48) until the final value $v_f = 0.001$. The final value of $\theta$ obtained must equal the initial guessed value. This leads to the final bank angle $\sigma_f = 0$. Fave's analysis is in good agreement with pure numerical analysis for low values of the maximum lift-to-drag ratio.

## References


1. Vinh, N.X., and Chern, J.S., "Three-Dimensional Optimum Maneuvers of a Hypervelocity Vehicle," IAF paper No. 79-F-184, presented at the XXXth Congress of the International Astronautical Federation, Munich, F.R.G., September 1979.

2. Shkadov, L.M., Bukhanova, R.S., Illarionov, V.F., and Plokhikh, V.P., "Mechanics of Optimum Three-Dimensional Motion of Aircraft in the Atmosphere," NASA TT F-777, 1975.

3. Gell, D.A., "Optimum Lateral Range," Progress Report, Ph.D. dissertation, The University of Michigan, 1979.

4. Eggers, A.J., Jr., "The Possibility of a Safe Landing," Space Technology, edited by H.S. Seifert, John Wiley and Son, Inc., Ch. 13, 1959.

5. Slye, R.E., "An Analytical Method for Studying the Lateral Motion of Atmosphere Entry Vehicles," NASA TN D-325, 1960.

6. Fave, J., "Approche Analytique du Problème du Domaine Accessible à un Planeur Orbital," La Recherche Aérospatiale, No. 124, pp. 3-11, 1968.